USAAMRDL-TR-73-98 B

ADA020327

# 3000-HP ROLLER GEAR TRANSMISSION DEVELOPMENT PROGRAM
## Volume II - Design Report

Sikorsky Aircraft
Division of United Technologies Corporation
Stratford, Conn. 06602

December 1975

Final Report

Prepared for

EUSTIS DIRECTORATE
U. S. ARMY AIR MOBILITY RESEARCH AND DEVELOPMENT LABORATORY
Fort Eustis, Va. 23604

## EUSTIS DIRECTORATE POSITION STATEMENT

This report is one of six volumes of the final report under this contract. The objective of this program is to conduct research on the feasibility of a high-reduction-ratio, 3000-horsepower roller gear transmission. This report covers the preliminary design and detail design of an S-61-type aircraft main transmission. In addition, extensive redesign effort of the roller gear unit's second-row compound pinions is included. This program incorporated the first known successful use of ZE-41 material for an aircraft main transmission housing of this size.

James Gomez, Jr., Propulsion Technical Area, Technology Applications Division, served as project engineer for this effort.

Unclassified

| REPORT DOCUMENTATION PAGE | | READ INSTRUCTIONS BEFORE COMPLETING FORM |
|---|---|---|
| 1 REPORT NUMBER  USAAMRDL-TR-73-98B | 2 GOVT ACCESSION NO. | 3 RECIPIENT'S CATALOG NUMBER |
| 4 TITLE (and Subtitle)  3000-HP ROLLER GEAR TRANSMISSION DEVELOPMENT PROGRAM, VOLUME II. DESIGN REPORT. | | 5. TYPE OF REPORT & PERIOD COVERED  Final Report., |
| | | 6. PERFORMING ORG. REPORT NUMBER  Sikorsky Report 611675 |
| 7 AUTHOR(s)  G. P. Gardner  J. Kish | | 8 CONTRACT OR GRANT NUMBER(s)  DAAJ02-69-C-0042 |
| 9 PERFORMING ORGANIZATION NAME AND ADDRESS  Sikorsky Aircraft  Division of United Technologies Corporation, Stratford, Connecticut 06602 | | 10. PROGRAM ELEMENT, PROJECT, TASK AREA & WORK UNIT NUMBERS  62207A 1G162207AA72 01  006 EK |
| 11 CONTROLLING OFFICE NAME AND ADDRESS  Eustis Directorate  U. S. Army Air Mobility R&D Laboratory  Fort Eustis, Virginia 23604 | | 12 REPORT DATE  December 1975 |
| | | 13 NUMBER OF PAGES  377 |
| 14 MONITORING AGENCY NAME & ADDRESS(if different from Controlling Office) | | 15 SECURITY CLASS. (of this report)  Unclassified |
| | | 15a DECLASSIFICATION DOWNGRADING SCHEDULE |

16 DISTRIBUTION STATEMENT (of this Report)

Approved for public release; distribution unlimited.

17 DISTRIBUTION STATEMENT (of the abstract entered in Block 20, if different from Report)

18 SUPPLEMENTARY NOTES

Volume II of a six-volume report.

19 KEY WORDS (Continue on reverse side if necessary and identify by block number)

| Rollers | Transmission | Design |
| Gear | Helicopters | Stress |
| Preload | Aircraft | Analysis |

20 ABSTRACT (Continue on reverse side if necessary and identify by block number)

The development of the roller gear drive indicated potential gains in the overall operational efficiency of turbine-powered helicopters. This report presents the design effort involved in the development of the Sikorsky S-61 roller gear transmission.

DD FORM 1 JAN 73 1473  EDITION OF 1 NOV 65 IS OBSOLETE

Unclassified

The roller gear drive is a combination of the roller transmission, which transmits power through friction, and a conventional geared planetary arrangement.

This report covers the initial design of the S-61 roller gear transmission wherein the number of reduction stages, their locations and the reduction ratio of the roller gear unit are determined. Various types and layouts of transmissions are discussed. The finalized layout, which receives 3,700 hp from twin turbines and transmits 3,000 hp to the main rotor, incorporates a 19.85:1 roller gear unit as the final stage in a three-stage reduction transmission. The detail design of the major components is discussed, and a stress analysis is presented in the appendixes.

A calculated efficiency of 98.9% for the roller gear unit and 96.5% for the transmission is comparable to high-reduction-ratio transmissions of conventional design. Dynamic testing of the transmission will be conducted during later phases of the program whereby the efficiency of the transmission will be measured.

## PREFACE

This report, the second of six volumes dealing with the development of a VTOL drive train using a roller gear unit as the primary reduction stage, covers the design of a 3,000-hp roller gear transmission. The report was prepared by Sikorsky Aircraft under Contract DAAJ02-69-C-0042 for the Eustis Directorate, U. S. Army Air Mobility Research and Development Laboratory, Fort Eustis, Virginia. The technical monitors for the contract, which encompasses the design, development, test and evaluation of the roller gear within a helicopter transmission, were Messrs. James Gomez and Leonard M. Bartone, Technology Applications Division.

Program responsibilities at Sikorsky Aircraft were divided among Messrs. L. R. Burroughs, P. Marin and G. F. Gardner. Other personnel contributing to the design phase of the program included Messrs J. Kish, A. Korzun, R. Costanzo and T. Lally. Acknowledgement of appreciation for technical assistance is extended to Dr. A. L. Nasvytis, who invented the roller gear concept.

# TABLE OF CONTENTS

3

# TABLE OF CONTENTS (continued)

## LIST OF ILLUSTRATIONS

7

LIST OF ILLUSTRATIONS (continued)

8

LIST OF ILLUSTRATIONS (continued)

9

LIST OF ILLUSTRATIONS (continued)

13

## LIST OF ILLUSTRATIONS (continued)

## LIST OF TABLES

15

## LIST OF TABLES (continued)

# INTRODUCTION

## BACKGROUND AND HISTORY OF THE ROLLER GEAR DRIVE

Most high-power rotary speed reductions, such as those in helicopter transmissions, are accomplished by means of conventional gear planetaries. While transmissions employing this type of reduction unit perform satisfactorily, there has been continual research and development aimed at improving the performance of helicopter transmissions. One of the developments resulting from this effort has been the roller gear drive. As the name implies, the roller gear drive employs both rollers and gears in a hybrid planetary system. The rollers are used for positioning and to react radial forces, while the gears are used to transmit power. This arrangement has been shown to compare favorably with conventional planetaries on a power to weight ratio basis.

Development of the roller gear drive began in 1963 with a parametric study of the concept by TRW Incorporated under the direction of Dr. A. L. Nasvytis, the inventor of the roller gear drive. The basic roller gear concept was investigated over a range from 250 to 4,000 hp, from 12,000 to 30,000 rpm, and with 20:1 to 100:1 reduction ratios. No significant obstacles were found which would prevent the roller gear reduction drive from being developed and used in helicopters. It was found that the roller gear drive showed promise of higher efficiency, lower vibration, longer life, improved reliability, greater rigidity and lower weight. The final report of the study[1] concluded that the roller gear drive was a viable candidate for use in helicopter transmissions, and it was recommended that a program be initiated to design, fabricate and test an experimental unit.

A 200-horsepower unit of 70:1 reduction ratio was designed, fabricated and tested for 1,000 hours in a back-to-back regenerative arrangement.[2] The primary purpose of this program was to determine the feasibility of roller gear drive arrangements for power reductions in helicopter transmissions and to determine initial design parameters for the drive. This 1,000-hour endurance test, conducted in 1964 and 1965 by TRW, Cleveland, Ohio, confirmed that the roller gear drive was a high-efficiency unit suitable for future helicopter transmissions. At the conclusion of the test, all rollers and gear contacts were in excellent condition. It was

1  Dr. A. L. Nasvytis and J. E. Bauer, PARAMETRIC STUDY ON THE ROLLER GEAR REDUCTION DRIVE, USAAVLABS Technical Report 64-29, USAAMRDL, Fort Eustis, Virginia, June 1965.

2  ENDURANCE TEST OF AN-1 ROLLER GEAR DRIVE, USAAVLABS Technical Report 65-31, USAAMRDL, Fort Eustis, Virginia, August 1965.

recommended that a full-sized unit be designed, fabricated and tested to determine the technical feasibility of using the roller gear drive in a helicopter.

In 1968 and 1969, the Bell Helicopter Company of Fort Worth, Texas, conducted an engineering design study to determine the feasibility of employing the roller gear concept in a transmission for the UH-1 helicopter.[3] This study, which compared the roller gear drive to the existing UH-1 transmission and a new three-stage planetary design, showed that in the areas of efficiency and reliability, the roller gear was the potentially superior design. The roller gear drive ranked last only in fabricability/cost of the areas examined, while ranking second to the new three-stage planetary in weight. Five different roller gear drives of 42.8:1 reduction ratio were designed and analyzed. The drives were designed for approximately 1,140 hp with 13,890 rpm input and 324 rpm output. The primary study criteria were cost, weight, efficiency and reliability.

Meanwhile, TRW was proceeding with the design, fabrication and test of a roller gear drive whose size was comparable to the UH-1 helicopter transmission.[4] This roller gear drive was designed for 1,100 hp with 34.8:1 reduction ratio, accepting an input speed of 11,300 rpm and an output speed of 324 rpm. A cam mechanism was used to provide roller preload, while a spherical bearing in the outer row of the two-row arrangement was used to eliminate any reactions introduced into the assembly as a result of gearbox housing deflections. The rollers of this design were press fitted onto the gears.

The test method employed the principle of back-to-back coupling of two test units in a closed loop. Efficiency of the unit, as determined by test, was found to be 98.9 percent, which is high for a unit of 34.8:1 reduction ratio. A total time of 76.5 hours was logged toward the test objective of 200 hours. Testing was halted due to test rig malfunction and minor design deficiencies which became apparent during the full-load portion of the test program. As a result of this test program, it was determined that future designs would require attention to the method of joining the rollers to the gears and also to the width of the roller-end flanges. It was

3  C. W. Bowen, C. E. Braddock, and R. D. Walker, INSTALLA-
   TION OF A HIGH-REDUCTION-RATIO TRANSMISSION IN THE UH-1
   HELICOPTER, USAAVLABS Technical Report 68-57, USAAMRDL
   Fort Eustis, Virginia, May 1969.

4  A. L. Nasvytis and J. H. Hemlein, 1100-HP ROLLER GEAR
   DRIVE, USAAVLABS Technical Report 70-3, USAAMRDL, Fort
   Eustis, Virginia, January 1970.

concluded that the basic design concept of the roller gear drive was sound and offered a practical solution for long life, high speed, high power and high efficiency for high reduction ratio helicopter transmissions.

Sikorsky first examined the roller gear drive in 1966,[5] with a feasibility study aimed at replacing the two-stage planetary system of the CH-54A helicopter main transmission with a roller gear drive reduction unit. This study was aimed at using a roller gear unit as a direct replacement for the two-stage planetary system of the CH-54A helicopter transmission. The required overall reduction ratio of 9.69:1, however, was found to be too low to take full advantage of the benefits of a roller gear drive. It was recommended that an evaluation of a roller gear drive be conducted at the inception of a new aircraft program where no existing hardware or configuration restraints had been previously imposed. While this study concluded that the roller gear drive concept was not applicable to the particular vehicle chosen, this program and subsequent independent research and development efforts led to the present roller gear program for the S-61 aircraft.

In March 1969, in response to USAAMRDL request for proposal No. DAAJ02-69-Q-0034, Sikorsky Aircraft proposed a program to design, fabricate and test a transmission incorporating a roller gear drive for the H-3 (Sikorsky S-61) series helicopter. A contract for this program was awarded in June 1969. This report covers the initial design of the roller gear main transmission which was developed under this contract.

5  L. R. Burroughs and N. L. Chivaroli, CH-54A HIGH SPEED ROLLER GEAR TRANSMISSION FEASIBILITY STUDY, Sikorsky Engineering Report SER-64202, January 1970.

## PRINCIPLE OF OPERATION OF THE ROLLER GEAR DRIVE

The principle of the operation of a roller gear drive is the integration of rollers with gears in an epicyclic planetary arrangement. This is illustrated in Figure 1, where the roller diameters are equal to the pitch diameter of the gears to which they are attached. This results in pure rolling for the rollers and ideal operating center distance for gear meshing. The rollers are usually designed to straddle the gear teeth for load equilibrium. Flanges on the edges of the rollers are used to restrain the gears in the axial direction.
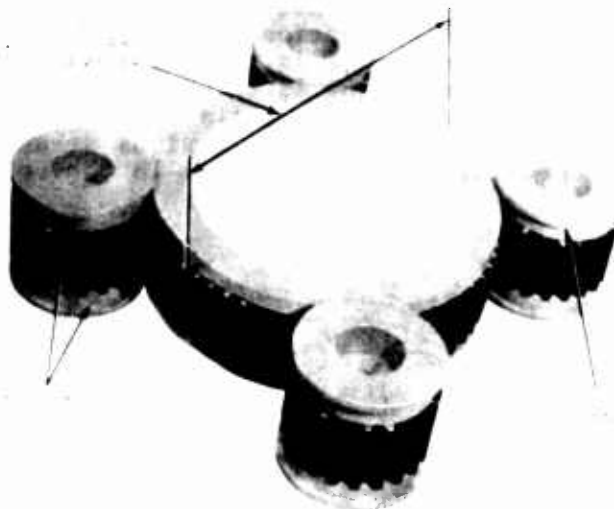


Figure 1. Roller Gear Concept.

To visualize how the rollers and gears are used in the epicyclic arrangement, it is convenient to examine a pure roller friction drive. Figure 2 depicts a simple planetary pure friction drive with sun roller driving, ring roller fixed, and carrier output. In this design, the ring roller is expanded to fit over the pinion-sun assembly giving the unit a preload at each contacting roller point. The maximum tangential load which can be transmitted before slippage occurs is equal to the preload force times the coefficient of friction.
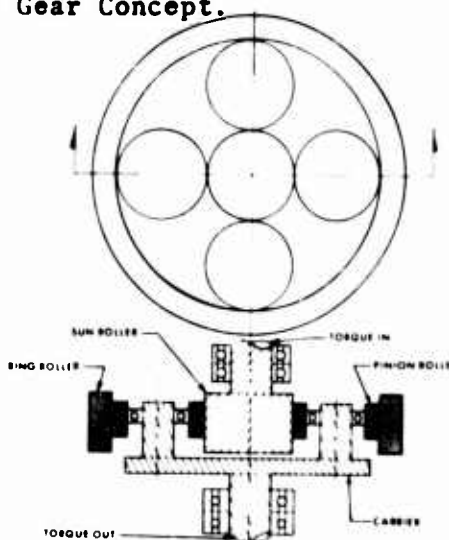


Figure 2. Pure Roller Friction Simple Planetary.

Higher reduction ratios can be obtained by the use of stepped
diameter rollers. This is illustrated in Figure 3 by a two-
row pure friction drive compound planetary with sun roller
driving, carrier output, and ring roller fixed. As in the
simple roller planetary, the ring roller is expanded over the
assembly to provide preload. This friction drive illustrates
the principle of a roller gear drive wherein the first-row
roller is supported at one inner point by the sun roller and
at two outer points by the second-row roller. Bearings are
not required to support the first-row roller since the rollers
serve the dual function of driving and supporting. The roller
gear drive is merely a pure friction drive with gear teeth in
place of the central roller portion of the rollers. Whereas
in the pure roller drive torque is transmitted by friction,
in the roller gear drive torque is transmitted by involute
gears. The teeth transmit torque while the rollers position
the components. A discussion of the various arrangements and
types of roller gear drives is presented in the following
section.
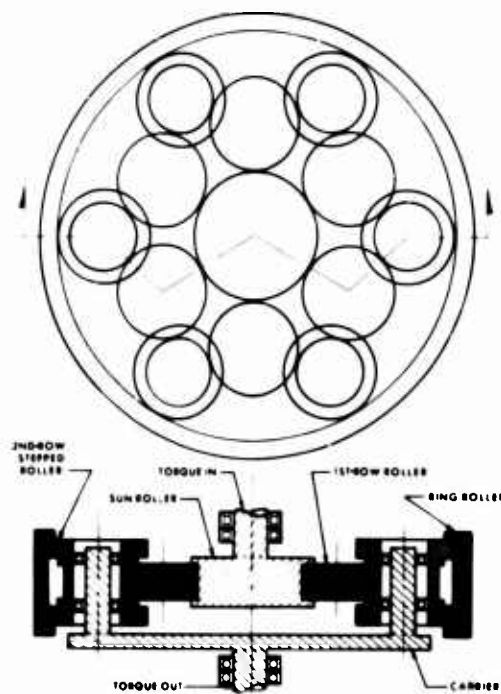


Figure 3.   Pure Roller Friction Compound Planetary.

22

## TYPES AND ARRANGEMENTS OF ROLLER GEAR DRIVES

The roller gear drive can take many forms and arrangements. Each type has its own advantages and disadvantages. Every roller gear drive design must have an input member, an output member and a fixed member. For speed reducing drives, the sun gear, or innermost central gear member, is used as the driving or input member. The driven, or output member, may be either the carrier or the ring gear, and the fixed or stationary member may also be either the carrier or the ring gear. In theory, row upon row of pinions may be added with no limitation. In practice, however, anything over three rows becomes unwieldy because of the large physical size of the last row pinions. Depending on the number of rows and whether the carrier or ring gear is fixed or rotating, the output member of a roller gear drive will rotate in a direction opposite to the input member or in the same direction as the input. With an even number of rows and with the ring fixed and carrier output, the carrier will rotate in a direction opposite to the input, while the opposite is true for ring output and carrier fixed. Conversely, for an odd number of rows and with the ring fixed and carrier output, the carrier will rotate in the same direction as the input, while the opposite is true for ring output and carrier fixed. This latitude leads to a large choice of designs.

The output gear of the roller gear drive may be an internal ring gear or an external output gear, Figure 4. Both designs have their advantages.
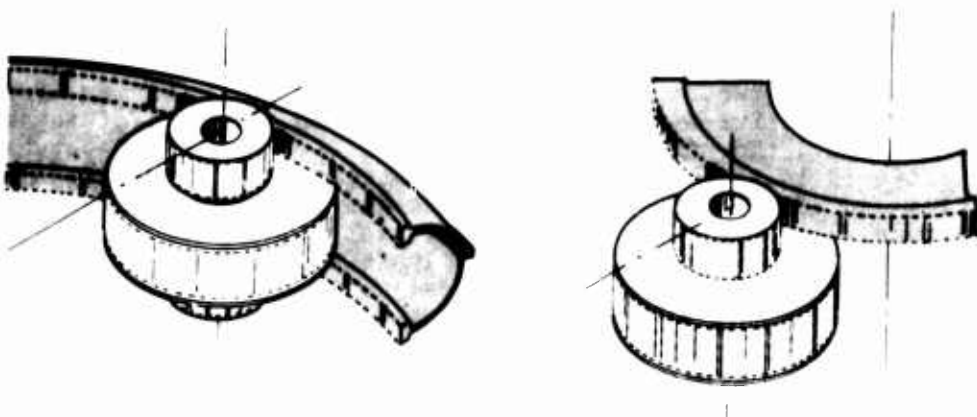


Figure 4.   Output Gear Design.

The ring gear, for example, can be designed as a split gear which straddles the last row pinions (one-half of the ring gear is located on each side of the last row pinion). This arrangement balances moments on the outer-row carrier bearings. With the external output gear, the design cannot be straddle-mounted and the nonsymmetrical arrangement induces a moment on the carrier bearing. The ring gear is located on the outside of the last row pinions, while the external output gear meshes on the inside of the last row pinion. Hence, the internal ring gear is larger, thereby producing higher reduction ratios for the same space envelope. For equal output torque and number of pinions, the tangential tooth load is lower on the larger diameter, internal ring gear. In addition, the axial gear length of the ring gear (face width), and hence weight, are lower. The separating gear forces of the internal ring gear design are in a direction which tends to induce preload on the rollers of the inner member. The separating forces on the rollers of the external output gear are in a direction which tends to unload the rollers of the inner members. Even if preloading devices are used to compensate for this, the loads required will be higher with the external output gear. On the other hand, the manufacturing cost of the external output gear is lower than that for the internal ring gear because it is smaller, has fewer teeth, and is easier to grind than an internal gear. Also, with an external output gear, accessory drives can be conveniently mounted on the outsides of the last row gears. In general, the advantages of the internal ring gear output member far outweigh the advantages of the external gear output member.

## Two-Row, Sun Driving, Ring Output, Carrier Fixed Design

The first specific roller gear drive arrangement to be discussed is the two-row, sun driving, ring output, carrier fixed roller gear drive as shown in Figures 5 and 6. Both of these designs have the same reduction ratio. The difference between the two is in the arrangement of the symmetry of the straddled gears and rollers. In Figure 5, the sun gear has two geared surfaces at either end of the shaft, while in Figure 6, the sun gear has only a single centrally located gear surface. The pinion arrangement for both designs then proceeds radially outward with alternating double and single gear members.

In any roller gear drive it is generally impossible to assemble the unit by starting at the outside and assembling inward. The only feasible way is to design a removable roller on the sun gear and a removable roller on the opposite side of the first-row pinion. Even for this case, care must be taken that the first-row pinion removable roller is not "trapped" by the second-row gears. Thus, in the design of
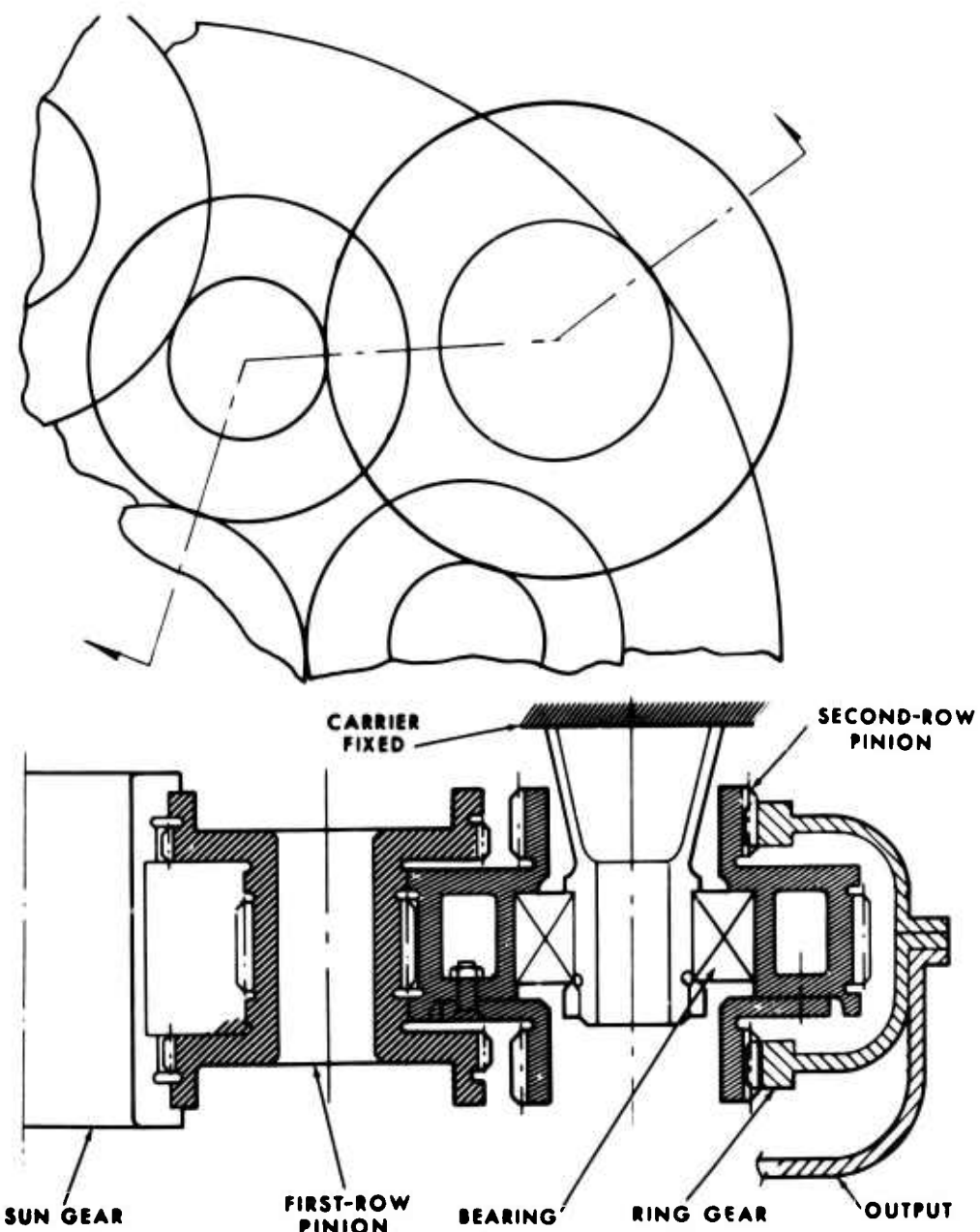
Figure 5. Two-Row, Double Sun Gear, Ring
Output Roller Gear Drive.

The labels in the figure are:
CARRIER FIXED, SECOND-ROW PINION, SUN GEAR, FIRST-ROW PINION, BEARING, RING GEAR, OUTPUT
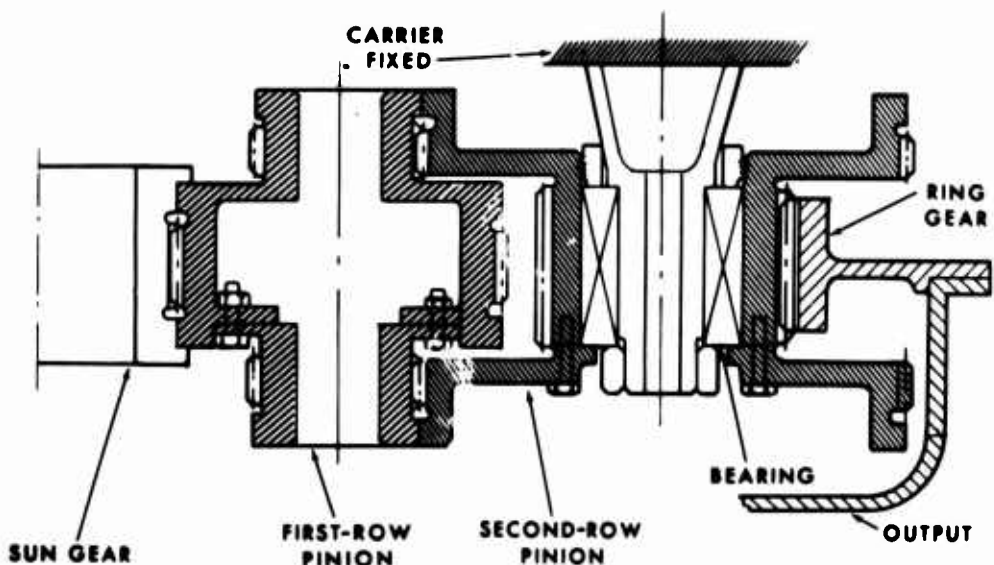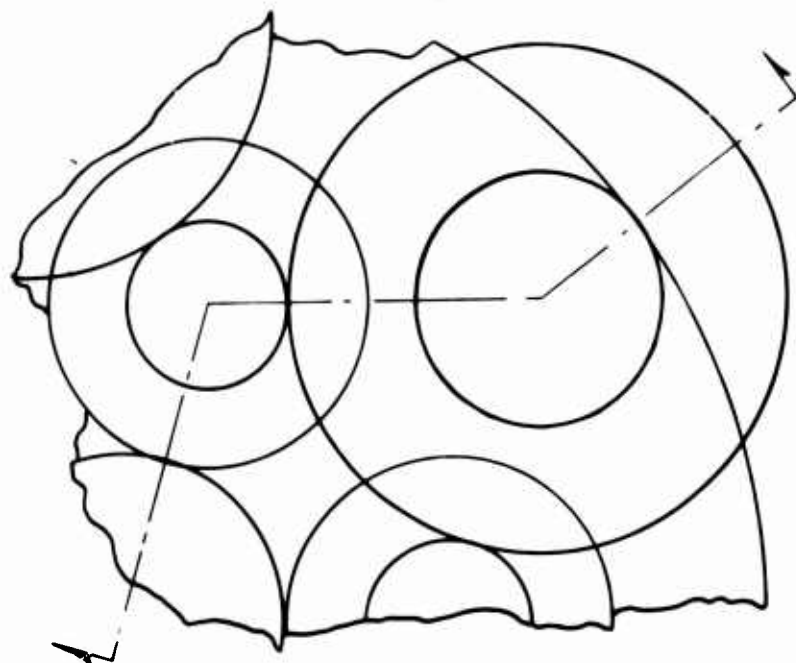
Figure 6.   Two-Row, Single Sun Gear, Ring Output
Roller Gear Drive.

26

Figure 6, with a single ring gear, the larger outer-row
gear must be removable so as not to "trap" the ring gear.
For this reason, the design of Figure 5 is preferable over
the design of Figure 6.

Note that both designs utilize stepped pinions with two
identical outer gear surfaces straddling the central gear
member. The teeth of the two identical outer gears must be
aligned parallel to each other and to the gear axis of
rotation in order to share the load equally. When the two
identical gears are larger in diameter than the central gear,
they can be machined together to provide alignment, but when
the two outer identical gears are smaller than the inner gear,
other methods must be used. If the gears are welded, such as
by electron beam welding or other processes, the original
angular location prior to welding may shift or creep during
the welding process. Alignment by final machining after
welding nullifies this problem; however, this is not always
possible and alignment by dowels, bolts or other positive
connections is required.

## Two-Row, Sun Driving, Ring Fixed, Carrier Output Design

The two-row, sun driving, ring fixed, carrier output is
similar in design to the two-row ring output, but has the
direction of rotation of the carrier opposite to the sun gear.
This design is shown with a double sun gear in Figure 7 and
with a single sun gear in Figure 8. Both designs have
identical reduction ratios and differ only in arrangement of
the straddled gear and roller members. In Figure 8, it is
seen that the second-row pinion must be split into two seg-
ments to permit assembly of the ring gear. The design of
Figure 7, which allows the ring gear to be assembled after
the sun gear, first-row pinion and second-row pinion is
preferable.

## Three-Row Design

Another family of roller gear drives can be designed with
three rows. The assembly problems associated with the two-
row drives, discussed above, also pertain to three-row drives.
In this instance, the preferable designs for three-row drives
start with a single sun gear and alternate with single and
double meshes radially outward to a split double ring gear.
The double ring gear is assembled last. Figure 9 depicts a
three-row drive with ring gear output, while Figure 10 shows
a three-row drive with carrier output. A ring gear output
drive rotates in a direction opposite to that of the sun
gear, whereas the carrier output drive rotates in the same
direction as the sun gear. Both of the three-row designs
shown are with a single sun gear.
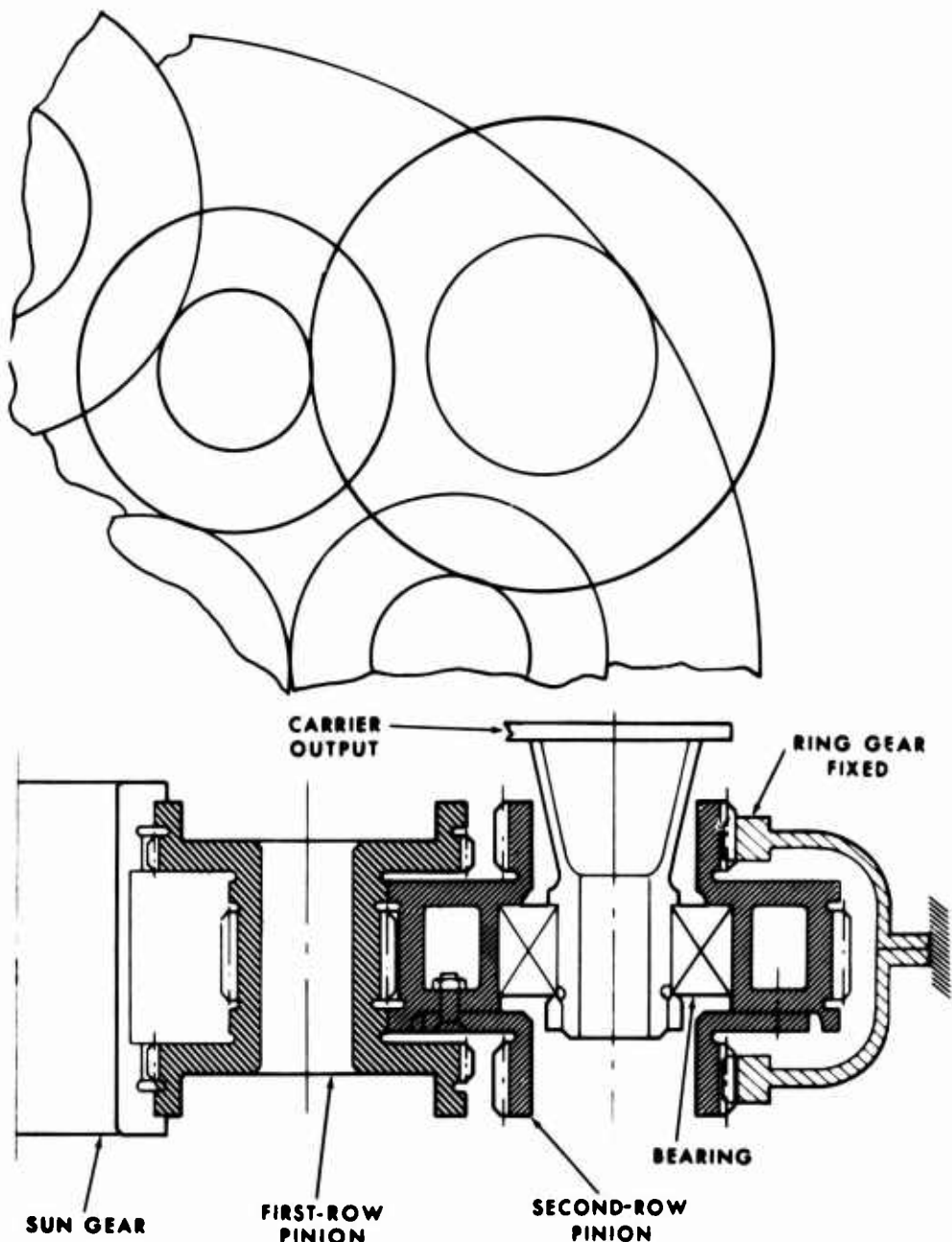
Figure 7.   Two-Row, Double Sun Gear, Carrier
Output  Roller Gear Drive.

Labels in figure:
CARRIER OUTPUT
RING GEAR FIXED
BEARING
SUN GEAR
FIRST-ROW PINION
SECOND-ROW PINION
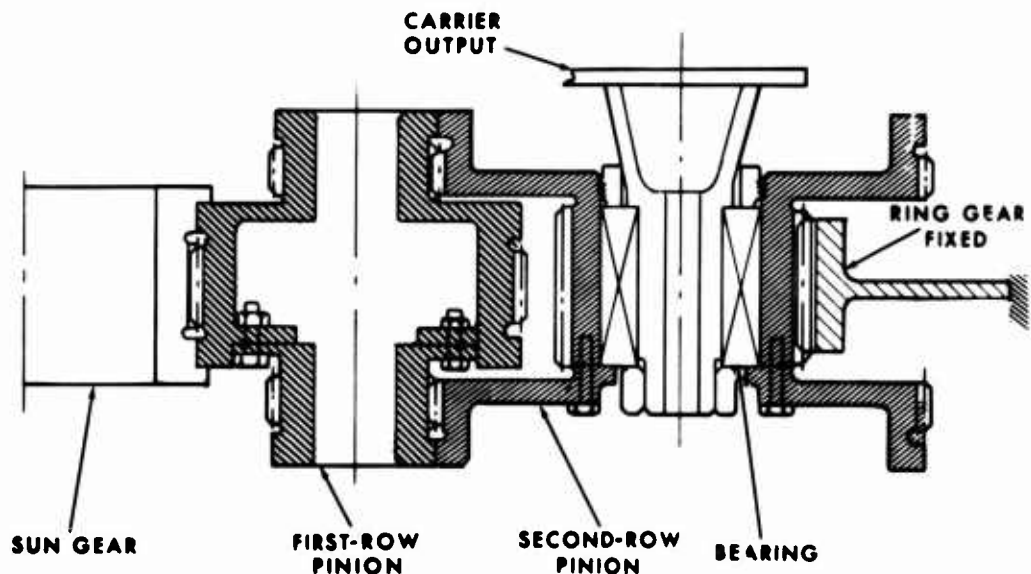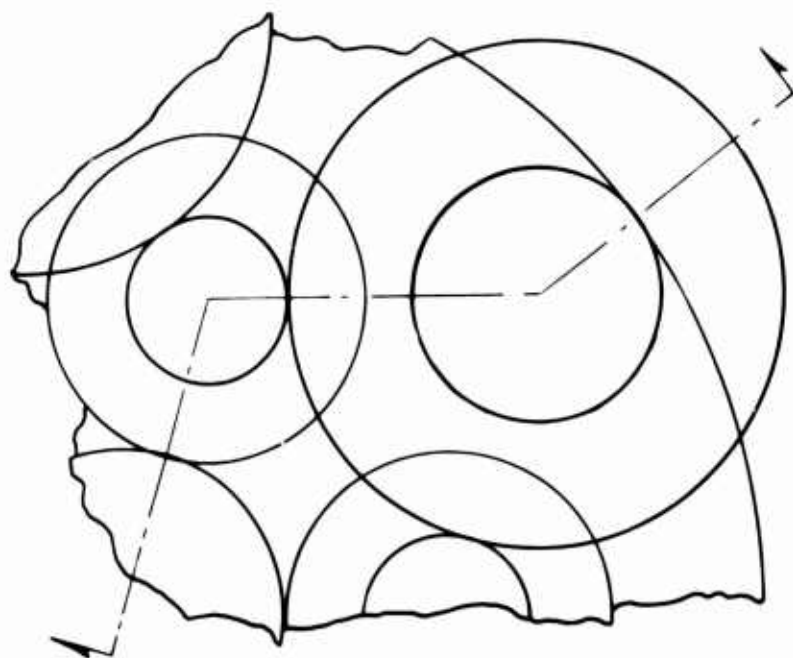
Figure 8.  Two-Row, Single Sun Gear, Carrier
Output  Roller Gear Drive.

29
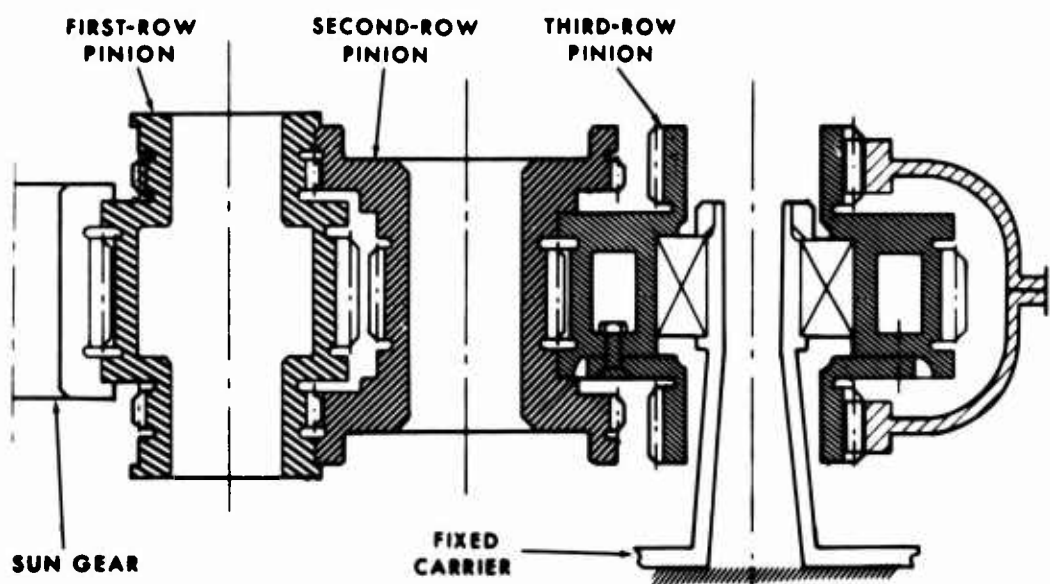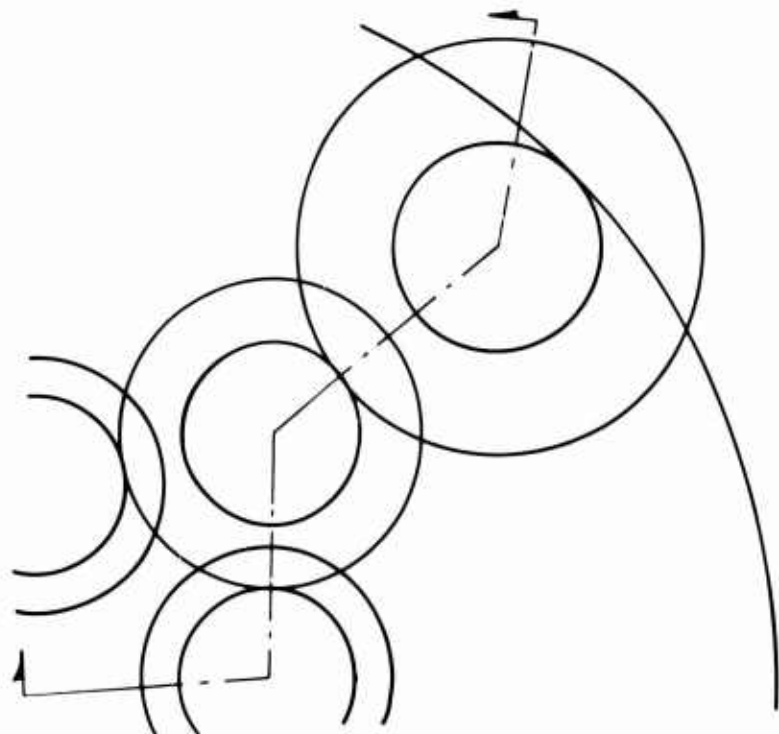
Figure 9. Three-Row, Single Sun Gear, Ring
Output Roller Gear Drive.

30
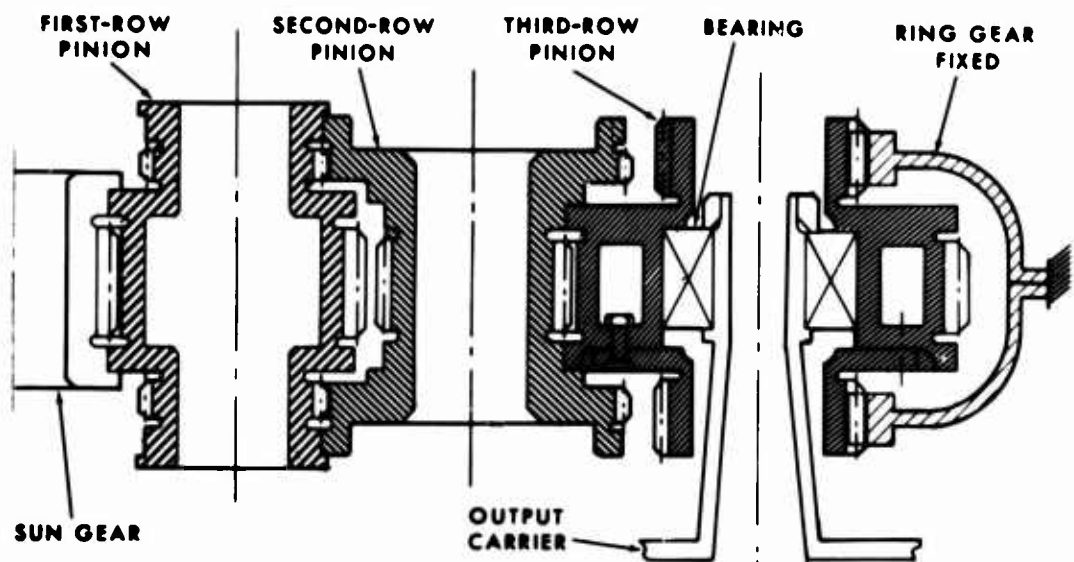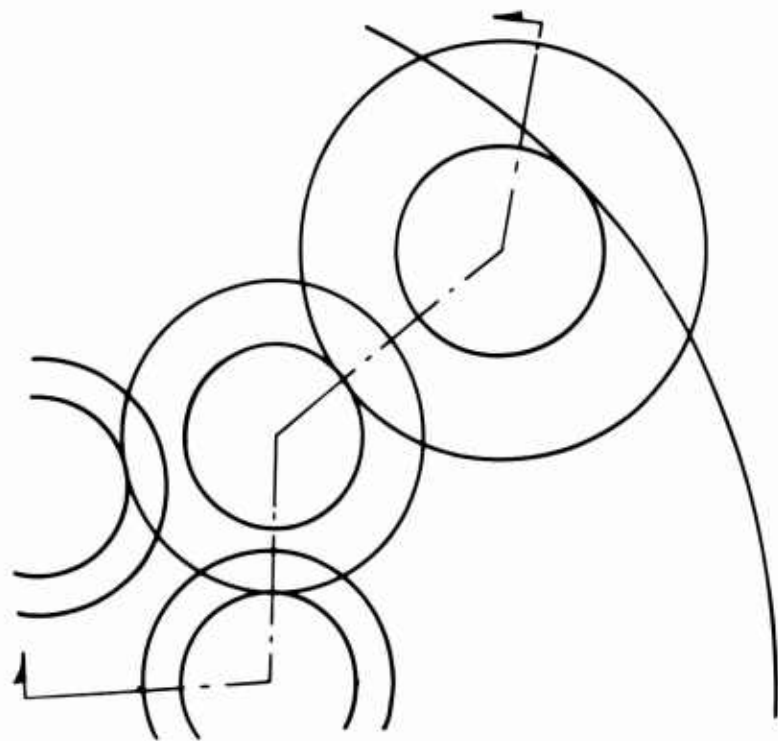
Figure 10.  Three-Row, Single Sun Gear, Carrier
Output  Roller Gear Drive.

31

A derivative of the three-row design is shown in Figure 11 where the last row is used as an idler and does not contain stepped pinions. This type of roller gear design can be used with carrier output, as shown, or with ring gear output for the opposite direction of rotation. Although this design loses some reduction ratio, it is attractive because its larger outer gear offers more space for a carrier output bearing.

## Staggered Gear Design

The last type of roller gear design to be discussed is the staggered gear concept. In all previous designs, clearance must be provided between pinions of adjacent gears in the same row. These gears may be designed to overlap with the staggered design shown in Figure 12. Since the gear diameters are larger, a higher reduction ratio can be obtained in the same envelope. The sun gear must be designed with two sets of teeth and rollers to mate with the staggered gears. An even number of pinions must be used with this arrangement.

## Multiple Row Design

Designs with four or more rows are feasible, but have not been included. The general arrangements are similar to the two- and three-row designs. As the number of rows increases, the diameter of the outer-row pinion must grow to fill the available space. For all practical purposes, sufficient ratio can generally be obtained in two or three rows with a reduction ratio of greater than 200:1 possible for a three-row drive.
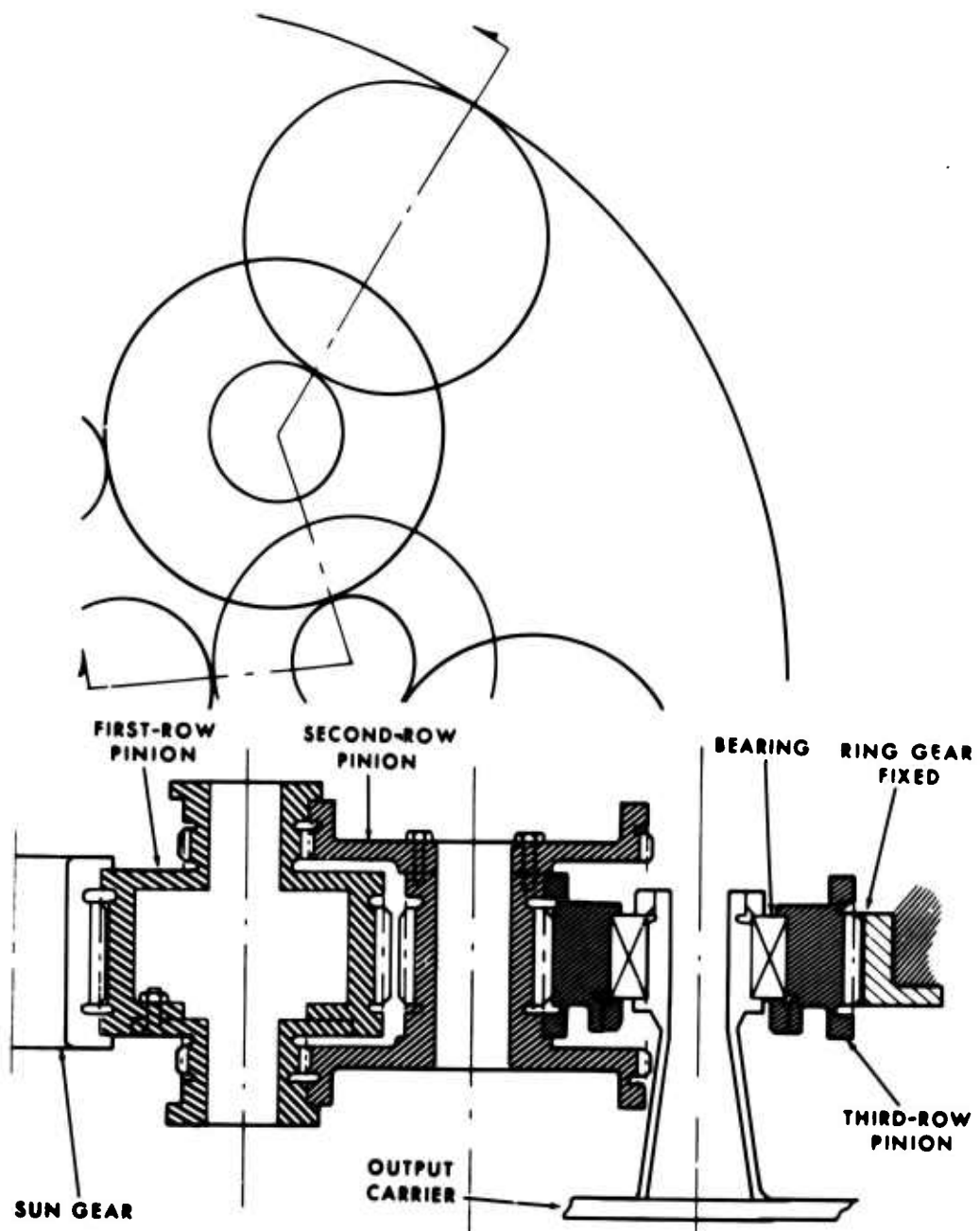
Figure 11. Three-Row, Single Sun Gear, Carrier Output, Single Last Row Gear, Roller Gear Drive.

33

SUN GEAR   STAGGERED FIRST-   SECOND-ROW   FIXED
           ROW PINION          PINION       CARRIER

                                            RING GEAR
                                            OUTPUT

FIRST-ROW
PINION

BEARING
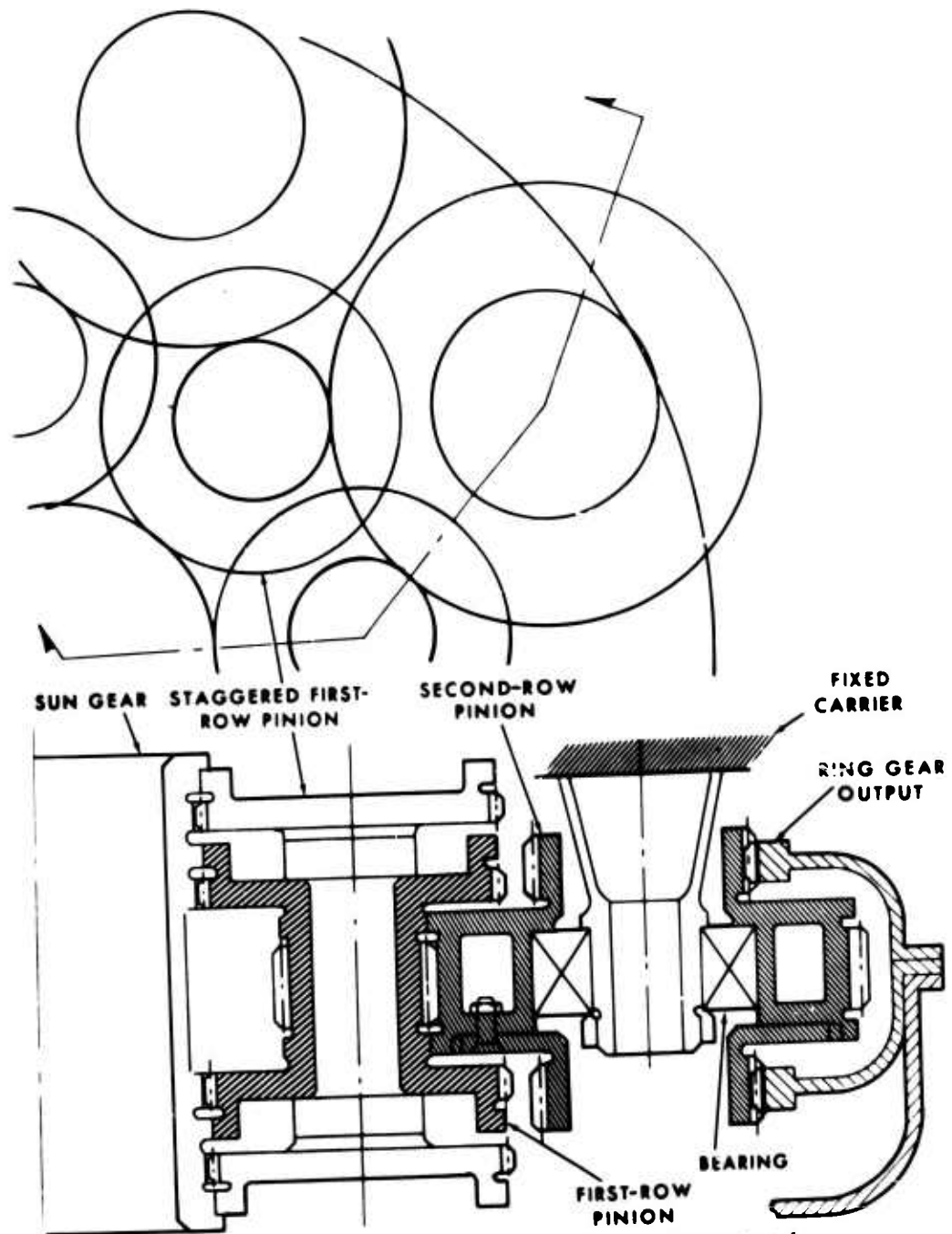
Figure 12.   Two-Row, Double Sun Gear, Staggered
First-Row Gears, Roller Gear Drive.

34

## APPROACH

### AIRCRAFT SELECTION

The roller gear drive was designed for a growth version of
Sikorsky Aircraft's S-61 helicopter. This type helicopter is
a single rotary-wing, twin turbine powered aircraft with a
single torque compensating tail rotor. The basic S-61 heli-
copter, Figure 13, has a gross weight of 21,000 pounds, and is
powered by two General Electric T58 engines, each developing
1,250 hp at 30 minutes rating.

The two turbine engines are mounted side-by-side; engine
driveshafts transmit power directly into the aft positioned
main gearbox. The rotary-wing assembly, to which five rotary
wing blades are attached, is splined to the main gearbox out-
put driveshaft. Shafting extends aft from the main gearbox
rear housing to the intermediate and tail gearboxes to drive
the tail rotor. A summary description of the S-61 aircraft
power system requirement is given in Table 1.

| TABLE 1.   S-61 AIRCRAFT DESCRIPTION. | |
|---|---|
| Helicopter Type: | S-61 |
| Engine Manufacturer: | General Electric |
| Engine Type (2): | T58-GE-8B |
| 30 Minute Rating | 2,500 hp |
| Maximum Continuous Rating | 2,100 hp |
| Main Gearbox Ratio: | 93.5:1 |
| Input Speed | 18,966 rpm |
| Main Rotor Speed | 203 rpm |
| Main Rotor Power | 2,100 hp |

Incorporating the latest version of the T58 series engine, the
YT58-GE-16, into a growth version of the S-61 helicopter will
raise the total power rating from 2,500 hp to 3,740 hp. This
will permit a roller gear drive transmission to transmit 3,000
hp to the main rotary-wing assembly.

### PROGRAM OUTLINE

After selecting the S-61 helicopter as the test bed for the
roller gear drive, preliminary studies of the main transmission
configuration were begun. Engine speeds and locations were
investigated and the gearbox input-output locations and reduc-
tion ratios determined. Several transmission configurations
were chosen for further study, and preliminary layouts were
made for the configurations selected.

Figure 13.   Sikorsky S-61 Type Helicopter.

For each preliminary main transmission configuration, various roller gear drive concepts were investigated to determine their relative advantages and disadvantages. The reduction ratio and space requirements were determined for each roller gear transmission combination. Preliminary layouts of the roller gear drive configurations were made, considering fabrication methods, bearing arrangements and manufacturing problems.

Upon completion of the preliminary design phase, a design review was conducted with the Eustis Directorate personnel and a final roller gear transmission configuration was selected. Detail layouts and casting drawings of the selected configuration were drawn concurrently because of the long lead time for the main casting.

Detail design and analysis commenced after the roller gear drive and main transmission configuration layout was completed. During the detail design phase of the program, liaison was maintained with manufacturing in the areas of fabrication of the roller gear components, gear timing and manufacturing tolerances which were all undeveloped at the time.

Upon completion of the detail design phase, the manufacture of the individual components commenced. A survey of the manufacturing methods used is given in Reference 6. While the parts were being manufactured, all necessary aircraft modifications were made. The modifications included installation of YT58-GE-16 engines, new forward engine mounts, new oil cooler and a new rotor control system.

After assembly of the main transmission, a series of tests was planned which, when completed, would provide the necessary information for a thorough evaluation of the roller gear transmission.

TEST PROGRAM

The test program encompassed bench tests, aircraft tiedown tests and reliability and maintainability tests.

The bench test program is designed to develop and debug the roller gear transmission and demonstrate that all catastrophic modes of failure are out of the planned operating range, and demonstrate that noncatastrophic modes are detectable. Upon the successful completion of the bench test program, an aircraft tiedown test is to be conducted to evaluate the compatibility of the roller gear transmission as the main transmission system in a helicopter. Finally, a 1,000-hour reliability and maintainability test is to be conducted to

6   G. F. Gardner and R. R. Cormier, ROLLER GEAR MANUFACTURE, 3000-HP ROLLER GEAR TRANSMISSION DEVELOPMENT PROGRAM, VOLUME III, USAAMRDL Technical Report 73-98C, USAAMRDL, Fort Eustis, Virginia, July 1975.

determine the long-term dynamic characteristics of the roller gear unit. At the conclusion of this test, overload stress condition tests will determine the mode of failure of the roller gear unit.

An outline of this program is shown in Figure 14. The following summarizes highlights of the objective of each test.

BENCH TESTS

No-Load Lubrication Test

No-load lubrication tests determine the optimum lubrication parameters. The factors under evaluation are the amount of lubricant and jet sizes required to provide adequate transfer of heat from the dynamic components of the gearbox while minimizing frictional losses caused by oil churning. In addition, the test is intended to locate and eliminate any lubricant flow problems which might be encountered such as restrictive oil paths, improper drainage, etc.

Gear Pattern Development Test

The second phase of bench testing to be performed includes gear pattern development tests to evaluate gear patterns generated when the gearbox operates under load. Examination of these gear patterns provides verification of the manufacture of the gears and the proper loading and alignment of gears and bearings.

Initial Development Test

Initial development testing provides data for evaluation of the manufacturing methods of the roller gear components. Since this program marked the first time electron-beam-welded gears were to be used extensively in a helicopter transmission, the initial development testing was considered necessary to check the endurance capabilities of these gears before the start of a 200-hour endurance test.

200-Hour Endurance Test

A 200-hour endurance test is designed to evaluate the effects on the roller gear transmission of long-term operation in a fatigue environment.

Efficiency Test

Coincident with the 200-hour endurance test, an efficiency test is to be conducted. The objective of this test is to accurately determine the efficiency of the roller gear drive transmission by means of heat loss calculation.

38
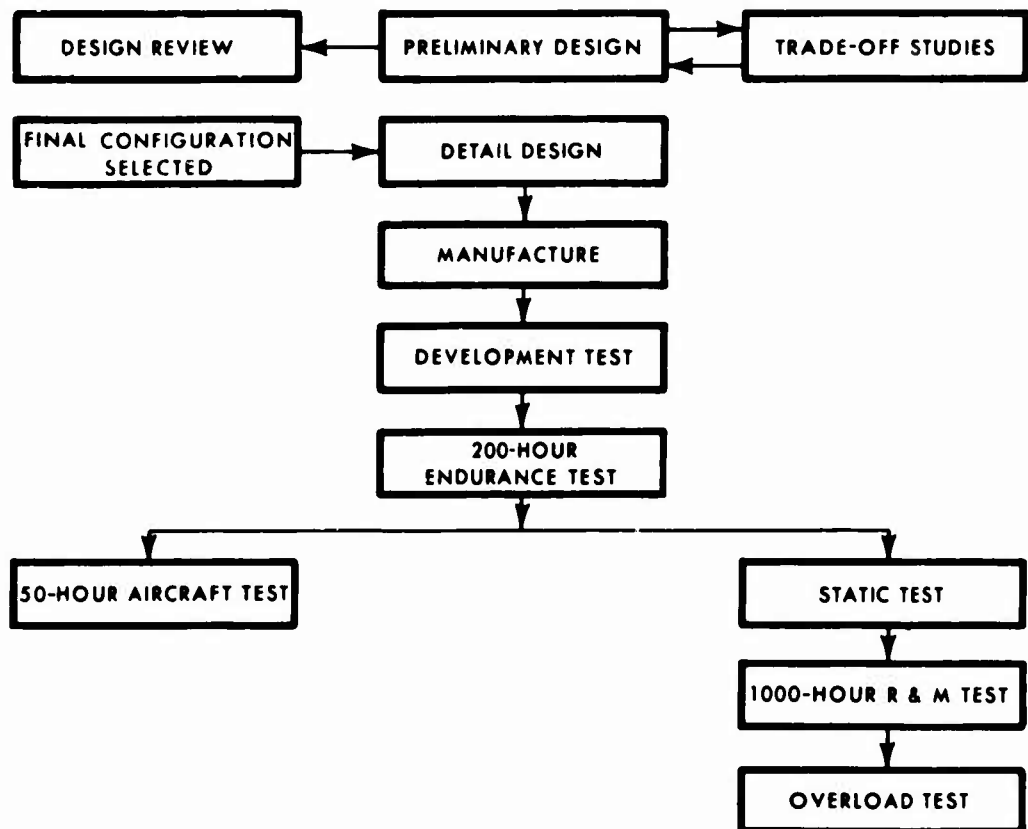
Figure 14.   Roller Gear Program - Flow Chart.

A report of the Bench Test Program is given in Reference 7.

AIRCRAFT TIEDOWN TEST

Upon the completion of the bench test phase of the program, an aircraft tiedown test program was planned. The primary purpose of this test is to evaluate the roller gear transmission in an aircraft installation during a 50-hour dynamic test.

This test phase of the program is documented in Reference 8.

1000-HOUR RELIABILITY AND MAINTAINABILITY TEST

This test is to establish failure modes and rates and subsequently the life characteristics of the roller gear drive. At the completion of the 1000-hour test, a series of overload tests are to be conducted to determine the mode of failure of the roller gear drive.

Prior to the commencement of a 1000-hour reliability and maintainability test, a static load equivalent to the maximum transmitted power is to be applied to a roller gear transmission instrumented to measure strains in the ring gear, output flange, second-row pinion rollers and posts. Determination of these stresses will enable an evaluation of the load-sharing characteristics of the roller gear unit to be made.

7  G. F. Gardner and R. E. Haven, LABORATORY BENCH TEST REPORT, VOLUME IV, 3000-HP ROLLER GEAR TRANSMISSION DEVELOPMENT PROGRAM, USAAMRDL Technical Report 73-98D, USAAMRDL, Fort Eustis, Virginia, May 1974.

8  G. F. Gardner and D. O. Adams, AIRCRAFT TIEDOWN TESTING, VOLUME V, 3000-HP ROLLER GEAR TRANSMISSION DEVELOPMENT PROGRAM, USAAMRDL Technical Report 73-98E, USAAMRDL, Fort Eustis, Virginia, 1975.

## DESIGN REQUIREMENTS

With the selection of the S-61 helicopter as the test aircraft, and the twin YT58-GE-16 engines as the power plant, required transmission speed and power characteristics were established. A 32-inch center distance between engines (i.e., butt line 16) and a 200 waterline was chosen as the location for the engines, thereby dictating the position of the transmission inputs. The location of the main rotor head remained the same as the production S-61 helicopter. The accessory power takeoff requirements of the roller gear transmission were kept identical to the S-61 accessory drives. Figure 15 shows the aircraft general arrangement. Table 2 lists the speed and maximum horsepower design requirements for the roller gear main transmission.

| Location | Speed (rpm) | Power (hp max) |
|---|---|---|
| TABLE 2. S-61 ROLLER GEAR TRANSMISSION DESIGN REQUIREMENTS. | | |
| Input Drives: | | |
| Dual Engine | 18,966 | 3,700 |
| Single Engine | 18,966 | 1,870 |
| Main Rotor: | 203 | 3,000 |
| Tail Takeoff and Accessories (Total) | 7,031 | 700 |
| Tail Rotor Takeoff: | 3,026 | 565 |
| Accessory Drives: | | |
| Generator (Two) | 8,100 | 54 |
| Tach Generator | 3,900 | 1 |
| Servo Hyd Pump | 4,197 | 6.5 |
| Aux Servo Hyd Pump | 4,005 | 6.5 |
| Utility Hyd Pump | 4,005 | 13.0 |
| Lubrication Pump | 5,149 | 4.0 |

The transmission components are designed for infinite life and bearings for 3,000 hours B.10 life minimum at the power and speeds listed in Table 2. Accessory drives were required to be located on the rear cover of the main transmission. With this basic preliminary data, configuration studies of the roller gear drive and main transmission were initiated.
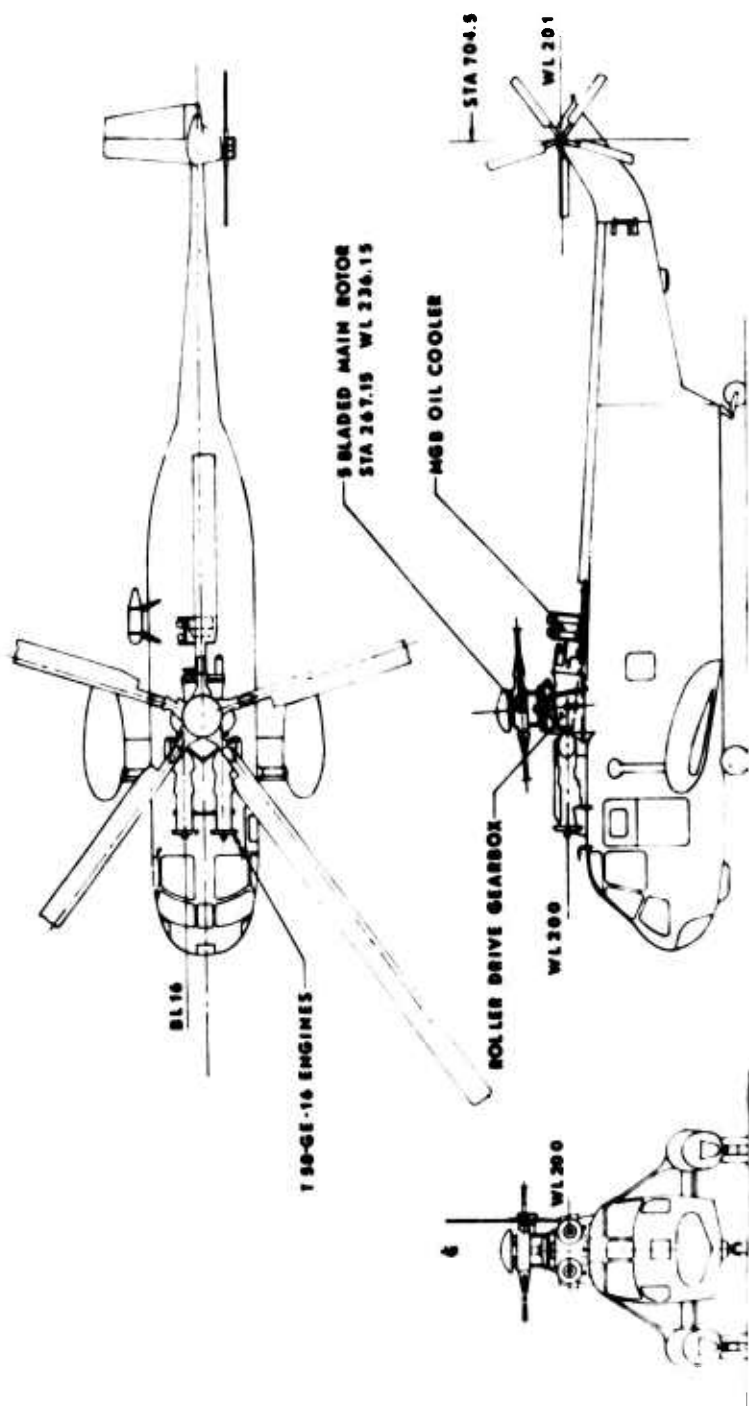
Figure 15. S-61 Roller Gear Aircraft.

5 BLADED MAIN ROTOR
STA 267.15   WL 236.15

MGB OIL COOLER

ROLLER DRIVE GEARBOX

WL 200

BL 16

T 58-GE-16 ENGINES

STA 704.5

WL 201

WL 200

42

## ENVELOPE, ROTATION AND RATIO RESTRICTIONS

The design of the roller gear drive transmission was dictated
by the physical geometry and characteristics of the S-61
helicopter. The YT58-GE-16 engines have an output speed of
18,966 rpm and develop 1,870 hp per engine. Since the S-61
was designed for a main rotor speed of 203 rpm, an overall
reduction ratio of the main transmission system of 93.4:1 was
required.

The production version of the S-61 helicopter main trans-
mission has four reduction stages, Figure 16. The first stage
is a spur gear reduction which drives through a freewheel unit
to a second-stage combining helical gear mesh. The third
stage is a spiral bevel mesh with the driven gear concentric
with the main rotor shaft. The driven gear of the spiral
bevel mesh drives the tail takeoff as well as the fourth
reduction stage, a single-stage planetary. The planetary is
of the single row type with sun gear input, carrier output,
and ring gear fixed. The carrier drives the main rotor shaft.
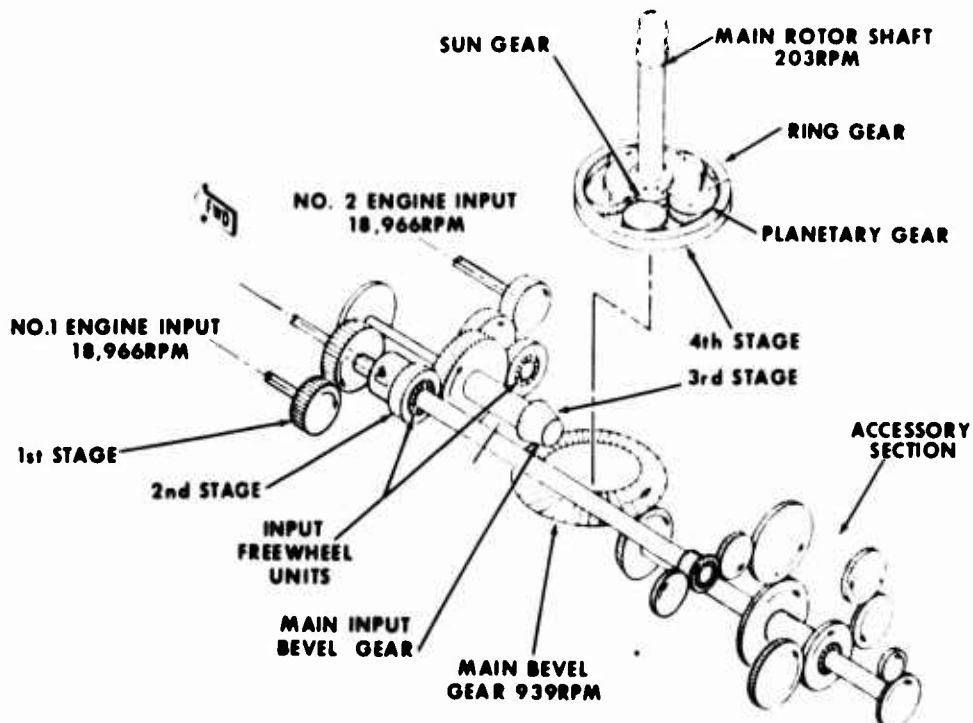
Figure 16.   S-61 Main Transmission Schematic.

With the location of the engines and the overall reduction ratio established, the number of reduction stages needed to deliver power from the engines to the main rotor shaft was examined. With a high reduction ratio obtainable from a roller gear unit, three configurations were examined which would deliver the power in three stages rather than the present four stages of the S-61. In general, the fewer the stages, the lighter the weight.

TRANSMISSION LAYOUT ARRANGEMENTS

Dual High-Speed Bevel Gear Inputs

The first design, Figure 17, employs a spiral bevel pinion driven by the engine to a spiral bevel gear whose shaft is parallel to the main rotor shaft. The spiral bevel gear drives through a freewheel unit to the second reduction stage which is a combining spur gear mesh. The driven gear of the combining mesh is concentric with the main rotor shaft and drives both the tail takeoff and the final reduction stage. The final stage is a roller gear planetary reduction unit with output to the main rotor shaft.
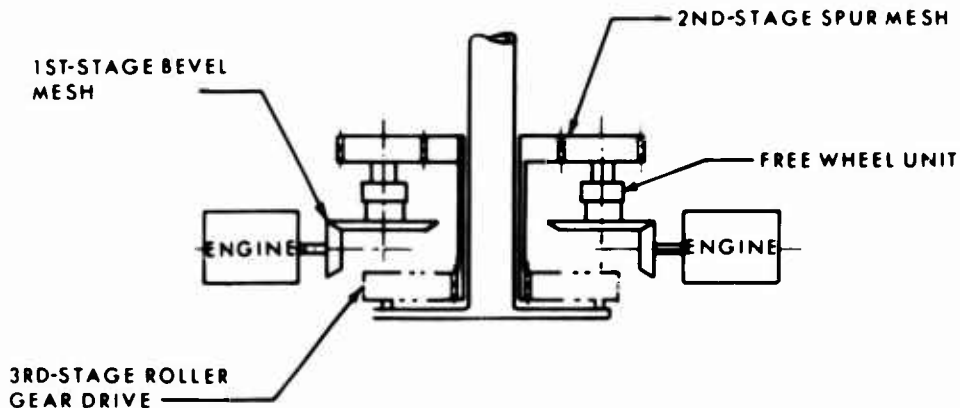
Figure 17. Dual High-Speed Bevel Gear Input Schematic.

## Dual High-Speed Crossed Helical Gear Inputs

The second configuration considered is shown in Figure 18. The first stage of this system is a crossed helical mesh which allows the wide engine centerline displacement required by the YT58-GE-16 engines. The driven helical gear transmits power through a freewheel unit to the second-stage combining spiral bevel mesh. The driven gear of the spiral bevel mesh is concentric with the main rotor shaft and drives both the tail takeoff and the third-stage roller gear reduction unit. This possibility was rejected because crossed helical gears are inefficient and are not recommended for high power and high torque applications[9].
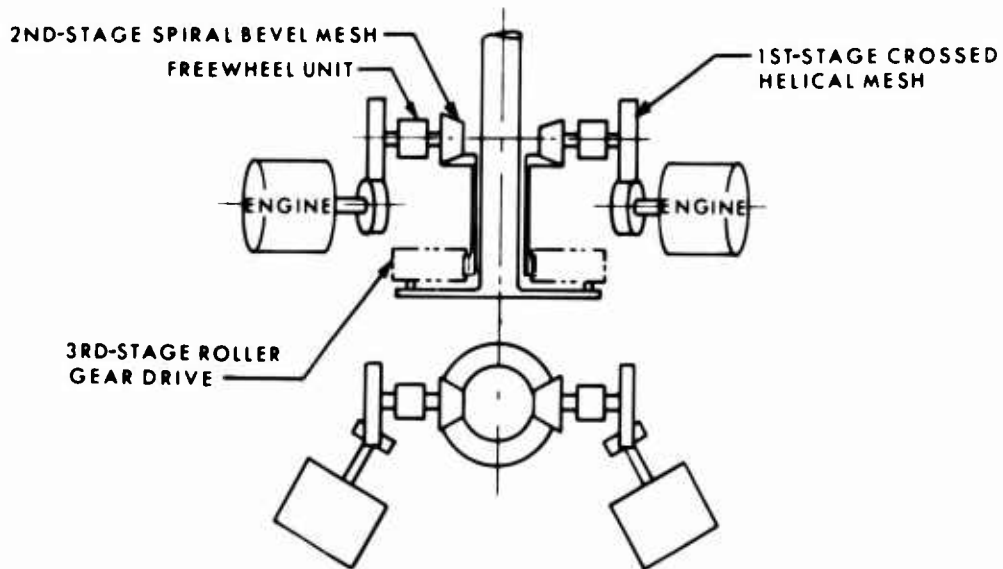
Figure 18.   Dual High-Speed Cross Helical Gear Input   Schematic.

9   J. E. Shigley, MECHANICAL ENGINEERING DESIGN, McGraw Hill Book Company, 1963, p. 449-451.

## Dual High-Speed Spur Gear Inputs

The third possibility is shown schematically in Figure 19.
In this configuration, the engine drives through a freewheel
unit to the first-stage combining spur gear mesh. The output
gear of the spur gear mesh in turn drives a single spiral
bevel mesh which turns the corner and aligns the shafting
parallel to the main rotor shaft. The driven gear of the
spiral bevel mesh drives the tail takeoff and the last stage
roller gear reduction unit. This design was rejected for two
reasons. First, during 1970 when the design was being formu-
lated, freewheel units were not developed to operate at the
high output speed of the YT58-GE-16 engines, and second, the
input spur gear mesh would require large gears due to the
engine spacing. These gears would have very high pitch line
velocities and a low power to weight ratio.
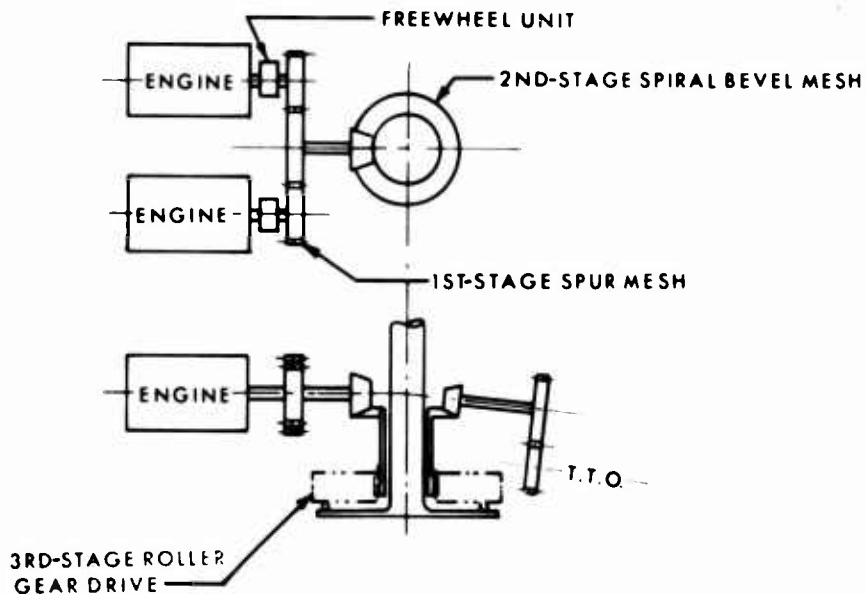
Figure 19. Dual High-Speed Spur Gear Input
Schematic.

46

Having eliminated the designs shown in Figures 18 and 19, the
configuration of Figure 17 was examined in greater depth.
Four possible layout variations of this configuration evolved.
The first-stage spiral bevel gear can be above or below the
bevel pinion and the second and third stages can be inter-
changed, Figure 20.
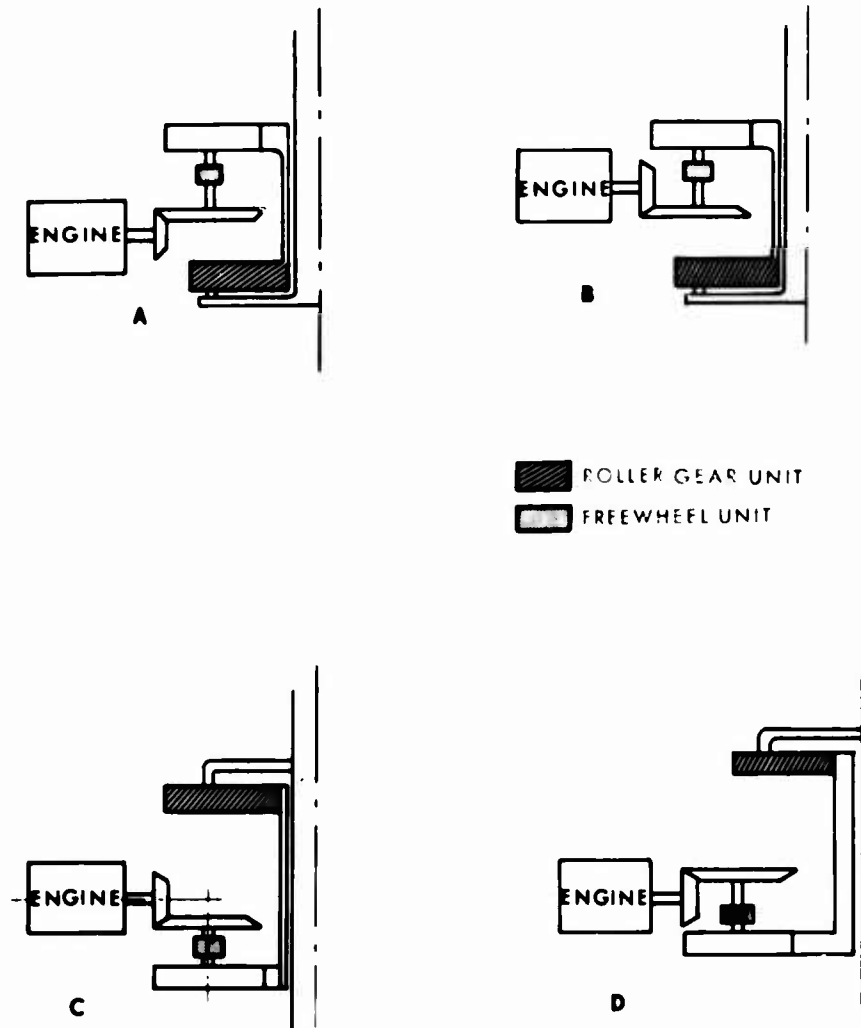


Figure 20.   High-Speed Bevel Gear Input Arrangement.

Before beginning layouts of these configurations, some limits were established for the transmission envelope. Since the main rotor shaft must pass through the center of the sun gear, the minimum possible diameter was set at 8.0 inches. The maximum ring gear diameter was established as 31.0 inches because of the size limitation of the quench press used during case hardening of the gear teeth. The roller gear drive design parameters which were established are listed in Table 3.

TABLE 3. ROLLER GEAR DRIVE DESIGN PARAMETERS.

| | |
|---|---|
| Minimum Sun Gear Diameter | 8.00 in |
| Maximum Ring Gear Diameter | 31.00 in |
| Output rpm | 203 |
| Input rpm | 4,000 - 5,00^ |
| Reduction Ratio (approximately) | 20:1 |
| Gear Allowable Compressive Stress* | 130,000 psi |
| Gear Allowable Bending Stress (one way) | 55,000 psi |
| Minimum Bearing Life (B.10 life) | 3,000 hr |
| Roller Allowable Compressive Stress | 150,000 psi |

\* Using AGMA calculation method

Preliminary layouts of the four possible candidate main transmission configurations show that with the roller gear unit located on top of the transmission (Figure 20, views C&D) the main housing was a poor design. First the housing would have had to be larger on top than on the bottom, which is inherently unstable; secondly, the larger diameter roller gear unit does not permit the main rotor servos to be mounted close to the rotor head. These two configurations were therefore eliminated.

This left two possible design configurations for the roller gear transmission, views A & B of Figure 20. The directions of rotation of these two possibilities are opposite to each other and thus affect the design of the roller gear drive. With the bevel gear on the bottom, Figure 20 B, the roller gear unit would have to be located lower in the main housing because room is required for the driven bevel gear bearings. This would require the main transmission to have greater overall height and increased weight. Thus, this design variation was eliminated and the final configuration of Figure 20, view A, selected. In this configuration, the roller gear input rotation is the same direction as the output rotation. This design decision eliminated 50 percent of all possible roller gear planetary designs since it determined input and output direction of rotation.

48

In general, the lightest transmission will result when the highest possible reduction ratio is located in the final reduction stage. Therefore, the earlier reduction stages should be as low as possible. With a roller gear drive reduction ratio of about 20:1, a combined 4.6:1 reduction ratio is required at the spur gear and spiral bevel gear meshes in order to obtain an overall ratio of 93.4:1.

For the teeth of the spiral bevel gears to be strong enough to transmit the design power, the face width of the bevel gears should be a maximum of 30 percent of the outer cone distance. When the face width is greater, the teeth become pointed on the toe of the gear. When a spiral bevel gear mesh is designed for the demanding conditions of the YT58-GE-16 engines, 3:1 is about the minimum ratio which will allow bevel gear stresses, scoring index, and pitch line velocity to remain within the state-of-the-art of spiral bevel gear capabilities.

The ratio of the combining spur gear was limited by envelope geometry and gear size to approximately 1.5:1.

With the envelope, direction of rotation, speed, power and reduction ratio of the roller gear drive unit known, work was initiated on possible candidate roller gear drive designs.

# ROLLER GEAR DRIVE, PRELIMINARY DESIGN

## DRIVE CONFIGURATIONS

Because of the limitations previously described, the roller gear drive was narrowed to four configurations:

 (1) Two-row, ring output, carrier fixed

 (2) Three-row, carrier output, ring fixed

 (3) Three-row, carrier output, no stepped gear in outer row

 (4) Two-row, ring output, carrier fixed, staggered first-row pinions.

These are shown schematically in Figure 21.

Within each candidate design, many design variants are possible. Roller and gear attachment methods, materials, tolerances, manufacturing methods to achieve gear timing, assembly order and ease of assembly, stresses, deflections, slopes, weight, envelope size, lubrication, reliability and tooth spacing relationships must all be considered when developing the layout designs of the roller gear drive. The preliminary layouts of these candidate roller gear drives, advantages and disadvantages, and selection of the final design are discussed in the "Roller Gear Drive Selection".
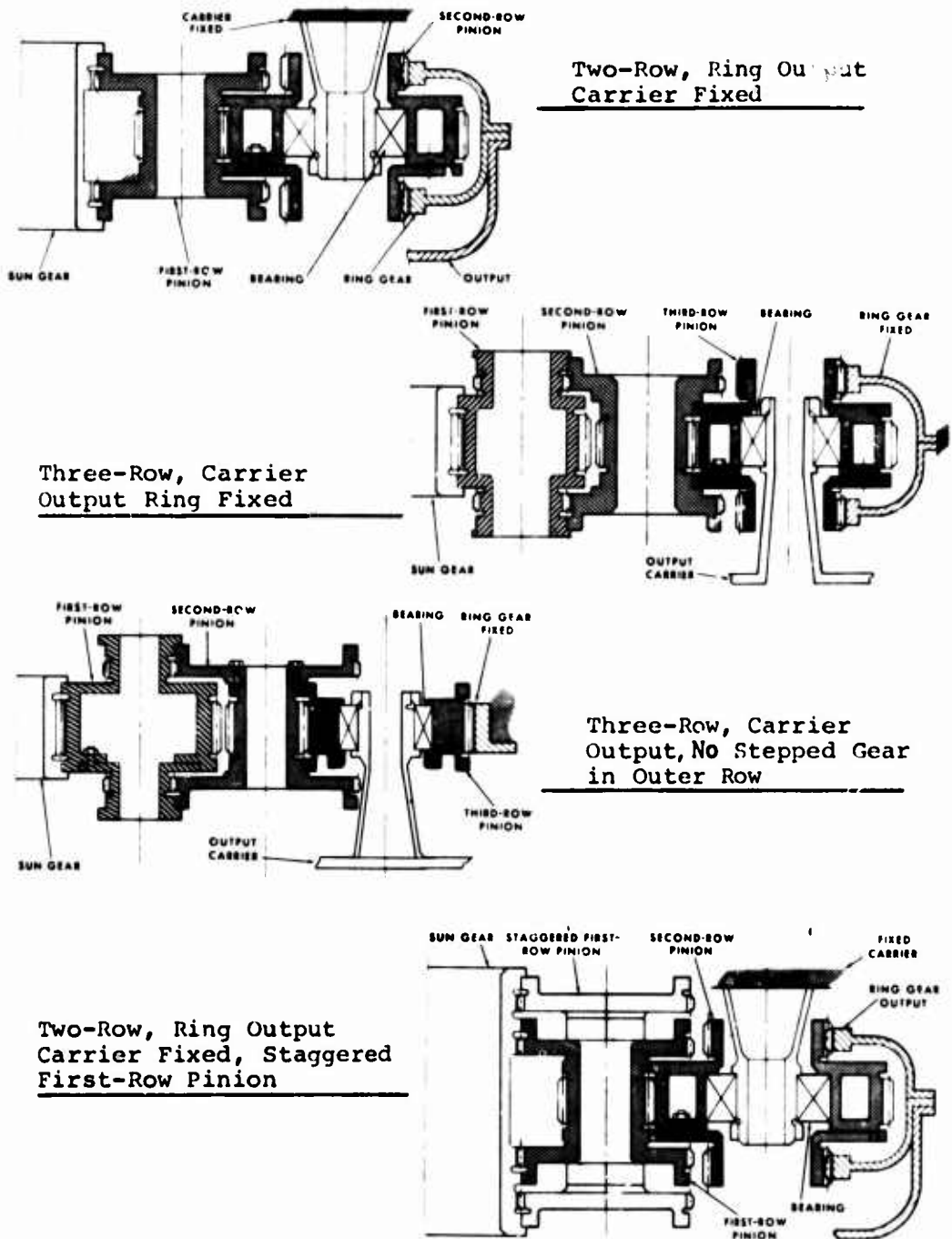
Figure 21.   Roller Gear Drive Configuration.

## BASIC NOTATION AND GEOMETRY

The basic roller gear drive notation used throughout this
report was developed in previous roller gear programs and has
been retained for clarity. The sun gear central member is
referred to as "a", while the ring gear is referred to as "c".
Pinions are referred to as "Y" for the smaller gear of each
row and "X" for the larger gear. The pinion row number is
subscripted. For example, the larger gear of the second-row
is "$X_2$," etc. Dimensions, angles, and gear nomenclature are
depicted in Figure 22.
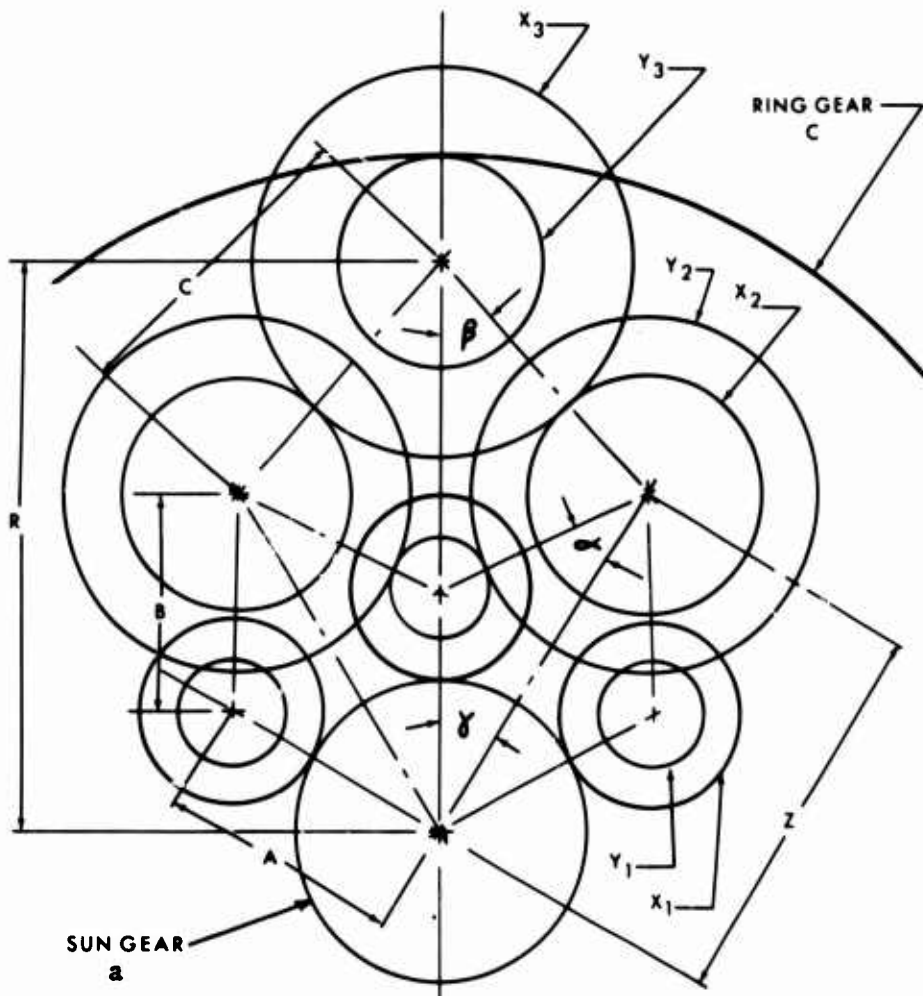


Figure 22. Notation, Roller Gear Geometry.

52

From the geometry of Figure 22, it is seen that

$$A = \frac{dX_1}{2} + \frac{da}{2} \qquad (1)$$

$$B = A \frac{\sin\gamma}{\sin\alpha} \qquad (2)$$

$$Z = A \cos\gamma + B \cos \qquad (3)$$

$$C = Z \frac{\sin\gamma}{\sin\beta} \qquad (4)$$

$$R = Z \cos\gamma + C \cos\beta \qquad (5)$$

An important geometric design consideration is the running clearance between adjacent gear members. Table 4 lists the possible gears between which tip to tip interference of teeth must be checked on the three-row design of Figure 22.

| TABLE 4. POSSIBLE INTERFERING ADJACENT GEARS. | |
|---|---|
| Driving Gear | Interfering Gear |
| $X_1$ | $X_1$ |
| $X_2$ | $X_2$ |
| $X_3$ | $Y_3$ |
| $X_2$ | $X_1$ |
| $X_3$ | $X_2$ |
| $X_2$ | $a$ |
| $X_3$ | $X_1$ |
| $X_2$ | $c$ |

The equations for determining tooth interference are derived from the roller gear drive geometry. To determine if interference exists between adjacent $X_1$ gears, the outside radius of the $X_1$ gear must be less than $A \sin\gamma$. Other geometric relations can be similarly determined.

## GEAR TEETH INDEXING

In any roller gear arrangement, certain tooth geometric relationships have to be maintained to assure proper meshing. When using stepped gears in a roller gear drive, or in any compound planetary, the gears must be "timed" to each other. That is, the angular relationship of a particular "master tooth" on one gear to a master tooth on another gear must be maintained exactly. This angular tooth relationship must be identical with all pinions of the assembly. This timing angle is shown by the dimension "X" in Figure 23. When "X" is given from the driving pitch points of the gear teeth, tooth thickness tolerances are eliminated.
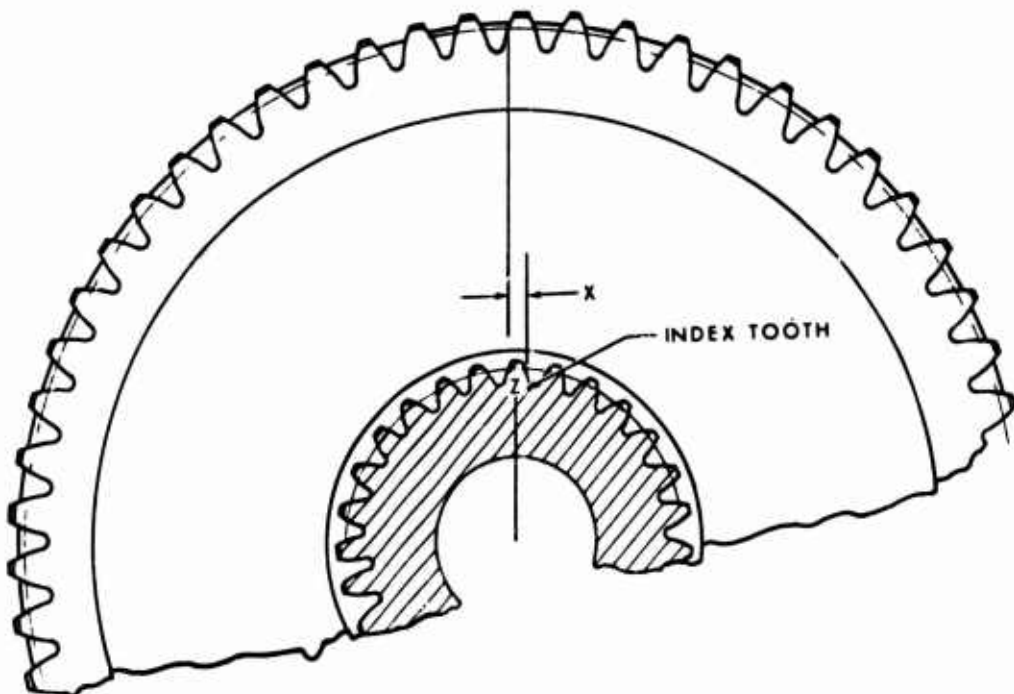


Figure 23. Timed Stepped Gears.

The requirement for assembly and tooth timing of the $X_2$ and $X_1$ gear of a typical stepped pinion roller gear mesh, Figure 24, is given by Equation (6).

$$\frac{(\text{no. of pinions}) (\text{arc length lmnop})}{\text{circular pitch}} = \text{no. of teeth} =$$

$$\text{where} \quad \gamma = \frac{\pi}{\text{no. of pinions}} = \text{integer} \qquad (6)$$

and

$$\text{circular pitch} = \frac{\pi}{\text{diametral pitch}}$$
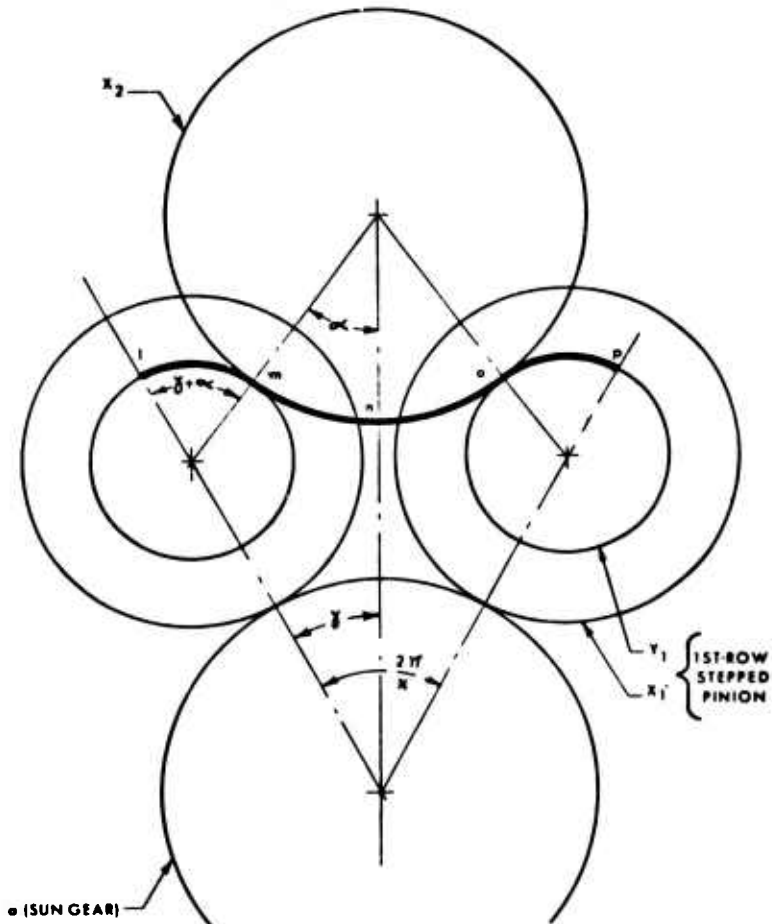


Figure 24. Stepped Pinion Mesh.

55

A special case of Equation (6) occurs when the resultant integer is also divisible by the number of pinions or when the mesh path lmnop corresponds to an integer number of teeth. In equation form, this reduces to

$$\frac{\text{arc length lmnop}}{\text{circular pitch}} = \text{integer} \qquad (7)$$

If Equation (7) is satisfied, Equation (6) will also be satisfied, but the converse is not always true. In those cases where the total mesh path around the roller gear unit corresponds to an integer number of teeth, as in Equation (6), but the requirement of Equation (7) is not met, the relationship between stepped pinions of an assembly must be different for each pinion of the assembly. This is not practical from a manufacturing standpoint, and hence the requirement of Equation (7) is more practical than that of Equation (6). Although this eliminates some candidate designs, numerous choices remain. Another requirement is that each individual segment of arc corresponds to an integer number of teeth; this is another special case of Equations (6) and (7) and may be written as

$$\frac{\text{arc length lm + arc length op}}{\text{circular pitch}} = \text{integer} \qquad (8)$$

and also

$$\frac{\text{arc length mno}}{\text{circular pitch}} = \text{integer} \qquad (9)$$

As in the previous case, if Equations (8) and (9) are both satisfied, Equations (6) and (7) are automatically satisfied. Again, the converse is not always true; i.e., Equations (8) and (9) are special cases. Each pinion of an assembly would require different timing angles if Equation (6) or (7) is used. It is easier and less expensive to manufacture each pinion with the same timing angle, and hence Equations (8) and (9) are used in the design of the roller gear unit. Although Figure 24 refers to the first-/second-row mesh, the same general procedure also applies for the second-/third-row mesh, etc.

arc length lm = arc length op = $\frac{d Y_1}{2} (\gamma + a)$

and

arc length mno = $2 a \frac{dX_2}{2}$

and

circular pitch = $\frac{\pi}{pitch}$

Substituting into Equation (8)

$$\frac{2 \frac{dY_1}{2} (\gamma + a)}{\frac{\pi}{pitch}} = integer$$

Also

$dY_1$ = number of teeth in $Y_1$ = $\frac{NY_1}{pitch}$

Hence

$$NY_1 \left[ \frac{\pi}{no.\ of\ pinions} + a \right] = integer \qquad (10)$$

By examination of Equation (10), it is evident that the only way this equation can be satisfied is if

$$a = \frac{\pi}{M} \qquad (11)$$

where

M = constant which defines the "toggle" angle

Substituting the definition of the toggle angle $a$ into (10) gives

$$NY_1 \left[ \frac{1}{no.\ of\ pinions} + \frac{1}{M} \right] = integer \qquad (12)$$

Equation (12) shows the basic relationship for the number of teeth in the $Y_1$ gear.

57

Also, by substitution into Equation (9)

$$\frac{dX_2}{\frac{\pi}{pitch}}\gamma = integer$$

Thus

$$\frac{NX_2}{M} = integer \qquad (13)$$

Equation (13) now defines the required relationship for the number of teeth in the $X_2$ gear.

When designing a roller gear drive, the tooth relationships must be as given by Equations (12) and (13) to ensure proper meshing. In Equations (12) and (13), the number of teeth and number of pinions are always integers. However, M does not necessarily have to be an integer to satisfy the equations; M can be an improper fraction. For example, consider the case of the angle $\alpha$ equal to 37° 30' when substituted in Equation (11):

$$\frac{37.5\pi}{180} = \frac{\pi}{M}$$

and

$$M = \frac{24}{5}$$

If the number of teeth in the inner row is divisible by 8 and the number of teeth in the outer row by 24, Equations (12) and (13) are satisfied. A computer program was written to determine all the possibilities of toggle angles and the lowest division of teeth such that Equations (12) and (13) are satisfied. The results of this effort are presented in Appendix A. When choosing a preliminary roller gear, only the particular discrete values of the toggle angles as shown in Appendix A may be used.

In addition to the meshing relationships discussed above, for equal spacing the number of teeth in the sun and ring gear must be divisible by the number of pinions.

$$\frac{Na}{no.\ of\ pinions} = integer \qquad (14)$$

$$\frac{Nc}{no.\ of\ pinions} = integer \qquad (15)$$

58

Equations (14) and (15) do not necessarily have to be held. However, if they are not, the timing angle between each stepped pinion would have to be different, which complicates manufacturing and assembly.

PRELOAD

At each gear contact point in the roller gear drive, there is a tangential tooth load, Wt, and a radial tooth load, Wr. These loads are related by the gear tooth pressure angle, $\theta$.

$$Wr = Wt ( \tan \theta )$$
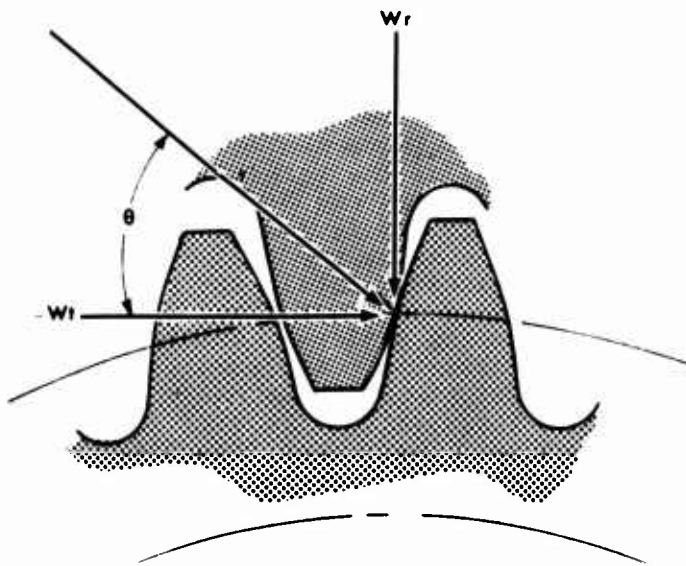


Figure 25. Gear Tooth Forces.

In a roller gear drive, the gear teeth tangential forces transmit torque through the system while the radial tooth forces are reacted by rollers. In a standard spur gear and shaft arrangement, bearings react the resultant gear loads. In a roller gear drive, the rollers take the place of the bearings and react the resultant gear loads to keep the system in equilibrium. A major difference between a roller gear pinion and a conventional gear and bearing arrangement is that in the conventional system the resultant bearing load can be in any direction since the gear surrounds the bearing; but in a roller gear drive, negative roller loads, i.e., separation at

the roller contact points, result in an unstable system. The roller loads must be positive for the system to be in equilibrium. Preloading is a method of insuring that the roller loads are always positive, thereby keeping the system stable. With the roller loads maintaining system equilibrium, the need for bearings is eliminated.

Preloading can be accomplished in two ways: by using external mechanisms or by designing a self-preloading system. In either design the roller loads must be sufficient to overcome inertia effects and gear tooth separating forces and yet not be so large as to require unnecessarily heavy rollers to react the loads.

Preloading mechanisms are designed to produce an initial positive preload and maintain a load on all roller contact points over the operating range of the roller gear unit. Several possible mechanisms for producing this preload are known. One employs a circular ring around the outer-row pinion bearing shafts. Bolts in this ring are used to apply inward radial loads to the pinion shafts and thus to the rollers of all the pinions of the assembly. Another mechanism uses an eccentric bushing which can be rotated to produce the desired preload and then locked in place. A third method is an eccentric bearing diameter on the pinion shaft itself. The pinion shaft is then rotated to obtain the preload before being held in place. These are just three examples of many possible external preloading devices. The major problem with these mechanisms, aside from the possible mechanical reliability and added weight of the mechanisms, is the necessity to induce a large initial load of a magnitude necessary to overcome gear loads when transmitting maximum power.

Preloading does not necessarily require an external mechanism. Inherent preloading can be achieved by proper choice of the number of gear teeth, toggle angles, number of pinions, distances and pressure angles. A self-preloading roller gear drive system can be designed by a careful choice of these geometric variables. One method is to employ varying gear teeth pressure angles between rows. A high gear tooth pressure angle can be used for the ring gear and progressively lower pressure angles for successive rows of pinions. Since the gear tooth radial load, $W_r$, decreases as the successive pressure angles decrease, the unit is forced radially inward from the force induced at the ring gear.

# ROLLER GEAR DRIVE, DESIGN SELECTION

## STAGGERED GEARS

This type of roller gear drive, a two-row, ring output, carrier fixed, with staggered $X_1$ gears, has the rotation of the input in the same direction as the output rotation. Staggered gears allow the same gears in each row to overlap, which in turn allows these particular gears to be larger in diameter, thereby increasing the overall reduction ratio of the unit. The reduction ratio using the number of teeth is given by

$$RR = \frac{X_1 \ X_2 \ c}{Y_1 \ Y_2 \ a} \tag{16}$$

Figure 26 is a layout of the staggered gear configuration with eight pinions per row. In the first row, four pinions are meshing with the inner sun gear members while four alternate pinions are meshing with the outer sun gear members.

An odd number of pinions cannot be used in the staggered design because symmetry of pinions is necessary. Analysis showed that eight pinions per row was the maximum possible number to obtain the required ratio of approximately 20:1. With ten or more pinions per row, the geometry is such that 20:1 cannot be obtained. With six pinions per row, the pinions become larger, face widths increase and the design weight becomes heavier. Within the envelope restrictions imposed, eight pinions is the optimum for minimum weight for a 20:1 ratio.

Because of the staggered configuration, the overall height of the roller gear unit becomes large and heavier when compared with other designs. Also, with the overlapping feature of the staggered first-row pinions, the unit is virtually enveloped by gears, thus restricting direct lubrication of the $Y_1$ - $X_2$ gear mesh. Because of lubrication, weight, overall height, and difficult manufacture of the sun gear, the staggered roller gear configuration was not considered as a candidate for the final design.

61
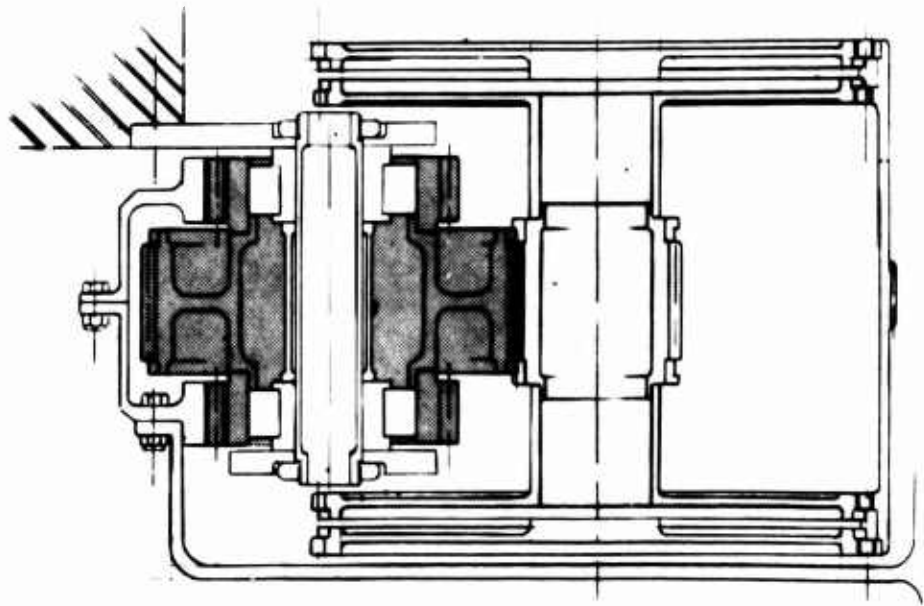
Figure 26.   Staggered Gear Layout.

63
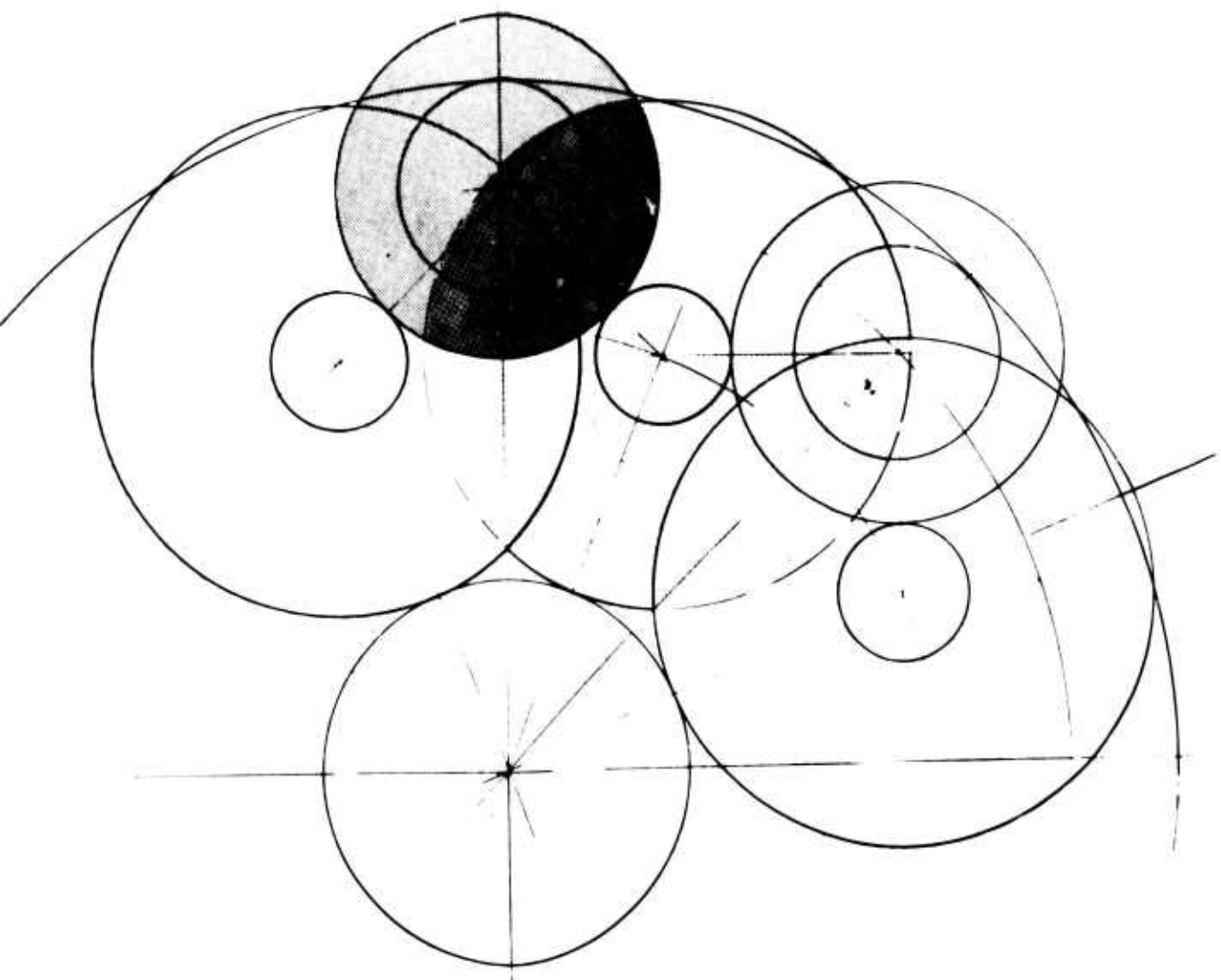
## THREE-ROW, NONSTEPPED OUTER-ROW GEARS

A three-row, carrier output with a nonstepped third-row pinion design appeared attractive because the third-row small pinion is eliminated. Not only does this reduce the number of fabricating joints, but it also allows for a much sturdier carrier/post design since the diameter of the third-row pinion can be large. A distinguishing feature of this design is the $Y_2 - X_3 - c$ mesh, Figure 27. This is the only roller gear drive in which three different gears mesh together in the same train. The $X_3$ in this instance is acting as an idler gear. A layout of this three-row drive configuration is shown in Figure 28.
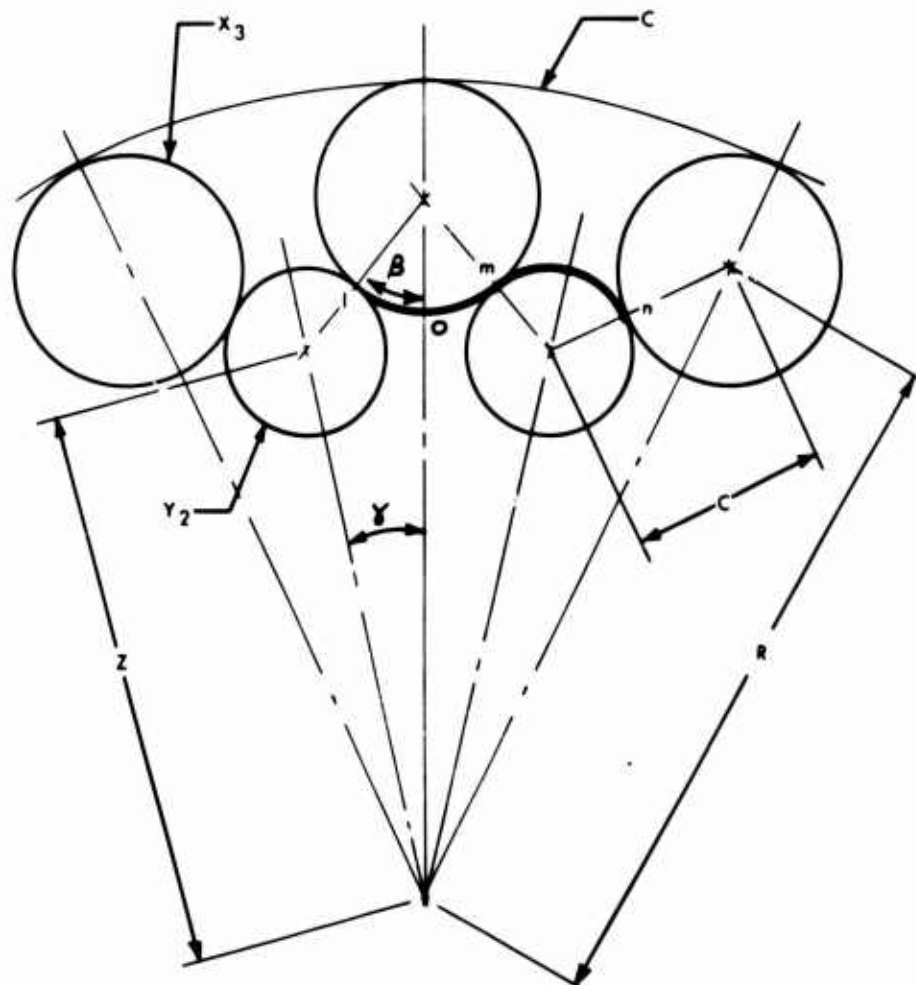


Figure 27. Three-Row Mesh Geometry.

65
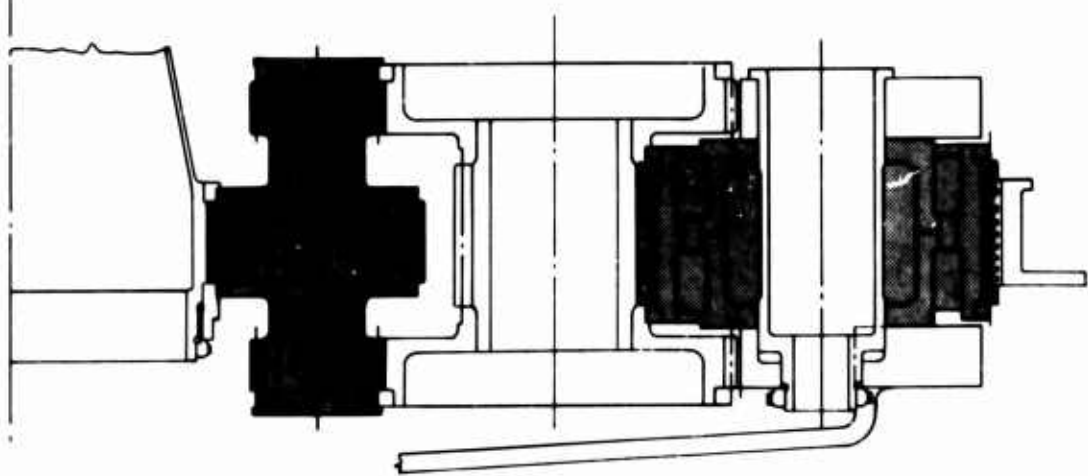
Figure 28.  Three-Row, Carrier Output Layout.

67
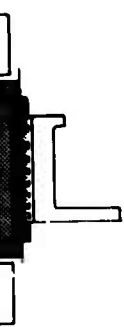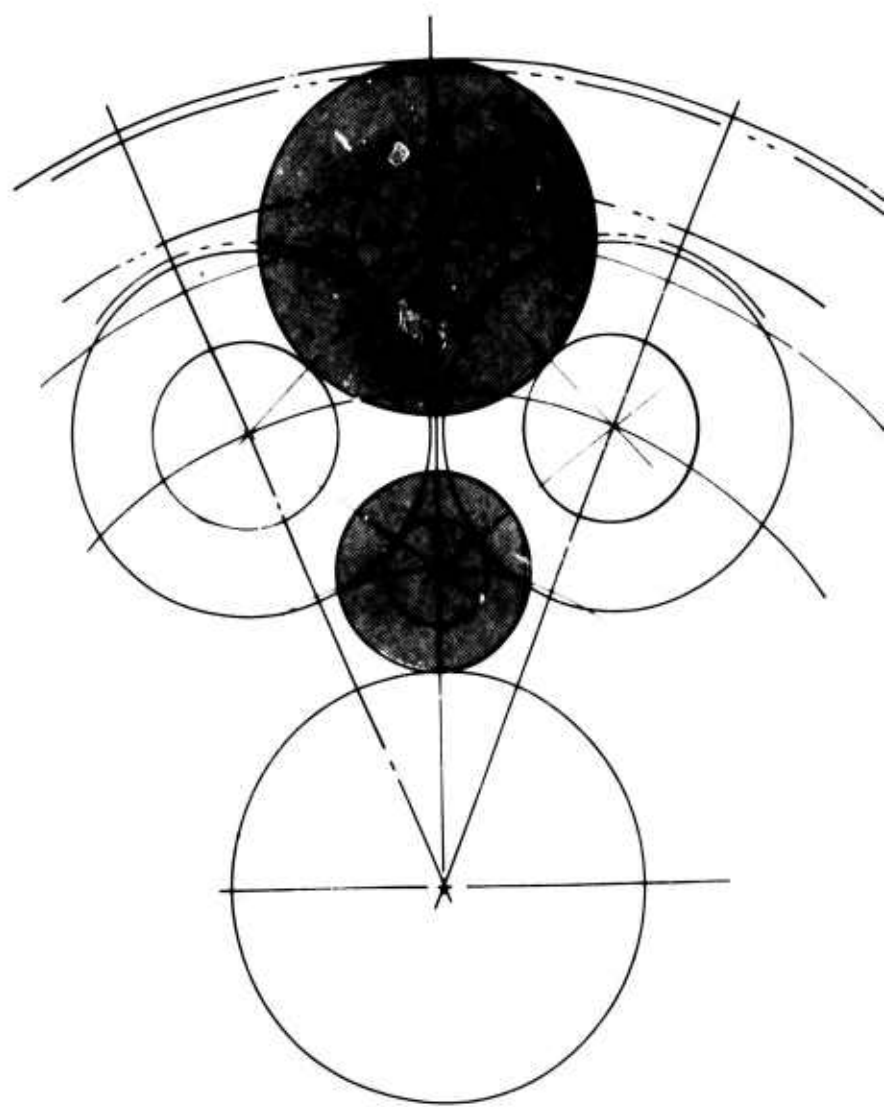
The reduction ratio of the three-row drive is

$$RR = 1 + \frac{X_1}{Y_1} \frac{X_2}{Y_2} \frac{c}{a} \qquad (17)$$

For proper meshing of the $Y_2$ - $X_3$ - c gear train, the arc lengths qt and ts must correspond to an integer number of teeth. This arc length mesh leads to equations similar to Equations (12) and (13). The number of teeth in the ring gear must also be divisible by the number of pinions. (These meshing relationships are required for any roller gear drive.) The additional requirement for the nonstepped outer-row pinion is the geometric relations that

$$\frac{Nc - NX_3}{NX_3 + NY_2} = \frac{R}{C} \qquad (18)$$

Substituting for R and C, the right side of the above equation can be expressed as a function of the toggle angles

$$\frac{Nc - NX_3}{NX_3 + NY_2} = \frac{\sin(\gamma + \beta)}{\sin} \qquad (19)$$

where

$\gamma$ = toggle angle for number of second-row pinions
$\beta$ = toggle angle for outer-row pinions

Also

$$\frac{NY_2}{\text{no. of pinions}} + \frac{NY_2}{M_2} = \text{whole number} \qquad (20)$$

$$\frac{NX_3}{M_2} = \text{whole number} \qquad (21)$$

$$\frac{Nc}{\text{no. of pinions}} = \text{whole number} \qquad (22)$$

Examination of Equations (18) through (22) shows that it is difficult to meet all of these requirements. In fact, an extensive computer analysis showed that within the practical limitations of number of teeth, angles, etc., there are no exact solutions to the above set of equations. The program was written in a series of nested loops in which each parameter was varied one at a time. The variables in this analysis were $NY_2$, $NX_3$, $N_c$, $M_2$, and number of pinions. These five variables

69

completely define the $Y_2$ - $X_3$ - c mesh. Even though there are no exact solutions, the requirement of Equation (19) does not have to be exact, but must be close. The error can be thought of as an error in center distance or a percent error in the ratio of R to C (see Figure 27).

In the computer analysis, the number of permutations of the five variables is 1,903,744,425. The variable $M_2$, which defines the toggle angle, $\beta$, between the second- and third-row pinions was considered to vary between four and six, which corresponds to angles of 30 to 45 degrees. Not only were integer values of $M_2$ attempted but also improper fractions with denominator varying between 2 and 12. Thus, 8/2, 9/2, 10/2, 11/2 and 12/2 were tried for $M_2$ along with 9/3, 10/3, 11/3, etc., in all combinations up to 72/12. The ring gear teeth were varied from 120 to 300, the teeth in $X_3$ from 40 to 100, the teeth in $Y_2$ from 18 to 36, and the number of pinions from 7 to 12 (excluding 11). Twelve solutions were found to satisfy Equation (19) within 0.5 percent error. These twelve feasible candidate designs are listed in Table 5. Thus, for a 30-inch ring gear, the center distance error would be a maximum of approximately 0.15 inch. The operation of this mesh with 0.15 inch error in center distance at the high power and speeds of a helicopter transmission is not feasible. For satisfactory operation, the maximum center distance error should be in the order of 0.005 inch in 30 inches, which amounts to 0.0167 percent.

| TABLE 5. GEAR TEETH AND ANGLE COMBINATIONS, NONSTEPPED OUTER-ROW CONFIGURATION. | | | | | |
|---|---|---|---|---|---|
| Number of Pinions | Toggle Angle Constant | Number of Teeth | | | Error (%) |
| | | $NY_2$ | $NY_3$ | $N_C$ | |
| 7 | 5 | 35 | 55 | 238 | .376 |
| 7 | 21/4 | 21 | 42 | 168 | .402 |
| 7 | 21/4 | 21 | 63 | 231 | .402 |
| 7 | 21/4 | 21 | 84 | 294 | .402 |
| 8 | 4 | 24 | 44 | 208 | .245 |
| 8 | 4 | 32 | 64 | 296 | .246 |
| 8 | 6 | 24 | 54 | 216 | .379 |
| 8 | 24/3 | 27 | 72 | 296 | .040 |
| 10 | 14/3 | 35 | 42 | 250 | .056 |
| 12 | 4 | 27 | 40 | 264 | .279 |
| 12 | 6 | 36 | 54 | 300 | .128 |
| 12 | 6 | 28 | 60 | 300 | .478 |

No cases were found to satisfy this condition in the 1,903,744,425 permutations. The two best cases found, with errors of 0.04 and 0.056 percent, have center distance errors of approximately 0.012 inch to 0.0168 inch which is high for aircraft gearing. As no combination of number of teeth could be chosen which satisfies the geometric and meshing relationships, the design, with nonstepped outer-row gears, was not considered feasible for the S-61 roller gear drive transmission.

## TWO-ROW DESIGN

A third candidate family of roller gear designs which satisfies the requirement of input direction of rotation equal to output is the two-row, carrier fixed, ring output. The reduction ratio for this type of roller gear drive is given by

$$RR = \frac{X_1}{Y_1} \frac{X_2}{Y_2} \frac{c}{a} \tag{23}$$

A two-row, carrier fixed, ring output roller gear drive layout with eight pinions per row is shown in Figure 29. This design has a single ring gear which is trapped inside the $X_2$ gear of the outer-row pinion. Assembly must commence from the ring gear and proceed inward for this design. The sun gear is assembled last, with the removable flanges on the sun gear and first-row pinion roller being bolted on after assembly of the sun gear. This first-row pinion flange must be placed loosely on the first-row pinion prior to assembly. After all the first-row pinions are in place and the sun gear assembled, the removable flanges are then bolted rigidly to the gears. One problem with the design of Figure 29, which has eight pinions per row, is that the $Y_2$ gear is relatively small, which creates a problem with the output bearing shaft design. There is insufficient room to obtain proper structural support for the bearing post. As the number of pinions increases, this problem becomes more and more acute. With nine or more pinions the required reduction ratio of approximately 20:1 cannot be obtained.

Figure 30 shows a similar design with seven pinions per row. The $Y_2$ gear is now larger, which allows a sturdier carrier post design than in the eight pinions per row design. Another unique feature of this design is the arrangement of the outer-row pinion which allows the outside diameter of the carrier bearing to be larger than the inside diameter of the $Y_2$ gear. This feature again allows a larger carrier post diameter to be used. Another design variation with seven pinions per row is shown in Figure 31.
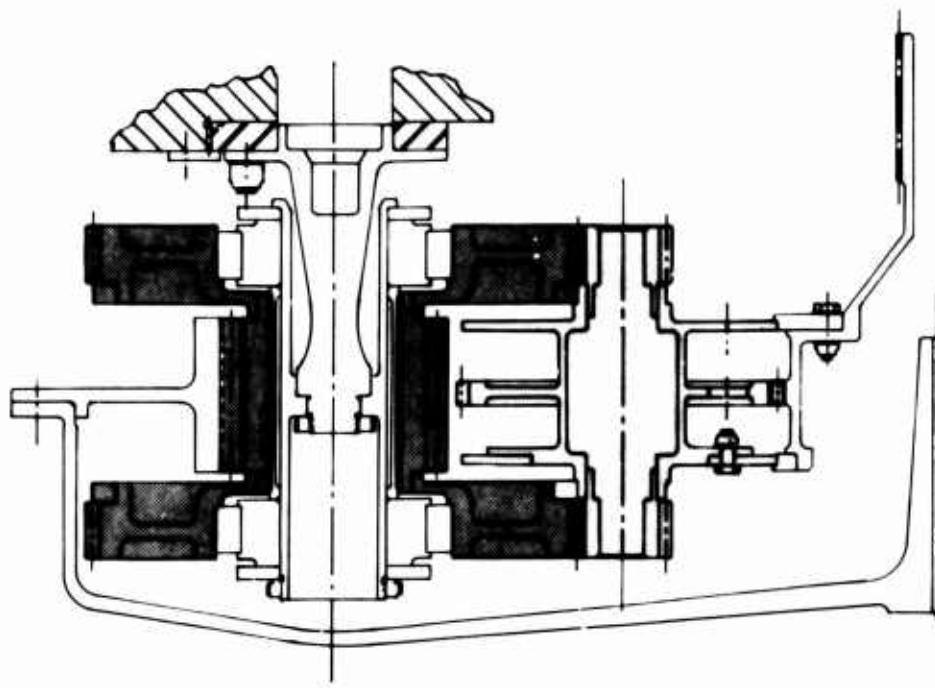
Figure 29.  Two-Row, Eight Pinions per Row Layout.
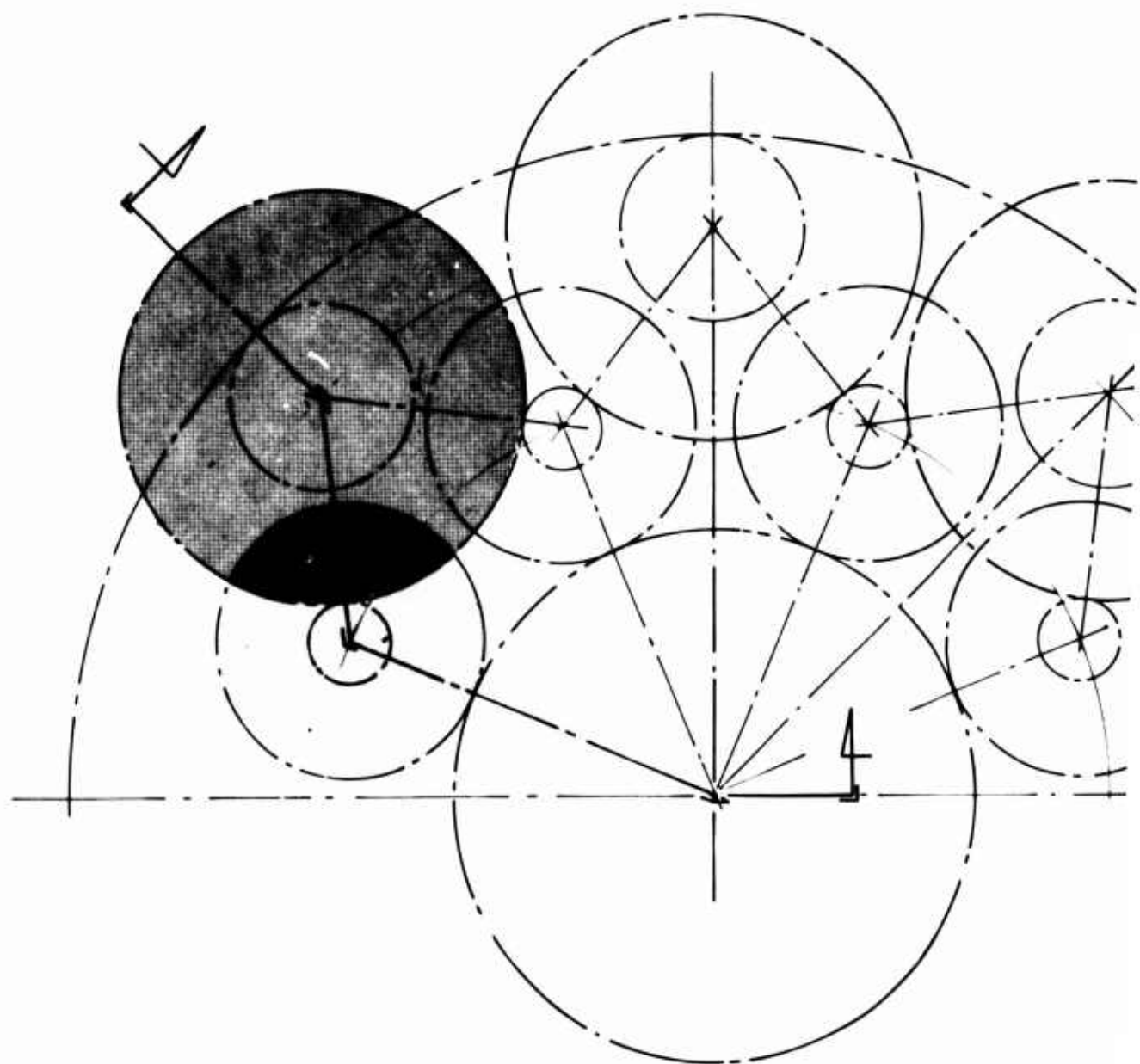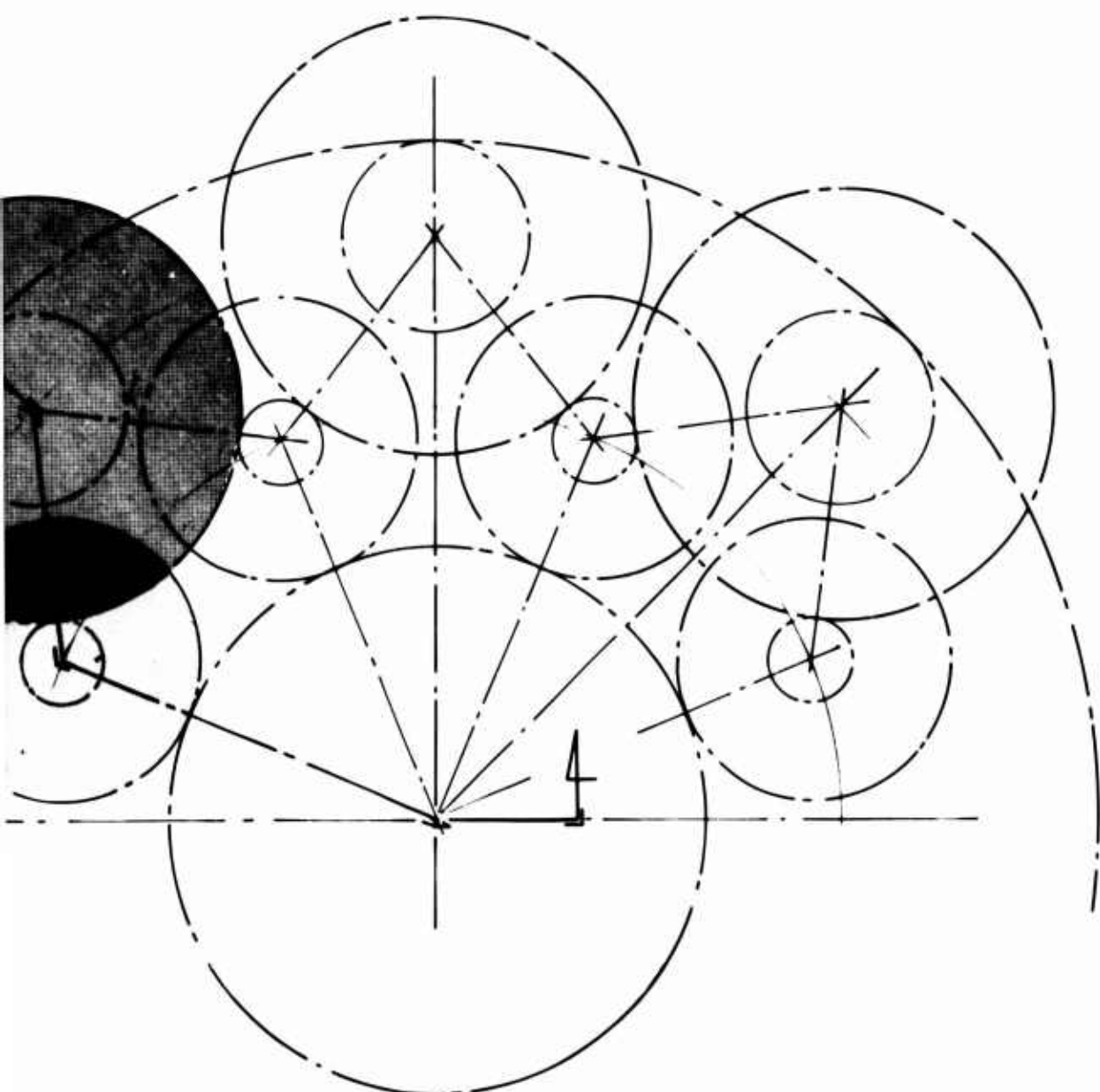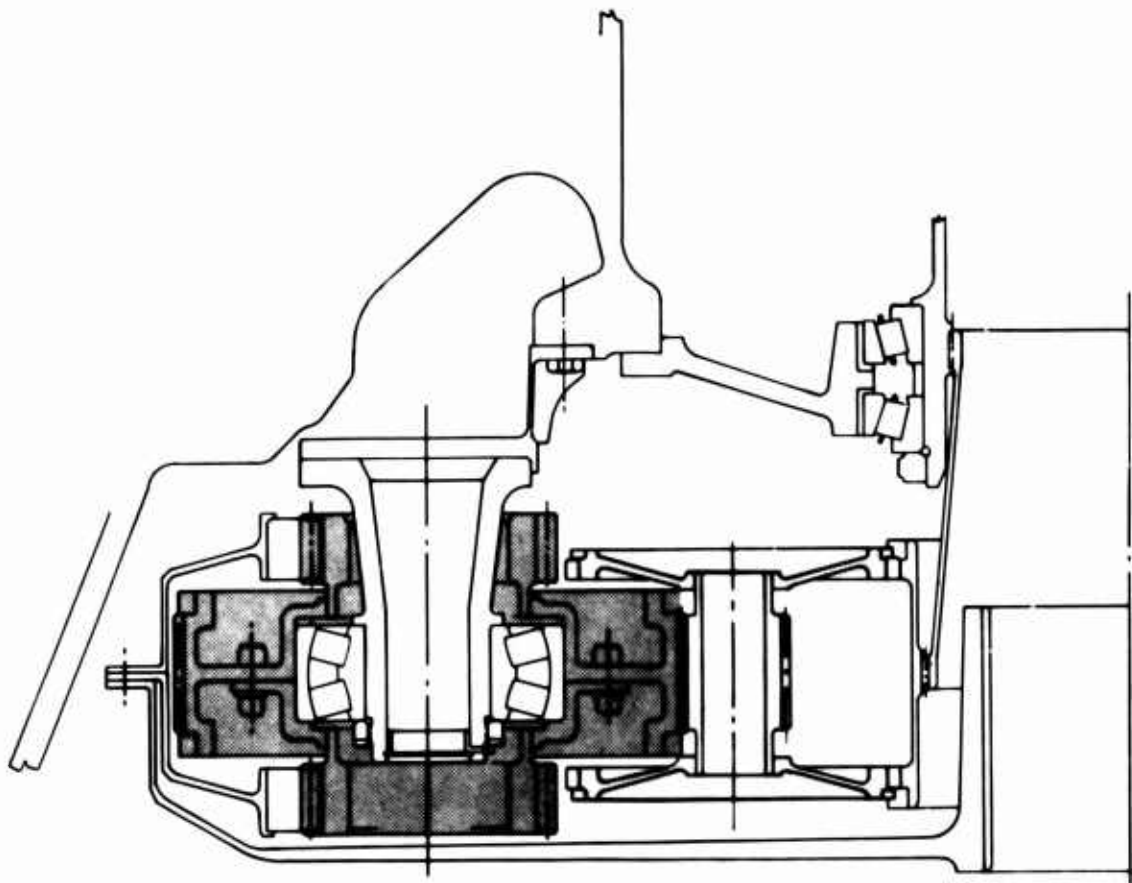
Figure 30.   Two-Row, Seven Pinions per Row Layout.

75
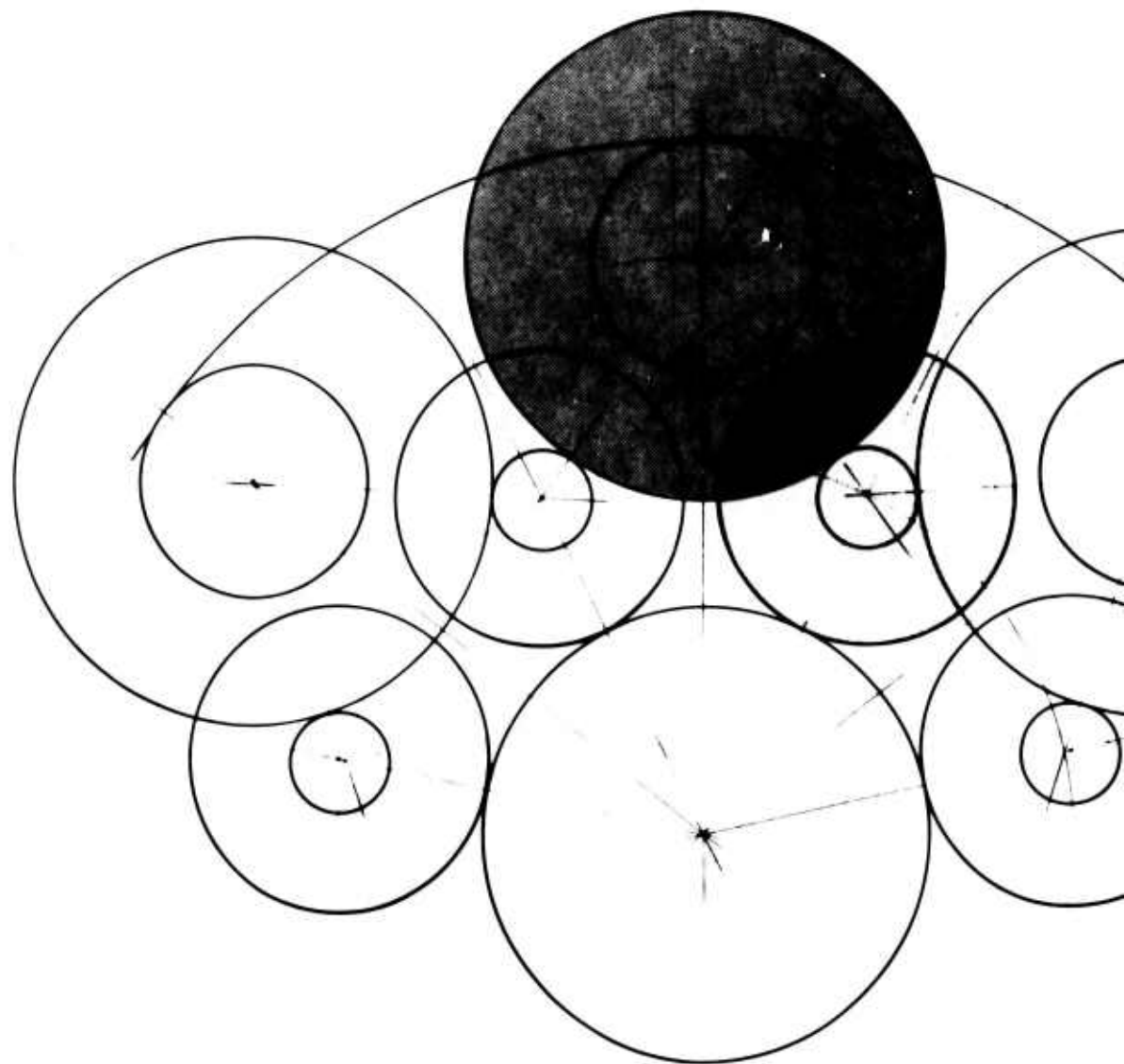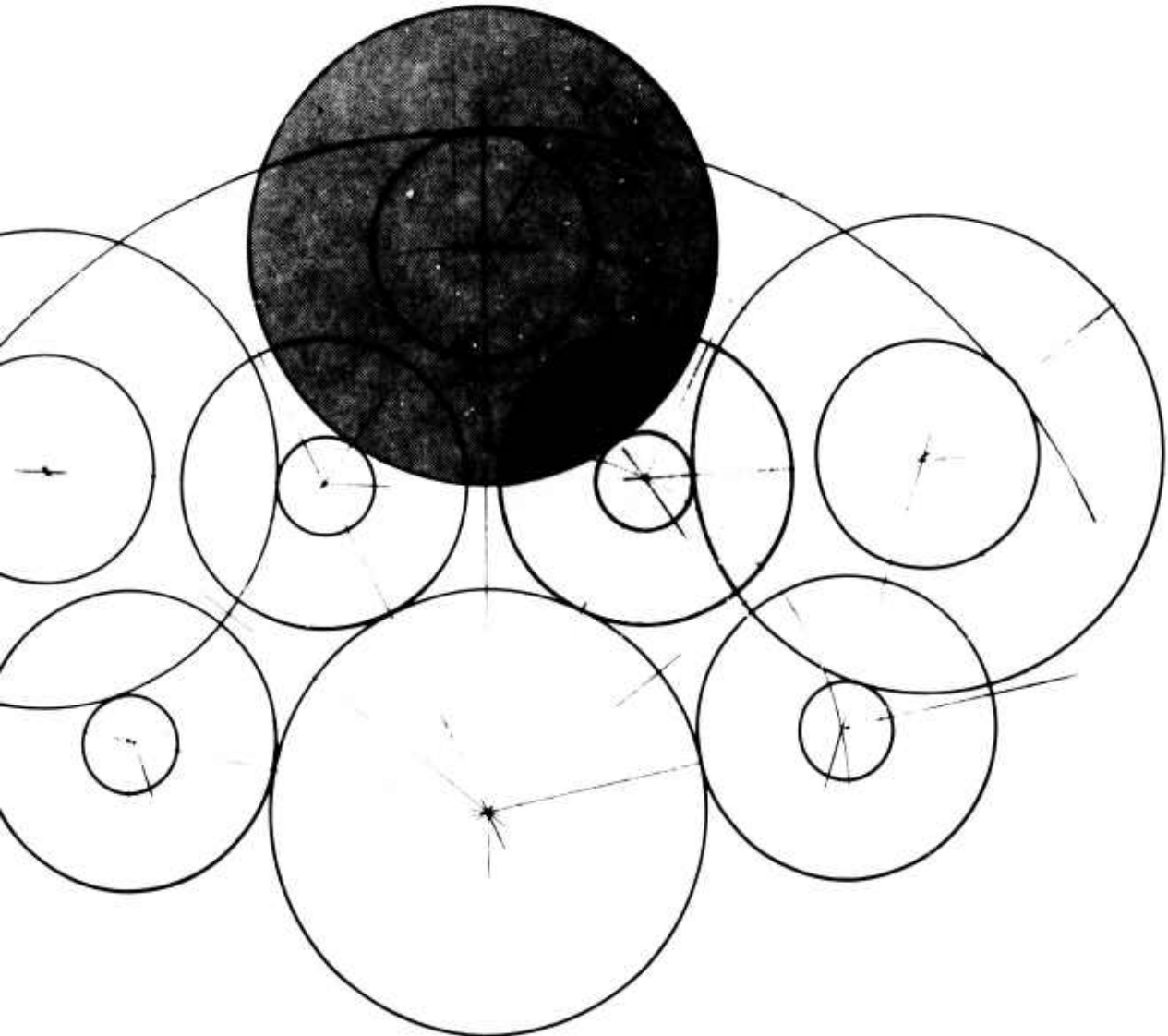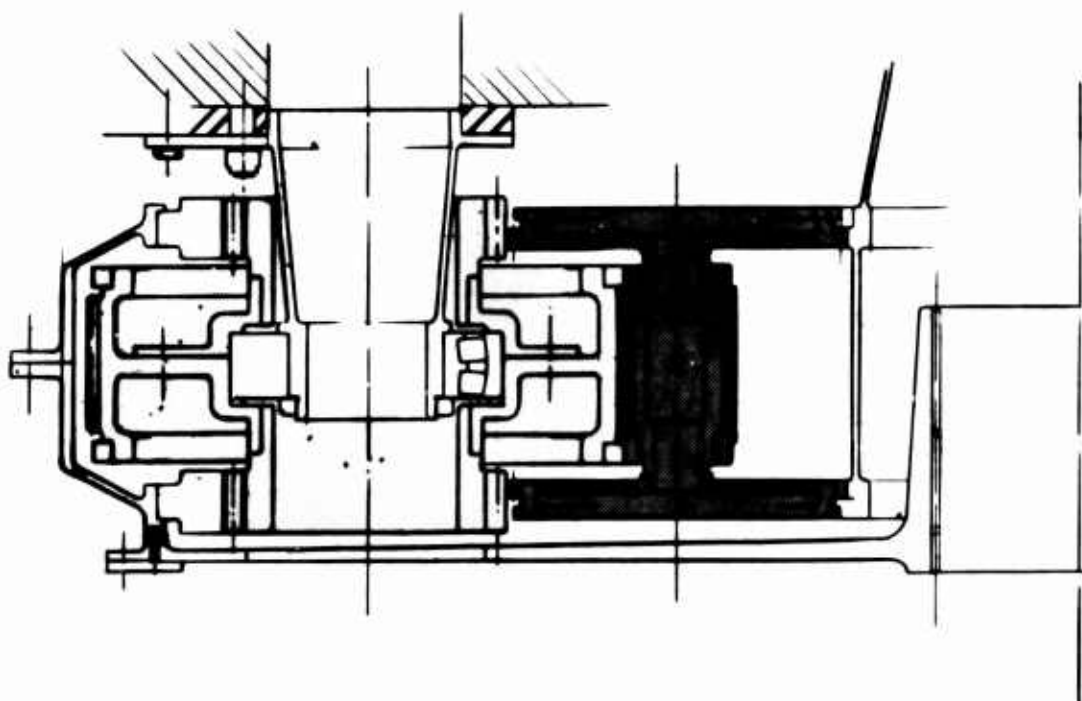
Figure 31. Two-Row, Seven Pinions per Row, Double
Ring Gear Layout.
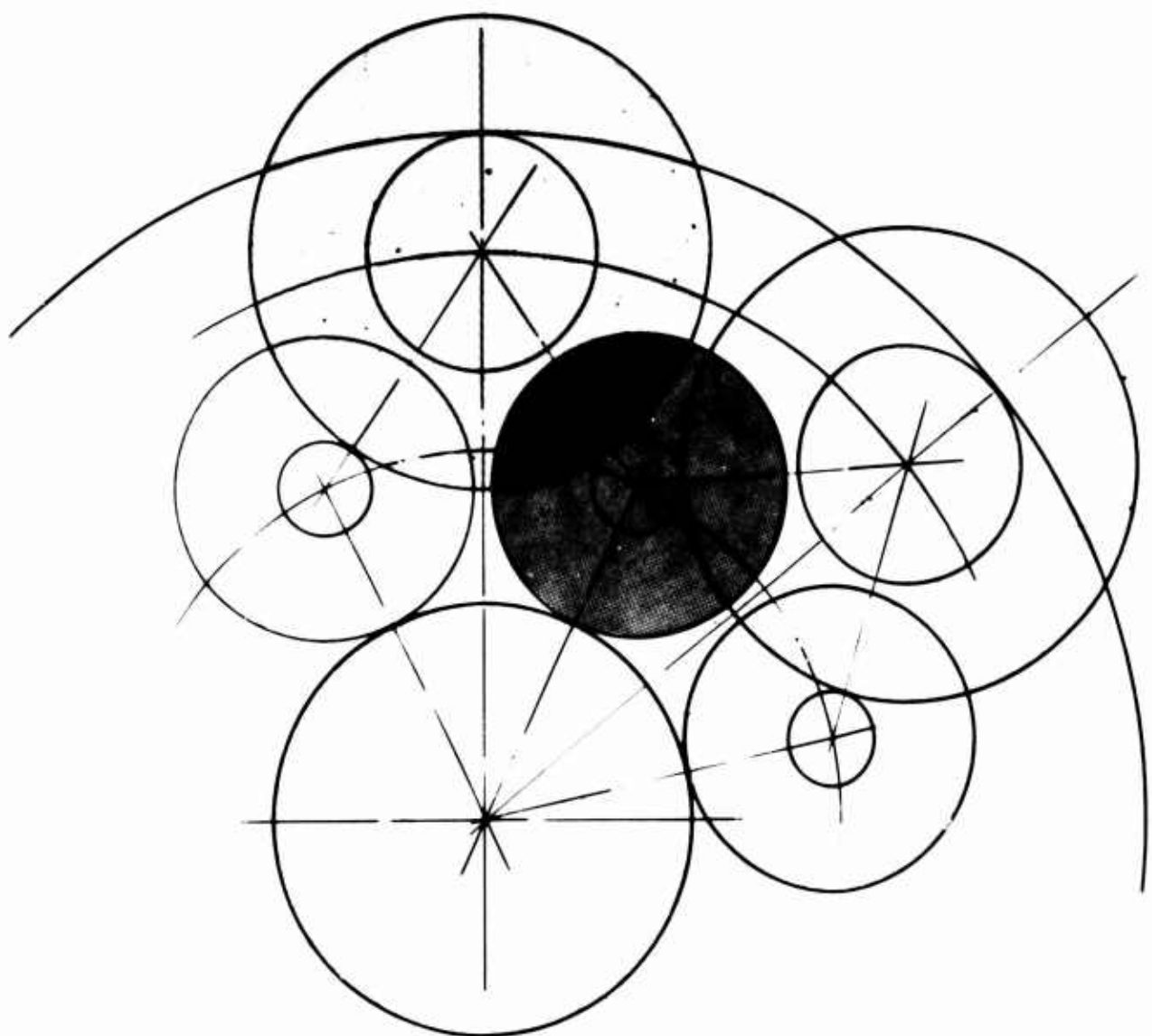
When six pinions per row or less are used in a two-row, ring output, roller gear drive, face widths increase and, in general, the gear diameters become larger and the designs are heavier than the seven-row designs. Hence, the optimum configuration within the restraints of the S-61 transmission is the seven pinions per row design. It is lighter in weight than designs with six or less pinions per row and retains a large enough $X_2$ gear diameter to allow a structurally sound output carrier post design which cannot be obtained with designs of eight or more pinions per row.

With seven pinions per row, it is possible to design a two-row, ring output roller gear drive unit to be self-preloading; i.e., the resultant roller loads are all positive, indicating inherent stability. This is accomplished by using a high gear tooth pressure angle on the ring gear mesh and using lower gear teeth pressure angles on successive pinion meshes toward the sun gear.

## THREE-ROW DESIGN

The final candidate roller gear drive configuration considered was the three-row, carrier output, fixed ring roller gear drive. As in the previous candidate designs, this drive has the same direction of rotation on the sun gear input as on the carrier output. The reduction ratio is given by

$$RR = 1 + \frac{X_1 \, X_2 \, X_3 \, c}{Y_1 \, Y_2 \, Y_3 \, a} \tag{24}$$

Figure 32 is a layout of a three-row, carrier output roller gear drive with six pinions per row. As with the two-row designs, the last row pinion can be disassembled to accommodate an output bearing whose diameter is larger than the inside diameter under the $Y_3$ gear. The assembly of this roller gear unit must start at the sun gear and proceed outward to the double ring gears. The bearing posts and carrier are assembled last. The spherical roller output bearing can accommodate large carrier plate post slopes and deflections while allowing the gears of the roller gear unit to remain in parallel alignment.

A design with seven pinions per row is depicted in Figure 33. The structural features of this seven-pinion design are similar to those of the six-pinion design. The weight is less in the seven-pinion design than in the six. Another seven-pinion layout is depicted in Figure 34. In this design, centralized flanges on the ring gears allow equal torsional deflection in each ring gear segment, which aids in equalizing load sharing of the entire assembly.

79
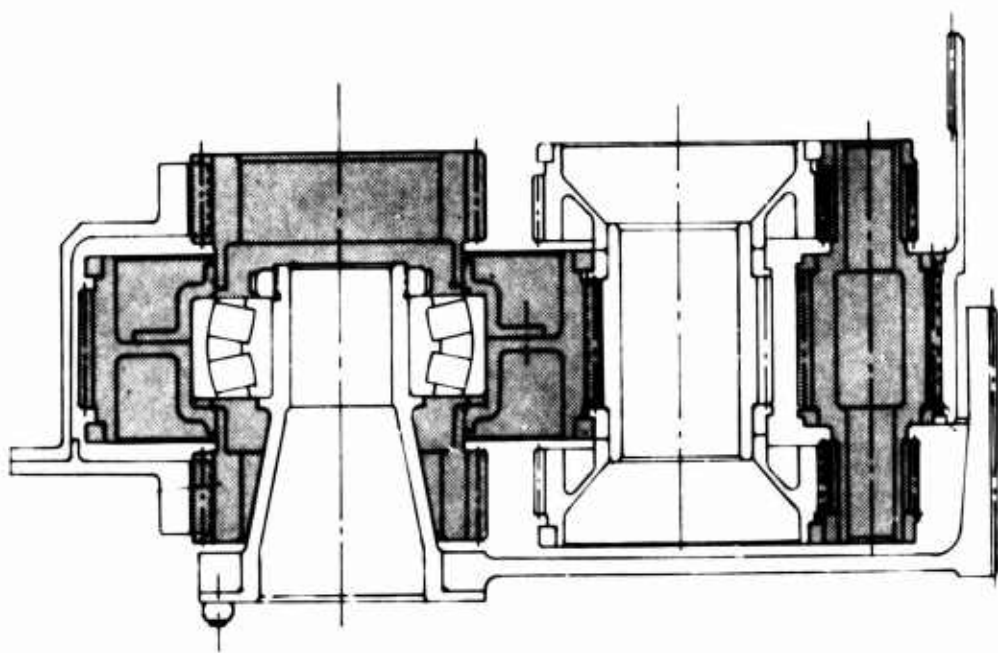
Figure 32.    Three-Row, Six Pinions per Row Layout.

81
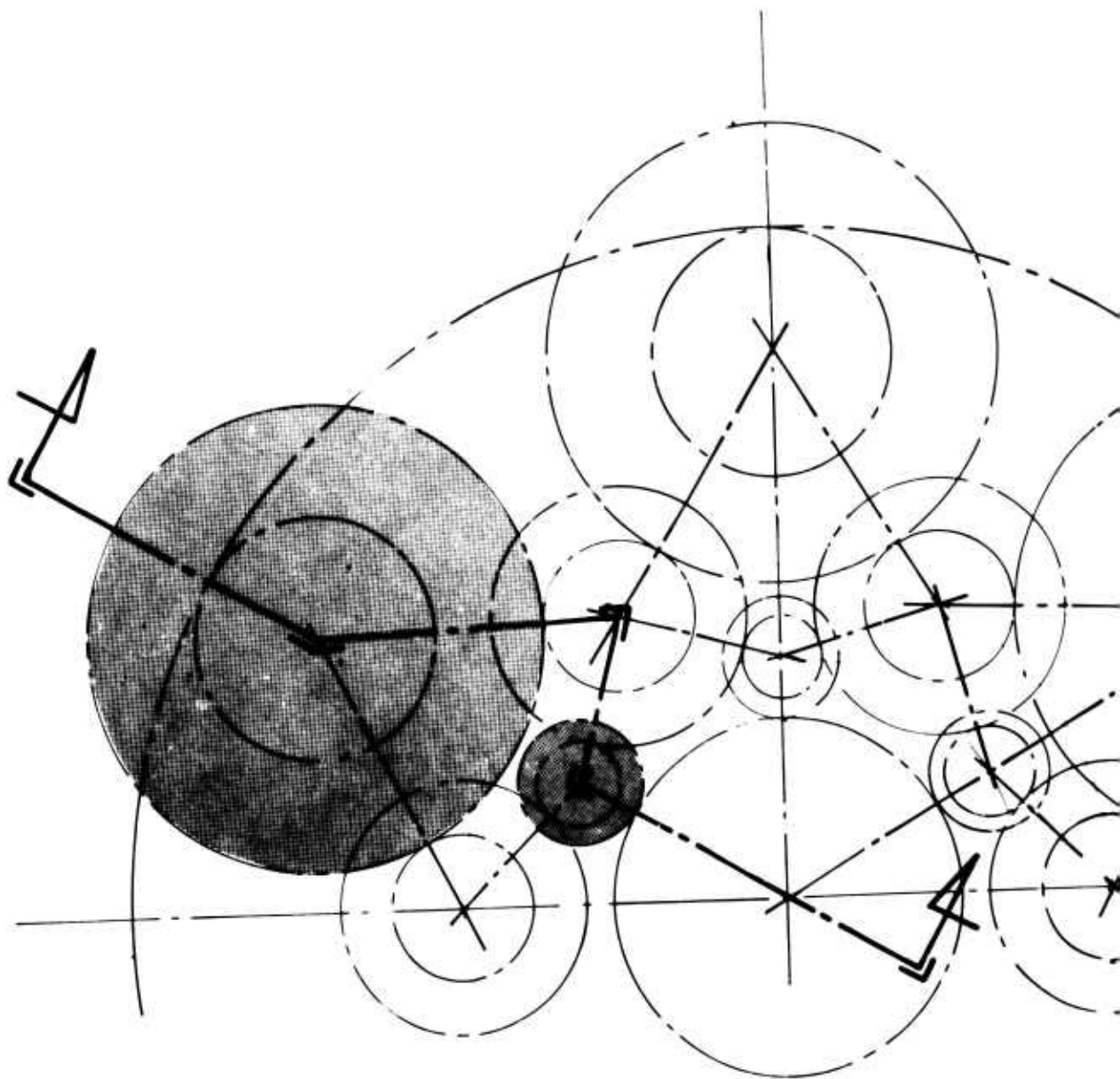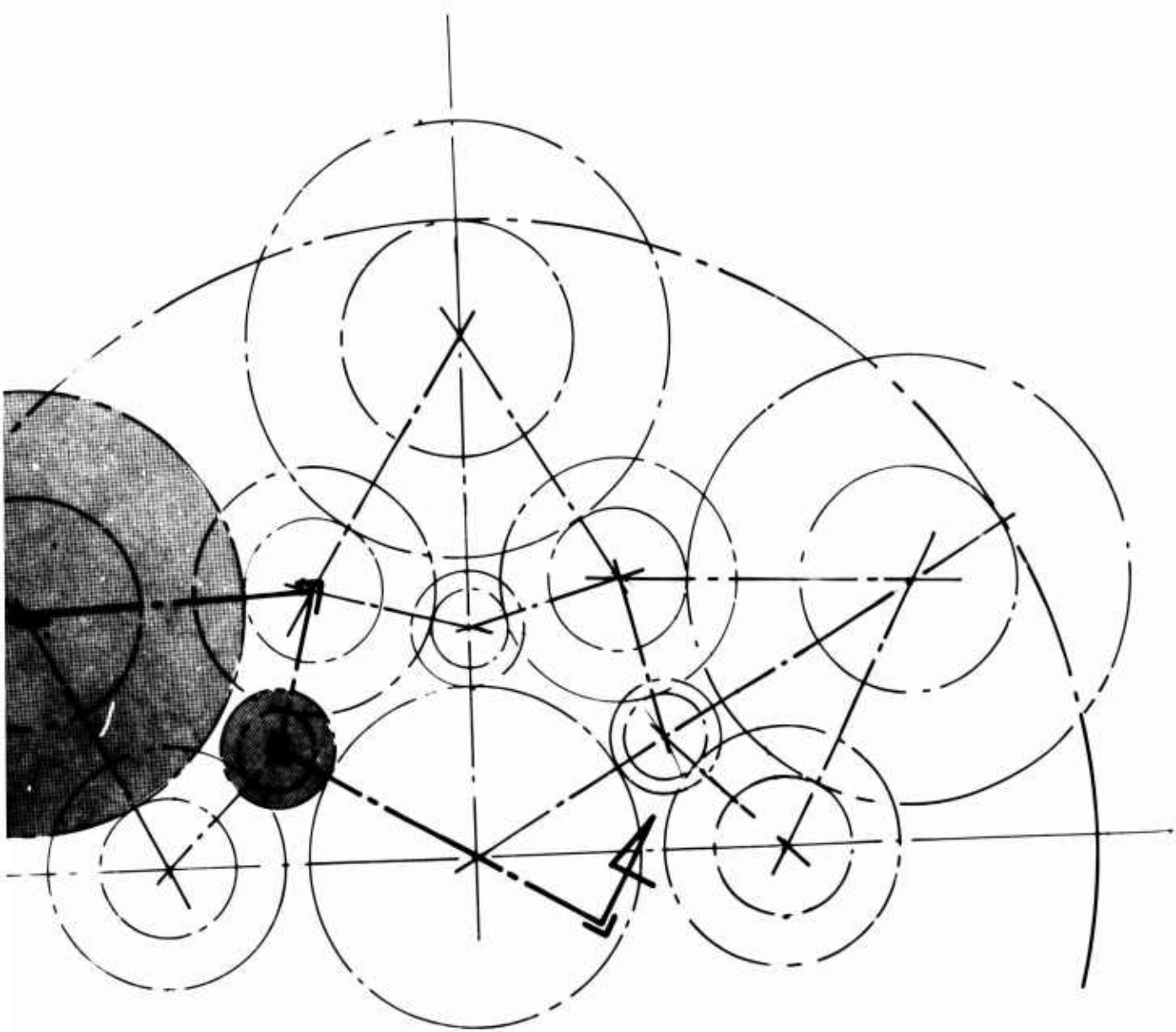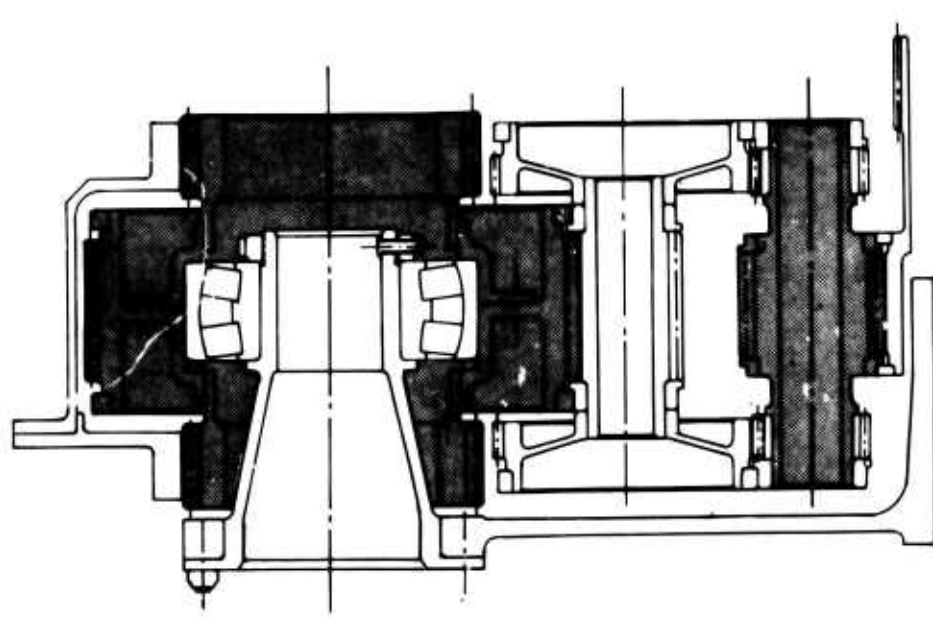
Figure 33. Three-Row, Seven Pinions per Row Layout.
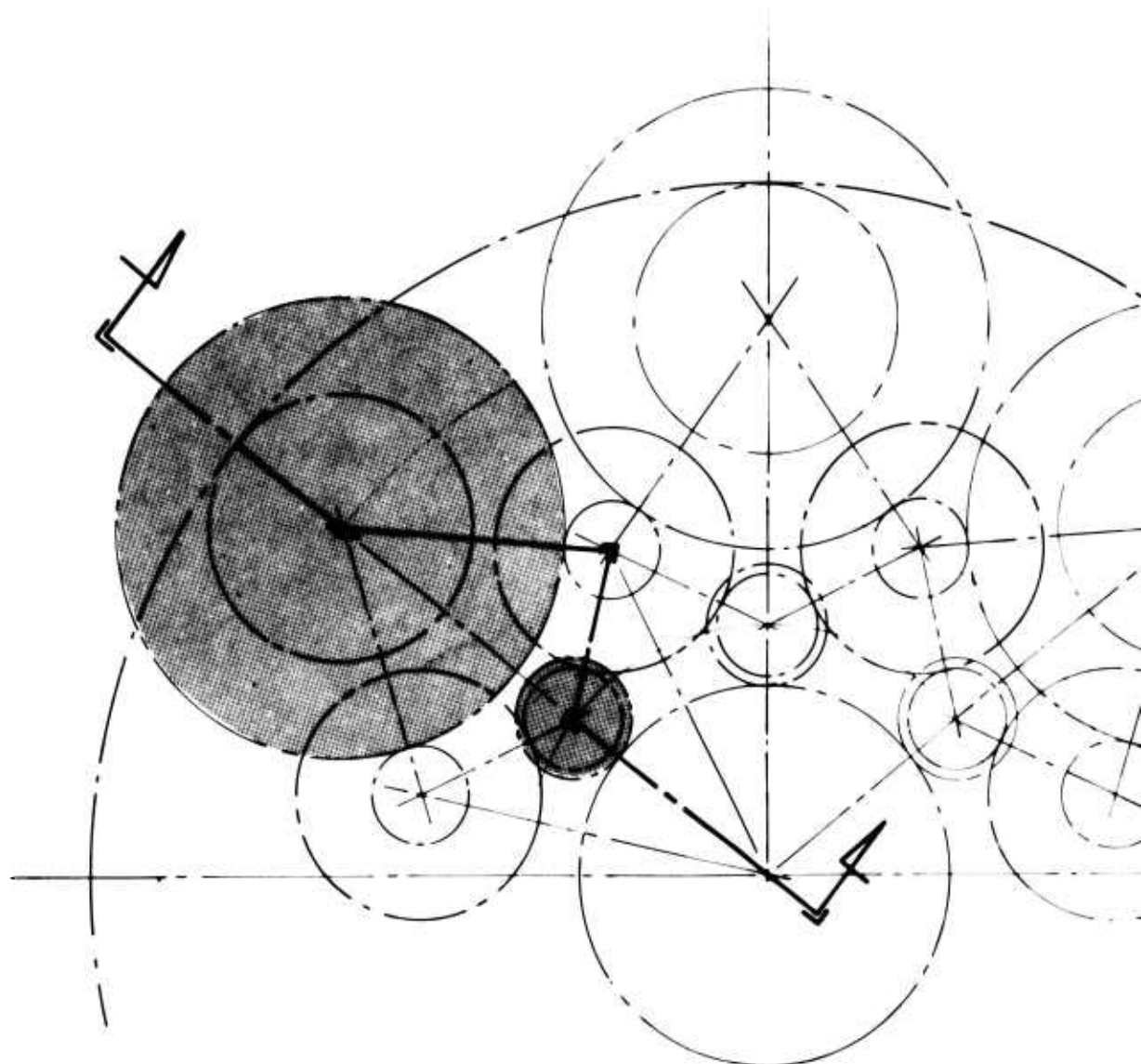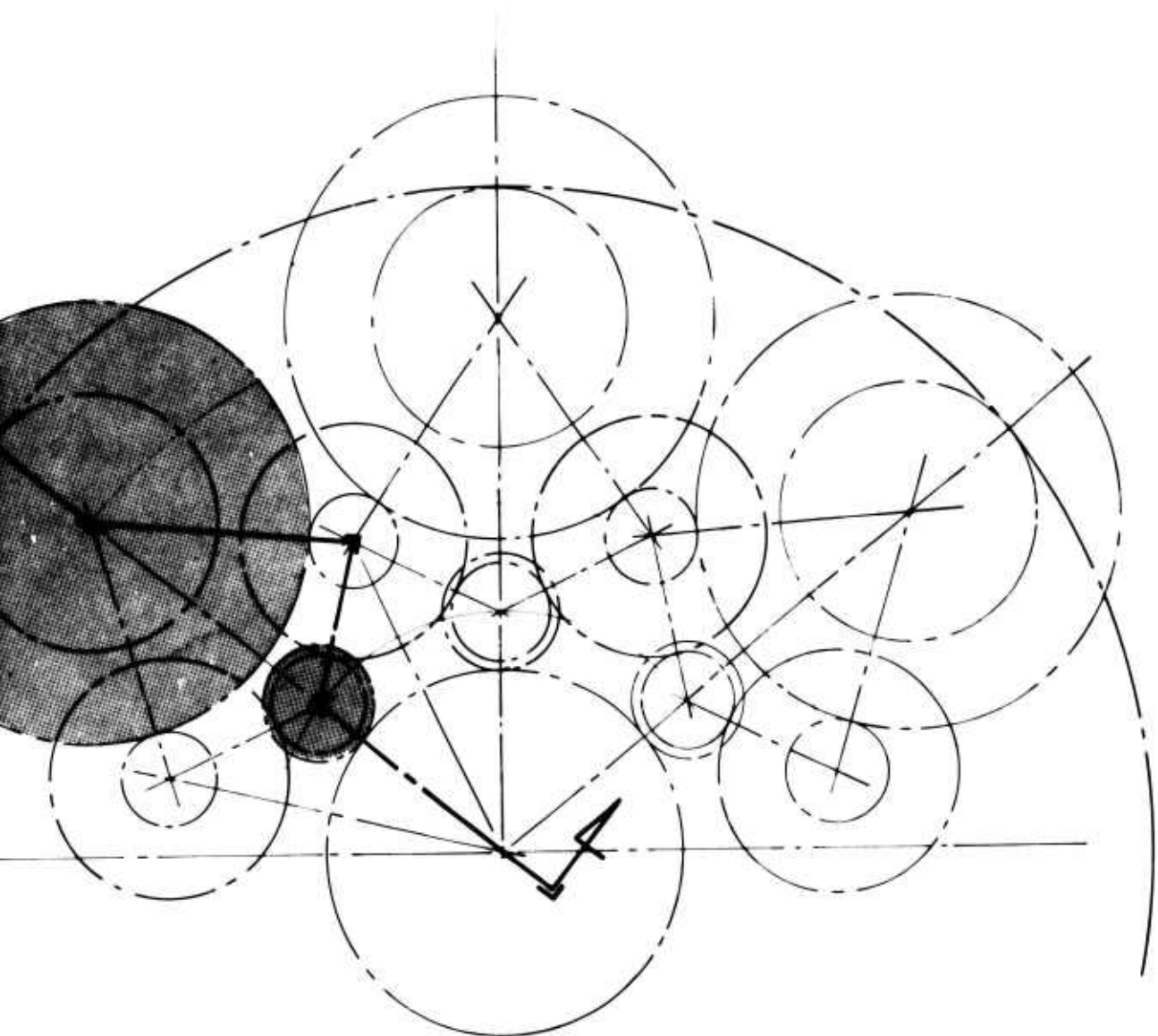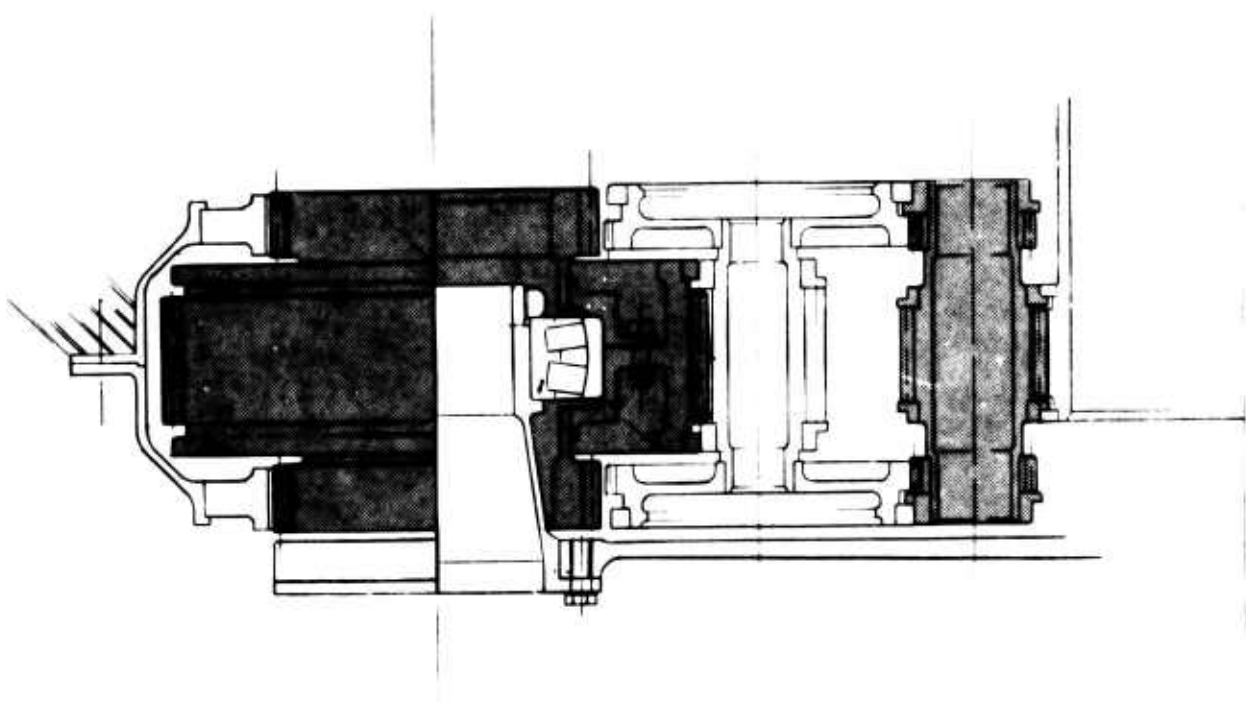
Figure 34. Three-Row, Seven Pinions per Row,
Carrier Output, Welded Ring Gear Layout.

85
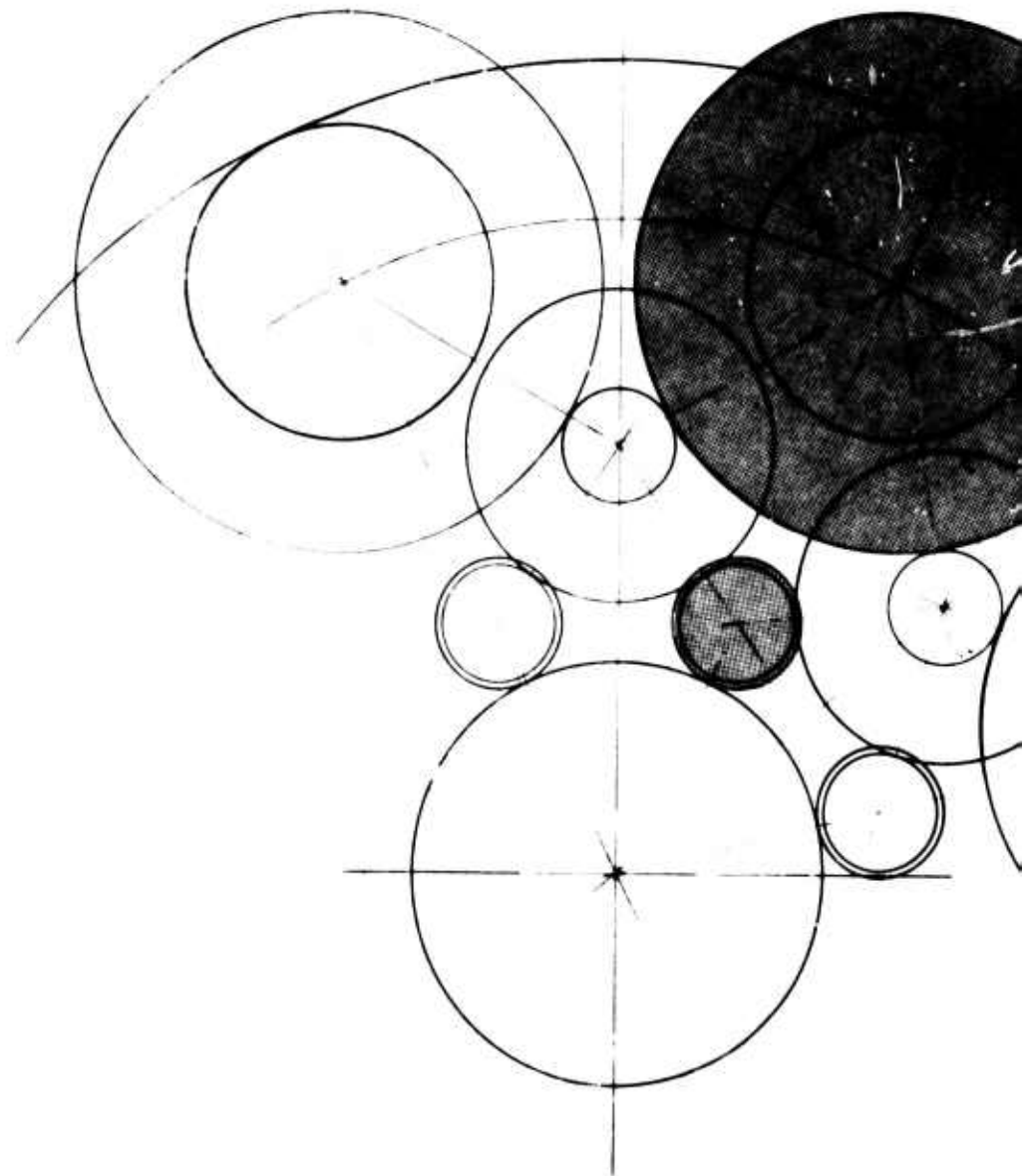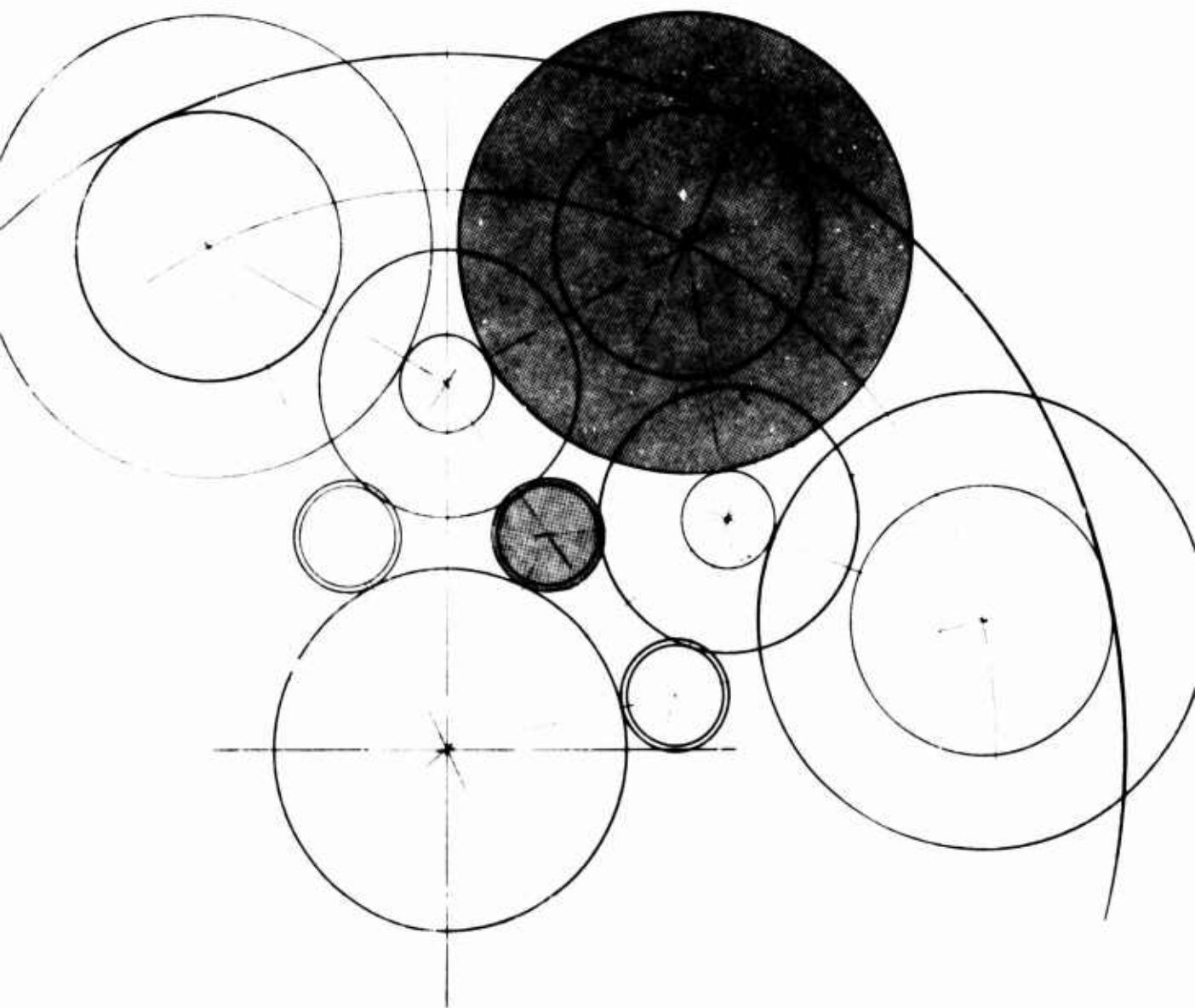
An eight pinion per row design is shown in Figure 35. This design also has a large diameter carrier post which provides for good support. However, a major problem with eight or more pinions per row is that self-preloading becomes more and more difficult to achieve because of the low toggle angles created by the eight and nine pinion geometry. Even for the cases where self-preloading is possible, the roller loads are low (less than 100 pounds at maximum horsepower).

A nine-pinion design is shown in Figure 36. In this design, the bearings have been spread outward and located under the smaller diameter outer-row gears ($Y_3$ gears). Although this spread bearing design has inherent stability, the carrier post has a relatively small diameter which weakens its structural carrying capability. Also, this roller bearing arrangement does not have the capability of high angular shaft misalignment, as does the spherical roller bearing of the previous three-row designs. For these reasons, the spread roller bearing configuration was not considered for the final design. As in the eight-pinion configuration, self-preloading is difficult to obtain with nine pinions.

A configuration with a single ring gear and single sun gear is also shown in Figure 36. This design has the same disadvantages as in the double ring gear design; i.e., the roller bearing support shaft is too small for proper support.

FINAL DESIGN SELECTION

The selection of the final roller gear drive configuration narrowed to the two-row, carrier fixed, ring gear output and the three-row, ring gear fixed, carrier output designs.

A primary consideration in these two candidate roller gear drives is weight. Preliminary layouts showed that in both designs, the optimum choice for minimum weight was seven pinions, with the two-row configuration weighing 573 pounds compared to 608 pounds for the three-row design[10]. A second consideration is efficiency. Using Buckingham,[10] the calculated efficiency of the two-row unit is 98.9 percent whereas for the three-row drive it is 98.1 percent. The number of gear elements in the two-row, ring output roller gear drive is $6n + 4$ while in the three-row, carrier output, the number of gear elements is $9n + 3$ (where n = number of pinions). Thus, the two-row design with seven pinions contains 46 gears whereas the three-row design contains 66 gears. The number of roller elements in the two-row, ring output roller gear drive is $6n + 2$ and in the three-row, carrier output, $10n + 2$. For the seven-pinion, two-row, there are 44 roller elements and for

10  E. Buckingham, ANALYTICAL MECHANICS OF GEARS, Dover Publications Inc., 1963, p. 395-408, New York, N.Y.

87
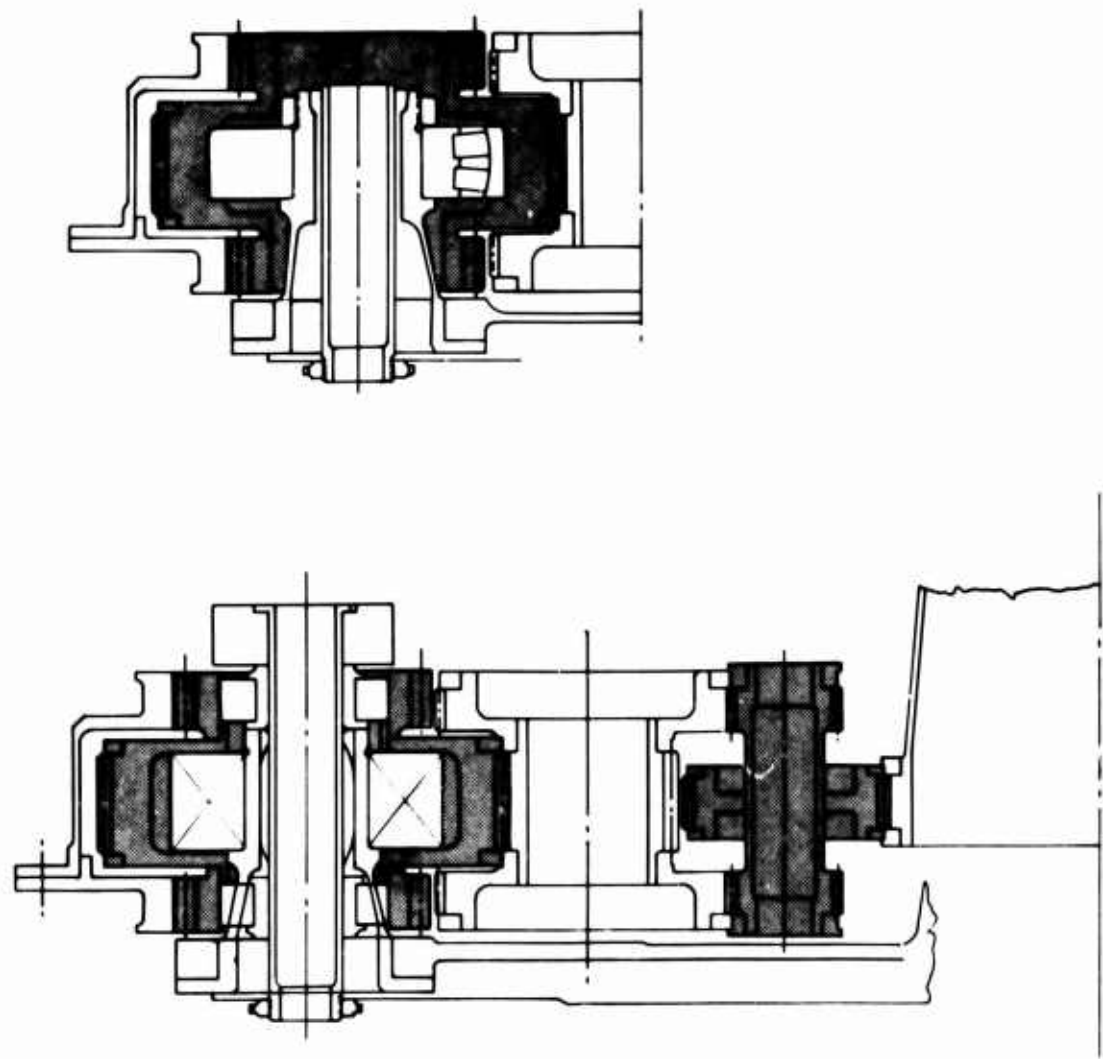
Figure 35. Three-Row, Eight Pinions per Row Layout.

89
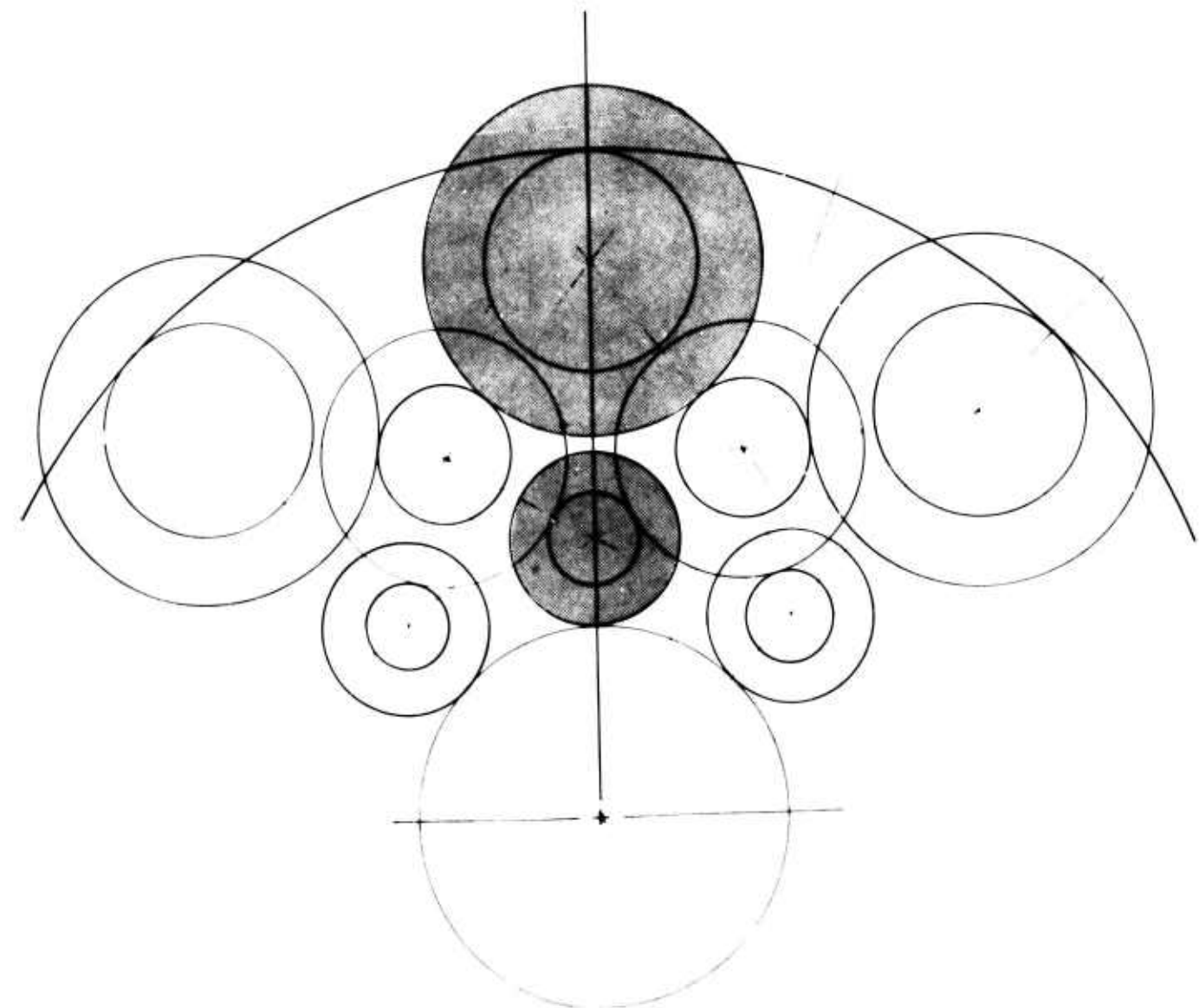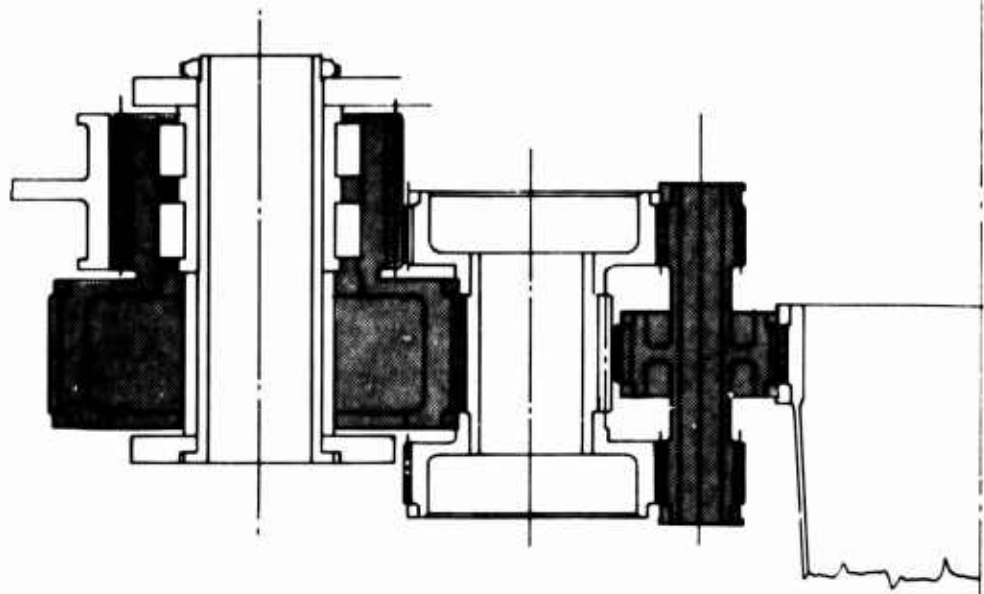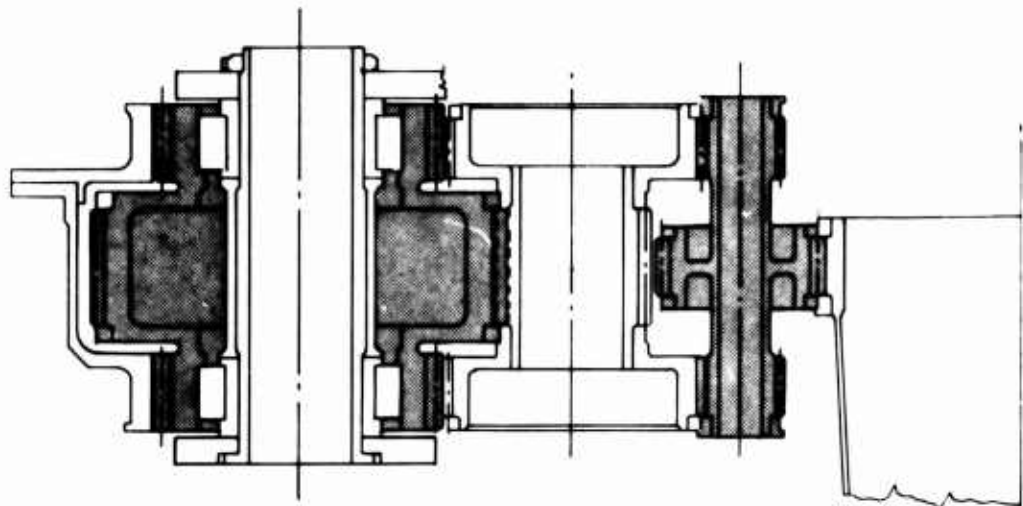
Figure 36. Three-Row, Nine Pinions per Row Layout.
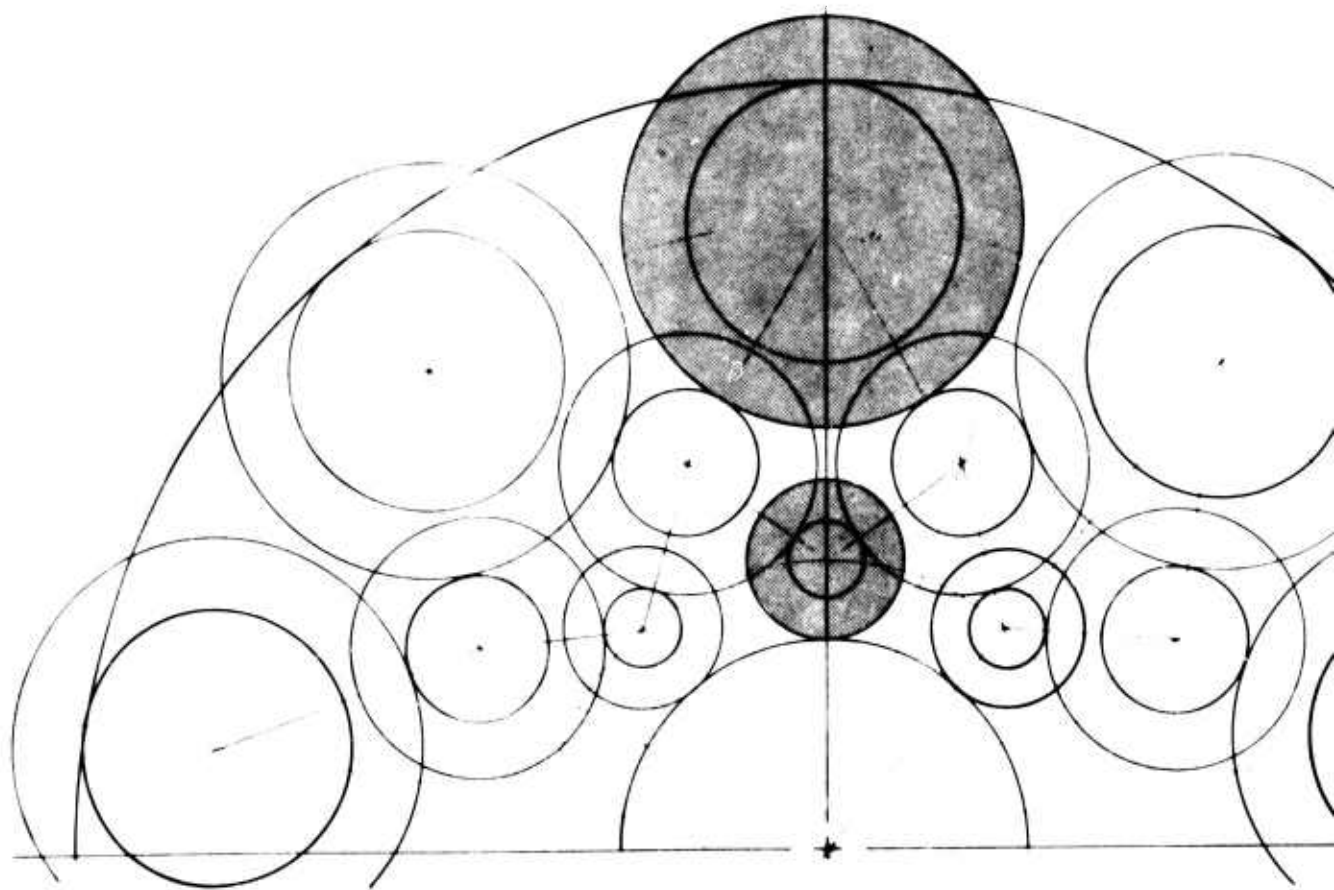
91
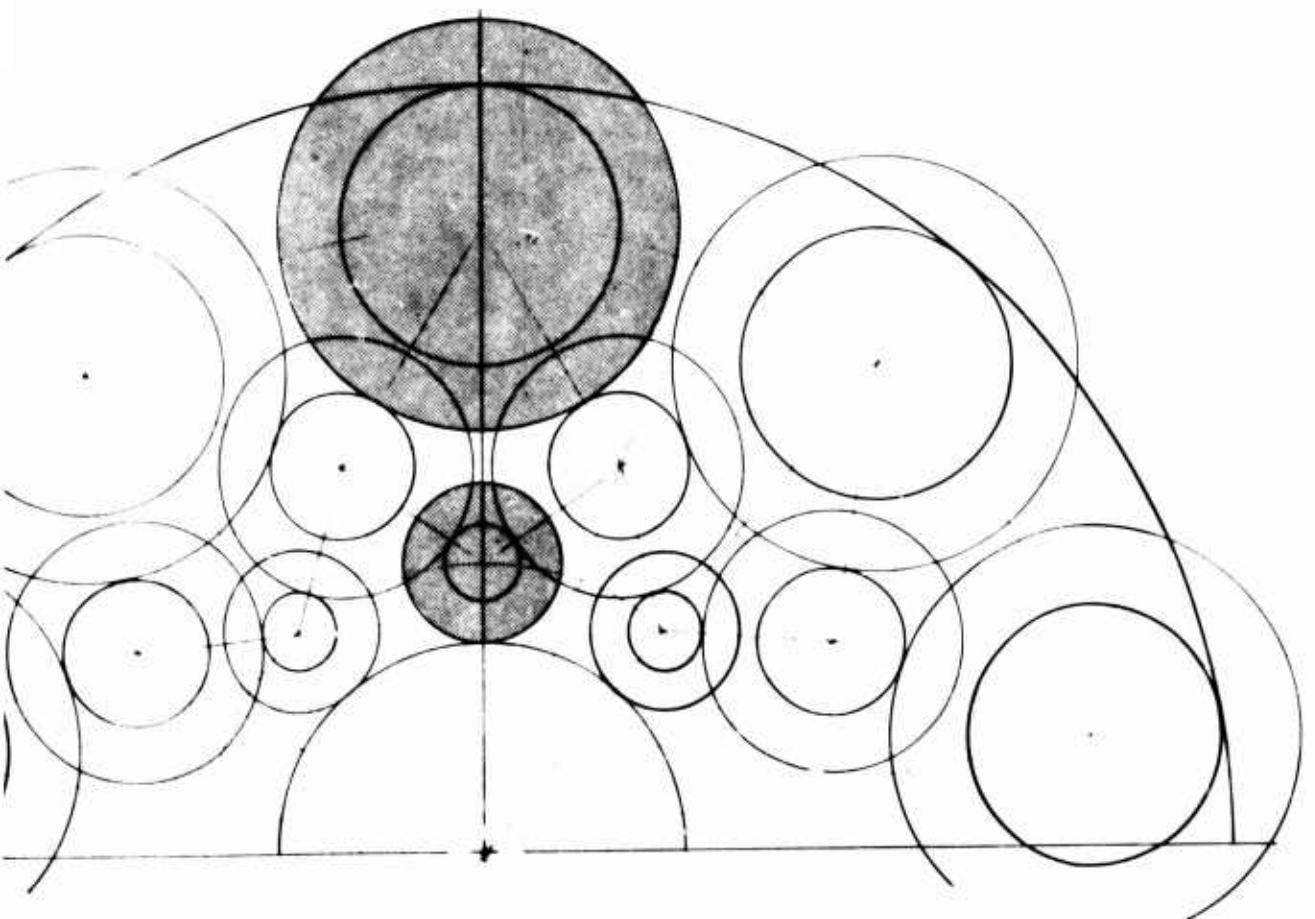
the three-row, 72 roller elements. Since there are more roller and gear elements in the three-row design than in the two-row, the reliability will be lower, assuming all components are designed for equal structural margins of safety. The cost will also be higher for the three-row configuration with more gear and roller components.

An additional consideration in the choice of a final roller gear drive is the accessibility to lubricate all gear and roller contact points. In the two-row, ring output configuration, the planet pinions in each row are stationary with respect to ground; thus, jets can be directed between the gears to lubricate all areas. In the three-row, carrier output configuration, the rows of pinions are rotating about the sun gear at the speed of the output carrier, and oil collector rings are required to meter oil to gear and roller contact points. This is a disadvantage for the three-row, carrier output design.

Rotation of the three rows of pinions about the sun gear in the carrier output roller gear drive imposes centrifugal loads on the pinions in a radial direction outward from the central sun gear. Centrifugal loads from inner rows impose themselves on each successive row toward the ring gear such that they significantly affect roller preload. This is a serious drawback of the three-row, rotating carrier output design. In the two-row, ring gear output configuration, no centrifugal forces are generated since the gears are stationary with respect to ground.

A further consideration is the effect of thermal expansion on the components of the candidate roller gear drive designs. A typical helicopter transmission operates between 200° and 250°F. Differential thermal expansion problems occur wherever an attachment is made between the steel internal transmission components and the magnesium cast housings. In the two-row roller gear drive there is a differential expansion between the carrier and housing, while in the three-row configuration, the differential expansion will take place between the housing and ring gear. The ring gear/housing differential expansion is not critical since the gear teeth will merely assume a new operating pitch line. In the two-row design, the differential expansion can be affected if the temperature induced deflection of the carrier is greater than the clearance in the carrier bearing. This disadvantage of the two-row design can be overcome by the design of a temperature compensating carrier to housing connection.

A summary of the comparative parameters for the two final roller gear drive candidate designs is presented in Table 6.

93

TABLE 6. COMPARISON, TWO-ROW VERSUS THREE-ROW DESIGN.

| Parameter | Two-Row Ring Output, Carrier Fixed 7 Pinions/Row | Three-Row Carrier Output Ring Fixed 7 Pinions/Row |
|---|---|---|
| Weight | 573 lb | 608 lb |
| Efficiency | 98.9% | 98.1% |
| Number of Gear Elements | 46 | 66 |
| Number of Roller Elements | 44 | 72 |
| Ease of Lubrication | Excellent | Poor |
| Effect of Centrifugal Force on Preload | None | Significant |
| Effect of Differential Thermal Expansion on Carrier | Significant | None |

The advantages and disadvantages of the final two candidate roller gear drive designs heavily favor the two-row, ring gear output as the best choice. Compared to the candidate three-row design, the two-row is lighter by 35 pounds, is more efficient, and has fewer numbers of gear and roller elements; therefore, it is less expensive to fabricate, is more reliable, is easier to lubricate, and has no centrifugal effects on its components. The sole disadvantage of differential thermal expansion between the carrier and housings can be eliminated by the design of a temperature compensating connection. The two-row, sun gear input, carrier fixed, ring gear output roller gear drive was therefore selected as the final design choice for the S-61 roller gear main transmission.

# ROLLER GEAR DRIVE, DETAIL DESIGN

## DESCRIPTION

The roller gear unit selected for the main transmission was the two-row, sun gear input, ring gear output, seven pinions per row design, Figure 37.

The input sun gear is spline driven by a floating quill shaft splined to the combining spur gear shaft. The sun gear splits the power to the first-row pinions into two paths to provide load equilibrium and to eliminate overturning moments about the axis of the pinions. The spline connection on the sun gear is centrally located to assure equal torsional deflection and therefore equal load on the gear teeth between both the upper and lower paths. Two rollers, located on the ends of the sun gear, are concentric with the gear pitch diameters. The sun gear is constrained in the axial direction by flanges on the ends of the rollers.

Seven first-row pinions, each containing two outer spur gears and rollers, mate with the sun gear; an inner spur gear meshes with the adjacent second-row pinions. Rollers, on each side of the inner spur gear, contain end flanges which constrain these pinions in the axial direction.

The roller gear unit is suspended from seven spherical roller bearings contained within each of seven second-row pinions. Roller side faces, adjacent to the outer spur gears of the second-row pinions, support the first-row pinions which in turn support the sun gear, Figure 38.

The central sun gear drives seven equally spaced first-row pinions. The rollers of two second-row pinions and the sun gear roller accurately position each first-row pinion. Each second-row pinion is similarly positioned by two first-row pinion rollers and, when not transmitting torque, the spherical bearing. However, when torque is being transmitted, the gear teeth mesh forces of the ring gear and second-row pinion result in the second-row pinion being reacted against two first-row pinion rollers. Figure 39 shows this star arrangement of the pinions and the roller contacts. The spherical bearings hold the second-row pinions in place and react the transmitted torque. The internal clearance of the bearing is such that under the worst case of roller tolerances plus deflections, the bearing does not react loads in the radial direction. The bearing reacts only loads in the tangential direction resulting from the reaction torque of the roller gear unit. The split ring gear has no rollers since the resultant load on the second-row pinion is radially inward.

95
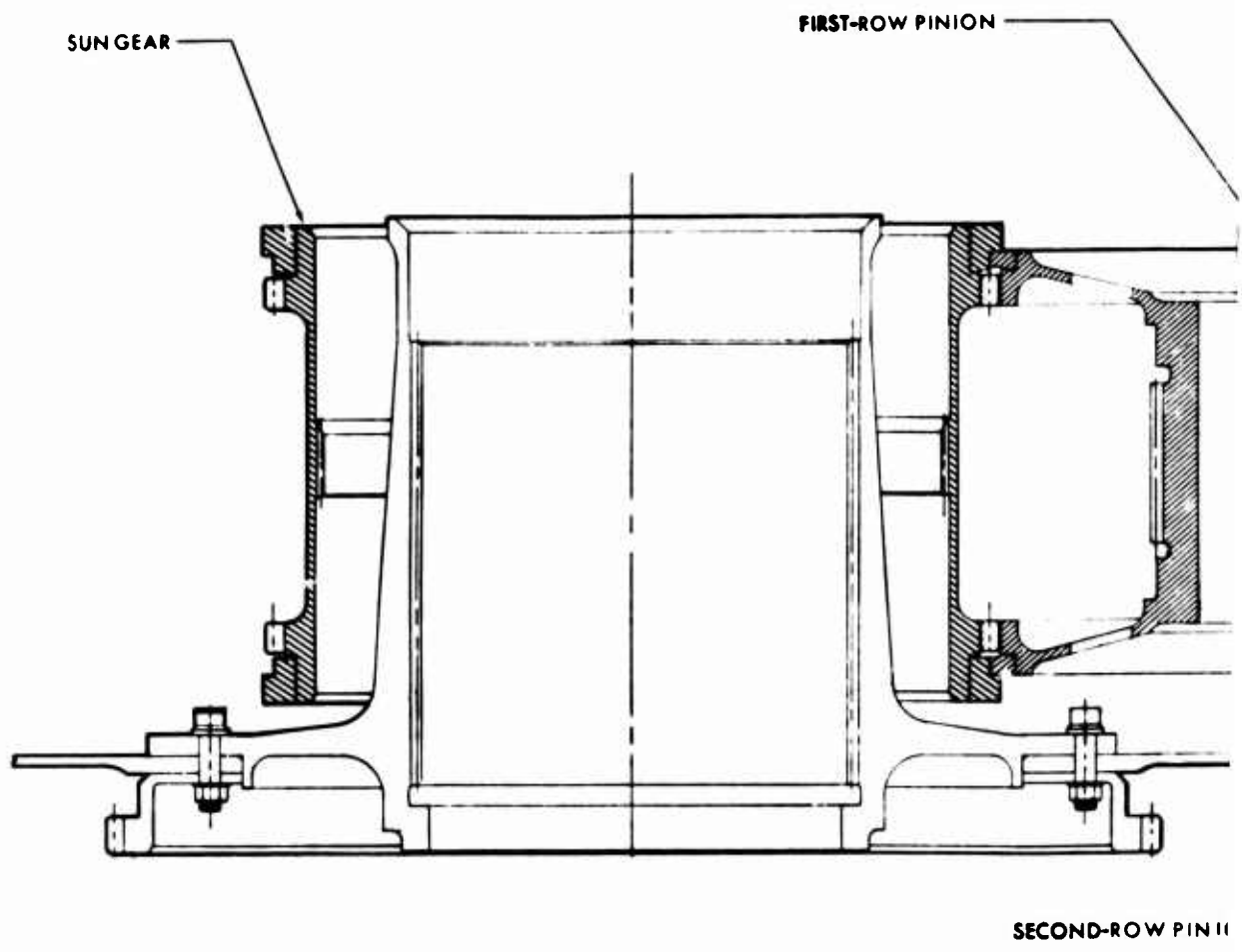
Figure 37.   Roller Gear Drive, S-61 Main Transmission.

TORQUE REACTION SPLINE
(PLATE ASSEMBLY)

POST

N

SECOND-ROW PINION

OUTPUT FLANGE ASSY

SPHERICAL BEARING

RING GEAR
ASSEMBLY
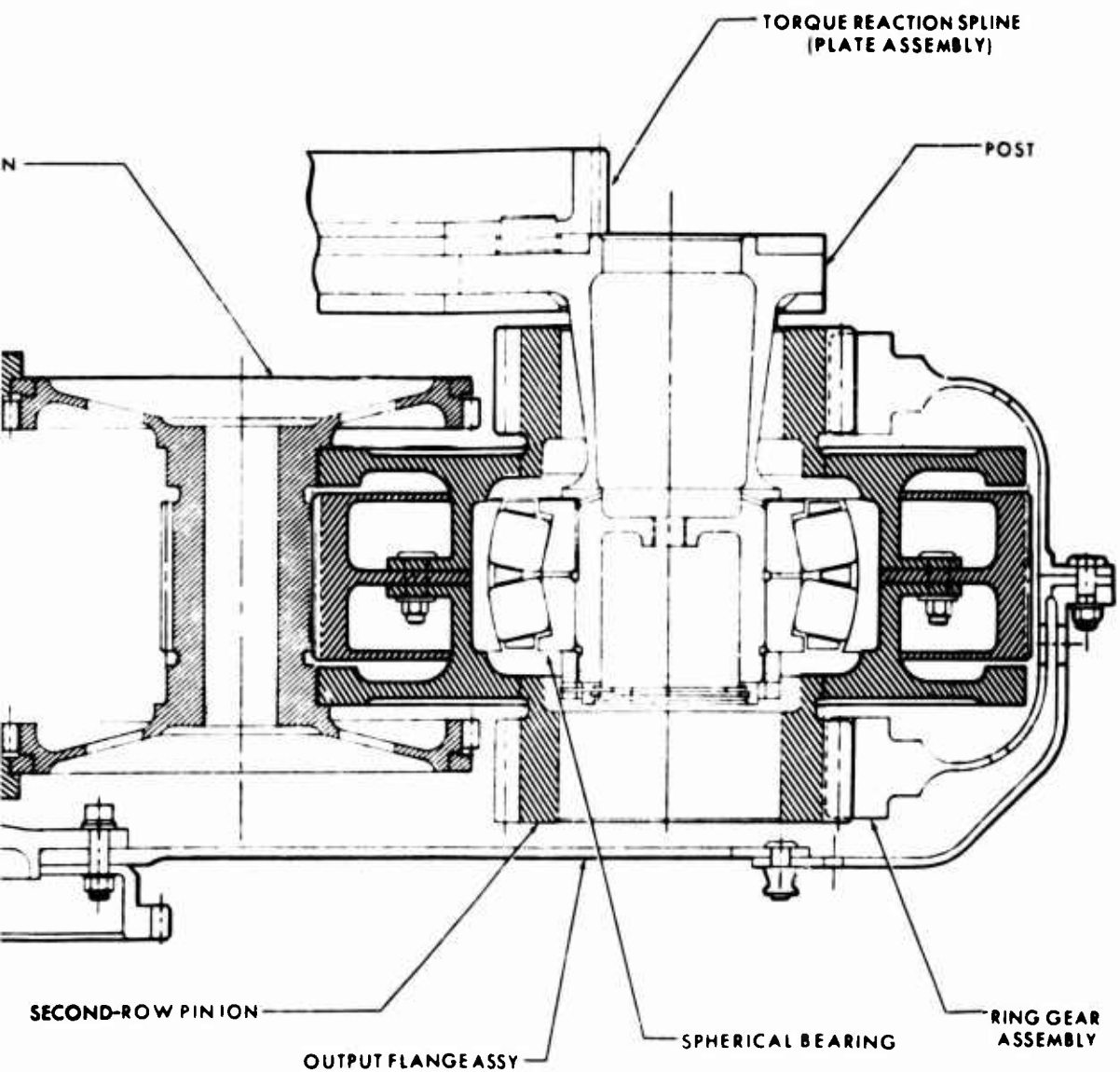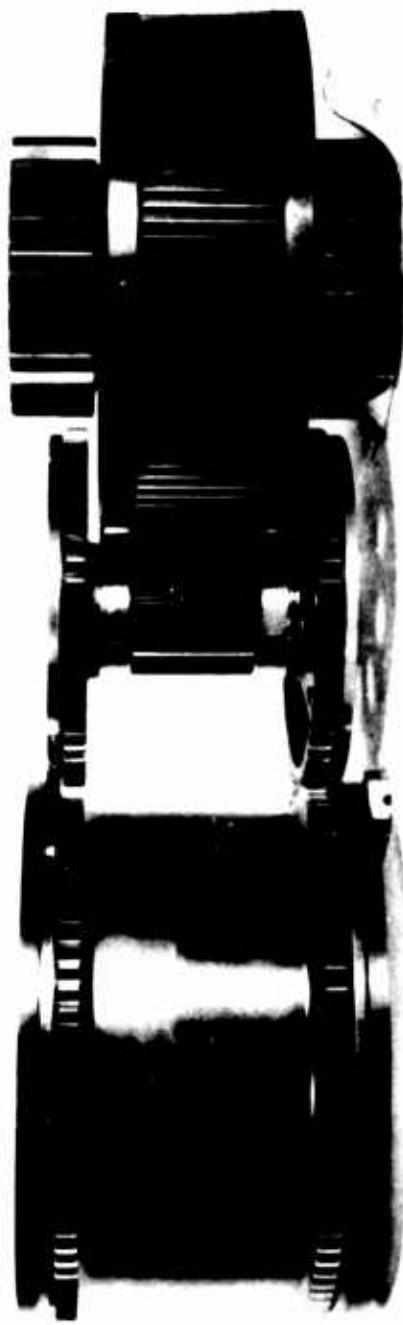
Figure 38. Roller Gear Sun, First-Row and Second-Row Pinions.

99
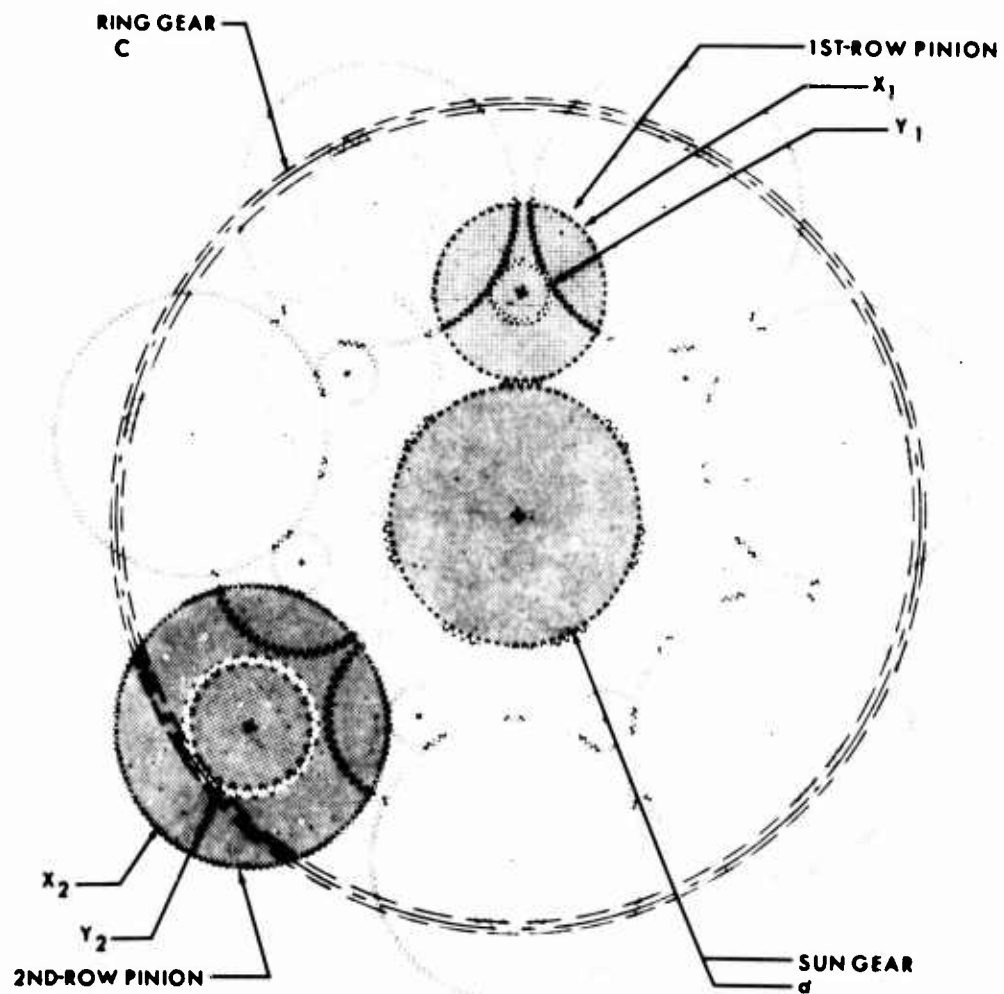
Figure 39. Star Arrangement, Roller Gear Unit.

The basic data for this roller gear unit is presented in Table 7.

| Location | Diametral Pitch | No. of Teeth | Pitch Diameter (in.) | Pressure Angle (deg) |
|---|---|---|---|---|
| | | TABLE 7. ROLLER GEAR BASIC DATA. | | |
| Sun - a | 9.448 | 84 | 8.89077 | 22.5 |
| First-Row - $X_1$ | 9.448 | 58 | 6.13887 | 22.5 |
| First-Row - $Y_1$ | 13.217 | 27 | 2.04282 | 25.0 |
| Second-Row - $X_2$ | 13.217 | 126 | 9.53318 | 25.0 |
| Second-Row - $Y_2$ | 5.583 | 25 | 4.47788 | 30.0 |
| Ring - c | 5.583 | 154 | 27.58374 | 30.0 |

The reduction ratio of the roller gear drive is

$$RR = \frac{(58)\ (126)\ (154)}{(27)\ (\ 25)\ (\ 84)} = 19.848$$

The roller loads in the roller gear drive are a function of gear loads and roller gear geometry. Whenever torque is trans- mitted in the roller gear drive unit, tangential and radial gear tooth loads are induced. The rollers, which transmit loads normal to the rolling surface, must react the resultant loads from the gear teeth. By careful choice of the roller gear design parameters, the roller reactive loads are made positive, i.e., "self-preloading", thereby ensuring stability of the three-point support. This is achieved by using successively higher gear teeth pressure angles for each gear mesh from the sun gear to the ring gear. The S-61 roller gear unit has no roller loads when at rest. As soon as power is applied, however, positive roller loads are generated and all the roller gear members move radially inward to contact each other, thus forming a preloaded assembly. A chart of the preload forces is presented in Figure 40.

101
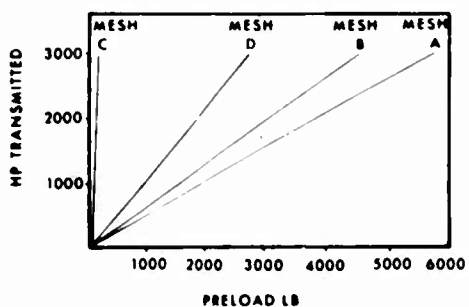
Figure 40.   Roller Preload Forces.

In order to ensure ideal gear operating conditions, the
rollers, which control the gear operating center distance, are
designed to equal the sun gear/first-row pinion pitch diameters
when transmitting full power.   The rollers are therefore
designed slightly oversize to compensate for the compressive
deflections induced by the roller preload forces shown in
Figure 40.   The first-row/second-row pinion preloads at B
(4,500 lb) and C (140 lb), however, vary so greatly when
transmitting 3,000 hp that no deflection compensation is made.
Table 8 gives the free state roller diameter.

Figure 41 shows the roller gear unit, mounted on an assembly
fixture and ready for installation in the main transmission
housing.   Identifying marks are visible on the sun gear and
first-row pinions which indicate the master teeth that have
to be aligned during assembly.

| TABLE 8.   ROLLER DIAMETERS | |
|---|---|
| Location | Diameter (in.) |
| Sun Gear Roller - a | 8.8917 8.8913 |
| First-Row Pinion Roller - $X_1$ | 6.1395 6.1391 |
| First-Row Pinion Roller - $Y_1$* | 2.0431 2.0427 |
| Second-Row Pinion Roller - $Y_2$* | 9.5335 9.5331 |

* These rollers are not corrected, as the two loading conditions vary greatly.
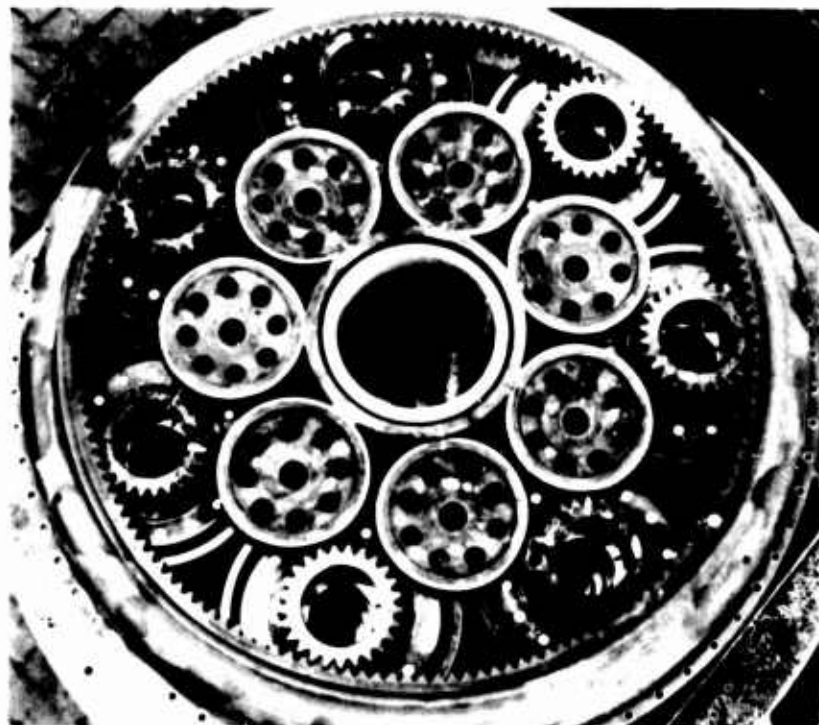


Figure 41.   Roller Gear Unit.

103

## SUN GEAR

The sun gear consists of three elements: a central gear shaft
and two identical end rollers, Figure 42. The rollers are
electron-beam-welded to the shaft to form an assembly.
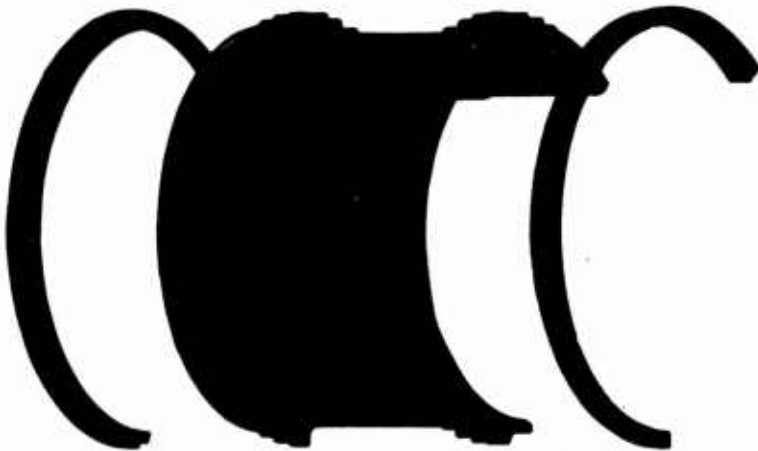


Figure 42.   Sun Gear, Exploded View.

An input spline drive is located in the center of the gear
shaft to equalize torsional wind up of the shaft at the gear
teeth.  Gear teeth parallelism then remains constant at all
levels of power transmission, thus ensuring equal load sharing.
The maximum permissible misalignment across the gear teeth is
.0004 inch, Figure 43.

To improve the gear meshing contacts, the gear teeth profiles
are modified.  The amount of modifying, or relieving, is equal
to the amount of deflection that occurs when the gear teeth
contact the driven gear when transmitting maximum power.  As
the teeth are cantilevered beams acting under elastic loading
condition, the gear tooth deflection is determined consider-
ing the shear, bending and compressive deflections induced on
the tooth.  The tip relief is incorporated onto the tooth
profile from the high point of single tooth contact.  The root
flank profile is also relieved, to eliminate high spots on the
tooth profile, Figure 44.
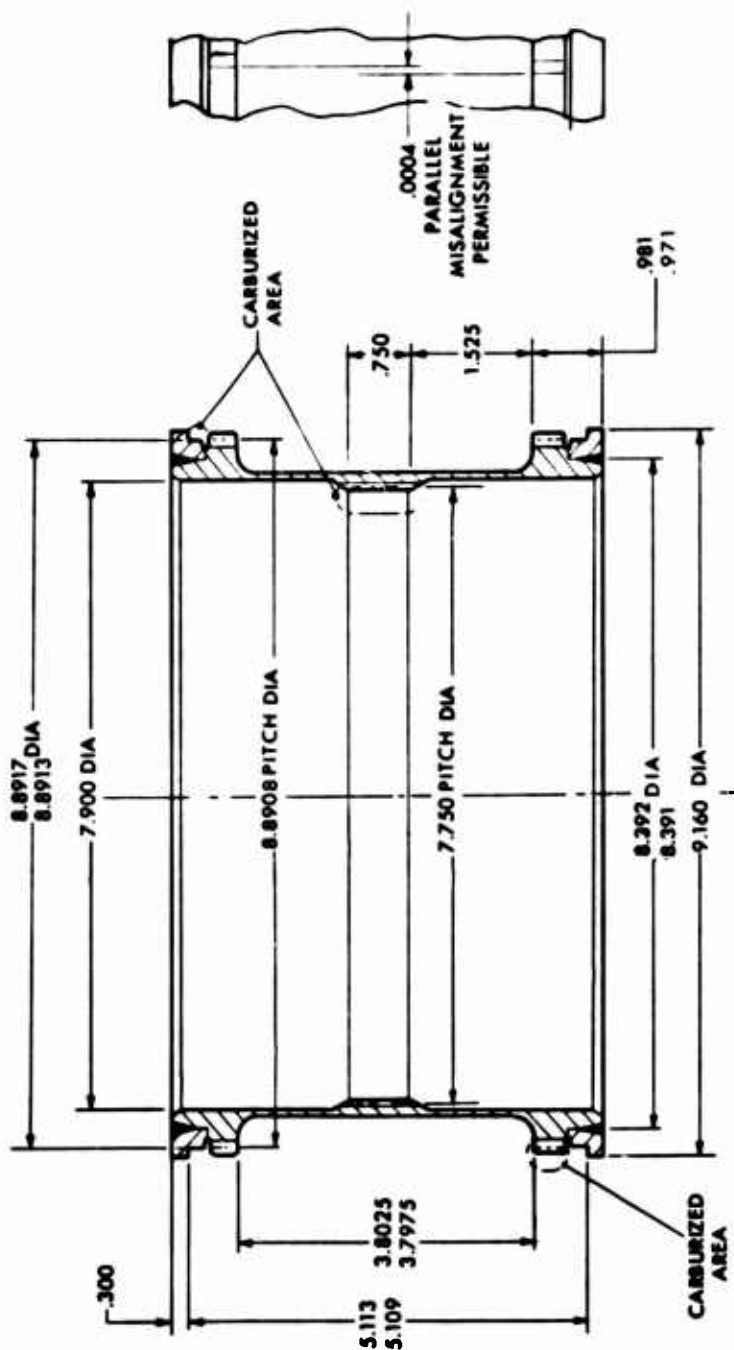
Figure 43. Sun Gear Dimensions.
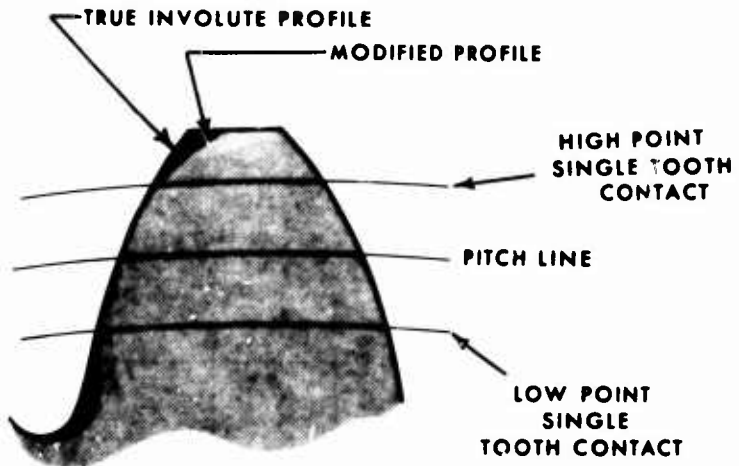
Figure 44. Modified Tooth Profile.

The electron beam welds are located at the centroid of the
section between the roller diameter and inside diameter of the
gear shaft. At this point, the tensile stresses due to bending
of the roller rim are a minimum; the shear stresses are a
maximum. Weld stresses are therefore a maximum in the direc-
tion of maximum weld strength.

Figure 45 shows the initial weld configuration. The undercut
between the roller and gearshaft is to accommodate weld
splatter. However, when the weld does not penetrate into the
undercut, voids remain at the root of the weld and incomplete
fusion of the joint occurs. To eliminate the stress risers
that these induce, the root area of the weld was removed as
shown in the modified configuration, Figure 45.



INITIAL DESIGN                    MODIFIED DESIGN
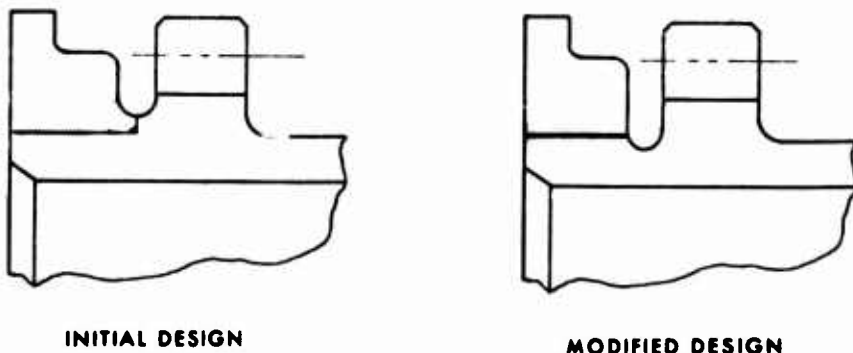
Figure 45.   Initial and Modified Design Weld Root Relief.

## FIRST-ROW PINION

The first-row pinion incorporates the $X_1$ - $Y_1$ gears and rollers and consists of a central gear member, two identical outer gears and two outer rollers, Figure 46. The design configuration permits the $Y_1$ gear to be carburized, hardened and finish machined prior to assembly of the outer gears. A close tolerance push-fit on the locating diameter of the inner/outer gears ensures concentricity while still allowing the semifinished outer gear teeth to be rotated to align with the inner gear prior to welding. After welding, the locating diameter is machined off and the outer gears are finish machined in relationship to an index tooth on the inner gear.
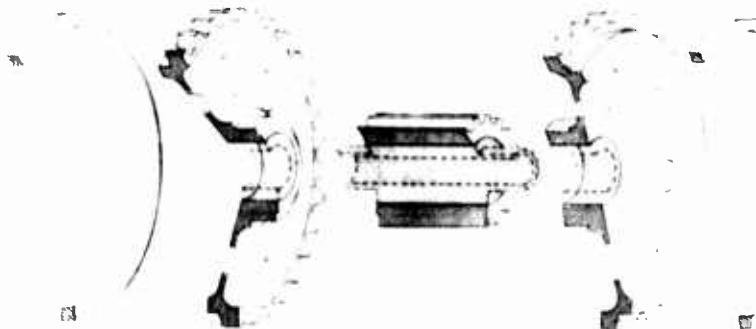
Figure 46. First-Row Pinion, Exploded View.

A set of seven pinions has to have the identical "X" dimension, shown in Figure 47, within ± .0002 inch. The "X" dimension can be of any value provided all seven pinions are identical. By measuring to the drive side of the inner and outer gear teeth, tooth spacing and thickness tolerances are not included. A method used to measure this dimension is shown in Figure 48. After finish machining of the outer gears, the rollers are electron-beam-welded and finish ground concentric to the pitch diameter of the gears. Figure 49 depicts the gear teeth alignment and concentricity requirements.
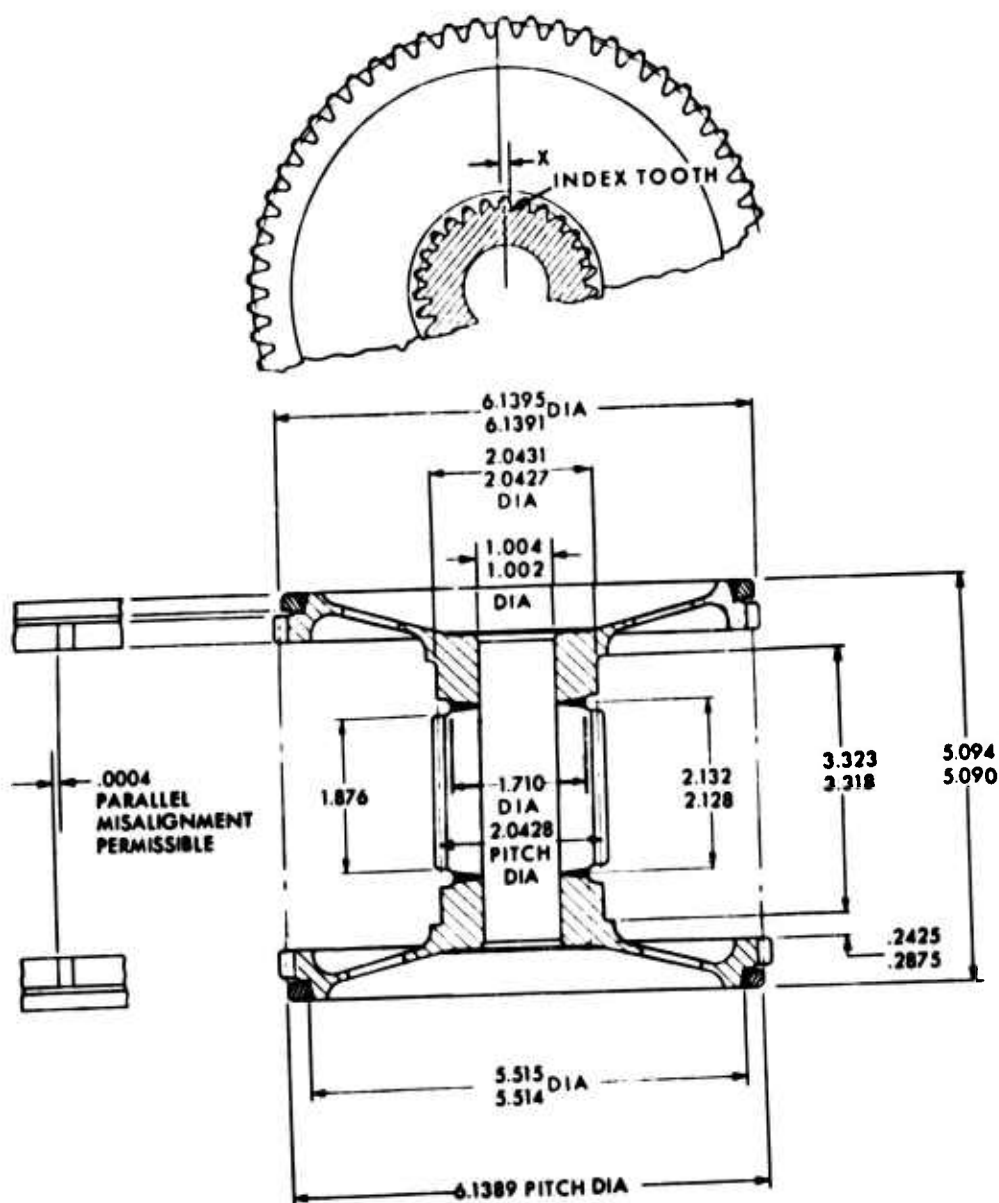
Figure 47. First-Row Pinion Dimensions.
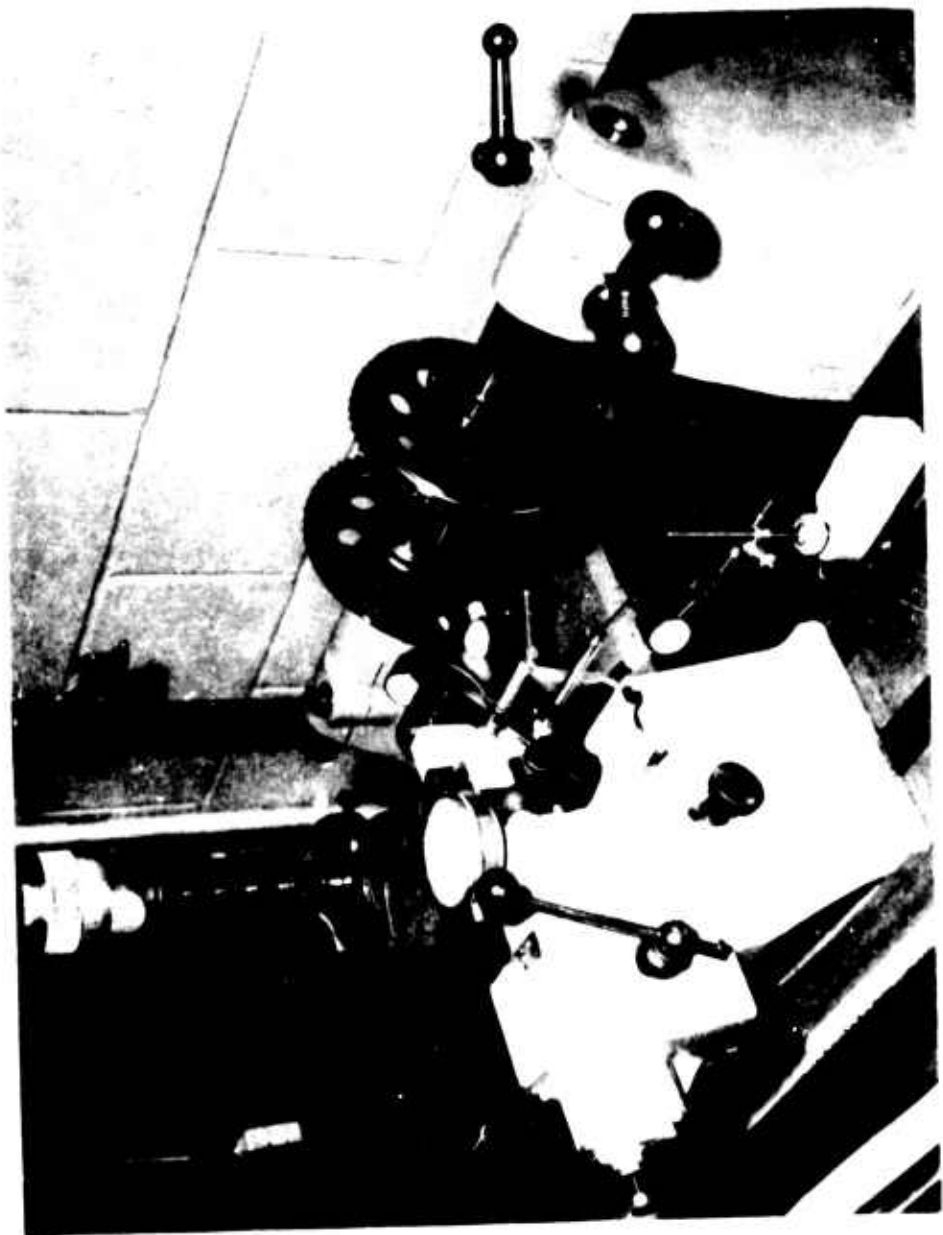
Figure 48. Inspection, First-Row Pinion.

109
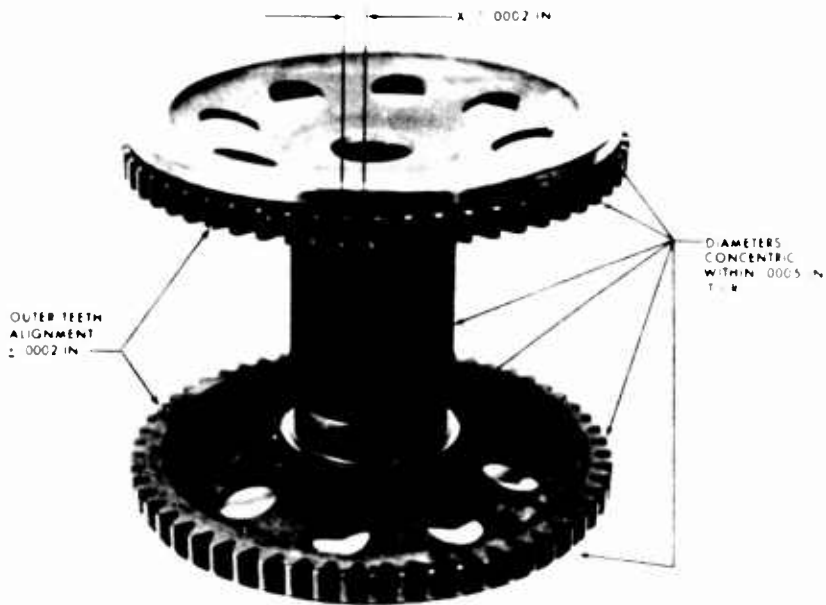
Figure 49.  Concentricity Requirements, First-Row Pinion.

The initial configuration of the first-row pinion, Figure 50, was designed with a longitudinal weld to join the outer gears to the inner gear.  Initial development testing of roller gear units with this design resulted in fracture of the $Y_1$ roller. Metallographic examination revealed a series of voids along the weld line with cracks extending from the voids.  It became apparent that the weld was too deep for the constraints imposed.  Increasing the depth of weld penetration would induce more heat into the part than is desirable.  This would temper the case-hardened surface of the $Y_1$ roller, thereby reducing the required $R_c$ 58-64 roller surface hardness.  The butt-welded joint was designed to eliminate the problem.

The outer roller weld was modified to remove any root weld porosity.  This was accomplished by machining out the root area of the weld similar to that accomplished on the sun gear.

110
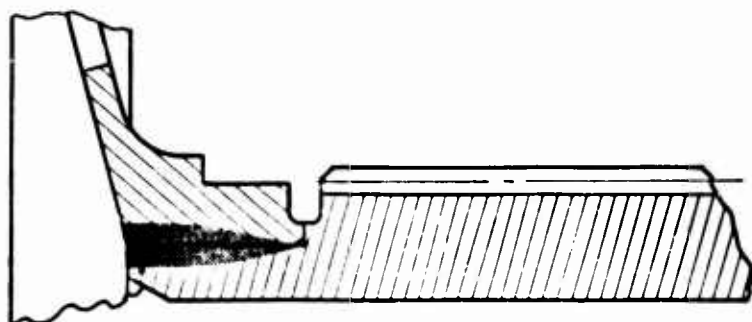
LONGITUDINAL WELD CONFIGURATION

VOIDS AT ROOT OF WELD
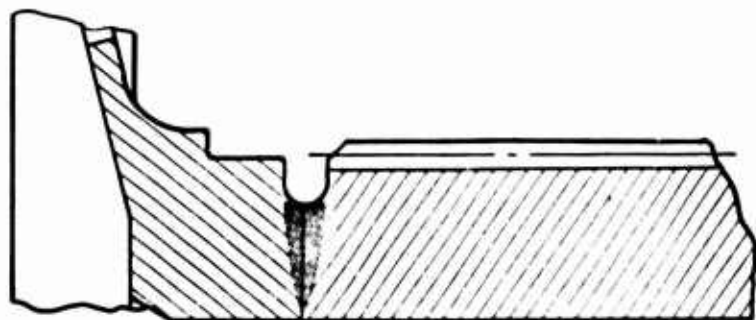
BUTT-WELD CONFIGURATION

Figure 50.  Weld Configurations, First-Row Pinion.

## SECOND-ROW PINION

The second-row pinion locates the spherical roller bearing which reacts the transmitted torque.

The initial pinion design, shown in Figure 51, consisted of an assembly of seven fabricated parts. These comprised two identical end gears $(Y_2)$, two rollers $(X_2)$, a central shaft and gear $(X_2)$ and an end flange which is bolted to the center gear web by taper-shank bolts.



Figure 51.   Second-Row Pinion (Initial Design).

To assist in the manufacture, each part was detailed separately and then assembled for further machining in the sequence depicted in Figure 52.

-051

-057

-053

-054

-055
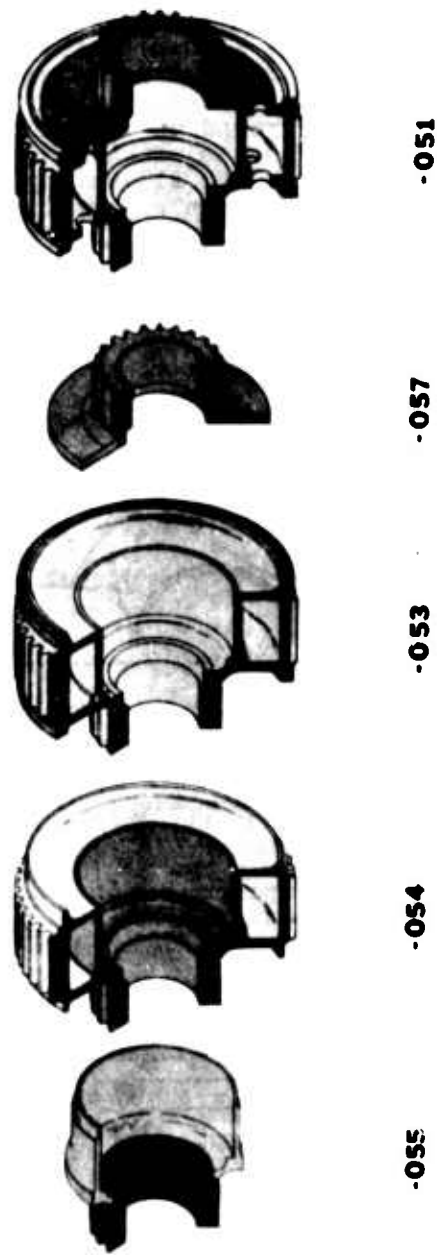
Figure 52. Fabrication, Second-Row Pinion (Initial Design).

The end gears are finish machined as a matched set to ensure that tooth spacing and gear teeth thickness tolerances are identical. A gear is then electron-beam-welded to the central shaft which is, in turn, welded to the semifinished carburized, hardened and rough ground center gear. Marked index teeth are aligned prior to welding. After welding, the center gear teeth are finish ground in relation to the small gear teeth. The "X" dimension to which the index teeth are ground can be of any value provided all seven pinions of one set are identical within ± .0002 inch allowable tolerance. The rollers are welded to the center gear assembly and the welded flange and gear assembly positioned by taper-shank bolts to obtain end gear alignment within ± .0002 inch, Figure 53.
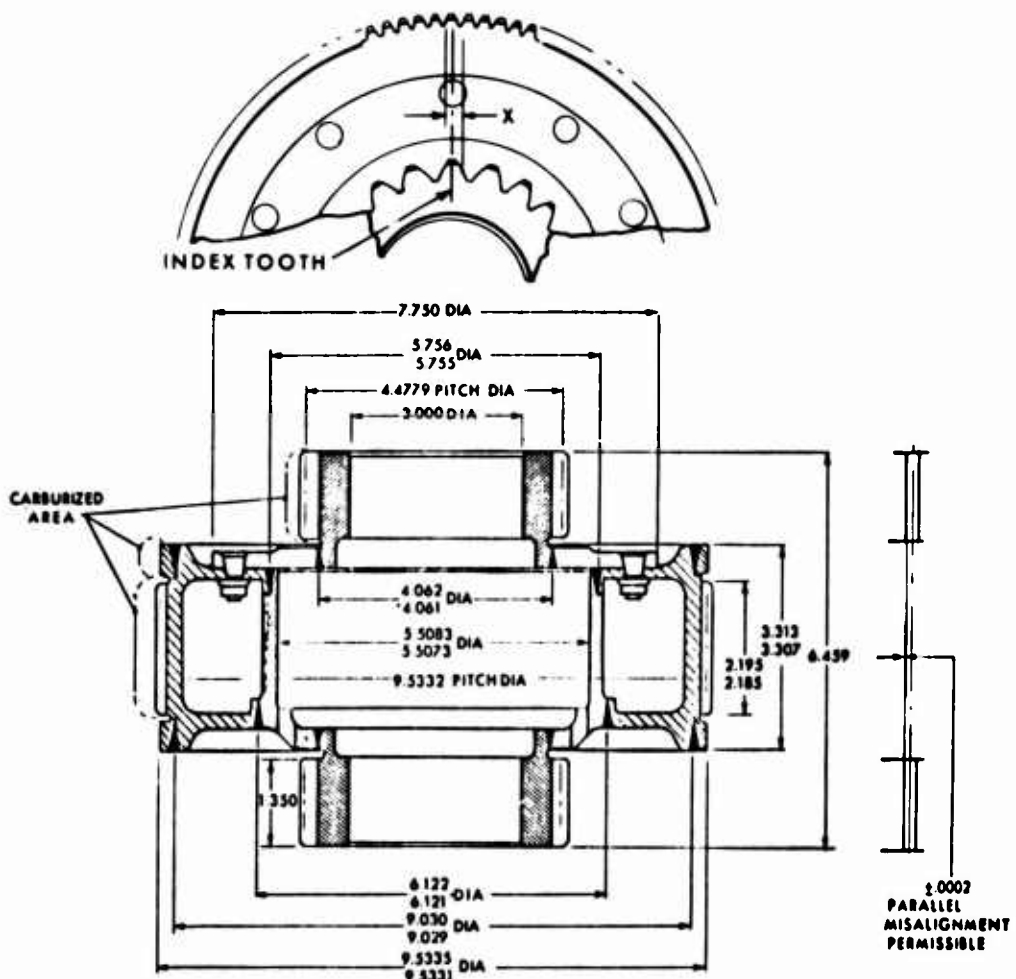


Figure 53. Second-Row Pinion Dimensions (Initial Design).

114

The second-row pinion, Figure 53, incorporates a design modification wherein the face width of the end gears, $Y_2$, was reduced from 1.440 inches to 1.350 inches. The resulting wider undercut between the end gear face and flange face allowed a thicker blast shield to be positioned under the electron-beam-welded joint. A wider, more powerful beam was then used to ensure complete fusion of this joint.

At the completion of tiedown testing of the roller gear transmission on a Sikorsky S-61 helicopter, ultrasonic inspection revealed cracks in the roller weld of the second-row pinions. Further testing was conducted in the regenerative facility, which was utilized for the Reliability and Maintainability test phase of this program.

At 15 and 40 hours of test, ultrasonic inspection revealed no significant increase in the flaw size. However, at 57.75 test hours, fracture of a second-row pinion occurred, Figure 54.

Initial fracture occurred at the bearing bore weld; at this time, secondary fracture occurred in the area of the outer roller weld due to the large leverage load from the unsupported ring gear mesh forces. Metallographic examination revealed that fracture initiated at voids in the root of the weld and progressed to the inside bearing bore, Figure 55. Fractographic analysis of the cracked roller weld, which did not contribute to the failure, Figure 56, showed that the fracture initiated from the root of the weld at the interface of the melt and heat-affected zones.

From this investigation, a redesign program resulted with the objective of eliminating blind electron beam welds.
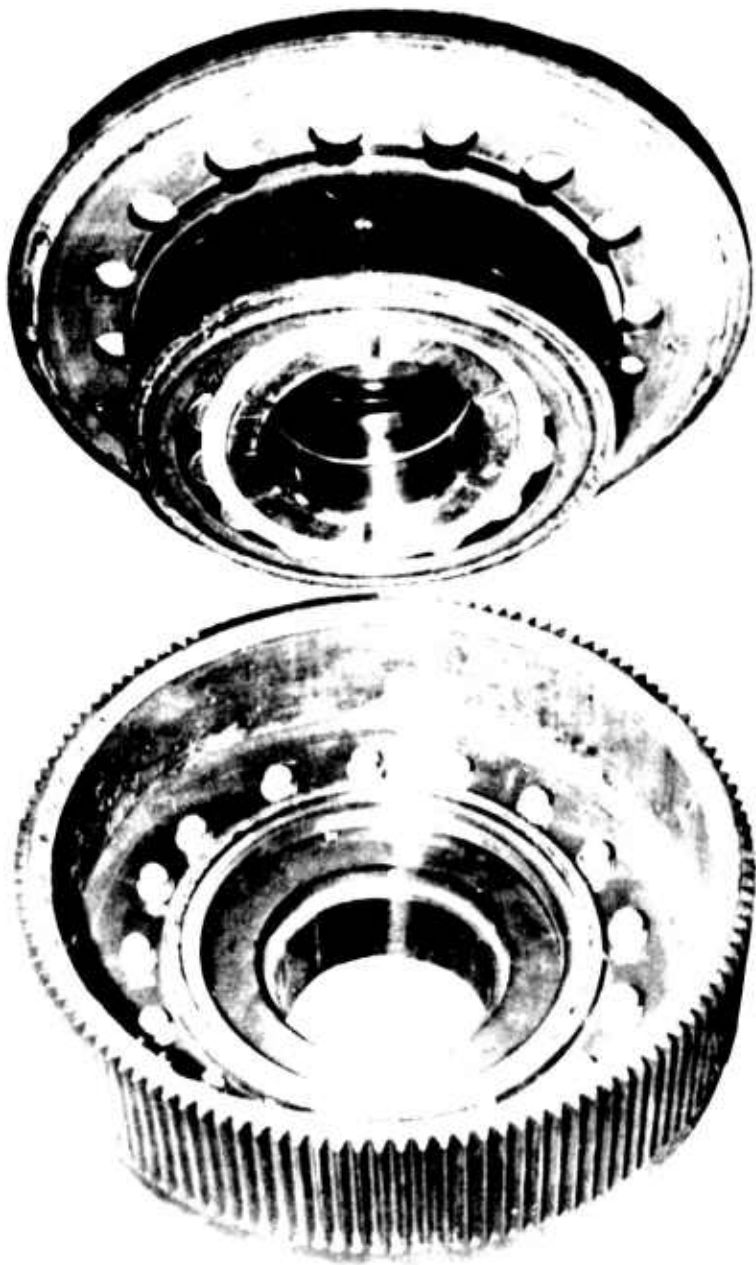
Figure 54. Fractured Second-Row Pinion.

116

CROSS SECTION
SECOND-ROW PINION

ELECTRON
BEAM WELD

FRACTURE LOCATION

MACHINED SURFACE

GAS HOLES
ORIGIN OF FRACTURE

FRACTURED SURFACE

SECTION A A DETAIL OF FRACTURE
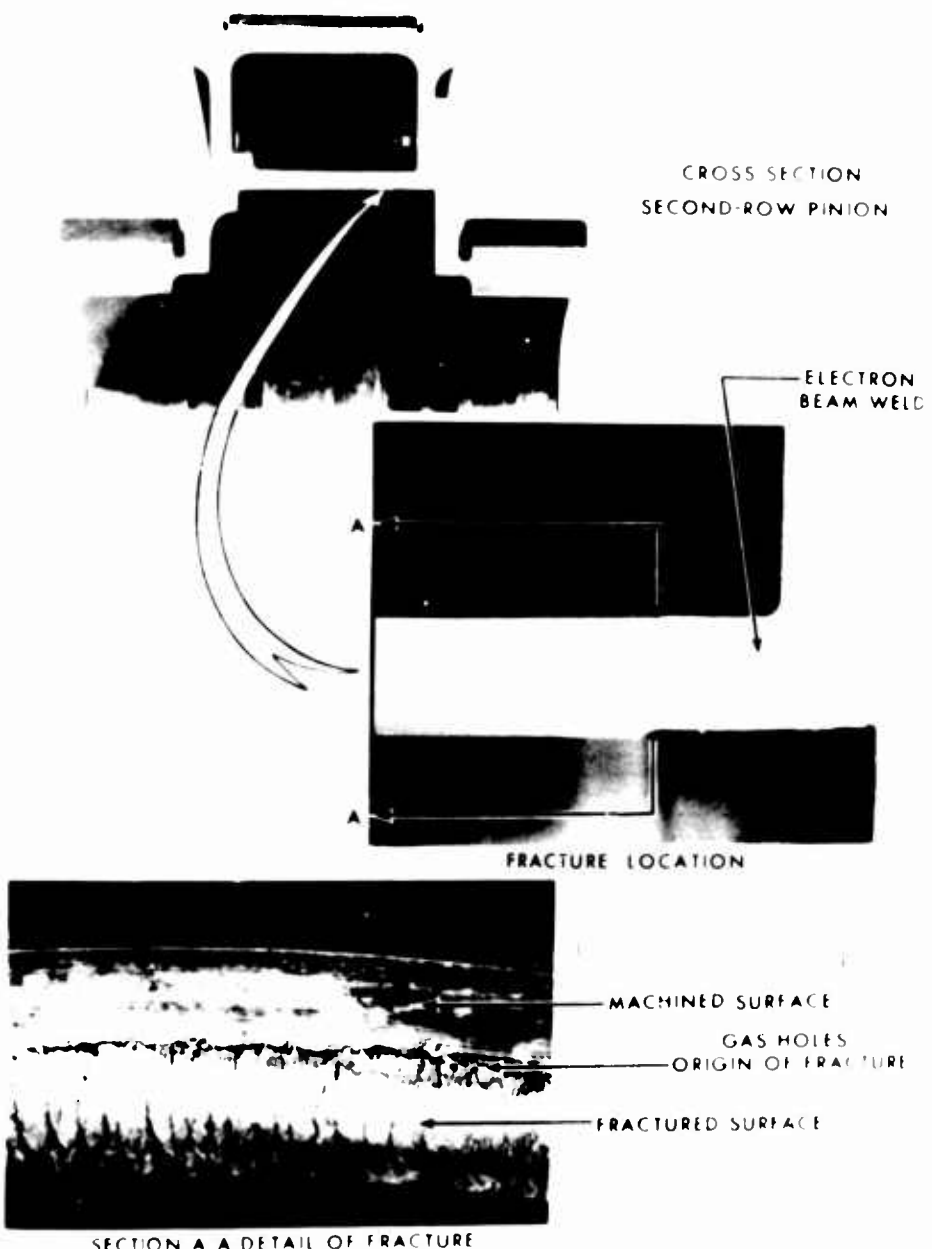
Figure 55.  Primary Fracture Surface, Second-Row Pinion.

117

ULTRASONIC
C SCAN RECORDING

Figure 56. Roller Fracture, Second-Row Pinion.

118

## STATIC TEST

As an initial step in the redesign program, a static evaluation test of the existing roller gear components was conducted to provide stress and load sharing data. The test consisted of assembling an instrumented roller gear unit in a transmission housing. The roller gear components under evaluation included seven strain gaged and calibrated roller gear posts, two strain gaged second-row pinions, a strain gaged ring gear and a strain gaged and calibrated main rotor shaft. The positioning of the strain gages in the post, second-row pinion and ring gear is shown in Figure 57. Their location within the roller gear unit is depicted in Figure 58.

The transmission was installed in a static rig and secured to react torque and main rotor shaft bending loads as illustrated in Figure 59. Main rotor thrust of 20,000 pounds was applied to simulate aircraft gross weight. Separate main rotor shaft bending and torque loads, representative of flight loads, were incrementally applied to determine each parameter's influence on the strain gaged roller gear components.

Main rotor shaft bending was applied in each of seven directions at increments of fifty-one 3/7° rotation for a full 360°, beginning in the forward direction. A single loading condition was also performed consisting of maximum bending, maximum thrust, and maximum torque.

## STATIC TEST RESULTS

The results of the static test indicated excellent load distribution between the roller gear posts. Figure 60 shows a ± 4 percent load sharing differential at maximum torque. The small amount of radial load present is attributable to the roller gear unit's not being allowed to turn.

Main rotor shaft bending introduced insignificantly small strains in the ring gear gages and pinion gages. The effect of main rotor shaft bending was absorbed by the output flange of the ring gear. Figure 61 illustrates the sinusoidal distribution of the output flange bending as a function of gage location and direction of applied loads.

Bending of the main rotor shaft resulted in insignificantly small tangential and radial roller post loads in all directions of load application.

Flange bending, ring gear bending, and second-row pinion strains were of a relatively low magnitude under all applied load conditions, and no evidence of significantly unequal upper and lower ring gear load distribution was observed.

119

ROLLER COMPRESSIVE STRAIN GAGES

ROLLER COMPRESSIVE STRAIN GAGES

FLANGE BENDING STRAIN GAGE

RING GEAR MESH BENDING STRAIN GAGE

DIRECTION OF APPLIED RADIAL LOAD

DIRECTION OF APPLIED TANGENTIAL LOAD

RING GEAR ASSY RG351 11186

OUTPUT FLANGE ASSY RG351 11185

4 ROWS OF 5 PAIR OF GAGES EQUALLY SPACED ON TOP SURFACE AND DIRECTLY OPPOSITE AS SHOWN TO READ PURE BENDING

Figure 57. Strain Gaged Components, Static Test.

120
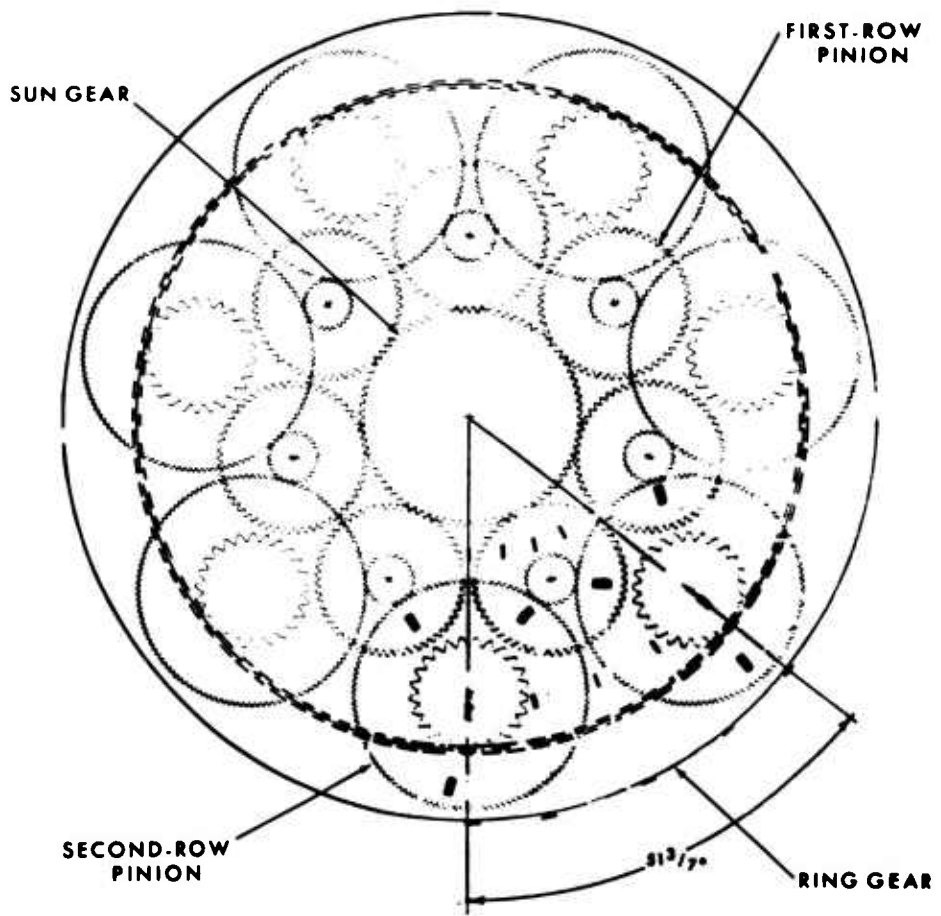
Figure 58. Location of Strain Gaged Second-Row
Pinions and Ring Gear.

121
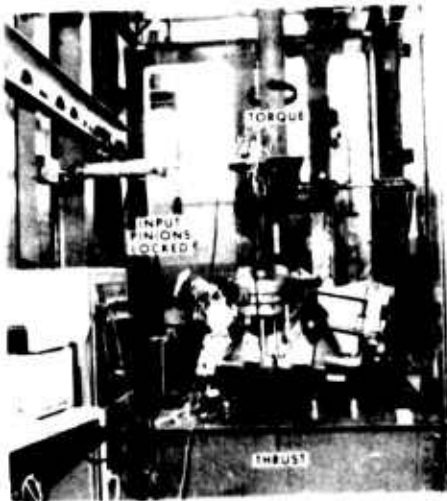
Figure 59.  Static Calibration Rig.
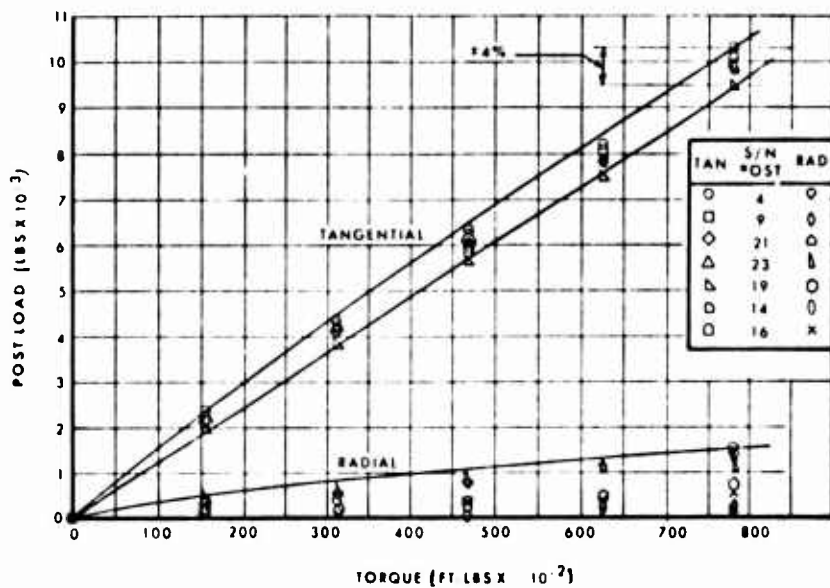
Figure 60. Post Loads, Roller Gear Unit.
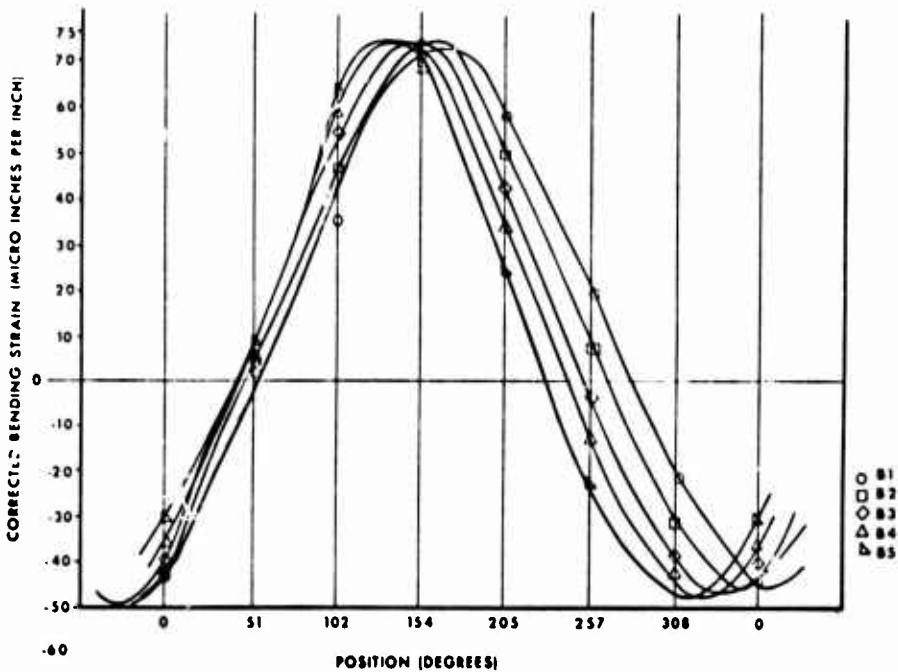


Figure 61. Output Flange Bending Strains due to
Main Rotor Shaft Bending.

123

## SECOND-ROW PINION REDESIGN

The redesign program for the second-row pinion produced three designs for further evaluation. These are shown in Figure 62. Each incorporates only two through electron beam welds, thus eliminating the blind welds of the previous design. An evaluation of the three candidate designs revealed the probability of fretting at the bolted interfaces. In the designs of A and B, this is more probable due to the lack of symmetry and varying stiffness at the bolted interface. The symmetrical design of "C" offers a direct path for the roller preload forces which are generated by the pinion/ring gear mesh.

The design "C" was selected as the candidate for fabrication and for further dynamic testing of the roller gear units. A detailed stress analysis of the final design, Figure 63, is included in Appendix D.

The design incorporates a split bearing bore. An interference fit of .003/.004 inch between the bearing and gear prevents rotation of the bearing outer race. Sixteen bolts on 7.080-inch pitch circle diameter and torqued to 165 in.-lb, provide sufficient clamping force to transmit the drive in friction from the large gear to the small gear. Threaded extraction holes provide for jack-out of the bearing.
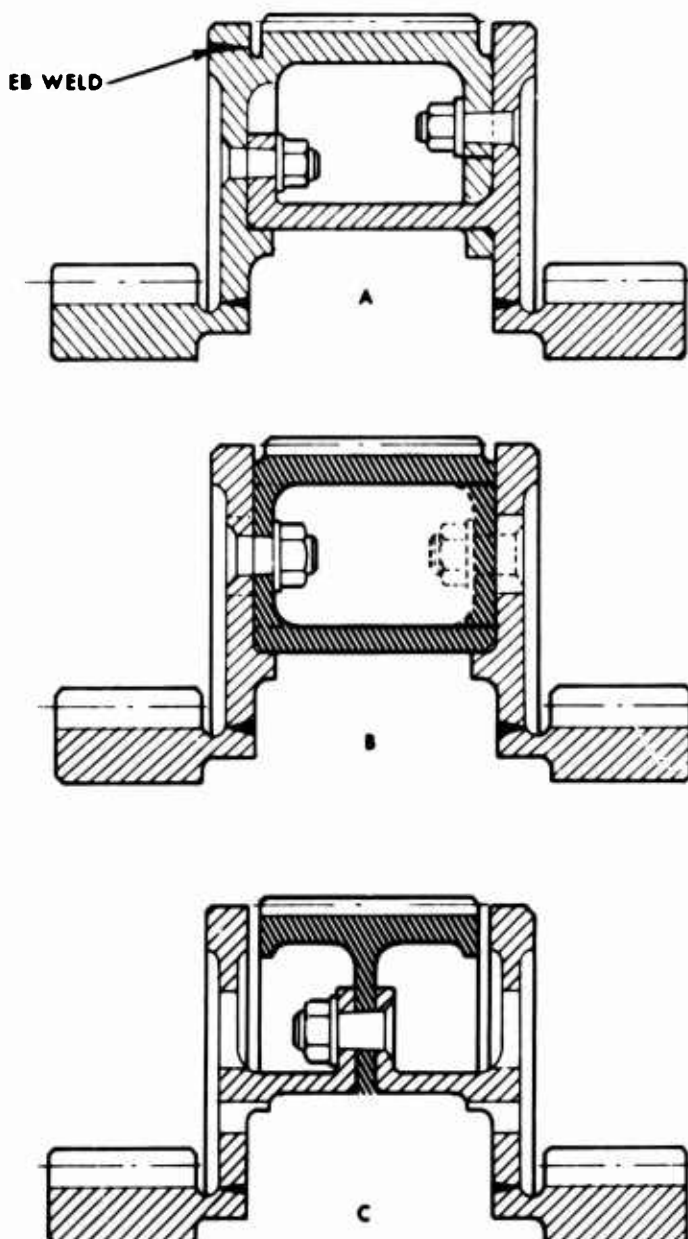
Figure 62.   Configurations, Redesigned
Second-Row Pinions.

125
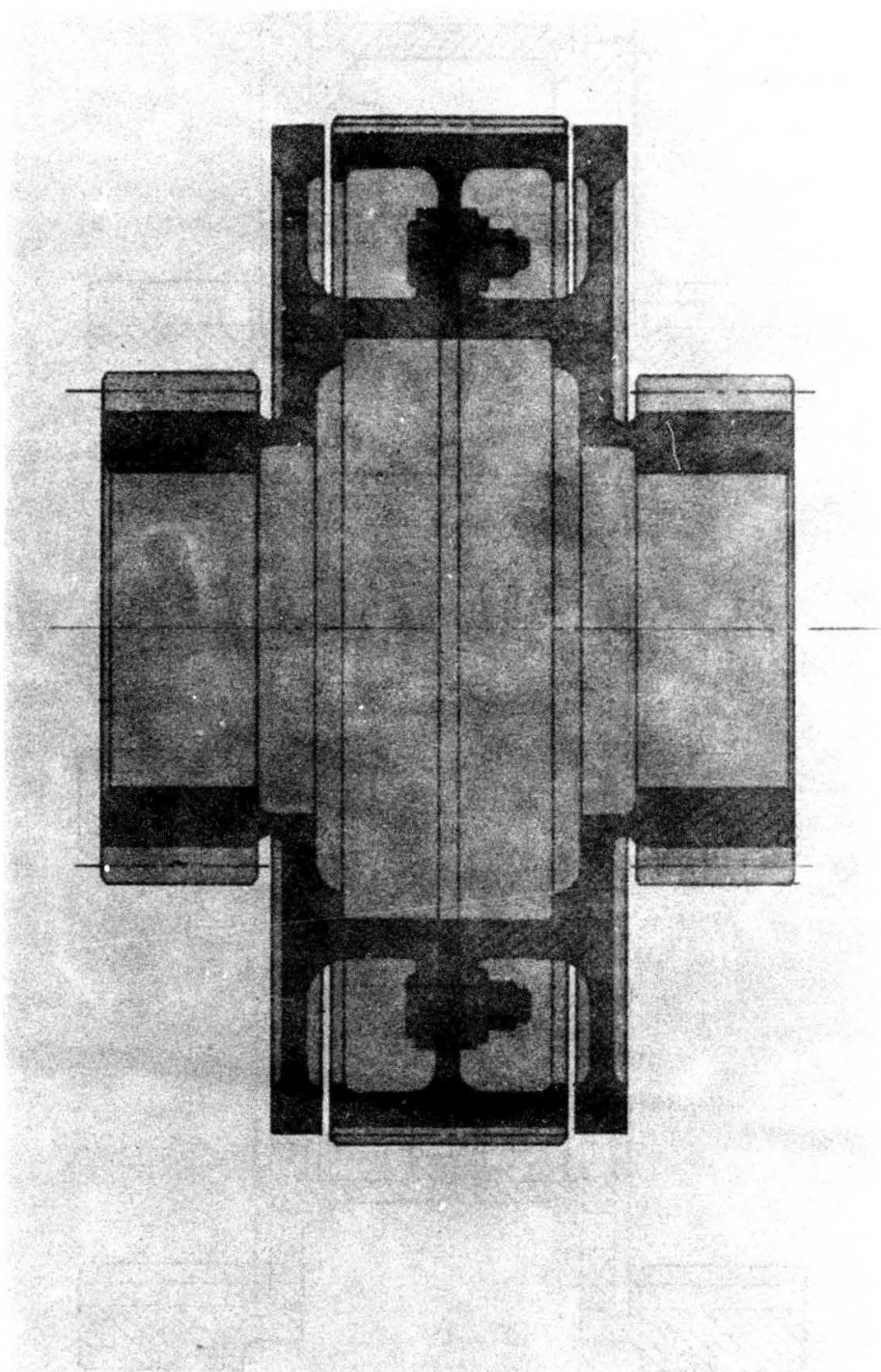
Figure 63. Redesigned Second-Row Pinion.

126

## RING GEAR

The ring gear consists of two nearly identical gears. These are fastened together during assembly of the roller gear unit by countersunk head bolts, Figure 64. These bolts are used only to ensure alignment of the gear teeth. The output flange assembly bolts transmit the output torque of the roller gear unit.

The dimensions of the ring gear are shown in Figure 65. The 30° pressure angle gear teeth are final machined, in the assembled condition, parallel to each other within ± .0002 inch. The curved web of the gear is designed to absorb the high vibratory ring gear stresses induced by the 30° pressure angle of the gear teeth. Holes in the web allow oil, centrifuged outward, to escape.
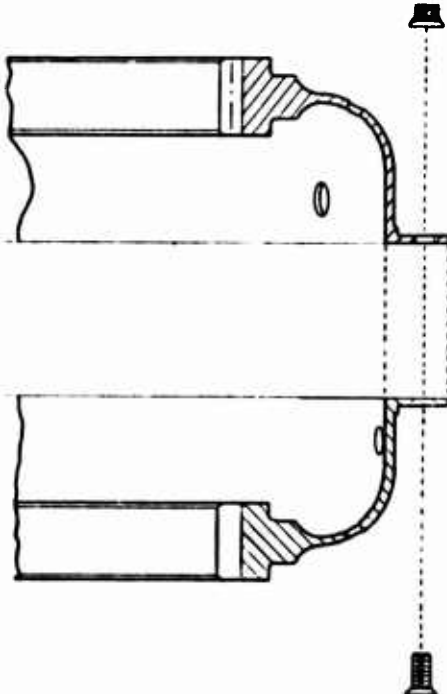


Figure 64. Ring Gear, Exploded View.
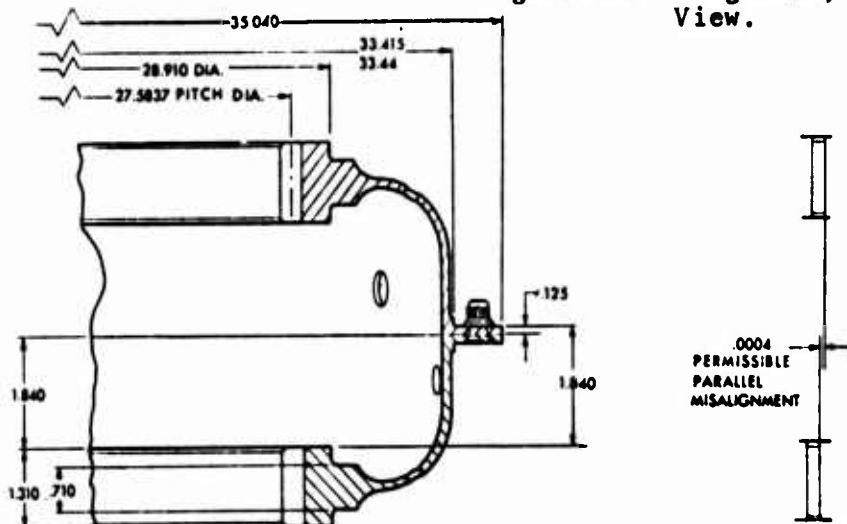


Figure 65. Ring Gear Dimensions.

127

## REACTION POST ASSEMBLY

The torque induced in the roller gear unit is reacted by the magnesium housing through a spline assembly. This spline assembly allows for the differing rates of thermal expansion of the magnesium housing and the steel components of the roller gear unit.

The torque generated within the roller gear unit is reacted by spherical bearings attached to posts. These posts, designed for constant stress throughout the tapered wall section, react 10,000 lb maximum tangential load, and induce a slope of .0018 inch/inch in the spherical bearings. The cantilevered posts are sandwiched between a built-up plate assembly which is bolted and doweled to an external spline. The roller gear unit, Figure 66, is assembled and located in the gearbox by the external spline mating with an internal spline rigidly fastened to the main housing. A double thickness tooth radially positions the roller gear unit. Seven bolts, one through each of the posts, statically support the roller gear unit. Gearboxes are designed to operate in the temperature range of -65°F to 250°F. The differing thermal expansion rate of magnesium and steel is absorbed in the working depth of the spline teeth without thermal stresses being imparted to the roller gear unit.

## SPHERICAL ROLLER BEARING

The spherical roller bearing is of the two-row design. The rollers and inner and outer races are fabricated from vacuum melt steel; the one cage is fabricated from silicon-iron bronze. The cage rides on the inner race and is silver-plated all over. The roller paths of the inner and outer races are machined to 6 AA (arithmetical average) surface finishes.

In order for the roller gear unit to be self-preloading, the bearing cannot detract from the radial loads induced on the rollers of the roller gear components. The bearings are therefore designed with an internal radial clearance of .0076-.0086 inch. When press fitted into the second-row pinion, the clearance closes to .0063-.0073 inch. An analysis is included in Appendix D which shows that the radial deflection of the second-row pinion, induced by roller preloads when transmitting 3,000 hp, is less than the radial clearance in the spherical bearing. Therefore, the bearing will remain unloaded in the radial direction.

MAIN TRANSMISSION ASSEMBLY

ROLLER GEAR UNIT

LUBRICATION JETS
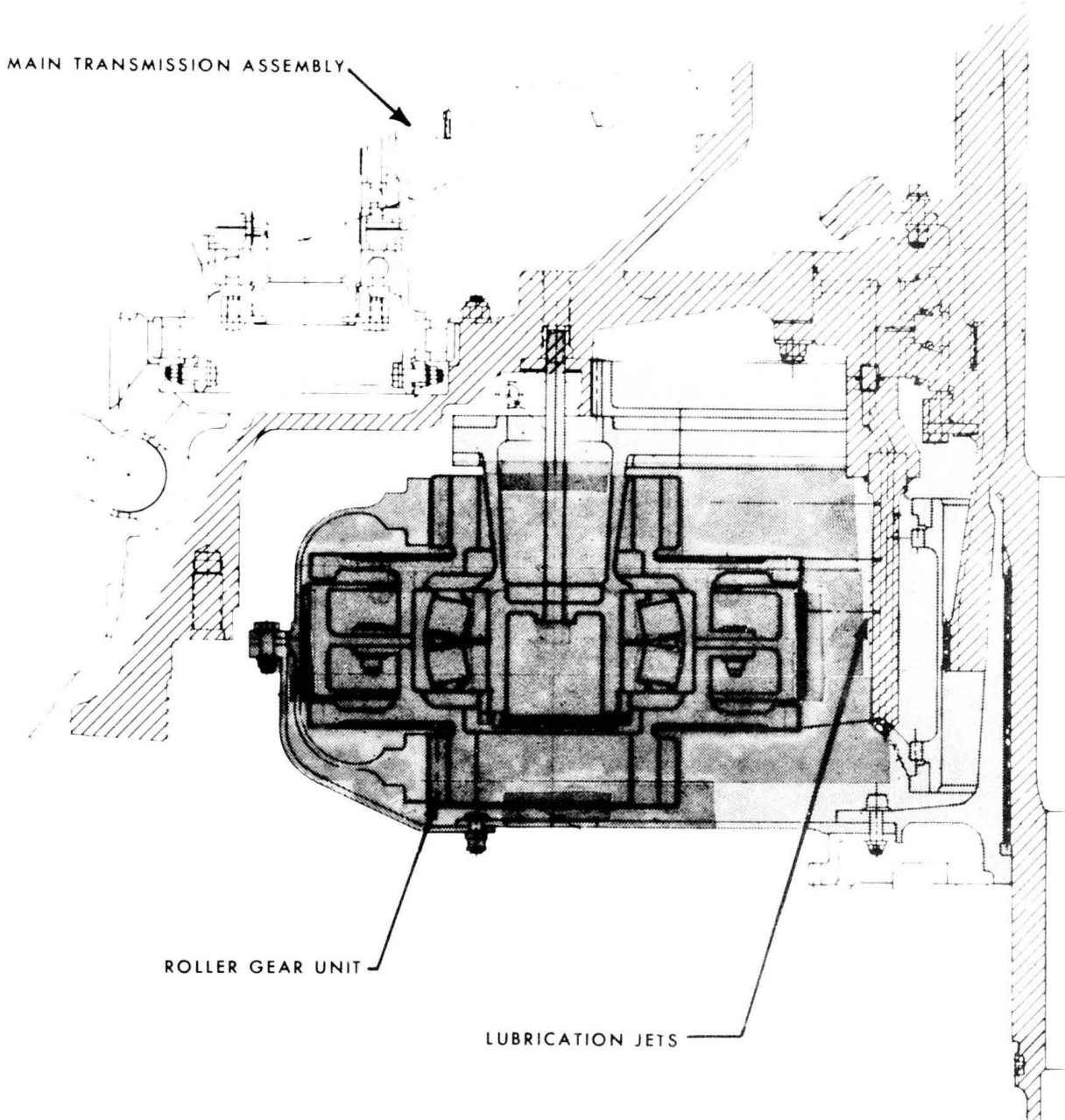
Figure 66.   Roller Gear Drive Installation.

129
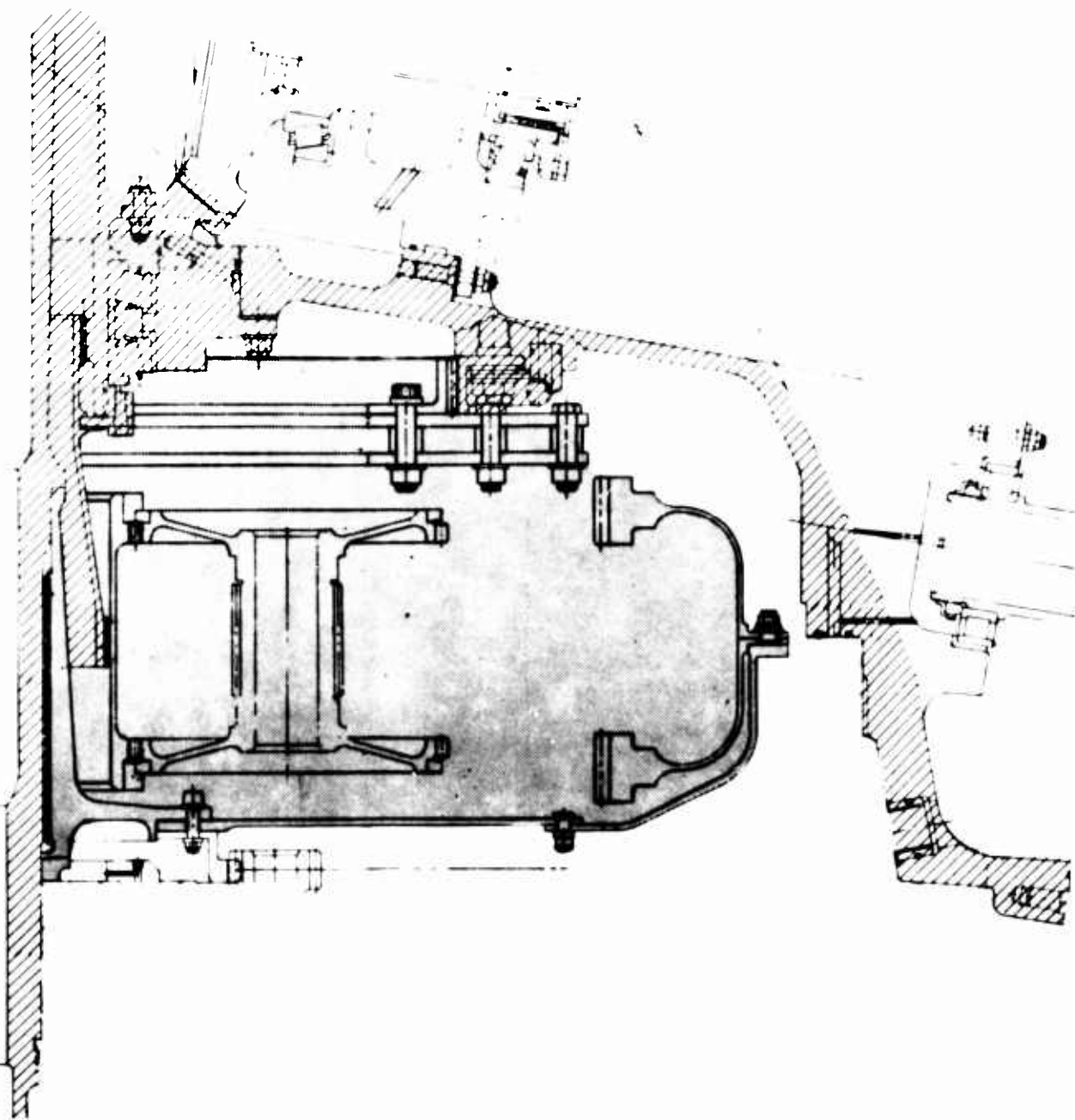
## ROLLER GEAR UNIT ASSEMBLY

Because of the unique geometry of the roller gear components, special attention was given to the assembly procedures of the roller gear unit. It was found that if assembly of the roller gear unit is attempted by first assembling all first-row pinions and then assembling all second-row pinions, the last second-row pinion cannot be placed in mesh with the first-row pinions. Assembly is prevented by the size of the toggle angle between the meshes with the two first-row pinions.

In order to overcome this difficulty, a special order of assembly was developed. The first step required the mating of one first-row pinion with the sun gear as shown in view A, Figure 67. Next, a mating pair consisting of one first-row and one second-row pinion assembly complete with spherical bearing was placed into mesh as shown in view B. This step was repeated until all but one first-row pinion and two second-row pinion assemblies were in place. The remaining three gears were then positioned as a set, as shown in view C, Figure 67. The second-row pinion bearing post assemblies were then installed, followed by placement of the output flange and hub assemblies. The two halves of the ring gear were then positioned to complete assembly of the roller gear unit. The completely assembled roller gear unit is shown in Figure 68.

Also illustrated in this figure are the timing marks on the sun and first-row pinions which aid in the assembly of the roller gear unit. Each first-row pinion is timed to the sun gear and two second-row pinions with which it mates.

131
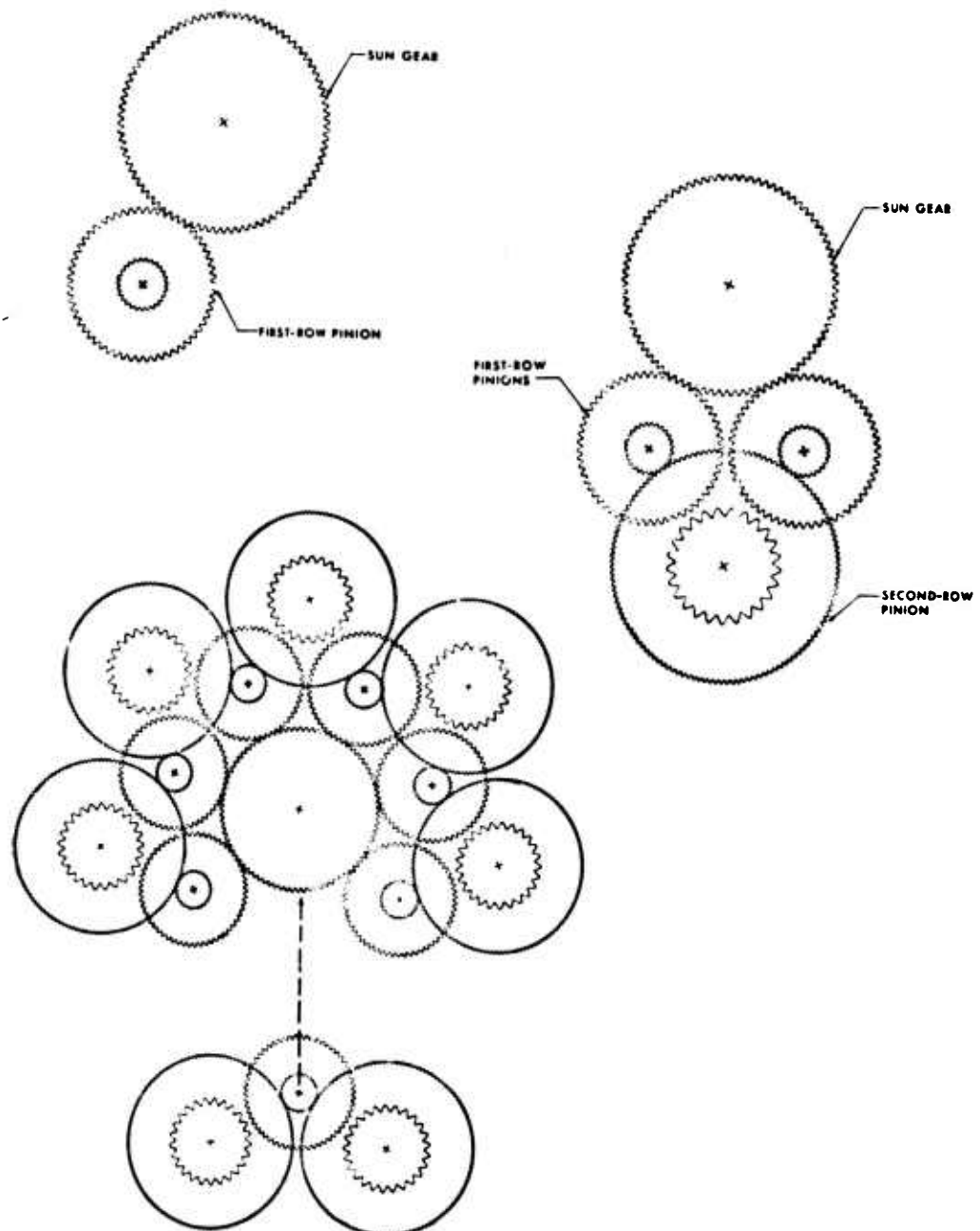
Figure 67.  Assembly Procedure, Roller Gear Unit.

Figure 68. Roller Gear Unit.

# MAIN TRANSMISSION, DETAIL DESIGN

## INTRODUCTION

This section of the report discusses, except for the roller gear drive unit itself, the detail design aspects of the S-61 roller gear drive main transmission.

A cross-sectional drawing of the main transmission is shown schematically in Figure 69.
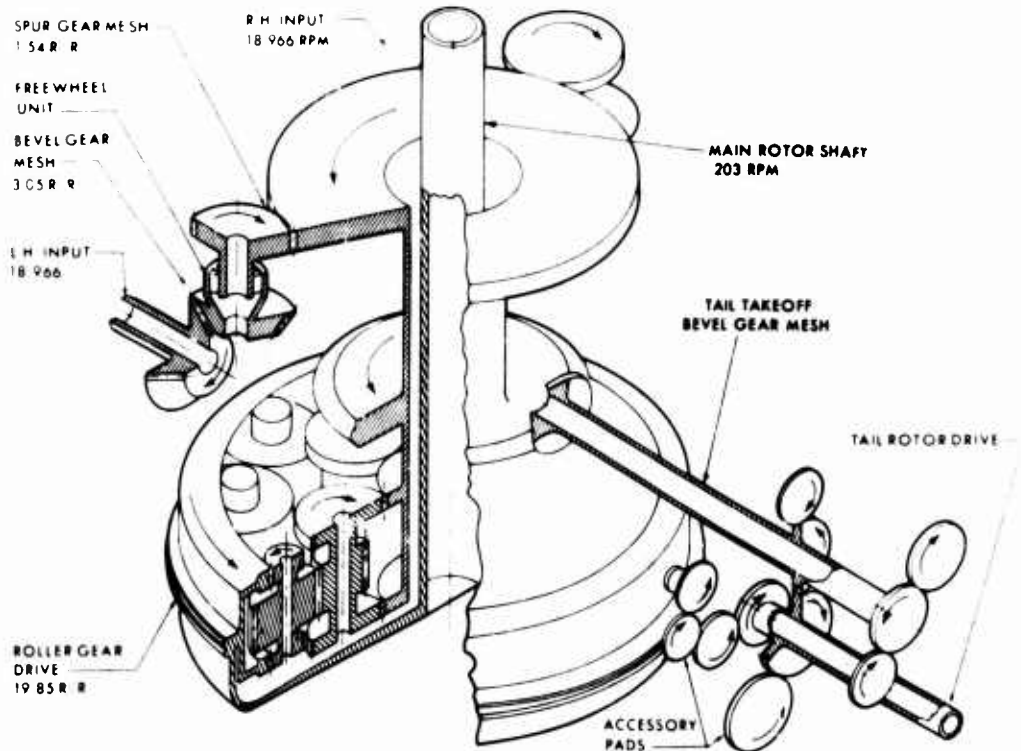


Figure 69.   Schematic, Roller Gear Transmission.

Power is fed from each engine at 18,966 rpm to a spiral bevel gear mesh. This first-stage spiral bevel mesh has a reduction ratio of 3.05 to 1 which reduces the speed at the output bevel to 6,223 rpm. Both the bevel pinion and gear are straddle mounted for rigidity and to minimize gear deflections. Concentric within each output bevel gear shaft is a ramp-roller type overrunning clutch. These clutches permit single-engine operation and also allow the rotor to overrun in the event of engine malfunction or engine shutdown. The output cam shaft of the ramp roller clutch drives a second-stage spur gear mesh. Power from each engine is combined to a single torque path at this spur gear mesh where the shaft speed is reduced from 6,223 rpm to 4,045 rpm.

The output shaft of the second-stage spur gear drives the accessory and tail drive section of the transmission. Mounted on the rear cover of the transmission are accessory drive packs which provide the drive adaptation for two generators, an auxiliary hydraulic pump, a utility hydraulic pump, a lubrication pump, an oil cooler drive, a primary hydraulic pump, a tachometer and a rotor brake. Also driven by the second-stage reduction is the input sun gear of the roller gear drive unit, the output of which drives the main rotor shaft.

The actual arrangement of these components is shown in the cross-sectional drawing, Figure 70.

The engines are attached to the transmission housing by gimbal rings. These provide a pivotal point about which each engine can swing through small angles to accommodate airframe deflection, temperature gradients, misalignment, etc. A crowned spline coupling, the pivotal center of which is in the plane of the gimbal, transmits the engine driveshaft power to the input bevel gear mesh. To provide the correct bevel tooth bearing patterns, the input and tail takeoff bevel pinion and gear assemblies are shimmed for proper location in the main housing. An adaptor gearbox is fitted onto the rear cover of the transmission to provide the correct speed for the tail rotor system of the S-61 helicopter. A multiple disc coupling absorbs the angular misalignment of the tail driveshafting and adaptor gearbox output.

The gimbal ring arrangement, shown in the top view of Figure 71, is on 32-inch centers to accommodate the side-by-side installation of the aircraft engines. The locations of the accessories on the rear cover are as shown on the lower picture.

MAIN

SECOND-STAGE
COMBINING SPUR GEAR MESH

CAM-ROLLER
FREEWHEEL UNIT

305:1 REDUCTION RATIO
BEVEL GEAR MESH

HIGH SPEED
INPUT 18966 RPM

INPUT BEVEL PINION
FIRST-STAGE GEAR MESH

19.85:1 REDUCTION RATIO
ROLLER GEAR UNIT
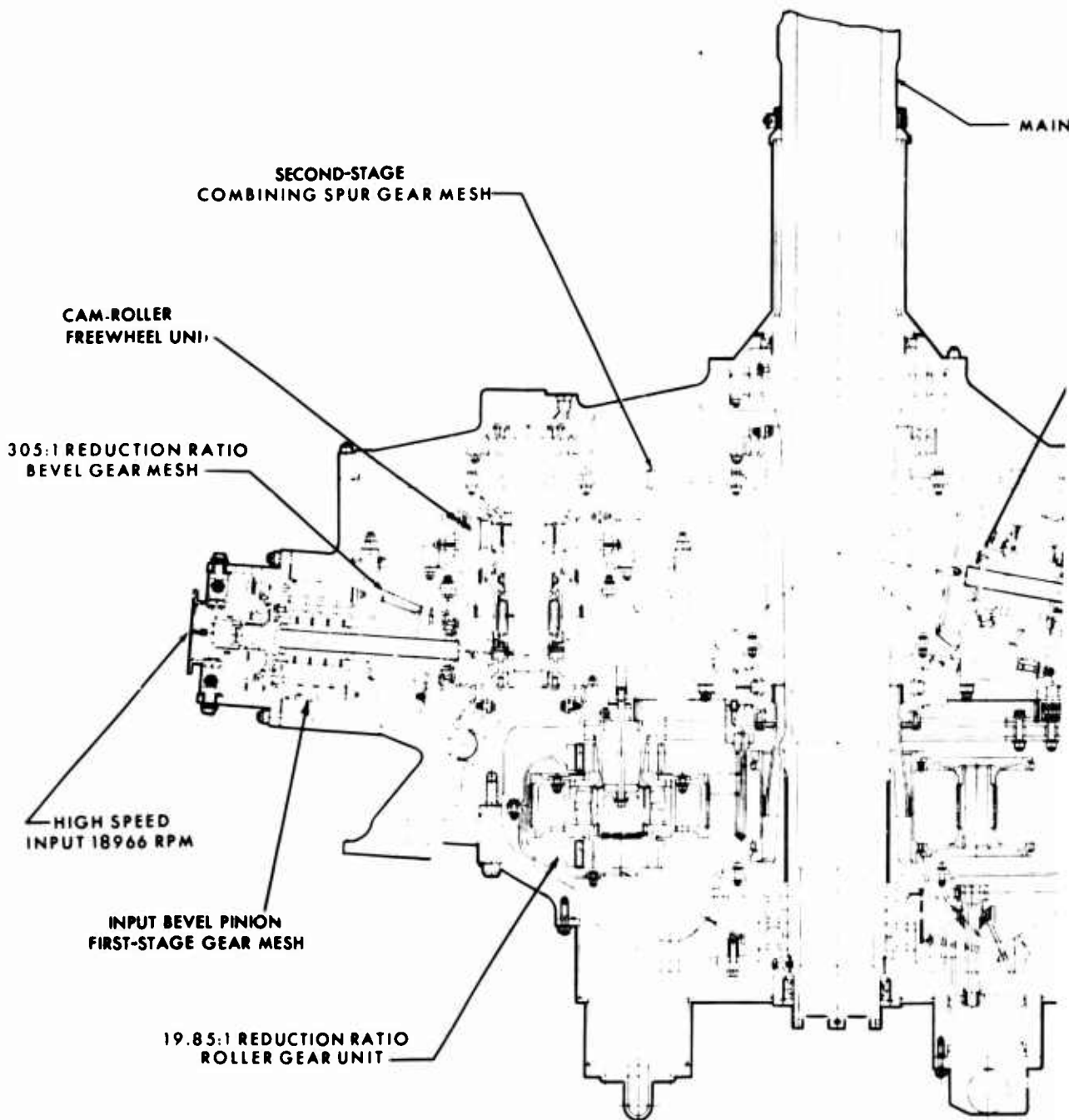
Figure 70.   Roller Gear Transmission Assembly Drawing.

137

MAIN ROTOR SHAFT
203 RPM

BEVEL GEAR TAKEOFF TAIL
ROTOR AND ACCESSORY DRIVE

ACCESSORY DRIVE PADS

OIL COOLER DRIVE
TAKEOFF 7031 RPM

TAIL ROTOR DRIVE
TAKEOFF 3026 RPM

ADAPTOR GEARBOX

MAIN ROTOR SHAFT

TOP COVER

REAR COVER

INPUT GIMBALS
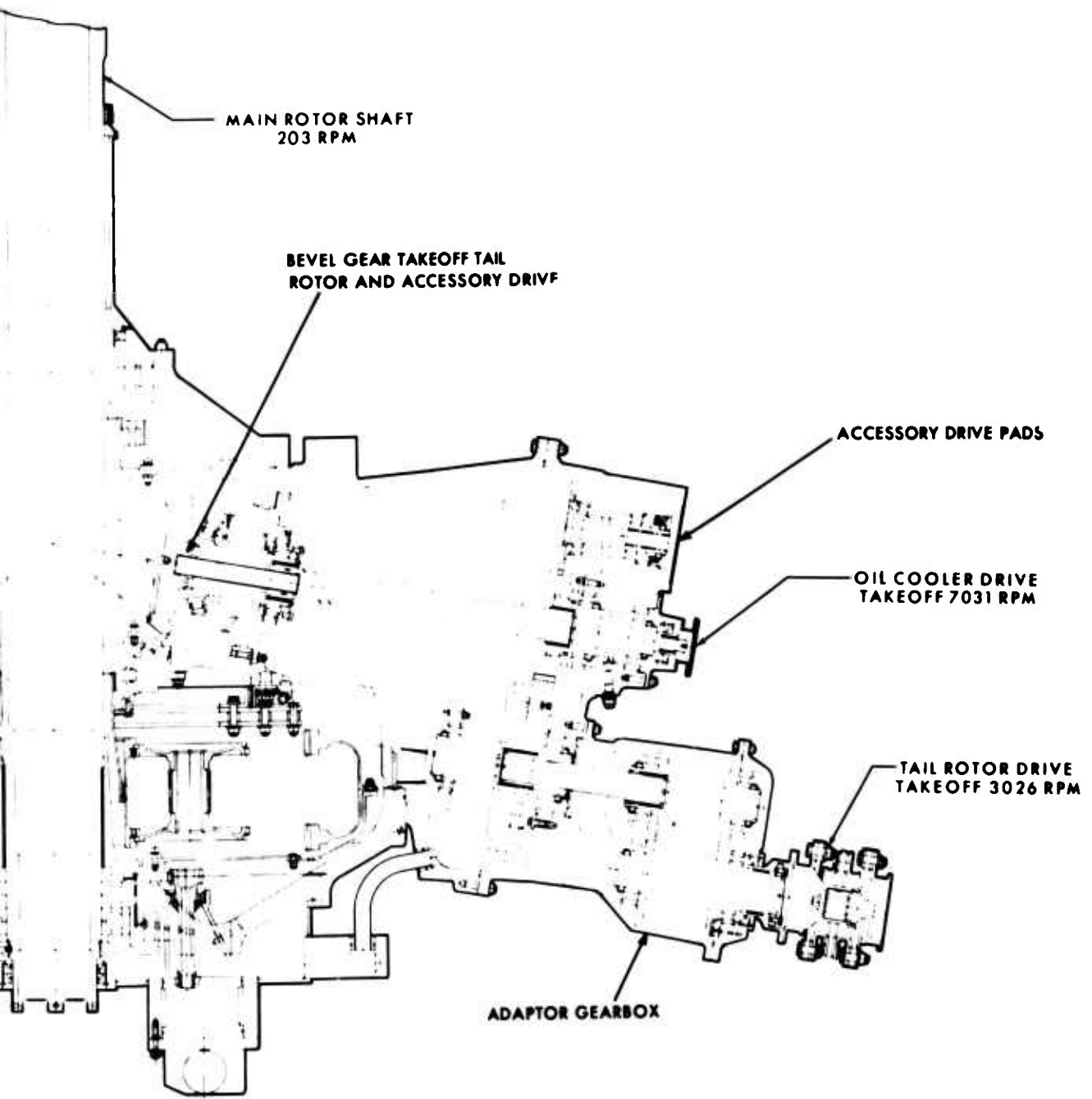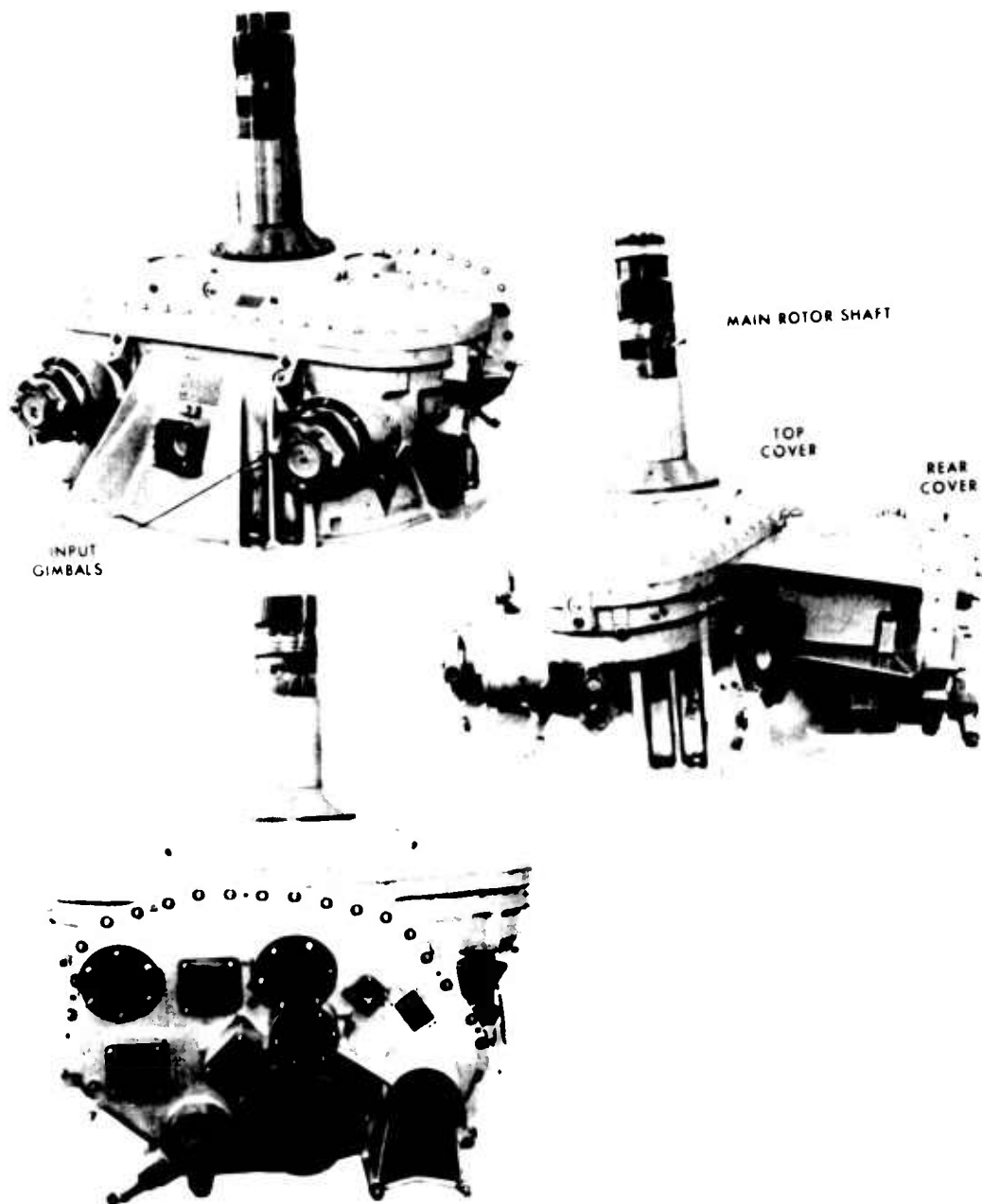
Figure 71. Roller Gear Transmission.

159

Appendix B presents a summary of the tooth bending and compressive stresses for all the gears in the roller gear drive main transmission. Appendix C summarizes the B-10 lives at prorated powers of all bearings in the main transmission, while Appendixes D through G present the structural analysis of the internal components of the main transmission.

## ENGINE DRIVESHAFT AND TORQUEMETER

The general arrangement of the engine installation on the S-61 aircraft is shown in Figure 72.
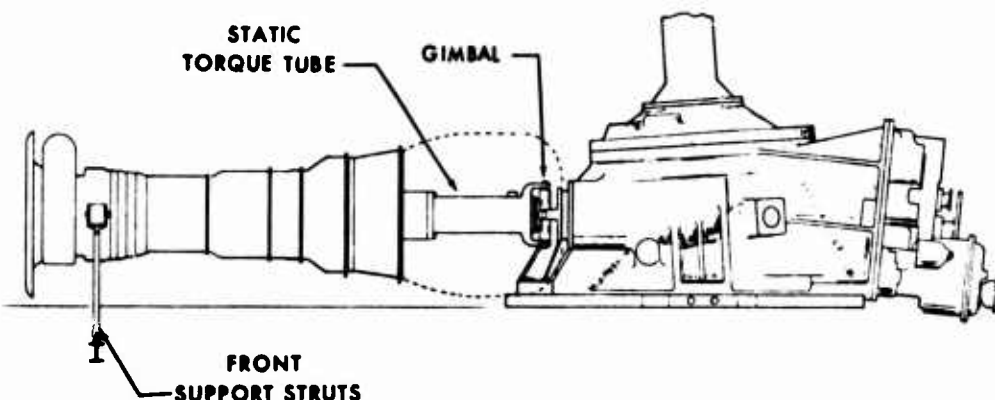


Figure 72. Engine Installation.

The engines are mounted on a three-point suspension system consisting of an aft gimbal and two elastomeric front supports. These front supports are attached through vertical struts to the engine/aircraft support ring. Each engine is supported at the rear by bolting a gearbox static torque tube to the engine power takeoff pad. This is attached to the gearbox through elastomeric mounts in a gimbal which allows two-axis motion to accommodate misalignment of the engine to the gearbox. The pivot point of this gimbal is coincident with that of a crowned spline coupling. This coupling, in conjunction with a flexible coupling on the engine power takeoff, accommodates driveshaft misalignment resulting from any engine/gearbox mismatch.

The engine/gearbox driveshaft is located within the static torque tube. A phase line torquemetering system is designed integral with the driveshaft to measure driveshaft windup due to engine torque. The torquemeter system, designed by National Water Lift, is shown schematically in Figure 73.

Attached to the engine output end of the driveshaft is an outer shaft which has three equally spaced pole pieces machined onto the free end of the shaft. Attached to the gearbox end of the driveshaft is another outer shaft also with three equally spaced pole pieces which intermesh with the pole pieces on the input end. As the engine driveshaft twists under the influence of shaft torque, the spacing between the pole pieces varies. As the shaft angle of twist is directly proportional to torque, the variation in distance is a measure of shaft torque. A single pickup located on the fixed engine torque tube detects the spacing of the pole pieces and transmits the signal to a signal conditioning junction (SCJ) box. The SCJ box converts the pulse type input signals into an analog output voltage proportional to the amount of driveshaft twist. This voltage is fed into a torque servo indicator which displays a signal as a percentage of transmitted torque. A shaft temperature sensor compensates for a change in driveshaft material modules over a range of -40°F to +450°F.

The driveshaft is designed for a nominal windup of 1.56° ± .06° when transmitting 100 percent torque (6,214 in-lb). The maximum windup at 130 percent torque is 2.03°. A torque simulator can be plugged into the SCJ box in place of the torque sensor to calibrate the system. This simulator electrically generates signals equivalent to dynamic operations at 18,966 rpm (100 percent speed); a continuously variable torque (0 to 130 percent torque) is then superimposed over the speed signal.

In the design of the torquemeter/driveshaft assembly, the natural frequency, or critical speed of the assembly, had to be determined to ensure that resonance would not occur within the operating range of 0 to 22,190 rpm, which corresponds to a 117 percent autorotative redline speed. The critical speeds were determined by computer analysis. Figure 74 shows the driveshaft layout and the normalized shaft deflection for the first critical speed. The method of solution was based on the Myklestad-Prohl numerical tabular method. A mathematical model of the driveshaft system was made where bearing supports were modeled as springs and couplings were modeled as pinned connections. The driveshaft outside diameter and wall thickness parameters were varied within the constraints of the torque tube diameter. The driveshaft length, between the flexible steel laminated coupling and crowned spline coupling, was predetermined by the requirement to accommodate the engine exhaust casing. Figure 75 shows the engine driveshaft.

141
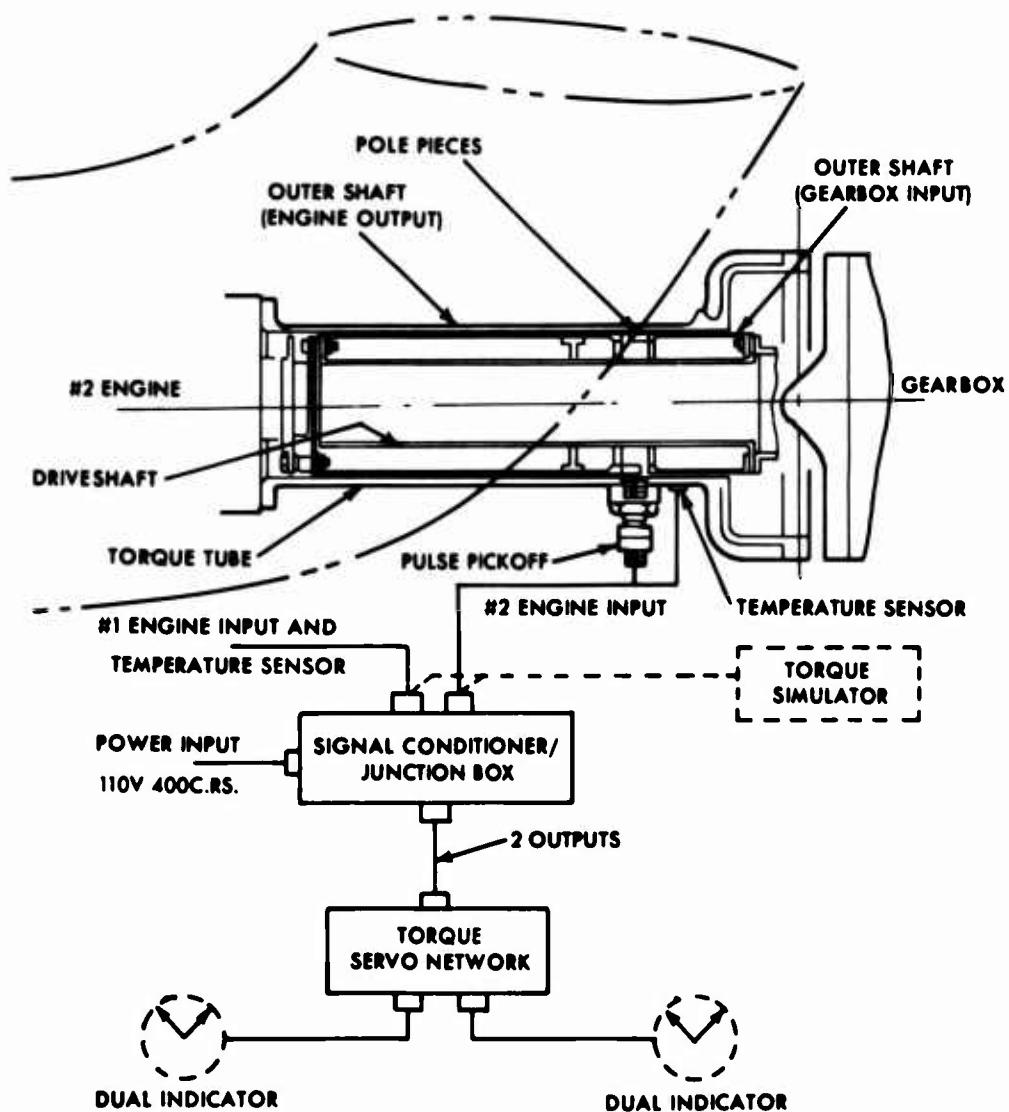
Figure 73. Engine Torquemeter System.
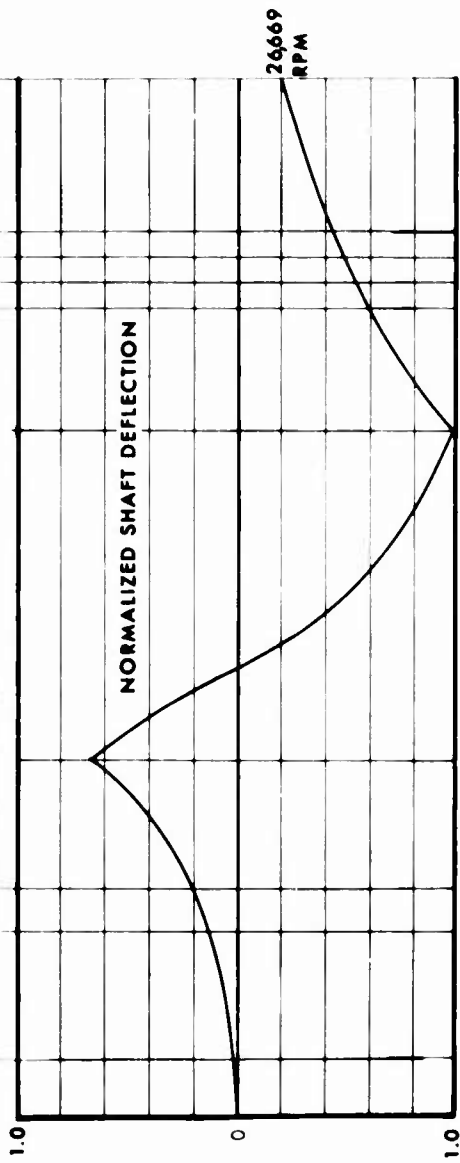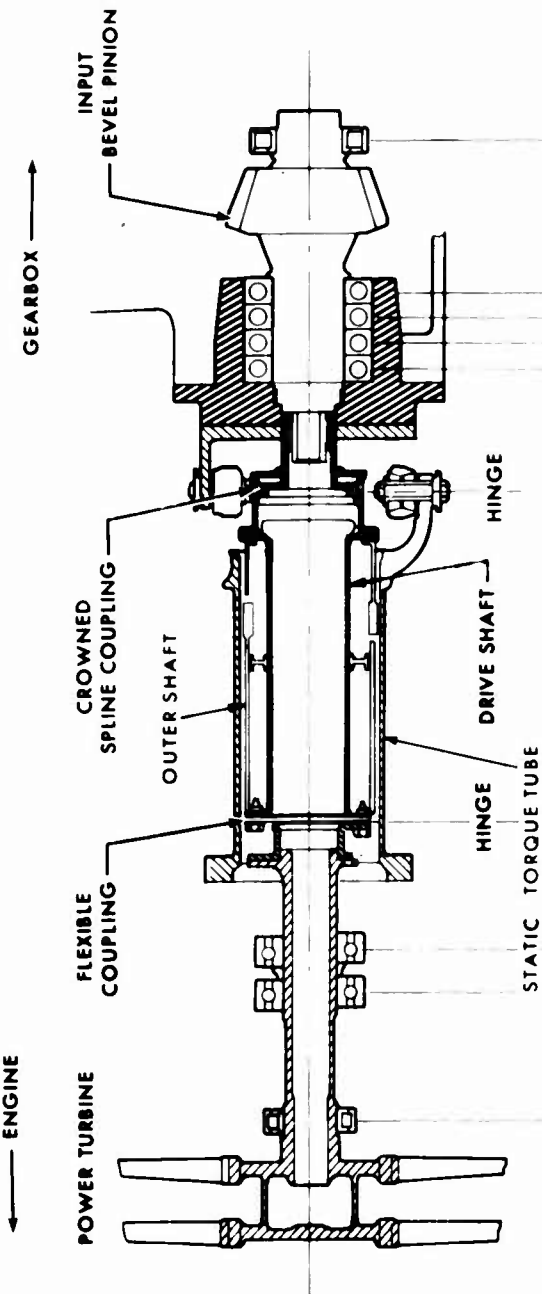
Figure 74. Input Driveshaft Layout - Critical Speed Analysis.

143
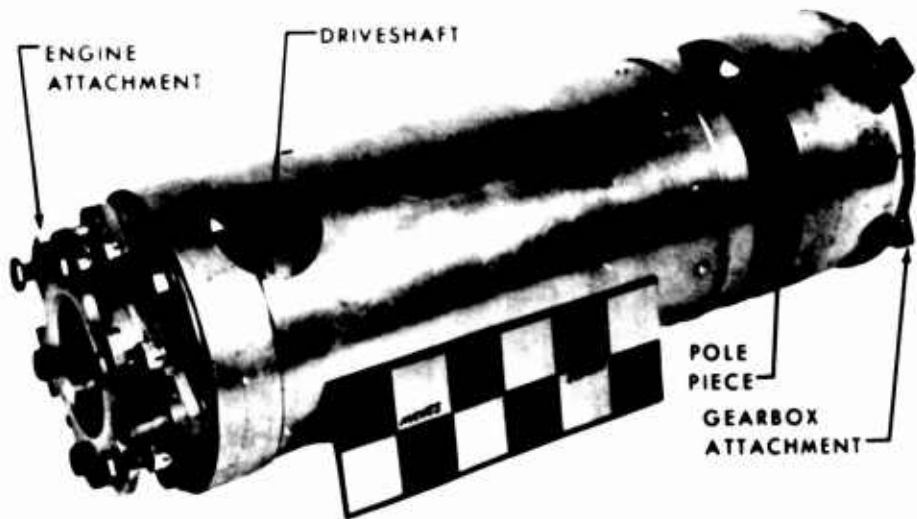
Figure 75. Engine Driveshaft.

## INPUT BEVEL STAGE

The first reduction stage of the roller gear drive main transmission consists of a spiral bevel gear set of 3.05:1 reduction ratio. This spiral bevel gear arrangement reduces the engine output speed from 18,966 rpm to 6,223 rpm and aligns the output gear shaft parallel to the main rotor shaft.

The requirements of this mesh were such that a compromise was required between bearing life and gear scoring. In order to obtain a high bearing life, the pinion pitch diameter should be as large as possible for the same torque. This decreases tooth loads and hence bearing reactions. To minimize gear scoring, the pinion pitch diameter should be as small as possible, thereby lowering pitch line velocity and sliding. Bearing life is improved by designing both pinion and gear shafts with straddle mounted supports.

During the preliminary design phase of the program, various tradeoff studies were performed in an effort to balance bearing life and gear scoring.

144

The input pinion bearing arrangement consists of a four-ball
bearing stack arrangement and a nose roller bearing strad-
dling the pinion. The last bearing of the ball stack is a pre-
load bearing. The remaining three share the thrust and
radial loads induced on the bevel pinion. The four bearings
of the stack are supplied by the bearing manufacturers as a
matched set. The retainers of the bearings are of one piece
construction of AMS 4616 iron silicon bronze and are silver-
plated all over. The bearings are lubricated by centrifugal
force from an oil distribution tube located in the center of
the pinion, Figure 76.
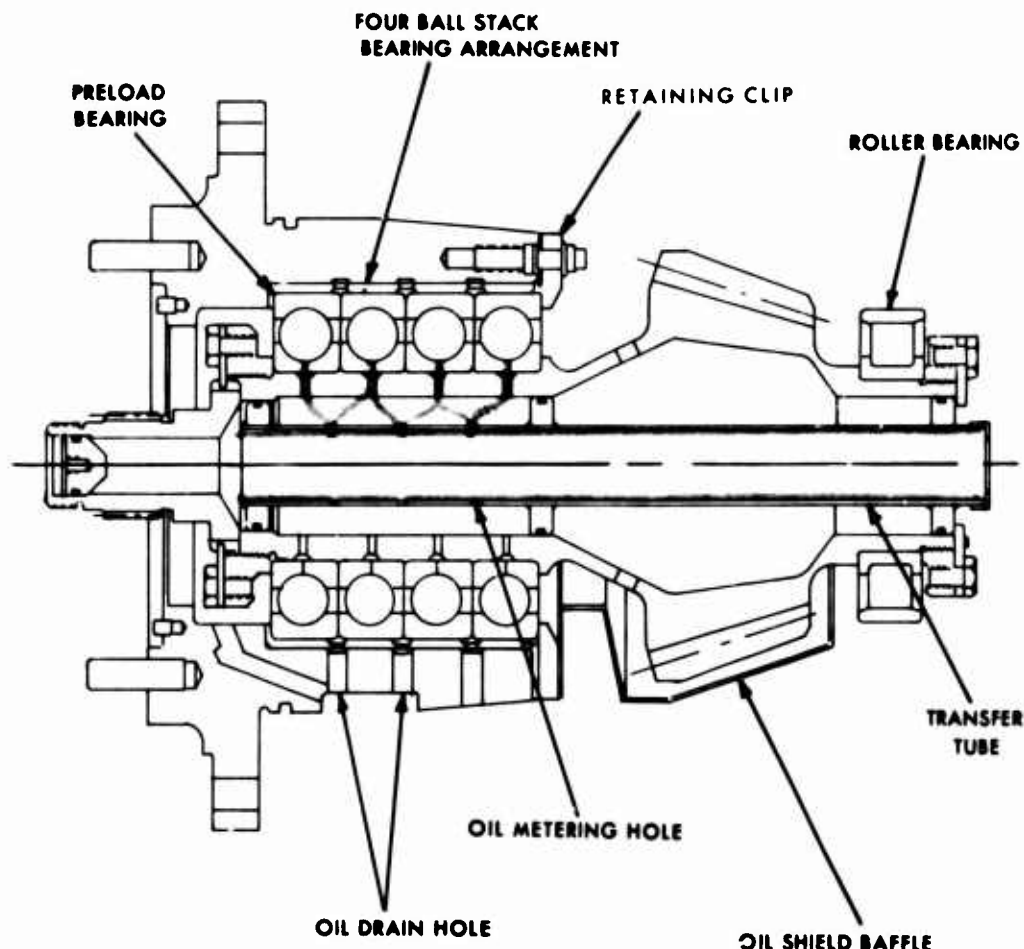
Figure 76. Input Bevel Pinion Arrangement.

145

A dimensional summary of the 3.05:1 reduction ratio set is given in Table 9.

The estimated tooth stresses for this bevel gear set when transmitting 1,870 hp at 18,966 rpm are shown in Table 10.

| TABLE 9. INPUT BEVEL SET GEOMETRY. | | |
|---|---|---|
| | Pinion | Gear |
| Number of Teeth | 21 | 64 |
| Diameter Pitch | 4.193 | 4.193 |
| Face Width (in.) | 2.100 | 2.100 |
| Pressure Angle | 20° | 20° |
| Shaft Angle | 86° | -- |
| Pitch Diameter (in.) | 5.008 | 15.264 |
| Addendum (in.) | .294 | .122 |
| Dedendum (in.) | .166 | .329 |
| Mean Spiral Angle | 30° | 30° |
| Backlash with Mate (in.) | .006/.008 | -- |
| Face Contact Ratio | 1.877 | 1.877 |

| TABLE 10. INPUT BEVEL GEAR TEETH PARAMETERS. | |
|---|---|
| Pinion Torque (in-lb) | 6,214 |
| Pinion Speed (rpm) | 18,966 |
| Pinion Bending Stress (psi) | 12,080 |
| Gear Bending Stress (psi) | 12,120 |
| Contact Stress (psi) | 132,500 |
| Load Distribution Factor | 1.1 |
| Lubricant Specification | MIL-L-7808 |
| Inlet Oil Temperature (°F) | 180 |
| Scoring Index | 251 |

The stress values listed are well within the design limits of 30,000 psi in bending stress and 200,000 psi in contact stress for AISI 9310 material, carburized and case hardened to Rockwell "C" 60 minimum. The calculated scoring index value is also within the limit of 500 for aircraft application using the MIL-L-7808 lubricant specified for the transmission and engines.

These low stress values arise mainly from a requirement to obtain a high contact face ratio of 1.877:1. This ensures smooth, quiet operation at the pitch line velocity of 24,866 feet per minute, the highest mesh velocity to date of any Sikorsky production or experimental bevel gear set. These high velocity gears are shown in Figure 77.



INPUT SPIRAL BEVEL PINION

INPUT SPIRAL BEVEL GEAR
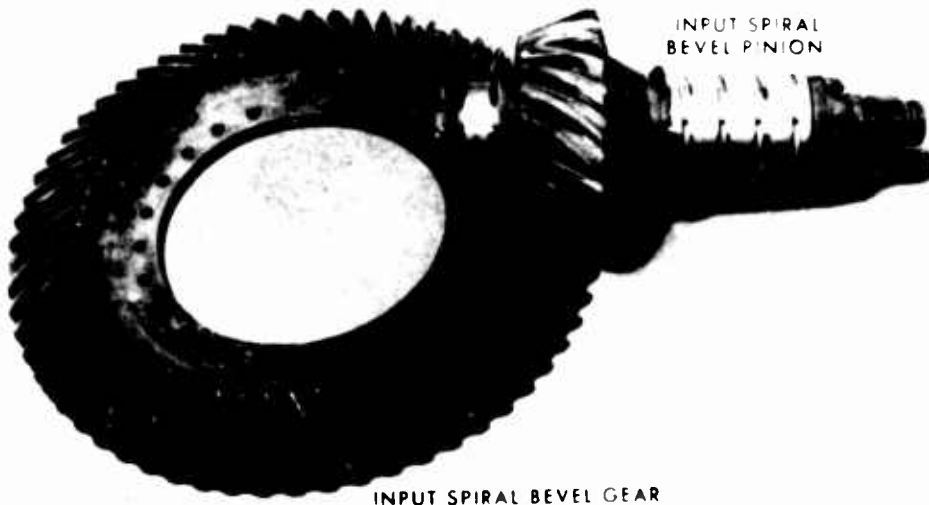
Figure 77. Input Bevel Pinion and Gear.

FREEWHEEL UNIT

Located within each vertical bevel gear shaft is an over-
running clutch. This clutch, sometimes known as a freewheel
unit, permits the output or driven member of the clutch to
freewheel whenever the input or driving member is stopped or
is rotating at a slower speed. In a helicopter transmission,
actuated overrunning clutches are used to disengage the
engines from the rotor, thus disconnecting the engine drive.
In dual engine arrangements, overrunning clutches permit one
engine to be started without rotating the remaining engine.
Safe landings may be executed by autorotation without the use
of engines as the overrunning clutch automatically disconnects
a stationary engine from the rotor head drive.

The principal components of the roller gear transmission ramp
roller overrunning clutch are the cam, rollers, outer housing
and cage as shown in Figure 78.
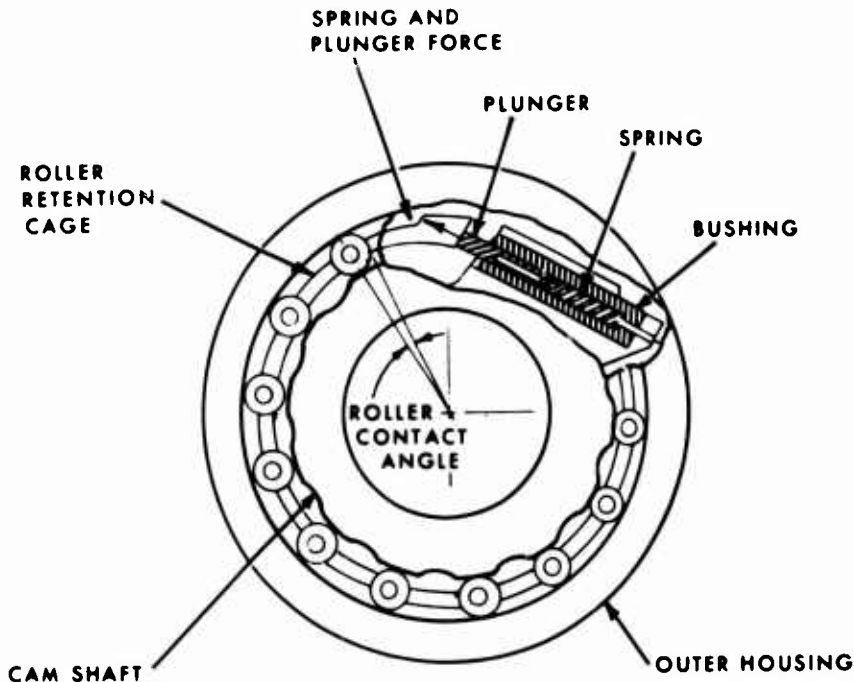
Figure 78. Principal Components, Ramp Roller Clutch.

Drive is obtained in a ramp roller clutch by the wedging
action of the rollers between the circular outer housing and
the flats of the cam. A spring and plunger mechanism acts
on the roller retainer, which in turn forces the rollers up
the ramps and against the outer housing. The wedging of the
rollers occurs only when the driving member attempts to turn
faster than the driven member. Overrunning occurs whenever
the driven member turns faster than the driving member. The
cam or the housing can be the driving member. In the roller
gear transmission the outer housing is the driving member,
Figure 79.
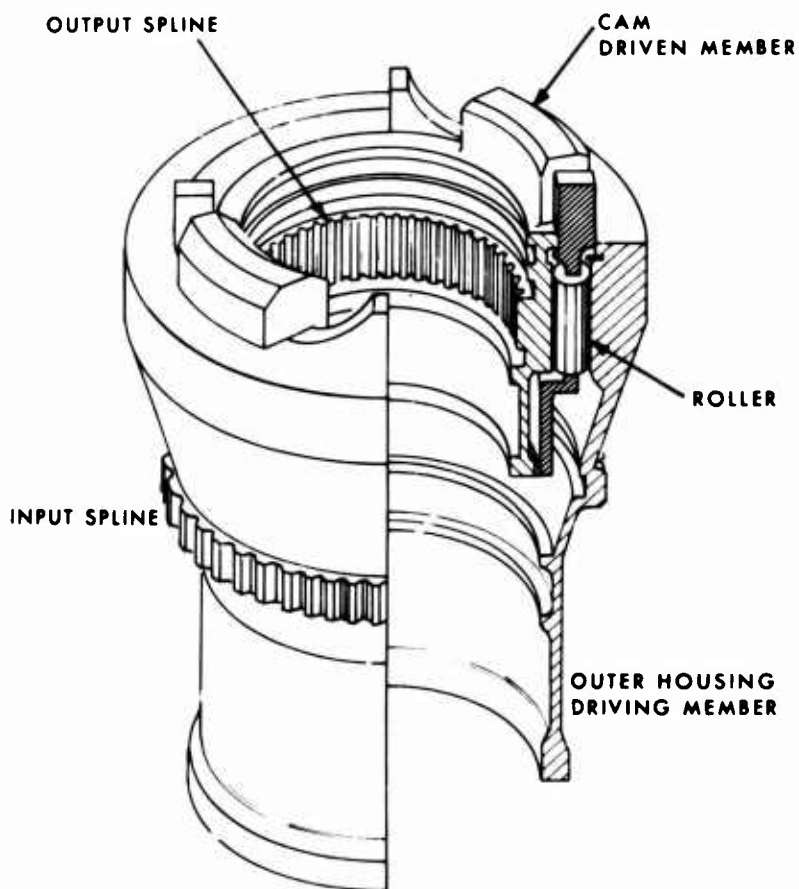


Figure 79. Ramp Roller Clutch, Roller Gear Transmission.

149

A free-floating quill shaft drive transmits power from the
bevel gear shaft to the clutch. Fourteen rollers are located
in a straddle supported cage on which two spring loaded
plungers apply a nominal torque of 9 in-lb. This force keeps
the rollers in intimate contact with the wedging surfaces and
ensures instantaneous clutch response. Four plunger stops are
incorporated into the cage design so the cage can be indexed
in the event of fretting and so provide new operating faces.
These are visible in Figure 80. The undercuts in the roller
pockets assist in the fabrication of the cage slots.
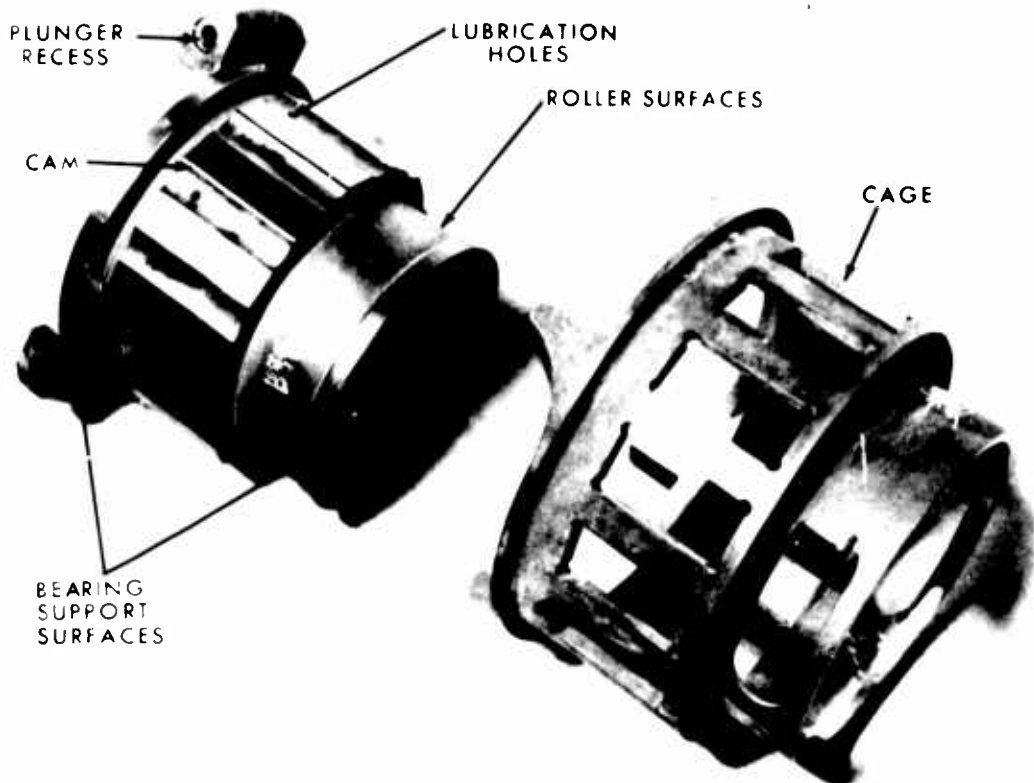
Figure 80. Cam and Cage, Ramp Roller Clutch.

150

Primary lubrication is provided by oil centrifuged from the
rotating spur gear shaft, Figure 81.  Additional lubrication
is provided by a jet directed between the cam and the housing.

The freewheel unit is of unitized construction.  This
facilitates replacement of the cam and housings in the eventual
wear of the flats.
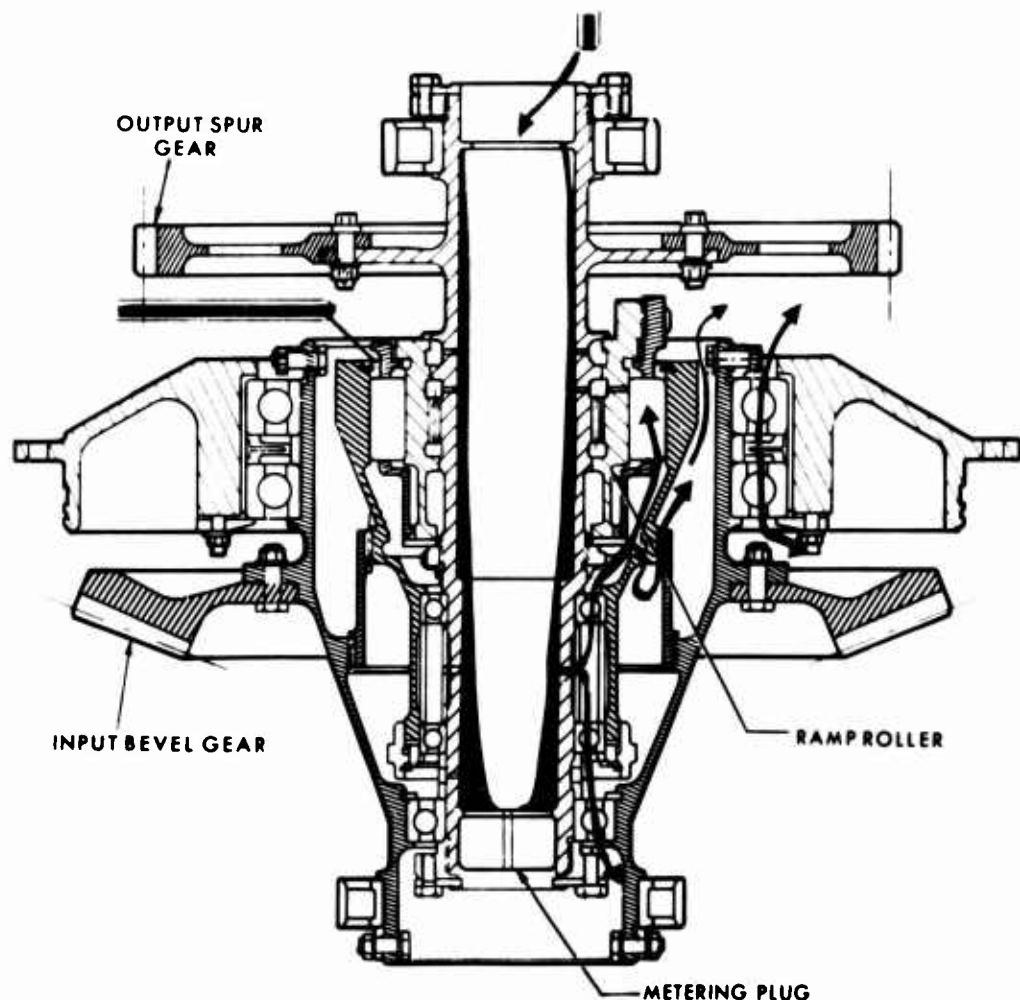


Figure 81.   Freewheel Unit Arrangement.

## COMBINING GEAR

Power from each engine is combined at the second-stage spur
gear reduction to a common driveshaft which transmits power
to the roller gear unit and the tail rotor drive and accesso-
ries. Two spur gears, driven by the cam outputs of the free-
wheel units, mesh with a common bull gear to combine the
power from each engine.

Maximum loads are induced in the bull gear shafting when single
engine maximum power is being transmitted by the right-hand
engine and maximum torque is absorbed by the tail drive and
accessory system. During normal dual engine operation, the
gear mesh loads on each side of the bull gear tend to cancel,
thereby lowering the stress levels in the shaft. The wall
thickness of the bull gear shaft is limited by manufacturing
technology which requires a nominal wall thickness of 0.100
inch to prevent excessive chatter while being machined.

The spur gear set, Figure 82, is designed to aircraft gear
practice. Holes in the gear webs lighten the structure.
Sufficient bolts are assembled to transmit the torque through
the friction achieved by the bolt clamping force. This is
normal design practice which is adhered to whenever possible.
The center bull gear teeth are crowned to reduce tooth contact
stresses. The resultant parabolic shaped gear teeth can
accommodate stress maldistribution resulting from misalign-
ment of the mating gear teeth.
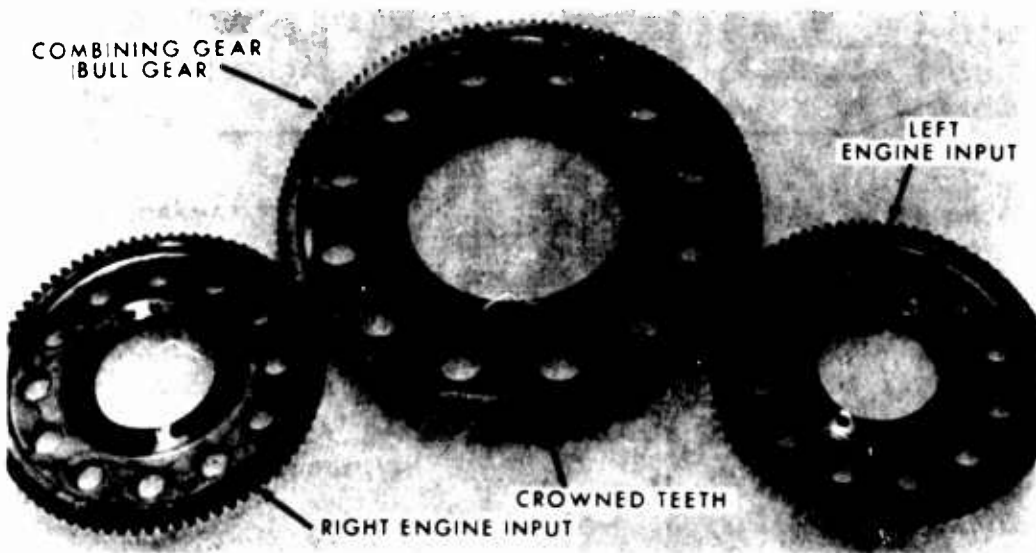
Figure 82. Second-Stage Reduction Gears.

A floating quill shaft transmits torque to the roller gear
unit. Two diametrically opposed clips axially support the
quill shaft. Lubrication of the quill shaft spline is by oil
centrifuged onto the shaft inner wall, Figure 83. An aluminum
spur shield prevents the oil from spilling out of the top of
the shaft.
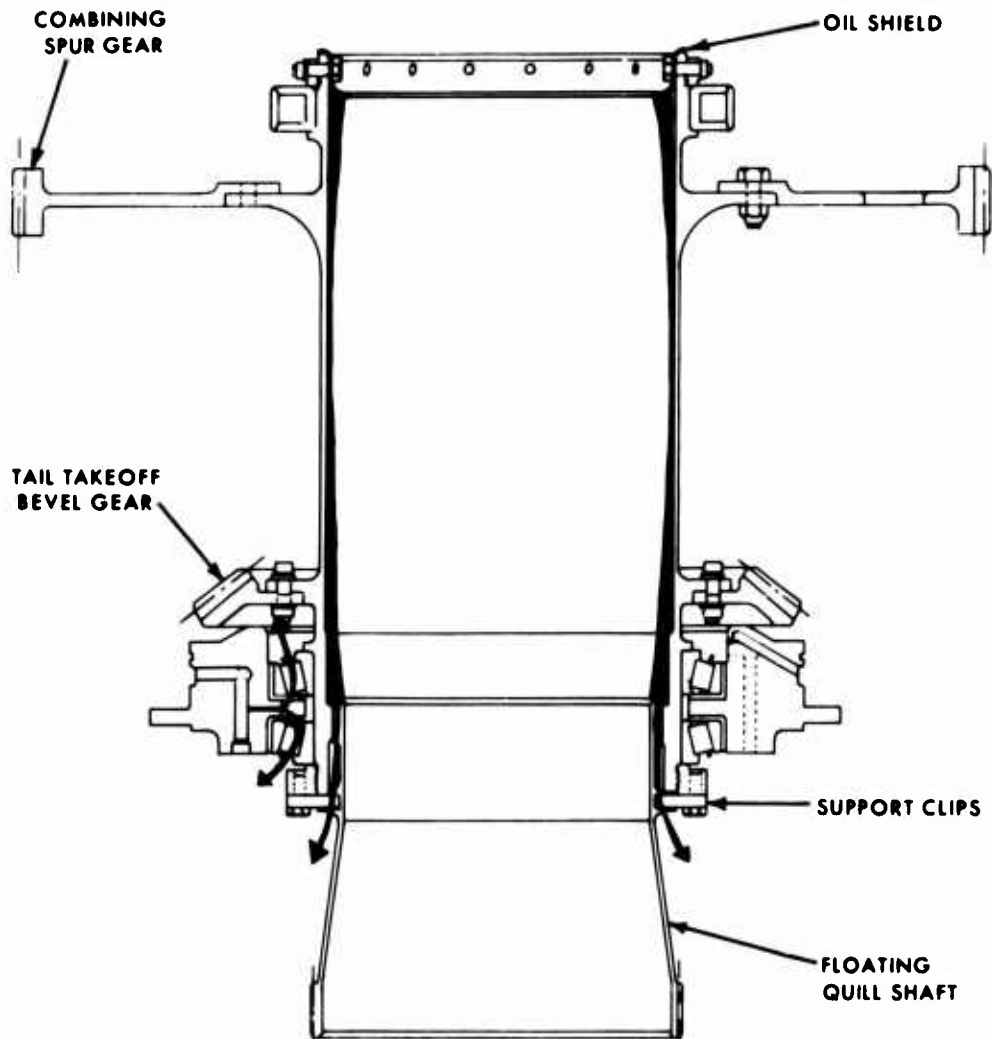


Figure 83. Combining Gear Shaft Arrangement.

## ACCESSORY DRIVE

The accessory gear train provides power for the accessories
listed in Table 11. Power for these drives is supplied from
the combining gear shaft through speed increasing spiral
bevel gears. The gears are all located on the rear cover of
the housing. During conceptual design, adequate clearance
has to be allowed to accommodate the size and accessibility of
the accessory units, and the requisite speed has to be obtained.
The fatigue design horsepower to which the accessory gears and
shaft and 3,000-hour minimum B-10 bearing life are designed
is assumed to be equal to the maximum power requirement of
each individual accessory.

| TABLE 11. ACCESSORY DRIVE TRAIN, MAIN TRANSMISSION. | | |
|---|---|---|
| | Fatigue Design hp | rpm |
| Generator Drive, Left Side | 53.6 | 8,010 |
| Generator Drive, Right Side | 53.6 | 8,112 |
| Auxiliary Hydraulic Pump Drive | 6.5 | 4,005 |
| Utility Hydraulic Pump Drive | 13.0 | 4,005 |
| Lubrication Pump Drive | 4.0 | 5,149 |
| Tail Takeoff Drive | 565.0 | 4,005 |
| Oil Cooler Drive | 15.0 | 7,031 |
| Primary Hydraulic Pump Drive | 6.5 | 4,197 |
| Tachometer Generator Drive | 1.0 | 3,906 |
| Rotor Brake Drive | 825.0 | 4,334 |

The arrangement of the accessory drives and their direction of rotation are shown in Figure 84. The primary tail drive is through a 45/90 spur gear reduction. A disc brake, driven off the 90-tooth output gear, is designed to stop the rotor in 12 seconds. Auxiliary supplied hydraulic pressure actuates four disc pucks, providing a brake torque of 11,990 in-lb.

Attached onto the rear cover is an adaptor gearbox. This gearbox enables the roller gear transmission to adapt to the speed and alignment requirements of the S-61 tail rotor drive system. In the eventuality of this transmission being incorporated into a growth production version of the S-61 helicopter, the adaptor gearbox would be eliminated and the tail drive system driven directly from the rear cover power takeoff.

The adaptor gearbox gears are straight spur teeth gears, 10 diametral pitch, and provide a 62 percent speed reduction through a 34/55/45 gear train. The 55-tooth idler gear is crowned to accommodate gear meshing misalignment of the input and output gears.
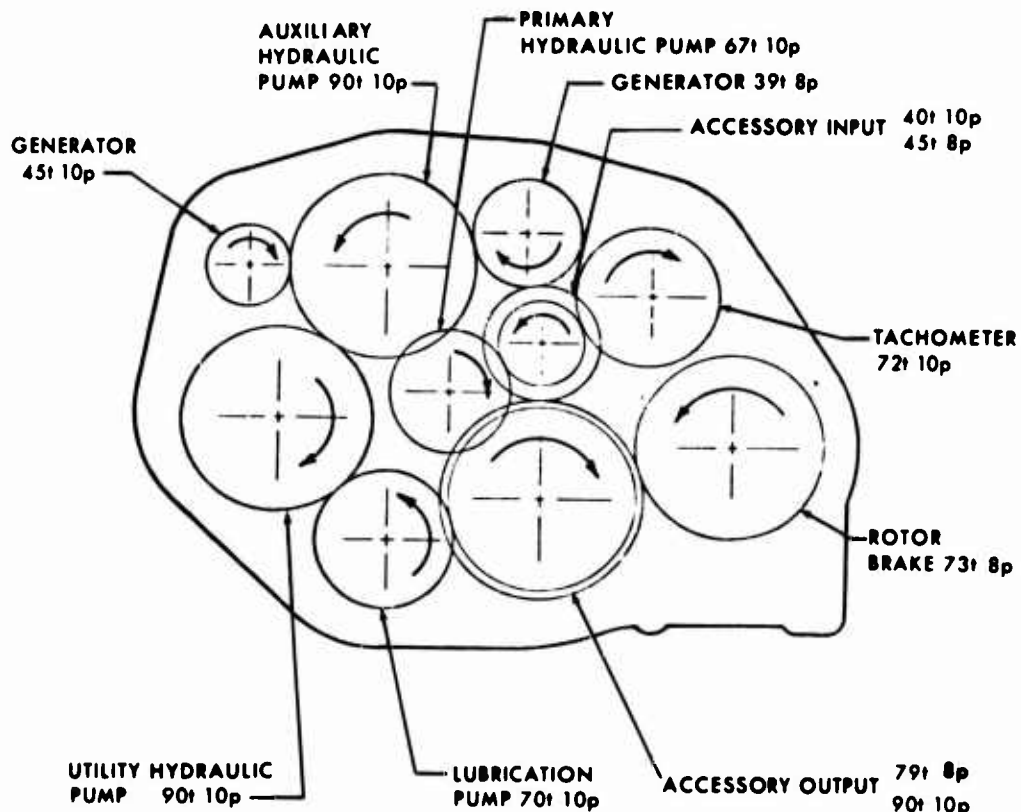


Figure 84.  Accessory Drive, Rear Cover.

155

## HOUSING

The transmission housing is three major castings which are
machined to form the main, the top and the rear cover housings.
The main housing contains the first- and second-stage reductions
and space for the roller gear unit.  The top cover is bolted
onto the main housing and provides the bearing supports for
the second-stage reduction and main rotor shaft.  The rear
cover contains the accessory gears and is bolted directly onto
the rear of the main housing.

As this was an experimental program, the housing design was
aimed at cost saving instead of weight saving.  Cored lines
were kept to a minimum, and bolt circle flanges were cast solid
instead of scalloped.  A cardboard model of the main housing,
Figure 85, was built and used as a geometric and structural
check by the casting foundry.



Figure 85.  Main Housing Design Model.
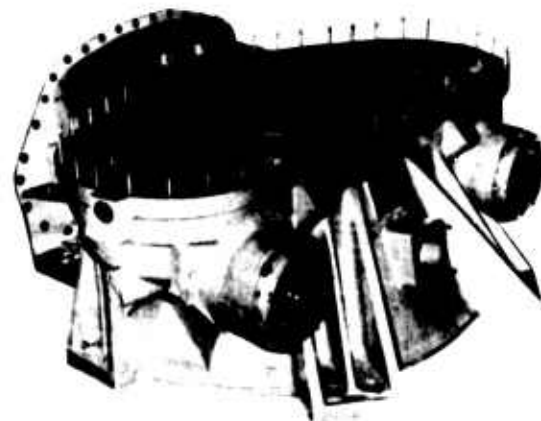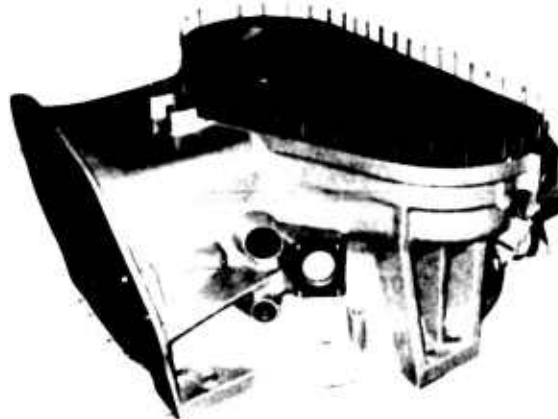
Figure 86.  Main Housing.

157

The three housings were cast from the magnesium alloy ZE41A. This alloy is stronger than the more conventionally used alloy AZ91C, Table 12, and casts virtually free of microporosity with a more homogeneous mass within the casting.

| TABLE 12. MECHANICAL PROPERTIES OF ZE41A AND AZ91C MAGNESIUM ALLOYS. | | |
|---|---|---|
| | AZ91C | ZE41A |
| Ultimate Tensile Strength (psi) | 17,000 | 26,000 |
| Yield Strength (psi) | 12,000 | 17,500 |
| Elongation (%) | 3.0 | 2.0 |
| Tensile Modulus of Elasticity ($10^6$ psi) | 6.5 | 6.5 |
| Shear Modulus of Elasticity ($10^6$ psi) | 2.4 | 2.4 |
| Thermal Expansion Coefficient ($10^{-6}$ in./in./°F) | 14 | 15.1 |

The main housing, Figure 86, provides three pads for the location of the main rotor head servos. These servos react the rotor head vibratory loads and are designed to statically withstand crash loads and fatigue loading induced by the rotor head vibratory forces.

The main housing ribs and mounting bolts are designed to withstand forward and downward crash loads of 20g and side crash loads of 10g. Transferring a rotor head weight of 2,590 lb and a gearbox weight of 1,900 lb to the centroid of the bolt pattern, Figure 87, gives the crash loads, Table 13, from which the forces in the gearbox hold-down bolts and housing rib sizes are determined.
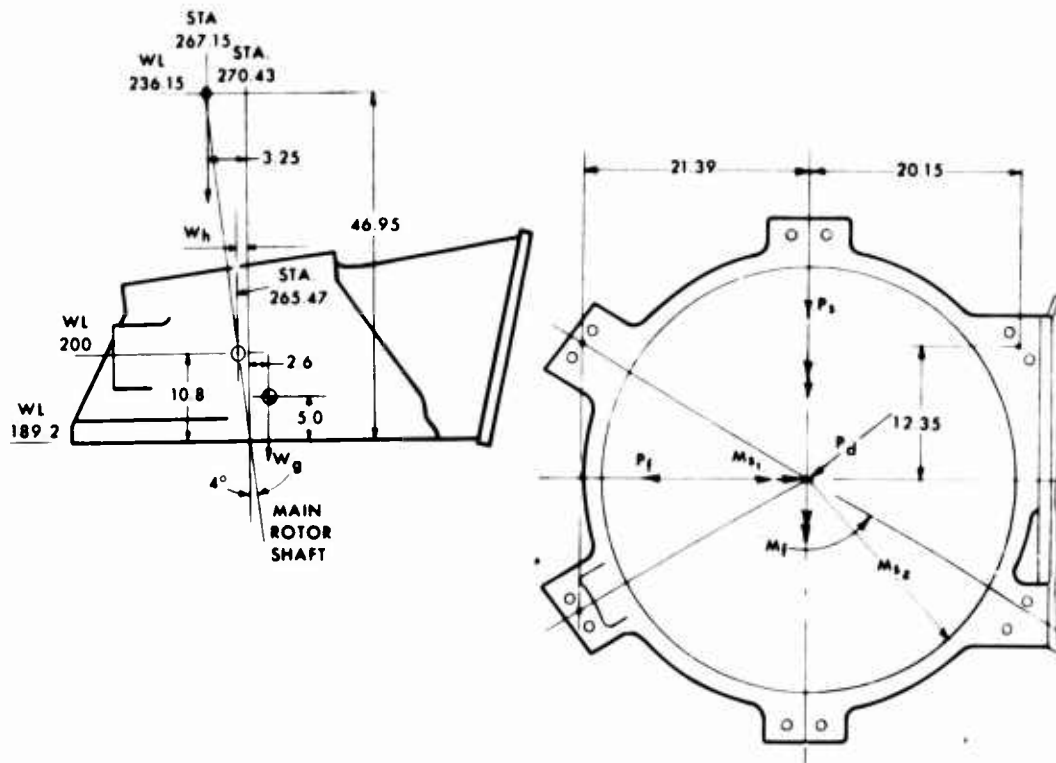
Figure 87. Crash Loads, Main Housing.

| TABLE 13. CRASH LOADS AT MOUNTING BASE, MAIN HOUSING. | | |
|---|---|---|
| Condition | Load (1b) | Moment (in-1b) |
| Condition I (20g forward) | $P_F$ = 89,800 | $M_F$ = 2,622,000 |
| Condition II (20g down) | $P_D$ = 89,800 | $M_D$ = 71,100 |
| Condition III (10g side) | $P_S$ = 44,900 | $M_{S1}$ = 1,311,000<br>$M_{S2}$ = 35,550 |

159

The ma n housing is designed for compartmentalization of the first- and second-stage reduction units, the roller gear unit and the accessory section. Magnetic type chip detectors, located as shown in Figure 88, allow lubrication oil to drain through while retaining magnetic particles which light remotely located chip indicators. This compartmentalization prevents contamination of the roller gear unit from debris which might be generated in the input and spur gear reduction units. It also assists in the accurate location of any malfunction of dynamic components.

SECOND-STAGE SPUR GEAR REDUCTION AND
TAIL TAKEOFF BEVEL GEAR CHIP DETECTORS

FIRST-STAGE BEVEL GEAR REDUCTION
LEFT-HAND & RIGHT-HAND INPUT
CHIP DETECTORS

ROLLER GEAR AND ADAPTOR
GEARBOX CHIP DETECTOR
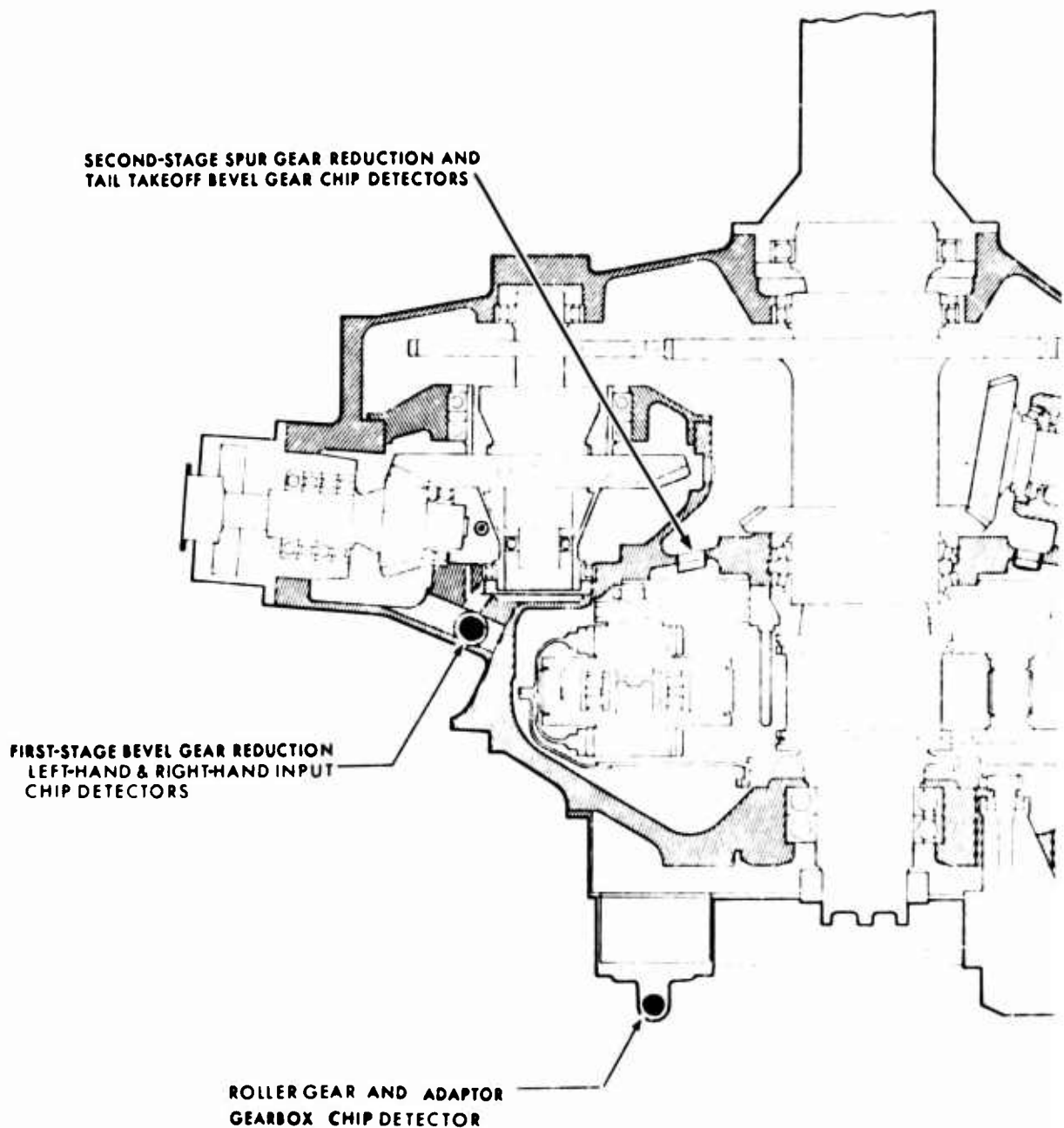
Figure 88.   Compartmentalization, Roller Gear Transmission.

161

ACCESSORY SECTION CHIP DETECTOR

TOR
R
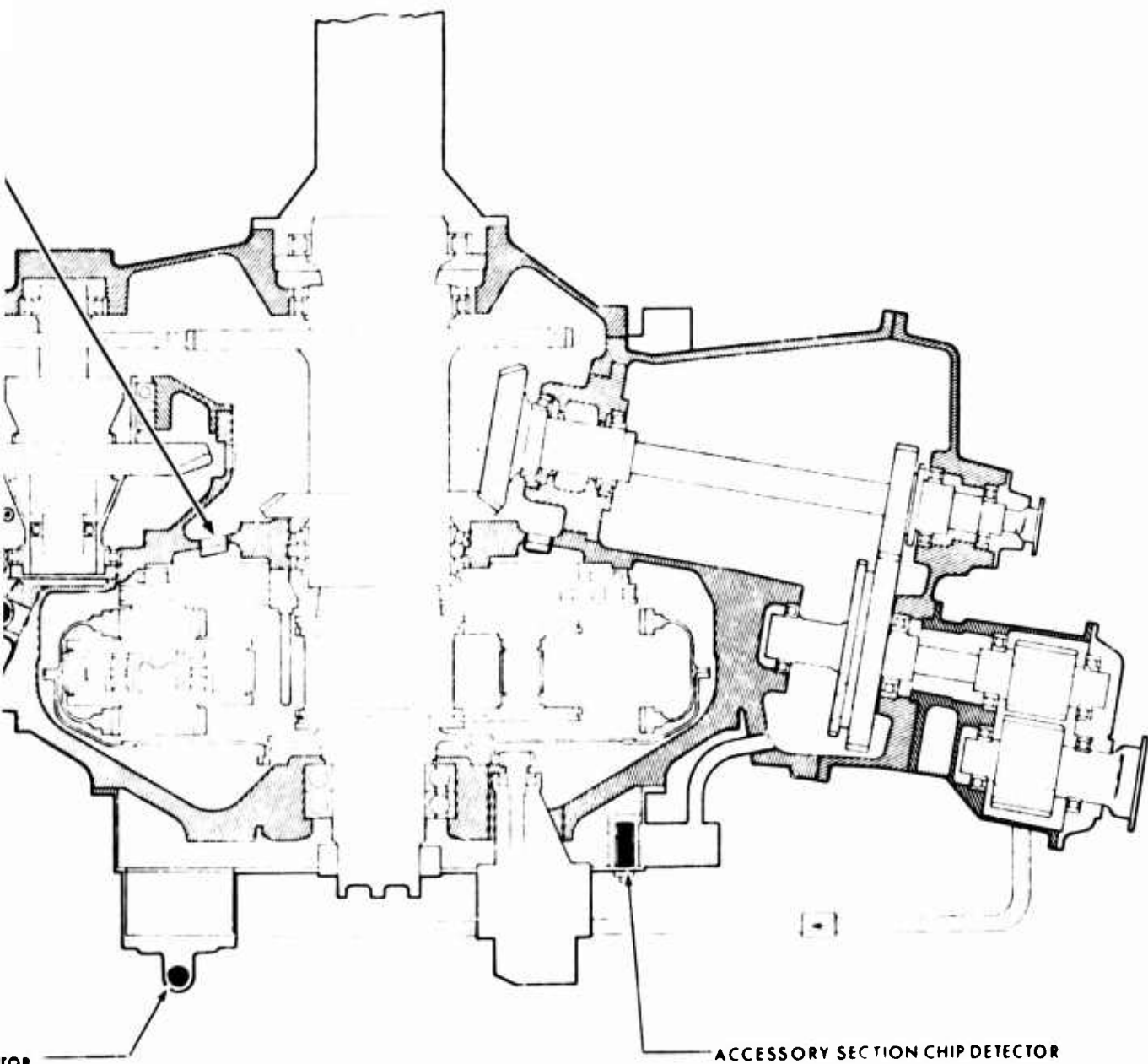
ler Gear Transmission.

# TRANSMISSION EFFICIENCY AND LUBRICATION

## INTRODUCTION

The efficiency of the roller gear unit is calculated to be 98.9 percent when transmitting full power. The efficiency of the complete transmission is 96.5 percent. These figures are based on calculations given in Appendix H whereby the heat generated within the gearbox is computed and then converted to friction power. This is then compared to the input power to obtain the efficiency. The transmission efficiencies result from the lubrication calculations (Appendix H) wherein the optimum cooling requirements for the gears and bearings are determined.

## LUBRICATION REQUIREMENTS

The primary drive train of the roller gear drive transmission has lubricant under pressure directed to the bearings and gear meshes. The input and tail takeoff bevel gears are lubricated into and out of the mesh by jets of oil; all other primary drive train gears have lubrication jets directed to the outgoing mesh. Primary drive train bearings have pressurized oil directed through them, though the input stack bearing oil pressure is created by centrifugal force which circulates the oil through the individual bearings.

In the roller gear drive unit each gear has oil directed to the outgoing mesh, and pressurized oil is directed to selected shoulder contact areas.

Accessory drive train gears are oil mist lubricated and the bearings are gravity fed from oil collected in scuppers.

In order to evaluate the lubrication requirements of gear meshes and bearings, it was necessary to determine the heat generated during operation. If sufficient lubricant is available to provide a heat balance between the heat generated and the heat dissipated, then lubrication should be good.

The heat generated during the operation of gears and bearings depends upon the energy loss due to friction. For the rolling contacts in the roller gear drive unit and gear meshes, the energy loss, i.e., the frictional horsepower, is directly related to the efficiency of the mesh and the transmitted power.

$$F_{hp} = (1 - \eta)hp$$

163

Bearing friction is normally witnessed as a temperature increase and is measured as a retarding torque. This loss falls into two categories: (1) the friction loss due to applied load $M_l$, and (2) the friction loss due to viscous effects Mv. The frictional horsepower is thus proportional to the total retarding torque $M = M_l + M_v$.

Thus,

$$F_{hp} = M \frac{rpm}{63,025}$$

For gears and bearings, the total heat generated in Btu's/minute is

$$H_1 = F_{hp} \times 42.42$$

and the oil required in gallons per minute is

$$Q = \frac{.13 \ H_1}{C_p \ \Delta T}$$

where

| | | |
|---|---|---|
| Q | = | required oil flow rate to cool $H_1$ (Btu/min), the amount, $\Delta T$ |
| $C_p$ | = | oil specific heat at average oil cooler temperature (Btu/lb/°F) |
| $\Delta T$ | = | change in oil temperature |

## LUBRICATION SYSTEM

Two fixed displacement vane pumps, one mounted in the sump and driven off the main rotor shaft through speed increasing gears, and the other mounted on the rear cover and driven by the primary hydraulic gear, are each capable of delivering 22 gallons per minute.

Oil from the sump is fed to each pump which combines into one line at the inlet to the oil filter. Upon exit, the oil passes through the oil cooler and onto the jets. The relief valve at the pump can be adjusted to ensure the desired pressure. In order to limit the amount of oil to the roller gear drive unit, a restrictor is placed in the line. Also affected by this restrictor are the lubrication jets to the tapered roller bearings on the outer shaft and tail takeoff bevel gear shaft. Figure 89 is a schematic of the lubrication system.
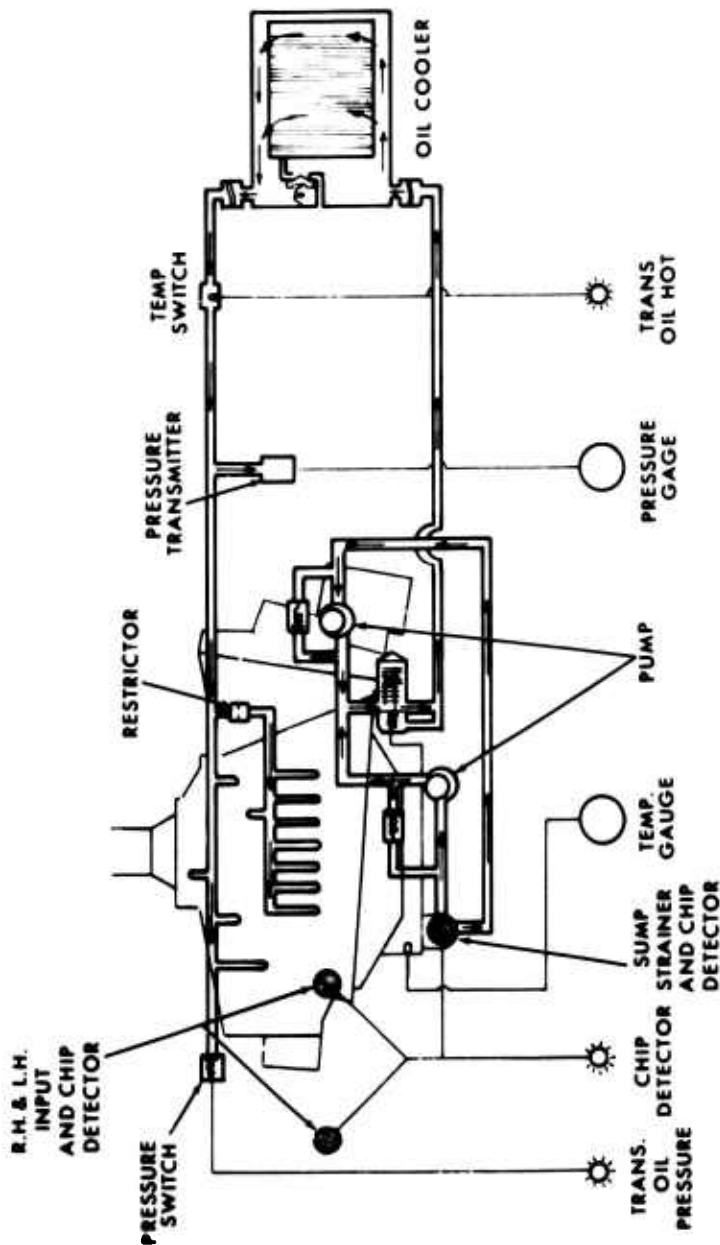
Figure 89. Lubrication Schematic, Roller Gear Transmission.

165

## TRANSMISSION EFFICIENCY

The efficiency of a transmission is a function of the heat that is generated in the gearbox. This heat, when converted to friction horsepower at the source of heat, i.e., the gear meshes and bearings, and compared to the input power, is the efficiency.

Heat is generated from friction, oil churning, windage and viscous shearing of the oil film at the contacts. In calculating the efficiency of the roller gear drive transmission, the effects of oil churning and windage were ignored; viscous shearing was incorporated in bearing friction horsepower, but neglected in gear mesh calculations.

The overall efficiency is a function of the power out and the power in. Thus

$$\eta_{overall} = \frac{P_{out\ main\ rotor} + P_{out TTO} + P_{out\ accessories}}{P_{in}}$$

## ROLLER GEAR DRIVE UNIT EFFICIENCY

The theoretical efficiency formula for the two-row, ring output, carrier fixed, sun gear input, roller gear drive is calculated from the efficiencies of the individual meshes. Since all gears are on fixed centers, the overall efficiency is the product of the three individual mesh efficiencies and is given by

$$\eta_{overall} = \eta_{ax1}\ \eta_{y1}\ \eta_{x2}\ \eta_{y2c}$$

where

| | | |
|---|---|---|
| $\eta_{overall}$ | = | overall efficiency of roller gear drive unit |
| $\eta_{ax1}$ | = | efficiency of sun gear with first-row pinion |
| $\eta_{y1\ x2}$ | = | efficiency of first-row pinion with second-row pinion |
| $\eta_{y2c}$ | = | efficiency of second-row pinion with ring gear. |

166

# APPENDIX A

## TOOTH SPACING RELATIONSHIPS

Proper meshing of gear teeth in a multistage roller gear drive can only be obtained with particular combinations of teeth. The meshing relationships shown herein pertain to the meshes between rows, i.e., first-row to second-row mesh, or second-row to third-row mesh, as shown in Figure A-1.

The equations derived in the "Gear Teeth Indexing" section of this report are

$$\frac{N_1}{M} + \frac{N_1}{n} = \text{whole number}$$

$$\frac{N_2}{M} = \text{whole number}$$

where

$N_1$ = teeth in gear of inner row
$N_2$ = teeth in gear of outer row
n = number of pinions
M = improper fraction defining the toggle angle as

$$a = \frac{\pi}{M}$$

All the possible toggle angles that can be used in a roller gear drive unit and the divisors of the number of teeth for each gear were determined. The results are presented in Table A-1 which gives the value of M for all combinations of number of pinions from five to twelve. In addition, the lowest integer divisors of each gear are given. The teeth of each gear must be divisible by these divisors with no remainder for the roller gear unit to mesh properly.

SECOND-ROW TO
THIRD-ROW MESH

FIRST-ROW TO
SECOND-ROW MESH
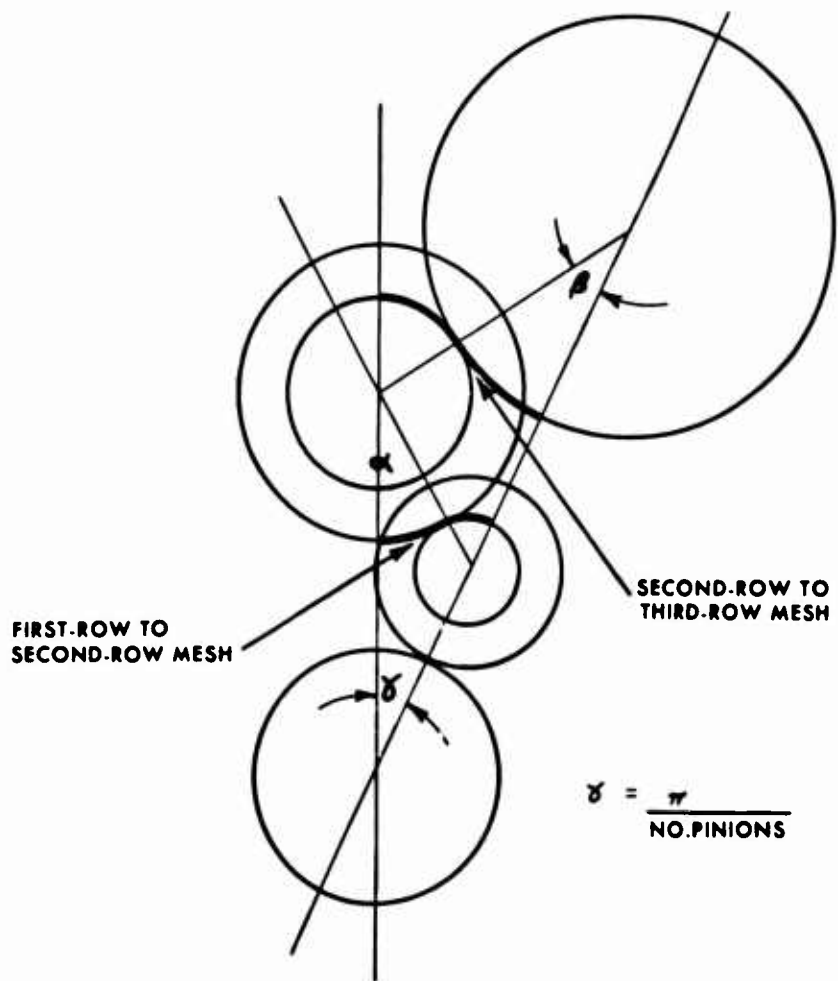
$$\gamma = \frac{\pi}{\text{NO.PINIONS}}$$

Figure A-1.   Gear Mesh Nomenclature.

168

| Number of Pinions | $a$ or $\beta$ (degrees) | M | Lowest Divisor of Inner Row Teeth | Lowest Divisor of Outer Row Teeth |
|---|---|---|---|---|
| 5 | 90 | 2 | 10 | 2 |
| 5 | 84 | 2 1/7 | 3 | 15 |
| 5 | 81 | 2 2/9 | 20 | 20 |
| 5 | 80 | 2 1/4 | 45 | 9 |
| 5 | 77 1/7 | 2 1/3 | 35 | 7 |
| 5 | 72 | 2 1/2 | 5 | 5 |
| 5 | 67 1/2 | 2 2/3 | 40 | 8 |
| 5 | 64 4/5 | 2 7/9 | 25 | 25 |
| 5 | 63 | 2 6/7 | 20 | 20 |
| 5 | 60 | 3 | 15 | 3 |
| 5 | 57 3/5 | 3 1/8 | 25 | 25 |
| 5 | 54 | 3 1/3 | 2 | 10 |
| 5 | 51 3/7 | 3 1/2 | 35 | 7 |
| 5 | 50 2/5 | 3 4/7 | 25 | 25 |
| 5 | 48 | 3 3/4 | 15 | 15 |
| 5 | 46 2/7 | 3 8/9 | 35 | 35 |
| 5 | 45 | 4 | 20 | 4 |
| 5 | 43 1/5 | 4 1/6 | 25 | 25 |
| 5 | 42 | 4 2/7 | 30 | 30 |
| 5 | 41 1/7 | 4 3/8 | 7 | 35 |
| 5 | 40 1/2 | 4 4/9 | 40 | 40 |
| 5 | 40 | 4 1/2 | 45 | 9 |
| 5 | 36 | 5 | 5 | 5 |
| 5 | 32 2/5 | 5 5/9 | 50 | 50 |
| 5 | 32 | 5 5/8 | 45 | 45 |
| 5 | 31 1/2 | 5 5/7 | 8 | 40 |
| 5 | 30 6/7 | 5 5/6 | 35 | 35 |
| 5 | 30 | 6 | 30 | 6 |
| 5 | 29 5/11 | 6 1/9 | 11 | 55 |
| 5 | 28 4/5 | 6 1/4 | 25 | 25 |
| 5 | 28 | 6 3/7 | 45 | 45 |
| 5 | 27 | 6 2/3 | 20 | 20 |
| 5 | 25 5/7 | 7 | 35 | 7 |
| 5 | 25 1/5 | 7 1/7 | 50 | 50 |
| 5 | 24 | 7 1/2 | 3 | 15 |
| 5 | 22 1/2 | 8 | 40 | 8 |
| 5 | 21 3/5 | 8 1/3 | 25 | 25 |
| 5 | 20 4/7 | 8 3/4 | 35 | 35 |
| 5 | 20 1/4 | 8 8/9 | 16 | 80 |
| 5 | 20 | 9 | 45 | 9 |
| 5 | 19 5/13 | 9 2/7 | 13 | 65 |
| 5 | 18 | 10 | 10 | 10 |
| 5 | 16 16/17 | 10 5/8 | 17 | 85 |
| 5 | 16 | 11 1/4 | 45 | 45 |

TABLE A-1.   TOGGLE ANGLES AND TOOTH INTEGER DIVISORS.

| Number of Pinions | $a$ or $\beta$ (degrees) | M | Lowest Divisor of Inner Row Teeth | Lowest Divisor of Outer Row Teeth |
|---|---|---|---|---|
| | | TABLE A-I. Continued | | |
| 5 | 15 3/7 | 11 2/3 | 7 | 35 |
| 6 | 90 | 2 | 3 | 2 |
| 6 | 85 5/7 | 2 1/10 | 14 | 21 |
| 6 | 84 | 2 1/7 | 30 | 15 |
| 6 | 80 | 2 1/4 | 18 | 9 |
| 6 | 78 3/4 | 2 2/7 | 48 | 16 |
| 6 | 77 1/7 | 2 1/3 | 42 | 7 |
| 6 | 75 | 2 2/5 | 12 | 12 |
| 6 | 73 7/11 | 2 4/9 | 33 | 22 |
| 6 | 72 | 2 1/2 | 30 | 5 |
| 6 | 70 | 2 4/7 | 9 | 18 |
| 6 | 68 4/7 | 2 5/8 | 42 | 21 |
| 6 | 67 1/2 | 2 2/3 | 24 | 8 |
| 6 | 64 2/7 | 2 4/5 | 21 | 14 |
| 6 | 62 4/13 | 2 8/9 | 39 | 26 |
| 6 | 60 | 3 | 2 | 3 |
| 6 | 57 3/11 | 3 1/7 | 33 | 22 |
| 6 | 56 1/4 | 3 1/5 | 48 | 16 |
| 6 | 54 | 3 1/3 | 15 | 10 |
| 6 | 52 1/2 | 3 3/7 | 24 | 24 |
| 6 | 51 3/7 | 3 1/2 | 42 | 7 |
| 6 | 50 | 3 3/5 | 9 | 18 |
| 6 | 48 6/13 | 3 5/7 | 36 | 26 |
| 6 | 48 | 3 3/4 | 30 | 15 |
| 6 | 46 2/13 | 3 9/10 | 26 | 39 |
| 6 | 45 | 4 | 12 | 4 |
| 6 | 43 7/11 | 4 1/8 | 22 | 33 |
| 6 | 42 6/7 | 4 1/5 | 42 | 21 |
| 6 | 42 | 4 2/7 | 5 | 30 |
| 6 | 40 10/11 | 4 2/5 | 33 | 22 |
| 6 | 40 | 4 1/2 | 18 | 9 |
| 6 | 38 4/7 | 4 2/3 | 21 | 14 |
| 6 | 37 1/2 | 4 4/5 | 8 | 24 |
| 6 | 36 | 5 | 30 | 5 |
| 6 | 35 | 5 1/7 | 36 | 36 |
| 6 | 34 8/13 | 5 1/5 | 39 | 26 |
| 6 | 34 2/7 | 5 1/4 | 14 | 21 |
| 6 | 33 3/4 | 5 1/3 | 48 | 16 |
| 6 | 32 4/13 | 5 4/7 | 26 | 39 |
| 6 | 31 11/19 | 5 7/10 | 38 | 57 |
| 6 | 30 | 6 | 3 | 6 |
| 6 | 28 4/17 | 6 3/8 | 34 | 51 |
| 6 | 27 3/11 | 6 3/5 | 22 | 33 |
| 6 | 26 1/4 | 6 6/7 | 16 | 48 |
| 6 | 25 5/7 | 7 | 42 | 7 |

170

| Number of Pinions | $a$ or $\beta$ (degrees) | M | Lowest Divisor of Inner Row Teeth | Lowest Divisor of Outer Row Teeth |
|---|---|---|---|---|
| | | TABLE A-1. Continued | | |

| Number of Pinions | $a$ or $\beta$ (degrees) | M | Lowest Divisor of Inner Row Teeth | Lowest Divisor of Outer Row Teeth |
|---|---|---|---|---|
| 6 | 25 | 7 1/5 | 36 | 36 |
| 6 | 24 6/11 | 7 1/3 | 33 | 22 |
| 6 | 24 | 7 1/2 | 10 | 15 |
| 6 | 23 1/3 | 7 5/7 | 27 | 54 |
| 6 | 22 1/2 | 8 | 24 | 8 |
| 6 | 22 2/19 | 8 1/7 | 38 | 57 |
| 6 | 21 3/7 | 8 2/5 | 7 | 42 |
| 6 | 20 20/23 | 8 5/8 | 46 | 69 |
| 6 | 20 10/13 | 8 2/3 | 39 | 26 |
| 6 | 20 | 9 | 18 | 9 |
| 6 | 19 1/11 | 9 3/7 | 11 | 66 |
| 6 | 18 3/4 | 9 3/5 | 48 | 48 |
| 6 | 18 6/13 | 9 3/4 | 26 | 39 |
| 6 | 18 | 10 | 15 | 10 |
| 6 | 17 11/17 | 10 1/5 | 34 | 51 |
| 6 | 17 1/7 | 10 1/2 | 42 | 21 |
| 6 | 16 4/5 | 10 5/7 | 50 | 75 |
| 6 | 16 2/3 | 10 4/5 | 27 | 54 |
| 6 | 16 2/13 | 11 1/7 | 39 | 78 |
| 6 | 15 | 12 | 4 | 12 |
| 7 | 90 | 2 | 14 | 2 |
| 7 | 85 5/7 | 2 1/10 | 21 | 21 |
| 7 | 77 1/7 | 2 1/3 | 7 | 7 |
| 7 | 72 | 2 1/2 | 35 | 5 |
| 7 | 68 4/7 | 2 5/8 | 21 | 21 |
| 7 | 64 2/7 | 2 4/5 | 2 | 14 |
| 7 | 60 | 3 | 21 | 3 |
| 7 | 57 6/7 | 3 1/9 | 28 | 28 |
| 7 | 51 3/7 | 3 1/2 | 7 | 7 |
| 7 | 46 2/7 | 3 8/9 | 5 | 35 |
| 7 | 45 | 4 | 28 | 4 |
| 7 | 42 6/7 | 4 1/5 | 21 | 21 |
| 7 | 41 1/7 | 4 3/8 | 35 | 35 |
| 7 | 38 4/7 | 4 2/3 | 14 | 14 |
| 7 | 36 36/49 | 4 9/10 | 49 | 49 |
| 7 | 36 | 5 | 35 | 5 |
| 7 | 34 2/7 | 5 1/4 | 3 | 21 |
| 7 | 33 3/49 | 5 4/9 | 49 | 49 |
| 7 | 32 1/7 | 5 3/5 | 28 | 28 |
| 7 | 30 6/7 | 5 5/6 | 35 | 35 |
| 7 | 30 | 6 | 42 | 6 |
| 7 | 29 19/49 | 6 1/8 | 19 | 49 |
| 7 | 25 5/7 | 7 | 7 | 7 |
| 7 | 23 29/77 | 7 7/10 | 11 | 77 |
| 7 | 22 2/49 | 8 1/6 | 49 | 49 |

| Number of Pinions | a or β (degrees) | M | Lowest Divisor of Inner Row Teeth | Lowest Divisor of Outer Row Teeth |
|---|---|---|---|---|
| 7 | 21 3/7 | 8 2/5 | 42 | 42 |
| 7 | 20 4/7 | 8 3/4 | 35 | 35 |
| 7 | 19 2/7 | 9 1/3 | 4 | 28 |
| 7 | 18 18/49 | 9 4/5 | 49 | 49 |
| 7 | 17 1/7 | 10 1/2 | 21 | 21 |
| 7 | 15 75/91 | 11 3/8 | 13 | 91 |
| 7 | 15 3/7 | 11 2/3 | 35 | 35 |
| 8 | 90 | 2 | 8 | 2 |
| 8 | 81 | 2 2/9 | 40 | 20 |
| 8 | 78 3/4 | 2 2/7 | 16 | 16 |
| 8 | 75 | 2 2/5 | 24 | 12 |
| 8 | 72 | 2 1/2 | 40 | 5 |
| 8 | 67 1/2 | 2 2/3 | 2 | 8 |
| 8 | 63 | 2 6/7 | 40 | 20 |
| 8 | 60 | 3 | 24 | 3 |
| 8 | 56 1/4 | 3 1/5 | 16 | 16 |
| 8 | 54 | 3 1/3 | 40 | 10 |
| 8 | 52 1/2 | 3 3/7 | 12 | 24 |
| 8 | 50 5/8 | 3 5/9 | 32 | 32 |
| 8 | 45 | 4 | 8 | 4 |
| 8 | 40 1/2 | 4 4/9 | 20 | 40 |
| 8 | 39 3/8 | 4 4/7 | 32 | 32 |
| 8 | 37 1/2 | 4 4/5 | 3 | 24 |
| 8 | 36 | 5 | 40 | 5 |
| 8 | 33 3/4 | 5 1/3 | 16 | 16 |
| 8 | 31 1/2 | 5 5/7 | 10 | 40 |
| 8 | 30 | 6 | 24 | 6 |
| 8 | 28 13/14 | 6 2/9 | 7 | 56 |
| 8 | 28 1/8 | 6 2/5 | 32 | 32 |
| 8 | 27 | 6 2/3 | 40 | 20 |
| 8 | 26 1/4 | 6 6/7 | 48 | 48 |
| 8 | 22 1/2 | 8 | 4 | 8 |
| 8 | 18 3/4 | 9 3/5 | 48 | 48 |
| 8 | 18 9/22 | 9 7/9 | 22 | 88 |
| 8 | 18 | 10 | 40 | 10 |
| 8 | 17 1/2 | 10 2/7 | 9 | 72 |
| 8 | 16 7/8 | 10 2/3 | 32 | 32 |
| 8 | 16 1/14 | 11 1/5 | 14 | 56 |
| 8 | 15 | 12 | 24 | 12 |
| 9 | 90 | 2 | 18 | 2 |
| 9 | 84 | 2 1/7 | 45 | 15 |
| 9 | 80 | 2 1/4 | 9 | 9 |
| 9 | 75 | 2 2/5 | 36 | 12 |
| 9 | 72 | 2 1/2 | 45 | 5 |
| 9 | 70 | 2 4/7 | 2 | 18 |

| Number of Pinions | α or β (degrees) | M | Lowest Divisor of Inner Row Teeth | Lowest Divisor of Outer Row Teeth |
|---|---|---|---|---|
| | | | Continued | |

TABLE A-1. Continued

| Number of Pinions | α or β (degrees) | M | Lowest Divisor of Inner Row Teeth | Lowest Divisor of Outer Row Teeth |
|---|---|---|---|---|
| 9 | 66 2/3 | 2 7/10 | 27 | 27 |
| 9 | 60 | 3 | 9 | 3 |
| 9 | 53 1/3 | 3 3/8 | 27 | 27 |
| 9 | 50 | 3 3/5 | 18 | 18 |
| 9 | 48 | 3 3/4 | 45 | 15 |
| 9 | 46 2/3 | 3 6/7 | 27 | 27 |
| 9 | 45 | 4 | 36 | 4 |
| 9 | 40 | 4 1/2 | 3 | 9 |
| 9 | 36 | 5 | 45 | 5 |
| 9 | 35 | 5 1/7 | 36 | 36 |
| 9 | 33 1/3 | 5 2/5 | 27 | 27 |
| 9 | 32 | 5 5/8 | 45 | 45 |
| 9 | 30 | 6 | 18 | 6 |
| 9 | 28 | 6 3/7 | 15 | 45 |
| 9 | 26 2/3 | 6 3/4 | 27 | 27 |
| 9 | 25 | 7 1/5 | 4 | 36 |
| 9 | 24 | 7 1/2 | 45 | 15 |
| 9 | 22 6/7 | 7 7/8 | 21 | 63 |
| 9 | 20 | 9 | 9 | 9 |
| 9 | 18 2/11 | 9 9/10 | 33 | 99 |
| 9 | 17 1/2 | 10 2/7 | 24 | 72 |
| 9 | 16 | 11 1/4 | 5 | 45 |
| 9 | 15 | 12 | 36 | 12 |
| 10 | 90 | 2 | 5 | 2 |
| 10 | 84 | 2 1/7 | 30 | 15 |
| 10 | 80 | 2 1/4 | 20 | 20 |
| 10 | 72 | 2 1/2 | 2 | 5 |
| 10 | 70 | 2 4/7 | 45 | 18 |
| 10 | 67 1/2 | 2 2/3 | 40 | 8 |
| 10 | 64 4/5 | 2 7/9 | 50 | 25 |
| 10 | 64 2/7 | 2 4/5 | 35 | 14 |
| 10 | 63 | 2 6/7 | 20 | 20 |
| 10 | 60 | 3 | 30 | 3 |
| 10 | 57 3/5 | 3 1/8 | 50 | 25 |
| 10 | 54 | 3 1/3 | 5 | 10 |
| 10 | 50 2/5 | 3 4/7 | 50 | 25 |
| 10 | 50 | 3 3/5 | 45 | 18 |
| 10 | 48 | 3 3/4 | 30 | 15 |
| 10 | 46 2/7 | 3 8/9 | 14 | 35 |
| 10 | 45 | 4 | 20 | 4 |
| 10 | 43 1/5 | 4 1/6 | 50 | 25 |
| 10 | 42 | 4 2/7 | 3 | 30 |
| 10 | 40 1/2 | 4 4/9 | 40 | 40 |
| 10 | 38 4/7 | 4 2/3 | 35 | 14 |
| 10 | 36 | 5 | 10 | 5 |

| Number of Pinions | $u$ or $\beta$ (degrees) | | M | | Lowest Divisor of Inner Row Teeth | Lowest Divisor of Outer Row Teeth |
|---|---|---|---|---|---|---|
| 10 | 32 | 2/5 | 5 | 5/9 | 25 | 50 |
| 10 | 32 | | 5 | 5/8 | 18 | 45 |
| 10 | 31 | 1/2 | 5 | 5/7 | 40 | 40 |
| 10 | 30 | | 6 | | 15 | 6 |
| 10 | 28 | 4/5 | 6 | 1/4 | 50 | 25 |
| 10 | 27 | | 6 | 2/3 | 4 | 20 |
| 10 | 25 | 1/5 | 7 | 1/7 | 25 | 50 |
| 10 | 24 | | 7 | 1/2 | 30 | 15 |
| 10 | 23 | 1/7 | 7 | 7/9 | 35 | 70 |
| 10 | 22 | 10/11 | 7 | 6/7 | 22 | 55 |
| 10 | 22 | 1/2 | 8 | | 40 | 8 |
| 10 | 21 | 3/5 | 8 | 1/3 | 50 | 25 |
| 10 | 20 | 4/7 | 8 | 3/4 | 14 | 35 |
| 10 | 19 | 1/17 | 9 | 4/9 | 34 | 85 |
| 10 | 18 | | 10 | | 5 | 10 |
| 10 | 16 | 8/13 | 10 | 5/6 | 26 | 65 |
| 10 | 15 | 3/4 | 11 | 3/7 | 16 | 80 |
| 10 | 15 | 3/19 | 11 | 7/8 | 38 | 95 |
| 11 | 90 | | 2 | | 22 | 2 |
| 11 | 81 | 9/11 | 2 | 1/5 | 11 | 11 |
| 11 | 73 | 7/11 | 2 | 4/9 | 2 | 22 |
| 11 | 65 | 5/11 | 2 | 3/4 | 11 | 11 |
| 11 | 60 | | 3 | | 33 | 3 |
| 11 | 57 | 3/11 | 3 | 1/7 | 22 | 22 |
| 11 | 54 | 6/11 | 3 | 3/10 | 33 | 33 |
| 11 | 49 | 1/11 | 3 | 2/3 | 11 | 11 |
| 11 | 45 | | 4 | | 44 | 4 |
| 11 | 43 | 7/11 | 4 | 1/8 | 3 | 33 |
| 11 | 40 | 10/11 | 4 | 2/5 | 22 | 22 |
| 11 | 38 | 2/11 | 4 | 5/7 | 33 | 33 |
| 11 | 36 | 9/11 | 4 | 8/9 | 44 | 44 |
| 11 | 32 | 8/11 | 5 | 1/2 | 11 | 11 |
| 11 | 28 | 7/11 | 6 | 2/7 | 4 | 44 |
| 11 | 27 | 3/11 | 6 | 3/5 | 33 | 33 |
| 11 | 24 | 6/11 | 7 | 1/3 | 22 | 22 |
| 11 | 21 | 9/11 | 8 | 1/4 | 33 | 33 |
| 11 | 20 | 5/11 | 8 | 4/5 | 44 | 44 |
| 11 | 19 | 7/11 | 9 | 1/6 | 5 | 55 |
| 11 | 16 | 4/11 | 11 | | 11 | 11 |
| 12 | 90 | | 2 | | 12 | 2 |
| 12 | 84 | | 2 | 1/7 | 20 | 15 |
| 12 | 81 | | 2 | 2/9 | 15 | 20 |
| 12 | 80 | | 2 | 1/4 | 36 | 9 |
| 12 | 78 | 3/4 | 2 | 2/7 | 48 | 16 |

TABLE A-1. Continued

| Number of Pinions | $\alpha$ or $\beta$ (degrees) | | M | | Lowest Divisor of Inner Row Teeth | Lowest Divisor of Outer Row Teeth |
|---|---|---|---|---|---|---|
| | | | TABLE A-1. | Continued | | |
| 12 | 75 | | 2 | 2/5 | 2 | 12 |
| 12 | 70 | | 2 | 4/7 | 36 | 18 |
| 12 | 68 | 4/7 | 2 | 5/8 | 28 | 21 |
| 12 | 67 | 1/2 | 2 | 2/3 | 24 | 8 |
| 12 | 63 | | 2 | 6/7 | 30 | 20 |
| 12 | 60 | | 3 | | 12 | 3 |
| 12 | 57 | 6/7 | 3 | 1/9 | 42 | 28 |
| 12 | 56 | 1/4 | 3 | 1/5 | 48 | 16 |
| 12 | 54 | 6/11 | 3 | 3/10 | 44 | 33 |
| 12 | 52 | 1/2 | 3 | 3/7 | 8 | 24 |
| 12 | 50 | | 3 | 3/5 | 36 | 18 |
| 12 | 48 | | 3 | 3/4 | 20 | 15 |
| 12 | 45 | | 4 | | 3 | 4 |
| 12 | 42 | 6/7 | 4 | 1/5 | 28 | 21 |
| 12 | 40 | | 4 | 1/2 | 36 | 9 |
| 12 | 38 | 2/11 | 4 | 5/7 | 44 | 33 |
| 12 | 37 | 1/2 | 4 | 4/5 | 24 | 24 |
| 12 | 35 | | 5 | 1/7 | 18 | 36 |
| 12 | 33 | 3/4 | 5 | 1/3 | 48 | 16 |
| 12 | 32 | 1/7 | 5 | 3/5 | 42 | 28 |
| 12 | 31 | 2/13 | 5 | 7/9 | 39 | 52 |
| 12 | 30 | | 6 | | 4 | 6 |
| 12 | 28 | 7/11 | 6 | 2/7 | 33 | 44 |
| 12 | 27 | | 6 | 2/3 | 30 | 20 |
| 12 | 26 | 1/4 | 6 | 6/7 | 48 | 48 |
| 12 | 25 | | 7 | 1/5 | 9 | 36 |
| 12 | 22 | 1/2 | 8 | | 24 | 8 |
| 12 | 21 | 9/11 | 8 | 1/4 | 44 | 33 |
| 12 | 21 | | 8 | 4/7 | 5 | 60 |
| 12 | 20 | | 9 | | 36 | 9 |
| 12 | 19 | 2/7 | 9 | 1/3 | 21 | 28 |
| 12 | 18 | 3/4 | 9 | 3/5 | 16 | 48 |
| 12 | 17 | 4/13 | 10 | 2/5 | 39 | 52 |
| 12 | 17 | 1/7 | 10 | 1/2 | 28 | 21 |
| 12 | 15 | | 12 | | 6 | 12 |

# APPENDIX B

## GEAR TOOTH STRESS ANALYSIS

Calculations for the dynamic bending stresses and compressive stresses for the gear teeth of the drive train were preformed and compared to an allowable stress to obtain the margin of safety.

## BENDING STRESS EQUATION

The basic equation for the bending stress at the root of the tooth in a spur and bevel gear is calculated as follows:

$$f_b = \frac{W_t K_o}{K_v} \quad \frac{P_d}{F} \quad \frac{K_s K_m}{J}$$

where

$W_t$ = tangential tooth load, lb
$K_o$ = overload factor
$K_v$ = dynamic factor
$P_d$ = diametral pitch
$F$ = face width, in
$K_s$ = size factor
$K_m$ = load distribution factor
$J$ = geometry factor

All the roller gear drive gears are case carburized and ground to close tolerances, thereby minimizing dynamic effects. The dynamic factor is therefore taken as 1.00.

The overload factor makes allowances for the roughness or smoothness of operation of the driving and driven members. Again, this factor is taken as unity.

The load distribution factor accounts for the combined effects of deflection of mountings and misalignments of the gears. Since these factors are less critical in bevel gears, the load distribution factor is usually taken as 1.10 while for spur or helical gears, the load distribution factor is assumed to be 1.30.

The size factor reflects nonuniformity of material properties and is taken as unity for aircraft spur gears while for bevel gears, the size factor is a function of diametral pitch.

The geometry factor, J, evaluates the shape of the tooth, the position at which the most damaging load is applied, stress concentration due to geometric shape and sharing of load. In bevel gears the geometry factor is taken for the mean normal section of the tooth.

176

## COMPRESSIVE STRESS EQUATION

The contact stress for bevel gears can be calculated by

$$f_c = K_p \; \frac{2 T_p \, K_o}{K_v} \; \frac{1}{F \, d_p^2} \; \frac{K_s \, K_m \, K_f}{I}$$

where

$K_p$ = elastic coefficient
$K_o$ = overload factor
$K_v$ = dynamic factor
$T_p$ = pinion torque, in-lb
$d_p$ = pinion pitch diameter, in
$K_s$ = size factor
$K_m$ = load distribution factor
$K_f$ = surface condition factor
$I$ = geometry factor

For steel spur gears the contact stress is given by

$$F_c = \sqrt{\frac{21 \times 10^6 W_t}{\sin 2\phi \; F}} \; \left\{ \frac{1}{d_p} \pm \frac{1}{d_g} \right\} \quad \begin{array}{l} \text{+ for external} \\ \text{- for internal} \end{array}$$

## ALLOWABLE STRESSES

For carburized and ground gears, the allowable stresses are given in Table B-1 below.

| TABLE B-1.  ALLOWABLE GEAR BENDING AND CONTACT STRESSES FOR CASE CARBURIZED GROUND GEARS. | | |
|---|---|---|
| **Components** | **Allowable Stress (psi)** | |
| Spur Gears - one way bending | $F_b$ = | 55,000 |
| Bevel Gears - one way bending | $F_b$ = | 30,000 |
| Spur Gears | $F_c$ = | 130,000 |
| Bevel Gears | $F_c$ = | 200,000 |

The difference in allowable bending stresses for spur and bevel gears is due mainly to the different size factors used.

Table B-2 summarizes the bending and contact stresses for the gears in the drive train of the roller gear transmission.

177

| Part Number | Part Name | Design hp | $f_b$ (psi) | $f_c$ (psi) |
|---|---|---|---|---|
| | TABLE B-2.   GEAR STRESS SUMMARY. | | | |
| RG351-11113 | Input Bevel Pinion | 1870 | 12080 | 132500 |
| RB351-11128 | Input Bevel Gear | 1870 | 12120 | 132500 |
| RG351-11132 | Input Spur Pinion | 1870 | 43450 | 111600 |
| RG351-11154 | Input Spur Gear | 1870 | 41500 | 111600 |
| RG351-11155 | TTO Bevel Gear | 700 | 14350 | 112200 |
| RG351-11193 | TTO Bevel Pinion | 700 | 15030 | 112200 |
| RG351-11183 | Sun Gear         - a | 3000 | 46700 | 128000 |
| RG351-11182 | 1st-Row Gear   - $X_1$ | 3000 | 47790 | 128000 |
| RG351-11182 | 1st-Row Pinion - $Y_1$ | 3000 | 39260 | 129600 |
| RG351-11181 | 2nd-Row Gear   - $X_2$ | 3000 | 33350 | 129600 |
| RG351-11181 | 2nd-Row Pinion - $Y_2$ | 3000 | 33780 | 129000 |
| RG351-11184 | Ring Gear        - C | 3000 | 30030 | 129000 |
| RG351-11170 | Oil Pump Gear | 70 | 20050 | 126500 |
| RG351-11189 | Oil Pump Pinion | 70 | 7000 | 126500 |
| RG351-11196 | Spur Pinion TTO | 645 | 37570 | 121700 |
| RG351-11197 | Spur Gear TTO | 645 | 36390 | 121700 |
| RG351-11211 | Generator Gear #2 | 53.6 | 15060 | 87900 |
| RG351-11219 | Tachometer Gear | 1.0 | 520 | 15200 |
| RG351-11213 | Primary Servo Gear | 6.5 | 3000 | 37700 |
| RG351-11209 | Accessory Gear | 6.5 | 2610 | 37700 |
| RG351-11212 | Generator Gear #1 | 53.6 | 22630 | 90200 |
| S6135-20181 | Auxiliary Servo Gear | 60.1 | 18540 | 90200 |
| S6135-20181 | Utility Servo Gear | 73.1 | 22850 | 82350 |
| RG351-11214 | Lubrication Pump Gear | 77.1 | 24360 | 94650 |
| RG351-11222 | Accessory Gear | 77.1 | 30200 | 94650 |

# APPENDIX C

## BEARING LIFE ANALYSIS

The B-10 lives of all the bearings in the roller gear drive transmission system are summarized in Table C-1. The B-10 life is that life in hours that 90% of a group of bearings will attain before failure. The equation used to calculate the lives shown in Table C-1 are as follows:

$$L = \left(\frac{c}{p}\right)^{3} \frac{16667}{rpm} \qquad \text{(ball bearing)}$$

$$L = \left(\frac{c}{p}\right)^{3.333} \frac{16667}{rpm} \qquad \text{(roller bearing)}$$

$$L = \left(\frac{3.86 \; BRR}{p}\right)^{3.333} \frac{16667}{rpm} \qquad \text{(tapered roller bearing)}$$

where

$C$ = bearing basic dynamic capacity at 33-1/3 rpm

$p$ = equivalent radial load in pounds

$BRR$ = basic radial rating for tapered roller bearings

$L$ = B-10 life in hours

When bearings are arranged in groups of two or more such as the four ball stack of the input pinion or the back-to-back duplex set of the input bevel gear, the above equations are modified to calculate a life of the bearing set. The four ball stack of the input bevel pinion has been analyzed by using a Sikorsky computer program. This program accounts for load sharing in the bearing set and also includes effects of centrifugal force.

All the B-10 lives have been calculated using prorated horsepower. The prorated horsepower is that single value which if steadily applied would give the same bearing life as a mission spectra of horsepower versus percent time. The prorated horsepower values quoted in Table C-2 were determined by assuming that the ratio of prorate horsepower to maximum horsepower was the same as that of previous designs. This assumption is valid since the ratio of prorate to maximum horsepower of previous designs falls within narrow limits regardless of the mission requirements.

| Location | Bearing No. | Load Radial | Thrust | B-10 (hours) |
|---|---|---|---|---|
| Input Bevel Pinion | { 9212 Ball Stack | | | 1950 |
| | R211 Roller | | | 4440 |
| Input Bevel Gear | { 1838 RDB Ball duplex | 1355 | 313 | 3250 |
| | R1922 Roller | 972 | | >5000 |
| Input Spur Pinion | { 111KS Ball | 320 | 50 | >5000 |
| | R213  Roller | 1600 | | >5000 |
| Freewheel Unit | { 1911 RDF Ball | - | - | >5000 |
| | 1911 RDF Ball | - | - | >5000 |
| Outer Shaft | { R1840 Roller | 845 | | >5000 |
| | LL639249/210 Taper | 955 | 52 | >5000 |
| Roller Gear 2nd Row | 22313 VAG Spherical | 6760 | 230 | 3090 |
| Main Rotor Shaft | { 9126 Ball duplex | 7130 | 24500 | 1090 |
| | R1838 Roller | 950 | | >5000 |
| TTO Bevel Pinion | { 34306/34478 Taper | 1235 | 720 | >5000 |
| | 395 S/394 A Taper | 511 | | >5000 |
| Spur Pinion TTO | { R113 Roller | 1080 | | >5000 |
| | 208 S Ball | 371 | | >5000 |
| Generator Gear #1, #2 | { R 108 Roller | 290 | | >5000 |
| | 107 KS Ball | 87 | | >5000 |
| Tachometer Gear | { 101 KS Ball | 7 | | >5000 |
| | 101 KS Ball | 2 | | >5000 |
| Lubrication Pump | { R 108 Roller | 525 | | >5000 |
| | 105 KS Ball | 181 | | 2900 |
| Primary Servo | { R 108 Roller | 84 | | >5000 |
| | 106 KS Ball | 30 | | >5000 |
| Auxiliary Servo | { R 108 Roller | 485 | | >5000 |
| | 106 KS Ball | 168 | | >5000 |
| Utility Servo | { R 108 Roller | 730 | | >5000 |
| | 106 KS Ball | 252 | | 4580 |
| Spur Gear TTO | { R111 Roller | 278 | | >5000 |
| | 212 S Ball | 910 | | 4100 |

TABLE C-1.  BEARING LIFE SUMMARY.

| Location | rpm | Max Horsepower | Max Continuous Horsepower | Prorated Horsepower |
|---|---|---|---|---|
| Input Pinion | 18966 | 1870 | 1770 | 1125 |
| Input Gear & Spur Pinion Shaft | 6223 | 1870 | 1770 | 1125 |
| Outer Shaft & Sun Gear | 4045 | 3700 | 3500 | 2250 |
| Main Rotor Shaft | 203 | 3000 | 2840 | 1850 |
| Tail Takeoff Bevel Gear | 7031 | 700 | 660 | 335 |
| Tail Takeoff | 3026 | 565 | 535 | 200 |

TABLE C-2. ROLLER GEAR DRIVE TRANSMISSION, DESIGN SYSTEM HORSEPOWER

STRUCTURAL AND FUNCTIONAL ANALYSIS,
ROLLER GEAR UNIT

ROLLER GEAR DRIVE BASIC DATA

Figure D-1 illustrates the geometry and nomenclature of the two-row, ring output, fixed cage roller gear drive. The basic data for this configuration is given in Table D-1 below.

| TABLE D-1. BASIC DATA - ROLLER GEAR DRIVE. | | | | |
|---|---|---|---|---|
| Location | Diametral Pitch | No. of Teeth | Pitch Diameter (in) | Pressure Angle (deg) |
| $i$ | Pitch | $N_i$ | $d_i$ | $\phi_i$ |
| a | 9.448 | 84 | 8.89077 | 22.5 |
| * $x_1$ | | 58 | 6.13887 | |
| * $y_1$ | 13.217 | 27 | 2.04282 | 25.0 |
| * $x_2$ | | 126 | 9.53318 | |
| * $y_2$ | 5.583 | 25 | 4.47788 | 30.0 |
| c | | 154 | 27.58374 | |
| *Number of pinions equal 7 | | | | |

Design load factors for the roller gear drive unit consist of a 1.5 static ultimate load factor and 1.15 static yield load factor based on the limit conditions. A value of 3000 hp was used for the limit design power; this is also conservatively assumed as the fatigue design horsepower. The output speed of the gearbox is 203 rpm.

From the geometry, the following equations for angles and distances are determined:
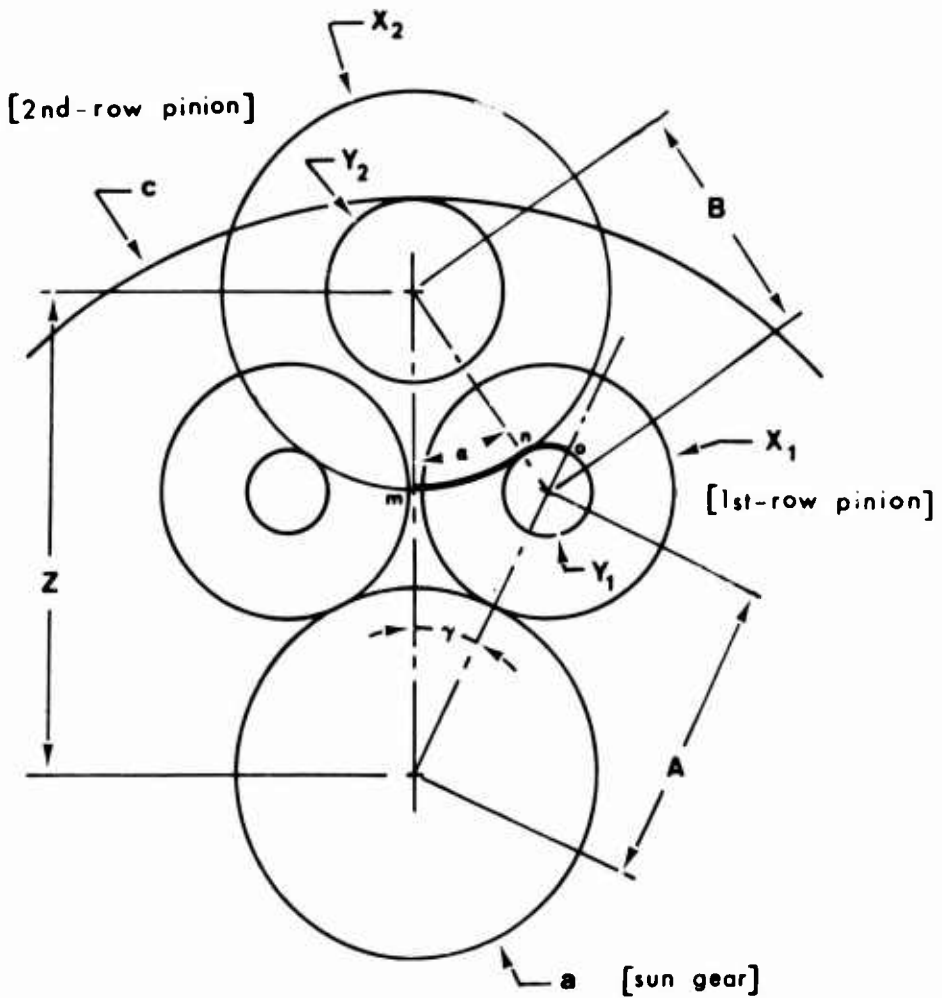
Figure D-1.  Roller Gear Drive Geometry and Nomenclature.

$$\gamma = \frac{180}{\text{no. of pinions}} = \frac{180}{7} = 25\frac{5}{7}$$

$$A = \frac{d_{x1}}{2} + \frac{d_a}{2} = \frac{6.13887}{2} + \frac{8.89077}{2} = 7.51482$$

$$\alpha = \frac{180}{M_1} = \frac{180}{5\frac{1}{4}} = 34\frac{2}{7}$$

$$B = A\,\frac{\sin\gamma}{\sin\alpha} = (7.51482)\,\frac{.43388}{.56332} = 5.78806$$

$$Z = A\cos\gamma + B\cos\alpha$$

$$= (7.51482)(0.90097) + (5.78806)(0.82624)$$

$$= 11.55295$$

## FUNCTIONAL ANALYSIS

The reduction ratio of this unit, cage fixed, ring gear output is given by

$$RR = \frac{N_{x1}\;N_{x2}\;N_c}{N_{y1}\;N_{y2}\;N_a}$$

$$= \frac{(58)(126)(154)}{(27)(25)(84)}$$

$$= 19.84888$$

For equal spacing of pinions:

$$\frac{N_a}{\text{no. of pinions}} = \text{whole number}$$

$$\frac{84}{7} = 12$$

$$\frac{N_c}{\text{no. of pinions}} = \text{whole number}$$

184

$$\frac{154}{7} = 22$$

For proper meshing of the $Y_1 - X_2$ mesh:

$$(2)\left(\frac{\text{arc length no}}{\text{circular pitch}}\right) = \text{whole number} \qquad \text{(Ref. Figure D-1)}$$

$$(2)\left(\frac{\text{arc length mn}}{\text{circular pitch}}\right) = \text{whole number} \qquad \text{(Ref. Figure D-1)}$$

where

$$\text{circular pitch} = \frac{\pi}{\text{Pitch}}$$

$$\text{arc length} = (\text{radius})(\text{angle})$$

Substituting for arc length, $\gamma$, and defining,

$$\alpha = \frac{\pi}{M_1}$$

leads to

$$\left(\frac{M_1 + \text{no. of pinions}}{M_1 \, (\text{no. of pinions})}\right) N_{y1} = \text{whole number}$$

$$\left(\frac{5\frac{1}{4} + 7}{(5\frac{1}{4})(7)}\right) 27 = 9$$

Similarly, the equation with arc length mn reduces to-

$$\frac{N_{x2}}{M_1} = \text{whole number}$$

$$\frac{126}{5\frac{1}{4}} = 24$$

For no $x_1 - x_1$ interference:

$$\text{no. of pinions} \leq \frac{\pi}{\arcsin\left(\frac{N_{x1} + 2}{N_a + N_{x1}}\right)}$$

$$7 \leq \frac{\pi}{\arcsin\left(\frac{58 + 2}{84 + 58}\right)}$$

$$7 < 7.2016$$

For no $x_2 - x_2$ interference:

$$\frac{d_{x2}}{2} + \frac{1}{\text{Pitch}_{x2}} \leq Z \, \text{Sin} \, \gamma$$

$$\frac{9.53318}{2} + \frac{1}{13.217} \leq (11.55295)(0.43388)$$

$$4.842 < 5.013$$

For no $y_2 - x_1$ interference:

$$B - \frac{d_{x1}}{2} - \frac{1}{\text{Pitch}_{x1}} \geq \frac{d_{y2}}{2} + \frac{1}{\text{Pitch}_{y2}}$$

$$5.78806 - \frac{6.13887}{2} - \frac{1}{9.448} \geq \frac{4.47788}{2} + \frac{1}{5.583}$$

$$2.613 > 2.418$$

For no $x_2 - a$ interference:

$$Z - \frac{d_{x2}}{2} - \frac{1}{\text{Pitch}_{x2}} \geq \frac{d_a}{2} + \frac{1}{\text{Pitch}_a}$$

186

$$11.55295 - \frac{9.53318}{2} - \frac{1}{13.217} \geq \frac{8.89077}{2} + \frac{1}{9.448}$$

$$6.711 > 4.551$$

Hence the roller gear drive unit meshes properly with equally spaced pinions and with no interference.

## LOAD ANALYSIS

A free body diagram of the 1st-row pinion with the applied loads is shown in Figure D-2, where

$N_i$ = applied roller loads

$W_{r_{x2}}$ = gear separating force from 2nd-row pinion

$W_{t_{x2}}$ = gear tangential force from 2nd-row pinion

$W_{r_{x1}}$ = gear separating force from sun gear

$W_{t_{x1}}$ = gear tangential force from sun gear

$\Delta$ = $\alpha + \dfrac{\pi}{\text{no. of pinions}}$

$\phi_i$ = pressure angle

$rpm_{out}$ = 203

$rpm_{in}$ = $(rpm_{out})(RR)$ = $(203)(19.84888)$ = 4029

$T_a$ = $\dfrac{63025 \text{ HP}}{rpm_a}$ = $\dfrac{(63025)(3000)}{4029}$ = 46930 in.-lb

$W_{ta}$ = $\dfrac{2 T_a}{d_a(\text{no. of pinions})}$ = $\dfrac{(2)(46930)}{(8.89077)(7)}$ = 1510 lb

**187**
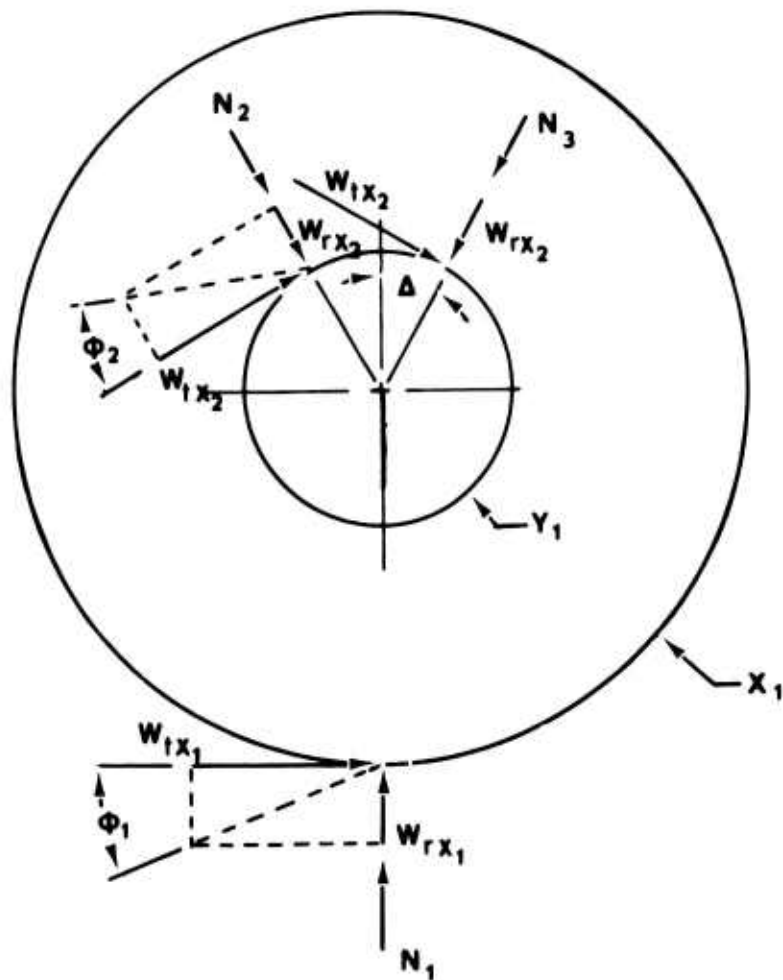
Figure D-2. Free Body Diagram - 1st-Row Pinion.

$$W_{ra} = W_{ta} \tan \emptyset = (1510)(.41421) = 630 \text{ lb}$$

$$W_{t_{x1}} = W_{ta}$$

$$W_{t_{y1}} = W_{t_{x1}} \left[ \frac{d_{x1}}{(2)(d_{y1})} \right] = 1510 \left[ \frac{(6.13887)}{(2)(2.04282)} \right] = 2270 \text{ lb}$$

$$W_{t_{y1}} = W_{t_{x2}}$$

$$W_{r_{x2}} = W_{t_{x_2}} \tan \emptyset_2 = (2270)(.46631) = 1060 \text{ lb}$$

Summing the forces in the horizontal and vertical directions leads to

$$N_2 \cos \Delta + W_{r_{x2}} \cos \Delta + N_3 \cos \Delta + W_{r_{x2}} \cos \Delta - N_1 - W_{r_{x1}} = 0$$

$$N_2 \sin \Delta + W_{t_{x2}} \cos \Delta - N_3 \sin \Delta + W_{t_{x2}} \cos \Delta + W_{t_{x1}} = 0$$

A free body diagram of the 2nd-row pinion with the applied loads is shown in Figure D-3, where

$N_i$ = applied roller loads

$W_{r_c}$ = gear separating force from ring gear

$W_{t_c}$ = gear tangential force from ring gear

$Q$ = bearing reaction force

$W_{r_{x2}}$ = gear separating force from 1st-row pinion

$W_{t_{x2}}$ = gear tangential force from 1st-row pinion

$\emptyset_i$ = pressure angle
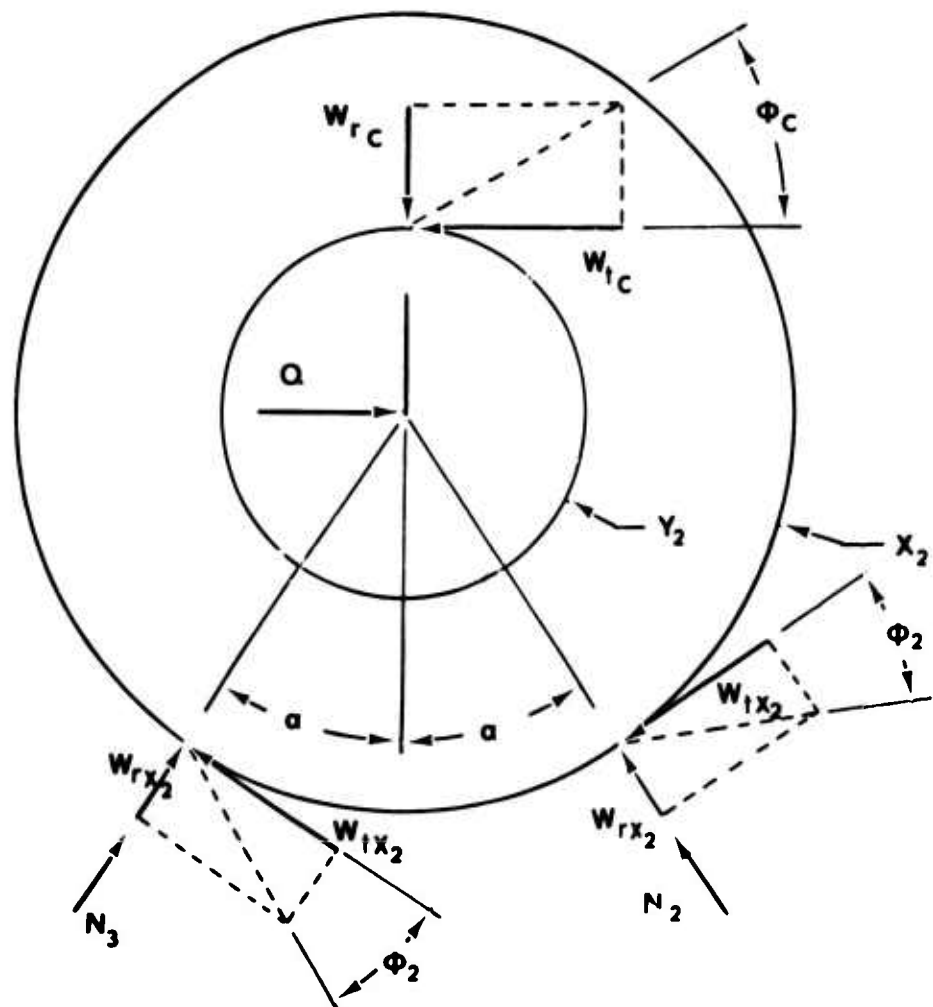
Figure D-3.  Free Body Diagram - 2nd-Row Pinion.

$$W_{t_c} = W_{t_{y2}}$$

$$= W_{t_{x2}} \left[ \frac{(2) \, d_{x2}}{d_{y2}} \right]$$

$$W_{t_{x2}} = W_{t_{y1}}$$

$$W_{t_{y2}} = W_{t_{x2}} \left[ \frac{(2) \, d_{x2}}{d_{y2}} \right] = 2270 \left[ \frac{(2)(9.53318)}{(4.47788)} \right] = 9660 \text{ lb}$$

$$W_{r_c} = W_{t_c} \tan \phi_c = (9660)(.57735) = 5580$$

Summing the forces in the horizontal and vertical directions leads to

$$N_3 \cos \alpha + W_{r_{x2}} \cos \alpha + N_2 \cos \alpha + W_{r_{x2}} \cos \alpha - W_{r_c} = 0$$

$$N_3 \sin \alpha - W_{t_{x2}} \cos \alpha - N_2 \sin \alpha - W_{t_{x2}} \cos \alpha + Q - W_{t_c} = 0$$

Solving the above equilibrium equations simultaneously with

$$\gamma = 25 \frac{5}{7}^{\circ}$$

$$\alpha = 34 \frac{2}{7}^{\circ}$$

$$\Delta = 60^{\circ}$$

Leads to

$$B_1 = \frac{W_{t_{x2}}}{\tan \Delta} + \frac{W_{t_{x1}}}{2 \sin \Delta}$$

$$B_1 = \frac{2270}{1.7320} + \frac{1510}{(2)(0.86603)}$$

$$B_1 = 2180 \text{ lb}$$

191

$$N_1 = W_{r_c}\left(\frac{\cos \Delta}{\cos a}\right) - W_{r_{x1}}$$

$$N_1 = (5580)\left(\frac{0.5000}{0.82624}\right) - 630$$

$$N_1 = 2750 \text{ lb}$$

$$N_2 = \frac{W_{r_c}}{2\cos a} - W_{r_{x2}} - B_1$$

$$N_2 = \frac{5580}{(2)(.82624)} - 1060 - 2180$$

$$N_2 = 140 \text{ lb}$$

$$N_3 = \frac{W_{r_c}}{2\cos a} - W_{r_{x2}} + B_1$$

$$N_3 = \frac{5580}{(2)(.82624)} - 1060 + 2180$$

$$N_3 = 4500 \text{ lb}$$

$$Q = W_{t_c} + 2W_{t_{x2}} \cos a - \sin a \ (N_3 - N_2)$$

$$Q = 9660 + (2)(2270)(.82624) - (.56332)(4500-140) = 10950 \text{ lb}$$

The roller loads as calculated indicate that positive roller separating forces exist under all loading conditions. Thus, the system is "self pre-loading".

The roller loads are directly proportional to power transmitted. The above calculations are based on 3000 horsepower transmitted while for 0 horsepower the roller loads will be 0 but will never be negative.

DEFLECTION ANALYSIS

A study of roller gear drive unit deflections was conducted to insure
that all rollers have positive separating loads and that the output bearing
remains unloaded in the radial direction. To meet these conditions, it is
sufficient to show that the radial difference in position between the de-
flected 2nd-row pinion centerline (from loads induced by 3000 HP input)
and the post location is less than the radial clearance in the post bearing.

Figure D-4 shows the roller gear drive geometry in the deflected and
undeflected conditions. Point D is the position of the ₵ of the 2nd-row
pinion as located by the actual roller sizes. Point P is the position of
the ₵ of the 2nd-row post as located by the reaction cage plate. Point B
is the position of the ₵ of the 2nd-row pinion under load as located by
the deflected rollers.

The roller sizes, $D_i$ given in Table D-2 are larger than the
theoretical pitch diameters of the gears to minimize roller sliding in
the loaded condition.

| TABLE D-2. ROLLER DIAMETERS. | | |
|---|---|---|
| Element | Symbol | Diameter (in.) |
| Sun Gear Roller | $D_a$ | 8.8917<br>8.8913 |
| 1st-Row Pinion Roller | $D_{x_1}$ | 6.1395<br>6.1391 |
| 1st-Row Pinion Roller* | $D_{y_1}$ | 2.0431<br>2.0427 |
| 2nd-Row Pinion Roller* | $D_{x_2}$ | 9.5335<br>9.5331 |
| *This roller is not corrected to minimize sliding, as the two loading conditions vary greatly. | | |

In the following calculations large errors can occur if an insufficient
number of significant figures are used. Nine significant figures are used in
the deflection analyses, but for clarity only five decimals are shown.
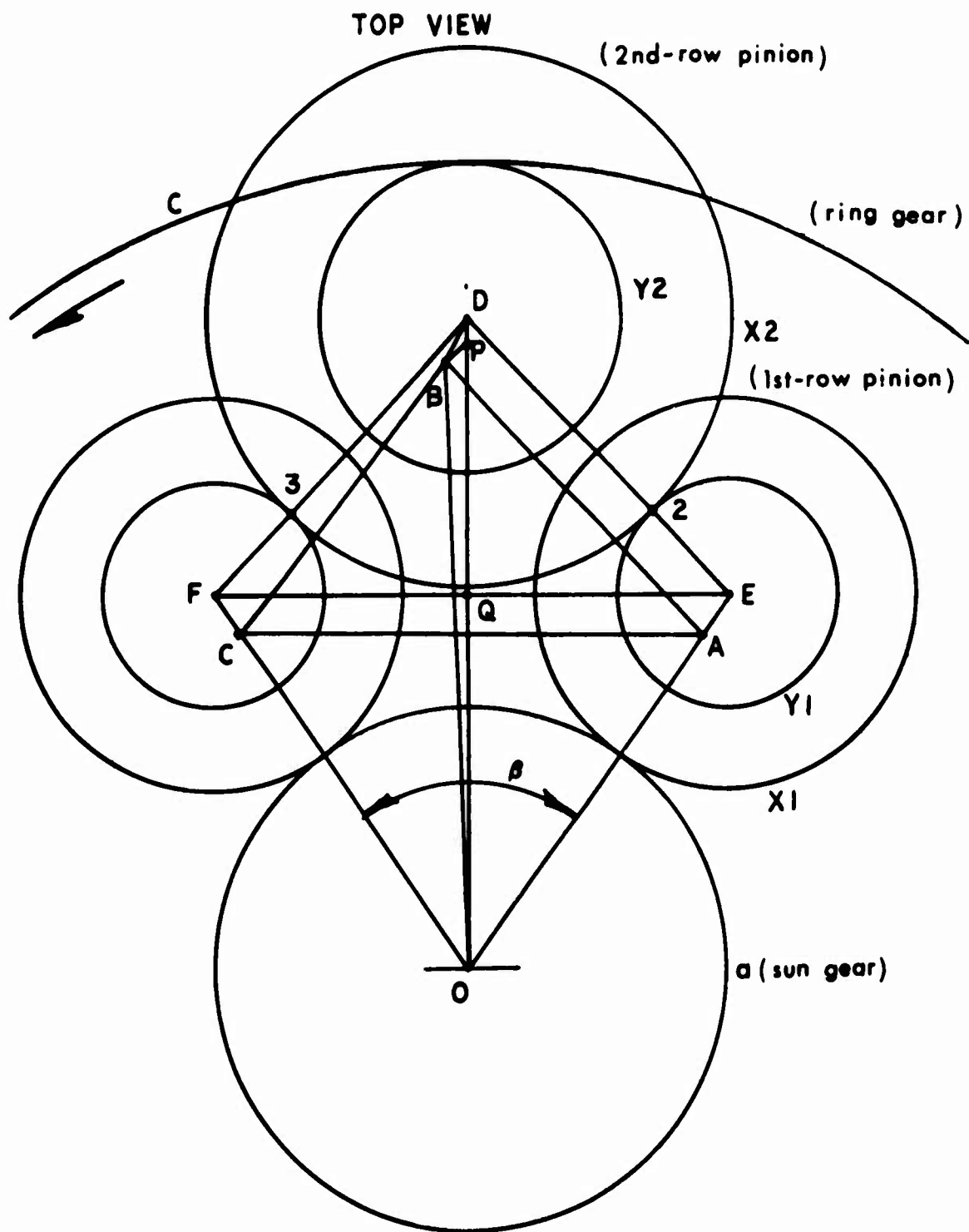
Figure D-4.  Roller Gear Drive Geometry Schematic.

From geometry of Figure D-4,

$$OF = \frac{D_a + D_{x1}}{2}$$

$$OC = \frac{D_a + D_{x1}}{2} - \delta_{a_{x1}}$$

where

$$D_a = \text{sun gear roller diameter}$$

$$D_{x1} = \text{pinion } x_1 \text{ roller diameter}$$

$$\delta_{a_{x1}} = \text{total deflection between a and } x_1$$

$$OQ = OF \cos \frac{\beta}{2}$$

where

$$\beta = \frac{2\pi}{\text{no of planets}}$$

$$AC = (2)(OC) \sin \frac{\beta}{2}$$

$$EF = (2)(OF) \sin \frac{\beta}{2}$$

The roller load at point 2 is 70 lb per roller and the deflection is assumed to be negligible.

$$\therefore AB = DF = DE = \frac{D_{x2} + D_{y1}}{2}$$

$$BC = \frac{D_{x2} + D_{y1}}{2} - \delta_{x2_{y1}}$$

Let $X_D$ and $Y_D$ be the coordinates of point D of the undeflected roller gear drive unit measured from point E.

$$Y_D = \sqrt{DE^2 - \left(\frac{EF}{2}\right)^2}$$

$$X_D = \sqrt{DE^2 - Y_D^2}$$

Similarly, for the deflected roller gear drive unit the coordinates of point B are determined with respect to point A.

$$Y_B = \sqrt{\left[\frac{AB^2 - BC^2 + AC^2}{2\,A\,C}\right]^2 - AB^2}$$

$$X_B = \sqrt{AB^2 - Y_B^2}$$

Measuring the coordinates of point B with respect to point E instead of A requires that

$$Y_D' = Y_B - \delta_{axl}\cos\frac{\beta}{2}$$

$$X_D' = X_B + \delta_{axl}\sin\frac{\beta}{2}$$

The coordinates of point B with respect to O (the centerline of the second-row pinion under load), measured from point O, are given by

$$Y_{BO} = OQ + Y_D'$$

$$X_{BO} = \frac{EF}{2} - X_D'$$

196

The coordinates of point D with respect to O (the centerline of the second-row pinion under no load) are given by

$$Y_{DO} = OQ + Y_D$$

$$X_{DO} = \frac{EF}{2} - X_D$$

The coordinates of point P with respect to O or the radial distance to the centerline of the post are given by $(X_{po}, Y_{po})$. The coordinates of points D and P do not in general coincide, and it can be shown by a suitable choice of point P due to tolerance buildup that the radial clearance required may be minimized.

If there is sufficient clearance in the bearing, then

$$C_L \geq BP_y$$

where

$C_L$ = radial clearance in the bearing installed and under load.

$BP_y$ = distance between $\cancel{\mathsf{C}}$ of the post and the radial component or "y" component of the second-row pinion in the deflected roller gear drive unit.

Only the radial or "y" component of BP is used, since this is the only component of deflection which insures that the bearing remains unloaded in the radial direction.

To assemble the gearbox it is necessary to show that:

$$C_u \geq DP$$

where

$C_u$ = radial clearance in the bearing installed.

DP = distance between $\cancel{\mathsf{C}}$ of the post and the $\cancel{\mathsf{C}}$ of the second-row pinion in the undeflected roller gear drive unit.

**197**

The terms $\delta_{x2_{y1}}$ and $\delta_{a_{x1}}$ are defined as the sum of the bending and compressive deflection for each roller contact.

The bending deflection for each roller is given in Table D-3. .

| TABLE D-3. ROLLER BENDING DEFLECTIONS. | | |
|---|---|---|
| Element | Symbol | Deflection (in) |
| Sun Gear Roller | $\mu_a$ | 0.00065 |
| 1st-Row Pinion Roller | $\mu_{x1}$ | 0.00032 |
| 1st-Row Pinion Roller | $\mu_{y1}$ | 0.00034 |
| 2nd-Row Pinion Roller | $\mu_{x2}$ | 0.00182 |

The bending deflections were calculated using ring theory, neglecting the shear deflections; the equations are outlined as follows.

For a roller subjected to a single concentrated load, the roller is put in equilibrium by uniform shear flow. The radial displacement at any point on the ring is given by

$$\mu \Big|_0^\pi = \frac{P\, r^3}{2\,\pi\, EI} \left[ \frac{\pi}{2} \sin\phi + \left(\frac{\pi^2}{6} - \frac{3}{8}\right) \cos\phi - \frac{\phi}{2} \sin\phi \right. $$
$$\left. - \frac{\pi}{2}\, \phi\, \cos\phi + \frac{\phi^2}{4} \cos\phi - 1 \right]$$

where

$\phi$ is the angle in radians measured from the point of load application

For a roller subjected to any number of concentrated equally spaced loads, the radial displacement of each load point is given by

$$\mu = \frac{P r^3}{2\, E\, I} \left[ \frac{1}{\sin^2\phi} \left(\frac{1}{2}\phi + \frac{1}{2}\sin\phi\cos\phi\right) - \frac{1}{\phi} \right]$$

198

where

> $\theta$ is the angle in radians measured from
> one half the distance between loads.

As an example of a roller subjected to a concentrated load consider
the 1st-row pinion roller $y_1$, where

$$r = .850 \text{ inch} = \text{radius to centroid of section}$$
$$I = 0.0059 \text{ in.}^4$$
$$E = 29 \times 10^6 \text{ psi}$$
$$P = 2250 \text{ lb per roller} = N_3/2$$

The maximum deflection occurs when $\phi = 0^\circ$

$$\mu_{y1} = 0.04296 \frac{P r^3}{E I}$$

$$\mu_{y1} = \frac{(0.04296)(2250)(0.850)^3}{(29)(10^6)(0.0059)}$$

$$\mu_{y1} = 0.00034 \text{ in}$$

As an example of a roller subjected to a number of concentrated
equally spaced loads, consider the sun gear roller - a, where

$$r = 4.156 \text{ inches} = \text{radius to centroid of section}$$
$$I = 0.0057 \text{ in.}^4$$
$$E = 29 \times 10^6 \text{ psi}$$
$$P = 1375 \text{ lb per roller} = N_1/2$$
$$\theta = 25^\circ 42'$$

$$\mu_a = \frac{(1375)(4.156)^3}{(2)(29)(10^6)(0.0057)} \left[ \frac{1}{(0.43388)^2} \left( \frac{25^\circ 42' \pi}{(2)(180)} + \frac{1}{2}(.43388)(0.90096) \right) - \frac{1}{25^\circ 42'}, \quad \frac{180}{\pi} \right]$$

199

$$\mu_a = 0.000654 \text{ in}$$

The compressive deflection for each roller pair is given in Table D-4.

<table>
<tr><td colspan="3">TABLE D-4. ROLLER COMPRESSIVE DEFLECTIONS.</td></tr>
<tr><td>Element<br>Pair</td><td>Symbol</td><td>Deflection<br>(in.)</td></tr>
<tr><td>Sun Gear Roller - a<br>1st-Row Pinion Roller - $x_1$</td><td>$\eta_{a_{x1}}$</td><td>0.00161</td></tr>
<tr><td>1st-Row Pinion Roller - $y_1$<br>2nd-Row Pinion Roller - $x_2$</td><td>$\eta_{y1_{x2}}$</td><td>0.00109</td></tr>
</table>

The compressive deflections were calculated considering the case of two parallel axis cylinders in contact with a load P. The deflection of the two cylinders in contact is given by

$$\eta = \frac{2(1 - \nu^2)}{E W \pi} P \left[ \frac{2}{3} + \ln\left(\frac{2D_1}{b}\right) + \ln\left(\frac{2D_2}{b}\right) \right]$$

where

$$b = 2.15 \sqrt{\frac{P \, D_1 \, D_2}{W E (D_1 + D_2)}}$$

As an example of the use of this equation, consider the calculation of $\eta_{y1_{x2}}$

200

$$D_1 = 2.0429 \quad \text{in.}$$

$$D_2 = 9.5333 \quad \text{in.}$$

$$P = 2250 \quad \text{lbs} = N_3/2$$

$$W = 0.481 \quad \text{in.}$$

$$E = 29 \times 10^6 \quad \text{psi}$$

$$\nu = .30$$

$$b = 2.15 \sqrt{\frac{(2250)}{(0.481)(29)(10^6)} \frac{(2.0429)(9.5333)}{(2.0429 + 9.5333)}}$$

$$b = 0.0354$$

$$\eta_{y_1 x_2} = \frac{(2)(1 - 0.3^2)}{(29)(10^6)\pi} \frac{2250}{0.481} \left[ \frac{2}{3} + \ln \frac{(2.0429)(2)}{0.0354} + \ln \frac{(2)(9.5333)}{0.0354} \right]$$

$$\eta_{y_1 x_2} = 0.00109 \quad \text{in.}$$

The total bending plus compressive deflections are given by

$$\delta_{x_2 y_1} = \eta_{y_1 x_2} + \mu_{y_1} + \mu_{x_2}$$

$$\delta_{a x_1} = \eta_{a x_1} + \mu_a + \mu_{x_1}$$

The total deflection between the $X_2$ and $Y_1$ roller under full load (3000 HP) is

$$\delta_{x_2 y_1} = 0.00109 + 0.00034 + 0.00182$$

$$\delta_{x_2 y_1} = 0.00326$$

201

The total deflection between the a and $X_1$ roller under full load (3000 HP) is

$$\delta_{ax_1} = 0.0016124 + 0.000654 + 0.000320$$

$$\delta_{ax_1} = 0.0025864$$

Using the previously derived geometry,

$$OF_{max} = \frac{8.8917 + 6.1395}{2}$$

$$OF_{max} = 7.51560$$

$$OF_{min} = 7.51520$$

$$OC_{max} = \frac{8.8917 + 6.1395}{2} - 0.00258$$

$$OC_{max} = 7.51301$$

$$OC_{min} = 7.51261$$

$$\frac{\beta}{2} = \frac{2\pi}{(7)(2)}$$

$$= 25.7142 \text{ deg}$$

$$\cos\frac{\beta}{2} = 0.90096$$

$$\sin\frac{\beta}{2} = 0.43388$$

$$OQ_{max} = (7.51560)(0.90096)$$

$$OQ_{max} = 6.77124$$

$$OQ_{min} = 6.77088$$

202

$$AC_{max} = (2)(7.51301)(.43388)$$

$$AC_{max} = 6.51933$$

$$AC_{min} = 6.51898$$

$$EF_{max} = (2)(7.51560)(.43388)$$

$$EF_{max} = 6.52158$$

$$EF_{min} = 6.52123$$

$$AB_{max} = \frac{2.0431 + 9.5335}{2}$$

$$AB_{max} = 5.78830$$

$$AB_{min} = 5.78790$$

$$BC_{max} = \frac{2.0431 + 9.5335}{2} - 0.00326$$

$$BC_{max} = 5.78503$$

$$BC_{min} = 5.78463$$

Determining the coordinates of point D with respect to E for the undeflected roller gear drive unit,

$$Y_D = \frac{4.78243}{4.78207}$$

$$X_D = \frac{3.26079}{3.26061}$$

**203**

Determining the coordinates of point B with respect to A for the deflected roller gear drive unit,

$$Y_B = \frac{4.78122}{4.78097}$$

$$X_B = \frac{3.26257}{3.26222}$$

Determining the coordinates of point B with respect to E for the deflected roller gear drive unit,

$$Y_D' = \frac{4.77889}{4.77864}$$

$$X_D' = \frac{3.26369}{3.26334}$$

The coordinates of point B with respect to 0 are

$$Y_{Bo} = \frac{11.55013}{11.54952}$$

$$X_{Bo} = \frac{-0.00255}{-0.00308}$$

The coordinates of the post location P relative to 0 are given by

$$Y_{po} = \frac{11.5525}{11.5515}$$

$$X_{po} = 0.0$$

The coordinates of point D with respect to 0 are

204

$$Y_{Do} = \frac{11.55368}{11.55296}$$

$$X_{Do} = \frac{+0.00017}{0.0}$$

The distances DP and BP are found from the x and y coordinates.

$$BP = \frac{0.00428}{0.00295} \quad \text{in.}$$

$$DP = \frac{0.002188}{0.00117} \quad \text{in.}$$

The y component of BP is

$$BP_y = \frac{0.00297}{0.00137} \quad \text{in.}$$

Since the radial clearance $C_l$ is 0.0036 in. min,

$$C_l > BP_y$$

Since the radial clearance $C_u$ is 0.0030 in. min,

$$C_u > DP$$

Hence, the bearing will never carry any radial load caused by excessive deflections and the roller gear unit will present no difficulty in assembly.

## ROLLER RIM STRESSES

The stresses in the roller rims are calculated on the basis of ring theory, neglecting the internal radial stresses. This method of analysis is somewhat conservative, as in some cases the model is closer in analogy to an edge loaded plate.

The sun gear roller is analyzed as a ring subjected to 7 equally spaced radial loads as shown in Figure D-5.
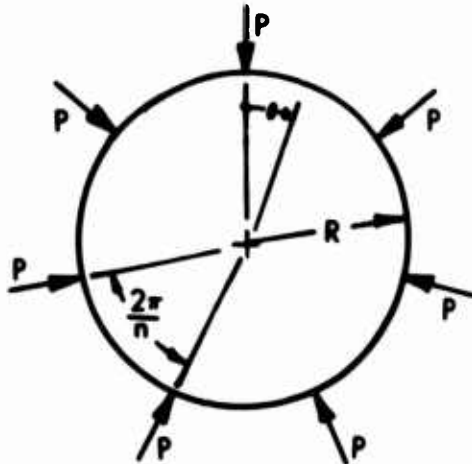


Figure D-5.   Load Diagram - Ring Subjected to Equally Spaced Radial Loads.

The equations for this case are given as follows:

$$M = K_m \, P \, \frac{R}{2}$$

$$N = K_n \, \frac{P}{2}$$

206

where

$$K_m = \frac{-\text{no. of pinions}}{\pi} + \sin\theta + \cot\left(\frac{\pi}{\text{no of pinions}}\right)\cos\theta$$

$$K_n = -\sin\theta - \cot\left(\frac{\pi}{\text{no of pinions}}\right)\cos\theta$$

M = internal moment

N = internal circumferential force

P = the applied roller load

R = the radius to the centroid of the section

$\theta$ = the angle measured from the point of load application

The first- and second-row pinion rollers are assumed to be analogous to a ring subjected to a concentrated radial load and kept in equilibrium by symmetric uniform shear flow as shown in Figure D-6.
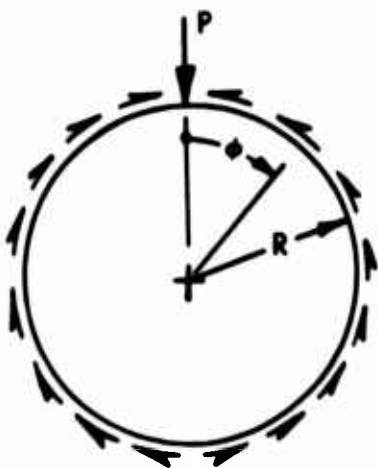


Figure D-6.   Load Diagram — Ring Subjected to Concentrated Load.

The equations for this case are given as follows:

$$M = K_m \frac{P\,R}{2}$$

$$N = K_n \frac{P}{2}$$

where

$$K_m = \frac{-(\pi - \phi)\,\sin\phi + .5\cos\phi + 1}{\pi}$$

$$K_n = \frac{(\pi - \phi)\,\sin\phi + 1.5\cos\phi}{\pi}$$

M     =     internal moment

N     =     internal circumferential force

P     =     the applied roller load

R     =     the radius to the centroid of the section

$\phi$     =     the angle measured from the point of load application

208

From the internal moments and internal forces the total axial plus
bending stress are determined for increments along the circumference of
the roller on both the inside and outside diameters. Figures D-7 to
D-9 are plots of the roller rim stresses versus angle for each
roller of the roller gear drive. Each roller is rotating while the point
of load application remains stationary (stress pattern stationary). This
means that at any cross section of the roller, the magnitudes of the
stresses are continually changing. Hence, a vibratory and steady stress
may be calculated for both the inside and outside diameters as follows:

$$\text{Steady Stress} = \frac{1}{2}\left(f_{a_{max}} + f_{b_{max}} + f_{a_{min}} + f_{b_{min}}\right)$$

$$\text{Vibratory Stress} = \frac{1}{2}\left(f_{a_{max}} + f_{b_{max}} - f_{a_{min}} - f_{b_{min}}\right)$$

where

$f_a$ = axial stress

$f_b$ = bending stress

The margin of safety is calculated from

$$MS = \frac{1}{\left(\dfrac{f_{st}}{F_{ty}} + \dfrac{K_f \, f_v}{F_{en}}\right)} - 1$$

where

$f_{st}$ = steady stress

$f_v$ = vibratory stress

Figure D-10 shows the assumed cross section used for each roller.
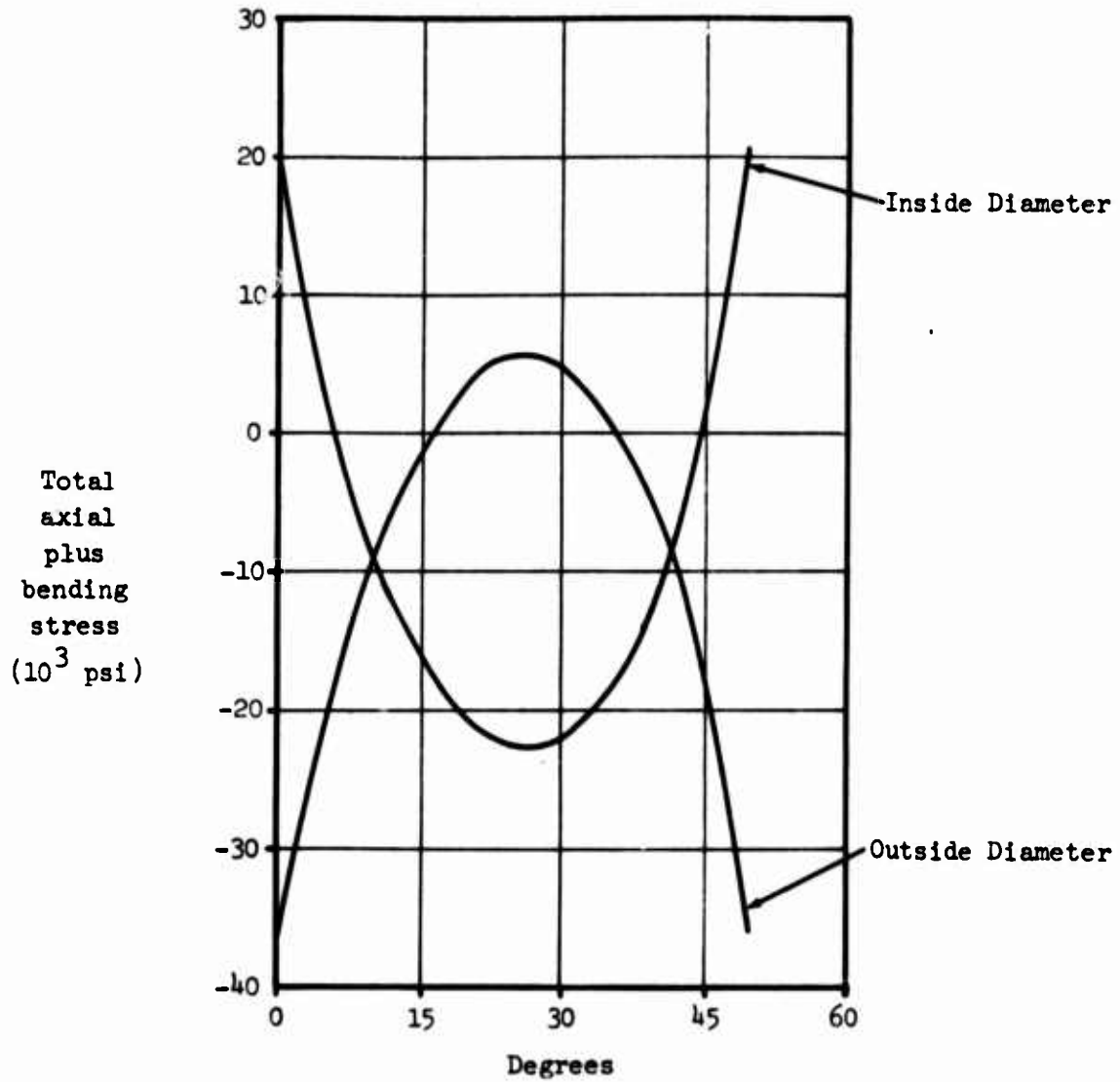
Figure D-7. Sun Gear Roller Rim Stresses.
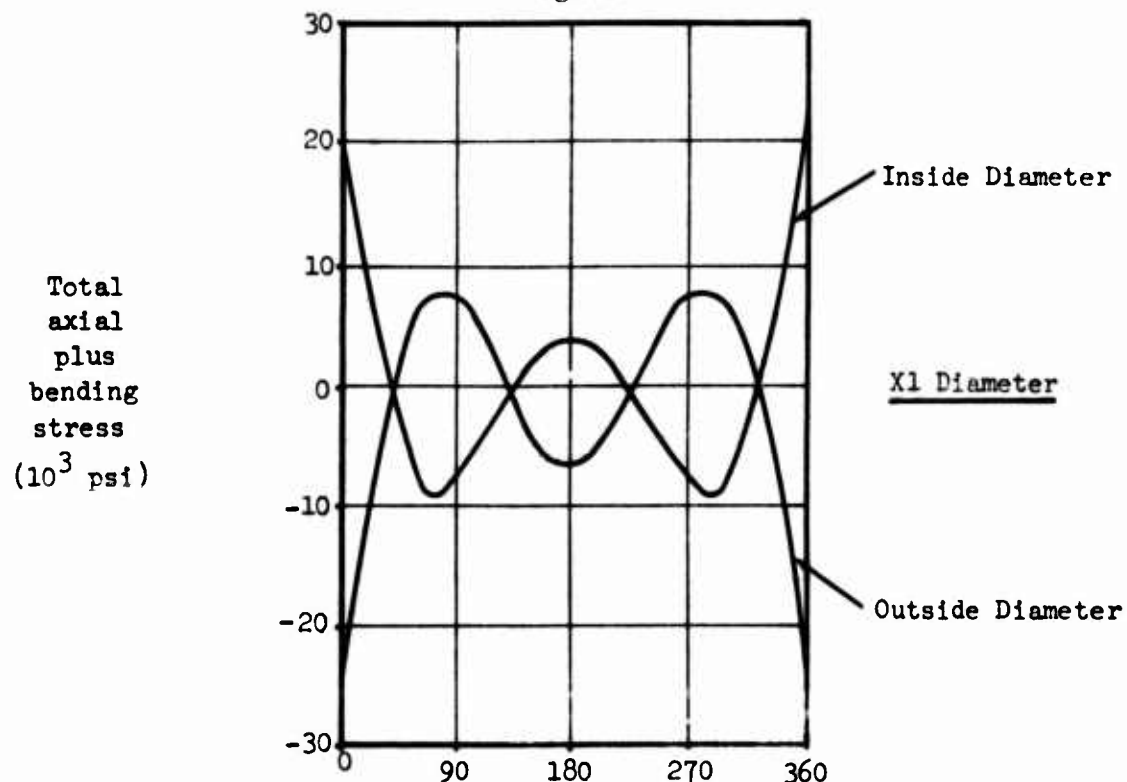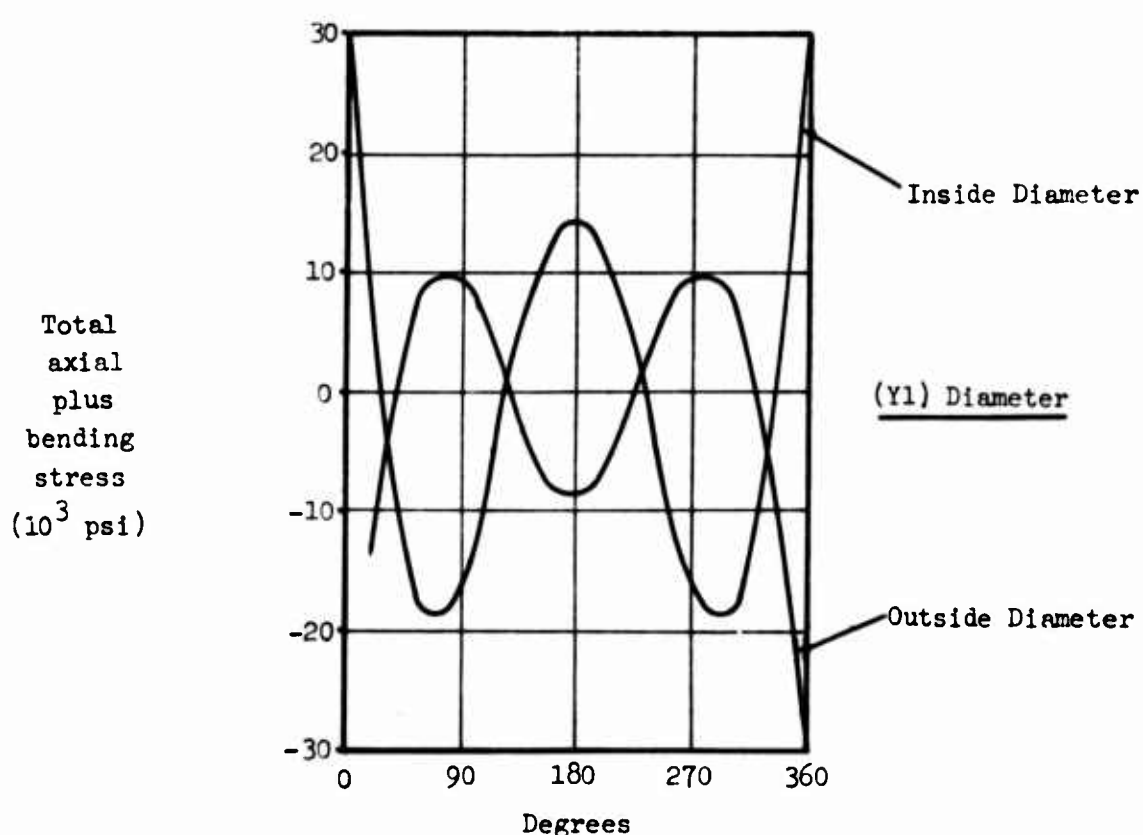
Figure D-8.   First-Row Pinion Roller Rim Stresses.
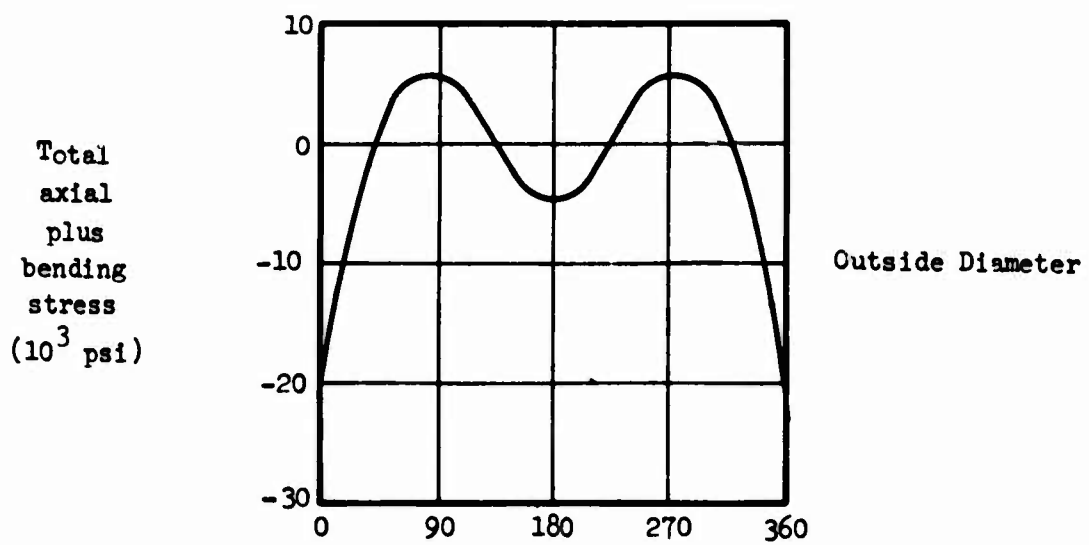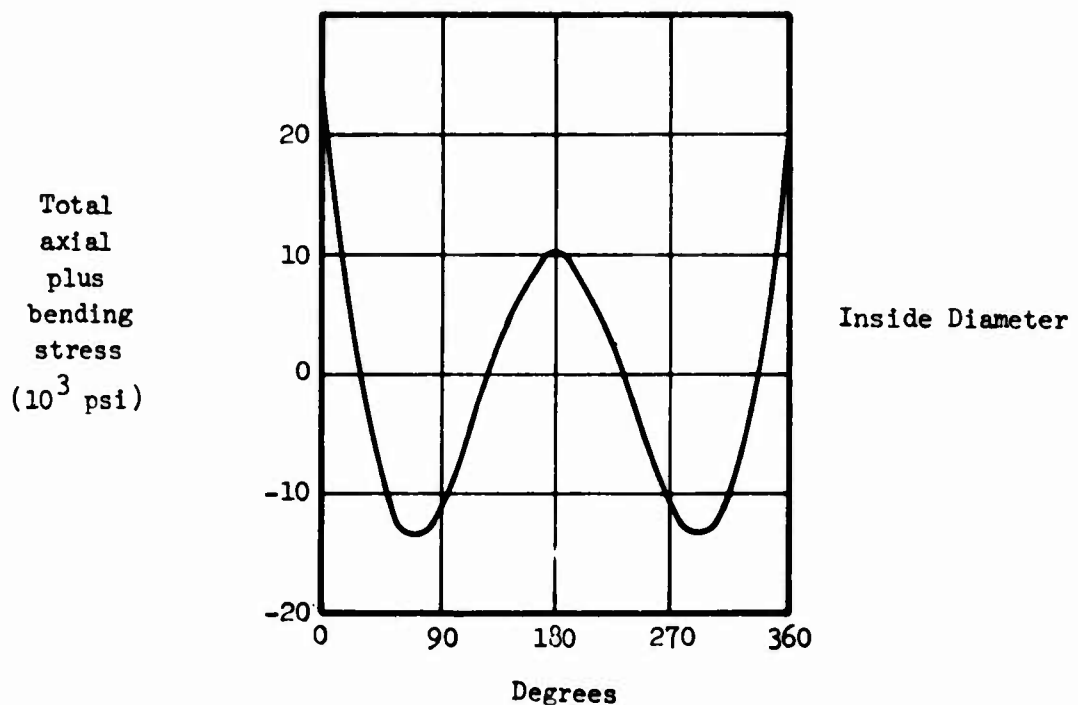
Figure D-9. Second-Row Pinion Roller Rim Stresses.

SUN GEAR

FIRST-ROW PINION

SECOND-ROW PINION
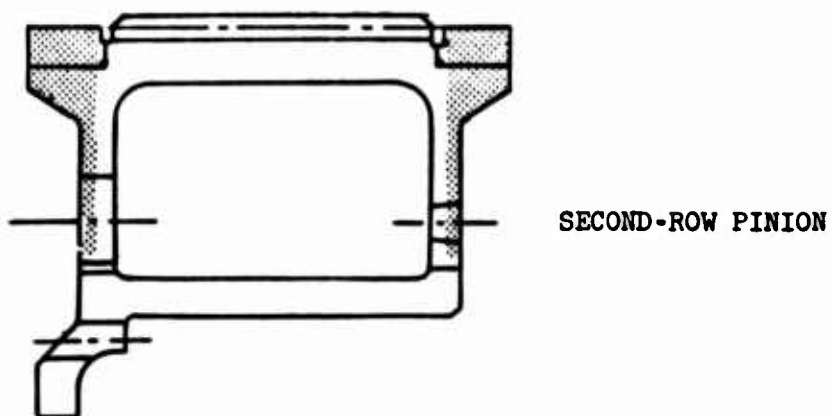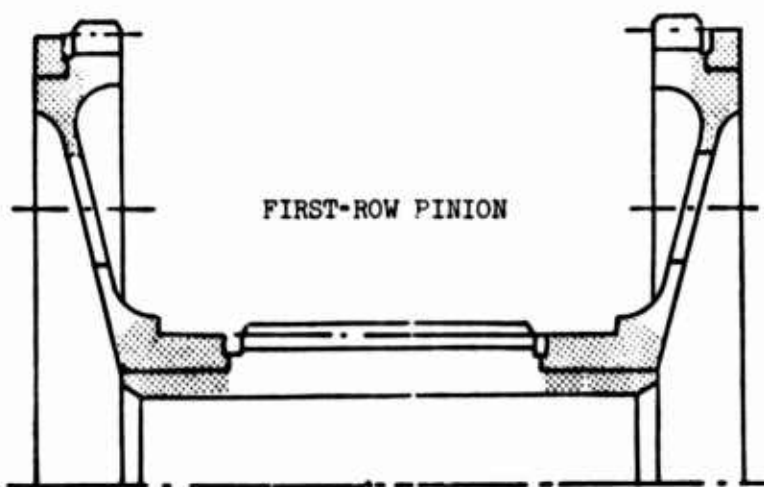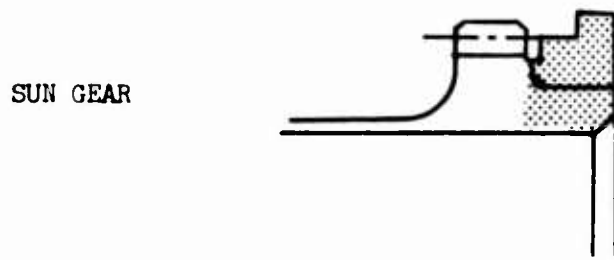
Figure D-10. Assumed Cross Section for Roller Rim Stress Analysis.

213

The minimum margin of safety for each roller with the section properties used is included in Table D-5.

| | Load per Roller (lb) | Section Properties | | | |
|---|---|---|---|---|---|
| Element | | $I$ (in$^4$) | $Z_{in}$ (in$^3$) | $Z_o$ (in$^3$) | Margin of Safety |
| Sun Gear Roller | 1375 | 0.0057 | 0.0157 | 0.0200 | + .16 (outside) |
| 1st Row Pinion Roller $X_1$ | 1375 | 0.01191 | 0.0239 | 0.0310 | +0.03 (inside) |
| 1st Row Pinion Roller $Y_1$ | 2250 | | | | |
| 2nd Row Pinion Roller $X_2$ | 2250 | 0.08671 | .0846 | 0.1156 | + .13 (inside) |

TABLE D-5.  ROLLER RIM STRESSES - MARGINS OF SAFETY.

As an example of the method of analysis consider the second row pinion roller:

$$\bar{x} = 4.0351 \text{ in.}$$

$$I = 0.08671 \text{ in.}^4$$

$$Z_o = 0.1156 \text{ in.}^3$$

$$Z_{in} = 0.0846 \text{ in.}^3$$

This roller is subjected to a concentrated load and is kept in equilibrium by symmetric uniform shear flow; although this roller has two contact points, one contact load is negligible   (70 lb  compared to 2250 lb ).

$$P = 2250 \text{ lb  per roller}$$

$$R = 4.0351 \text{ in.}$$

The values of the internal moments, internal forces, influence coefficients and stresses are calculated and given by Table D-6 for 22.5° increments.

## TABLE D-6.

### INTERNAL LOADS AND STRESSES FOR SECOND-ROW ROLLER RIM

| Angle $\theta$ | $K_m$ | $K_n$ | M | $fb_{outside}$ | $fb_{inside}$ | N | $fa$ | $ft_{outside}$ | $ft_{inside}$ |
|---|---|---|---|---|---|---|---|---|---|
| 0 | +0.23873 | 0.023873 | -2167. | -18741. | 25619. | -537. | -1647. | -20388. | 23972. |
| 22.5 | +0.06525 | 0.38798 | - 592. | - 5122. | 7002. | -872. | -2677. | - 7800. | 4324. |
| 45.0 | -0.04974 | 0.43398 | 451. | 3904. | -5336. | -976. | -2995. | 908. | -8332. |
| 67.5 | -0.09910 | 0.38007 | 899. | 7779. | -10634. | -855. | -2623. | 5156. | -13257. |
| 90.0 | -0.09085 | 0.25000 | 824. | 7131. | -9749. | -562. | -1725. | 5406. | -11474. |
| 112.5 | -0.04453 | 0.08187 | 404. | 3495. | -4777. | -184. | - 565. | 4060. | -4212. |
| 135.0 | +0.01450 | -0.08042 | - 131. | - 1137. | 1555. | +180. | 554. | - 584. | 2110. |
| 157.5 | +0.06172 | -0.19664 | - 560. | - 4845. | 6624. | +442. | 1357. | -3488 | 7981. |
| 180.0 | +0.07958 | -0.23873 | - 722. | - 6247. | 8540. | +537 | 1647. | -4599. | 10187. |

215

For the inside diameter the maximum and minimum values of stress as shown by Figure D-9 occur at 0 degrees and 72 degrees and are given by Table D-7.

| TABLE D-7. MAXIMUM AND MINIMUM VALUES OF STRESS, INSIDE DIAMETER – SECOND-ROW PINION | | | |
|---|---|---|---|
| Position (deg) | $f_a$ (psi) | $f_b$ (psi) | $f_a + f_b$ (psi) |
| 0 | -1650 | 25620 | 23970 |
| 72 | -2450 | -11070 | -13520 |

$$f_{st} + f_v = 5230 \pm 18750$$

$$K_t = 1.0$$

$$F_{en} = 22430 \text{ psi}$$

$$F_{ty} = 115000 \text{ psi}$$

$$MS = \left( \frac{5230}{115000} + \frac{18750 \ (1.0)}{22430} \right)^{-1} - 1$$

$$MS = + .13$$

For the outside diameter the maximum and minimum values of stress as shown by Figure D-9 occur at 0 degrees and 84 degrees and are given by Table D-8.

| TABLE D-8. MAXIMUM AND MINIMUM VALUES OF STRESS OUTSIDE DIAMETER - SECOND-ROW PINION | | | |
|---|---|---|---|
| Position (deg) | $f_a$ (psi) | $f_b$ (psi) | $f_a + f_b$ (psi) |
| 0 | -1650 | -18740 | -20390 |
| 84 | -2300 | 7860 | 5560 |

$$f_{s_t} + f_v = -7420 \pm 12980$$

$$K_t = 1.0$$

$$F_{en} = 27970 \text{ psi}$$

The compressive steady stresses on the outside of the roller may be neglected.

$$MS = \frac{F_{en}}{K_t f_v} - 1$$

$$MS = \frac{27970}{(1.0)(12980)} - 1$$

$$MS = +1.15$$

## GEAR RIM STRESSES

The gear rim thickness for each gear of the roller gear drive unit
is calculated from stresses in the rim. These stresses are determined
from thin ring theory, neglecting the effect of the internal radial shear
force.

The sun and ring gears are analyzed as a ring subjected to seven
equally spaced applied radial, tangential and moment loads. For the
sun or ring gear, the sign convention for the applied loads and factors
is given in Table D-9.

| TABLE D-9. SIGN CONVENTION FOR APPLIED LOADS AND FACTORS | | |
|---|---|---|
| Load | Sun Gear | Ring Gear |
| $W_r$ | – | + |
| $W_t$ | + | + |
| M | + | – |
| K | -1 | +1 |
| where | | |
| $W_r$ = applied radial load | | |
| $W_t$ = applied tangential load | | |
| M = resultant moment from tangential load acting at centroid of section. | | |

Figure D-11 is a sketch of the applied loads and the internal loads
for the sun and ring gears.

The internal moments $M_r$, $M_t$, and $M_m$ at any radial section $\theta$ due to
the applied radial, tangential and moment load, respectively, are given by

$$M_r = \frac{R}{2} W_R K_1$$

$$M_t = \frac{R}{2} W_t K_2$$

$$M_m = M K_3$$
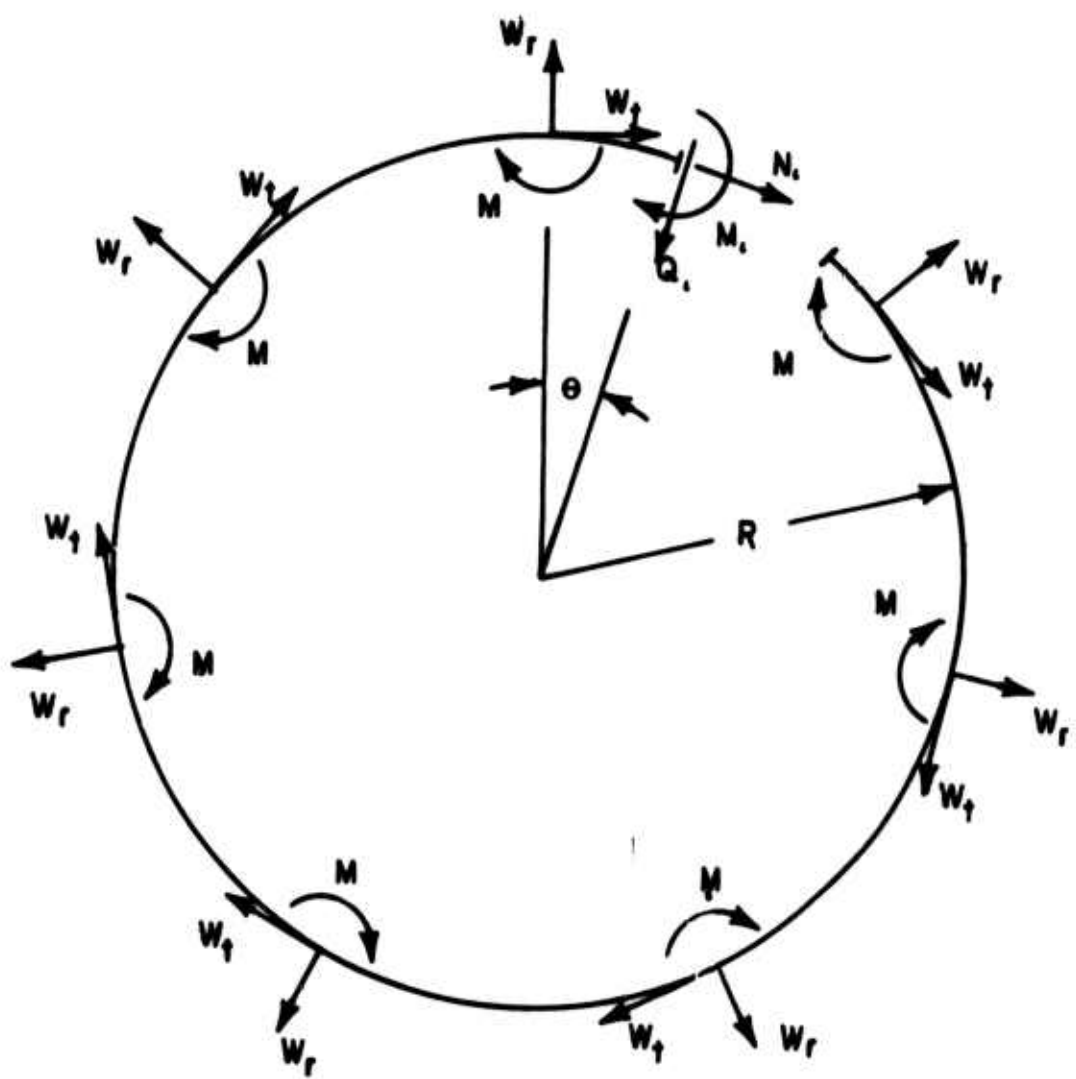
Figure D-11. Sun and Ring Gear Loads.

where

$$K_1 = \frac{(\text{no. pin})}{\pi} - \sin\theta - \cot\left(\frac{\pi}{\text{no. pin}}\right)\cos\theta$$

$$K_2 = \frac{(\text{no. pin})}{\pi} - 1 + \cos\theta - \cot\left(\frac{\pi}{\text{no. pin}}\right)\sin\theta$$

$$K_3 = \frac{(\text{no. pin})}{\pi} - 1$$

The circumferential internal forces $N_r$ and $N_t$ at any radial section $\theta$ due to the applied radial and tangential loads respectively are given by

$$N_r = K_4 W_r$$

$$N_t = K_5 W_t$$

where

$$K_4 = \frac{1}{2}\left[\sin\theta + \cot\left(\frac{\pi}{\text{no. pin}}\right)\cos\theta\right]$$

$$K_5 = \frac{1}{2}\left[\cot\left(\frac{\pi}{\text{no. pin}}\right)\sin\theta - \cos\theta\right]$$

The first- and second-row pinions are analyzed as rings subjected to applied radial, tangential, and moment loads and are placed in equilibrium by uniform shear flow. Referring to Figure D-1 for roller gear drive basic geometry and nomenclature, the $X_1$ and $Y_2$ gears have one mesh or applied load point, while the $Y_1$ and $X_2$ gears have two mesh or applied load points. For a gear with two mesh points the solutions for internal moments and internal forces are superimposed. Figure D-12 shows the applied loads and uniform shear flow necessary to keep the ring in equilibrium for the various loading conditions.
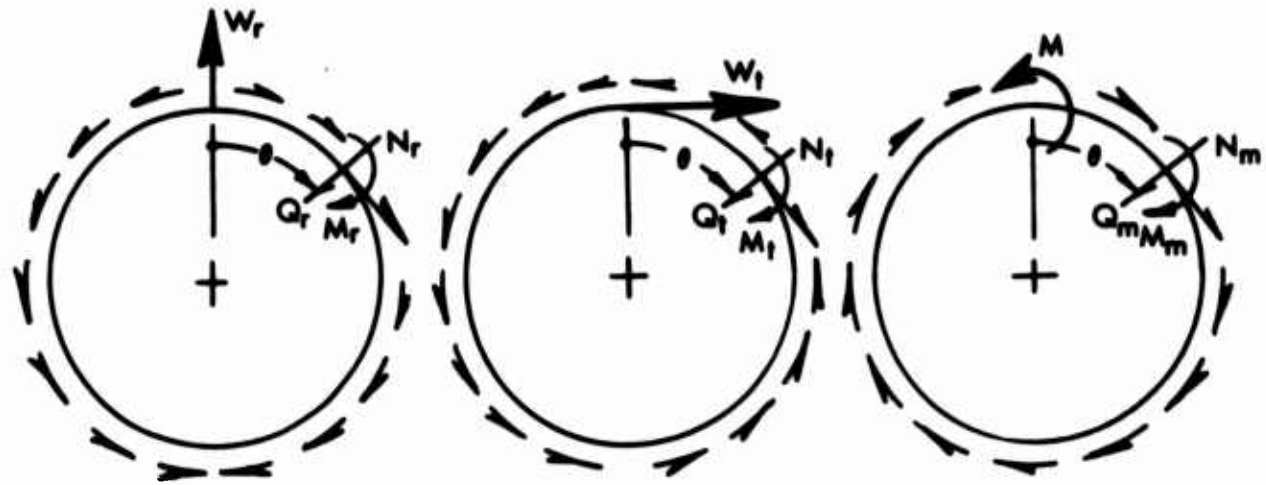
Figure D-12.   Applied Loads and Shear Flows
for Gear Rims.

The internal moments  $M_r$,  $M_t$, and $M_m$ at any radial section $\theta$   due to
the applied radial, tangential and moment load, respectively, are given by

$$M_r \ = \ K_6 \, W_r \, R$$

$$M_t \ = \ K_7 \, W_t \, R$$

$$M_m \ = \ K_8 \, M$$

where

$$K_6 \ = \ \left. \frac{-(\pi - \theta)\sin\theta \ + \ \frac{1}{2}\cos\theta \ +1}{2\pi} \right|_0^\pi$$

$$K_7 \ = \ \left. \frac{-(\pi - \theta) \ + \ \frac{3}{2}\sin\theta \ + \ (\pi - \theta)\cos\theta}{2} \right|_0^\pi$$

$$K_8 \ = \ \left. \frac{-\sin\theta}{\pi} \ - \ \frac{\theta}{2\pi} \ + \ \frac{1}{2} \right|_0^\pi$$

The circumferential internal forces $N_r$, $N_t$, and $N_m$ at any radial section $\theta$ due to the applied radial, tangential and moment load, respectively, are given by:

$$N_r = K_9 \, W_r$$

$$N_t = K_{10} \, W_t$$

$$N_m = K_{11} \, \frac{M}{R}$$

where

$R =$ distance from point of applied load to centroid of section.

$$K_9 = \left. \frac{(\pi - \theta) \sin\theta + \frac{3}{2}\cos\theta}{2\pi} \right|_0^\pi$$

$$K_{10} = \left. \frac{\frac{1}{2}\sin\theta - (\pi - \theta)\cos\theta}{2\pi} \right|_0^\pi$$

$$K_{11} = \left. \frac{\sin\theta}{\pi} \right|_0^\pi$$

From the total internal moments and total internal forces, the total axial plus bending stresses are determined for increments along the circumference of the gear on both the inside and outside diameters. Figures D-13 to D-18 are plots of the total axial plus bending gear rim stresses versus angle for each gear of the roller gear drive. Each gear is rotating while the point of load application remains stationary (stress pattern stationary) such ahat at any cross section of the gear rim, the magnitudes of the stresses are continually changing. Hence, a vibratory and steady stress may be calculated for both the inside and outside diameters. The maximum and minimum stress occurs at

$$\frac{\pi}{\text{no. of teeth}} \quad \text{or multiples of} \quad \frac{\pi}{\text{no. of teeth}} \quad \text{from the load point, since}$$

these are the weakest sections and not at the points of maximum moment. Figure D-19 of a typical gear tooth illustrates this point. The steady
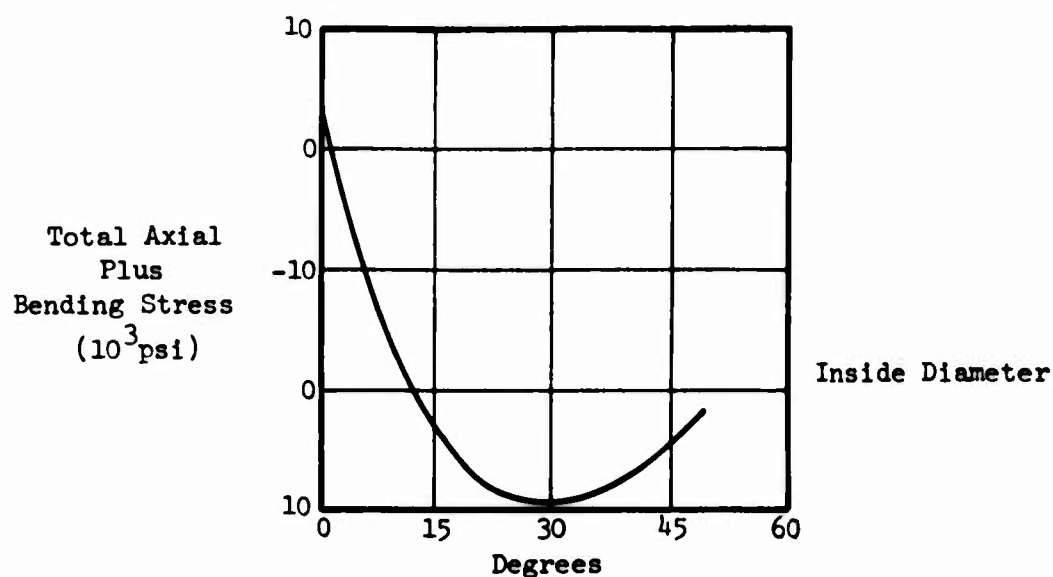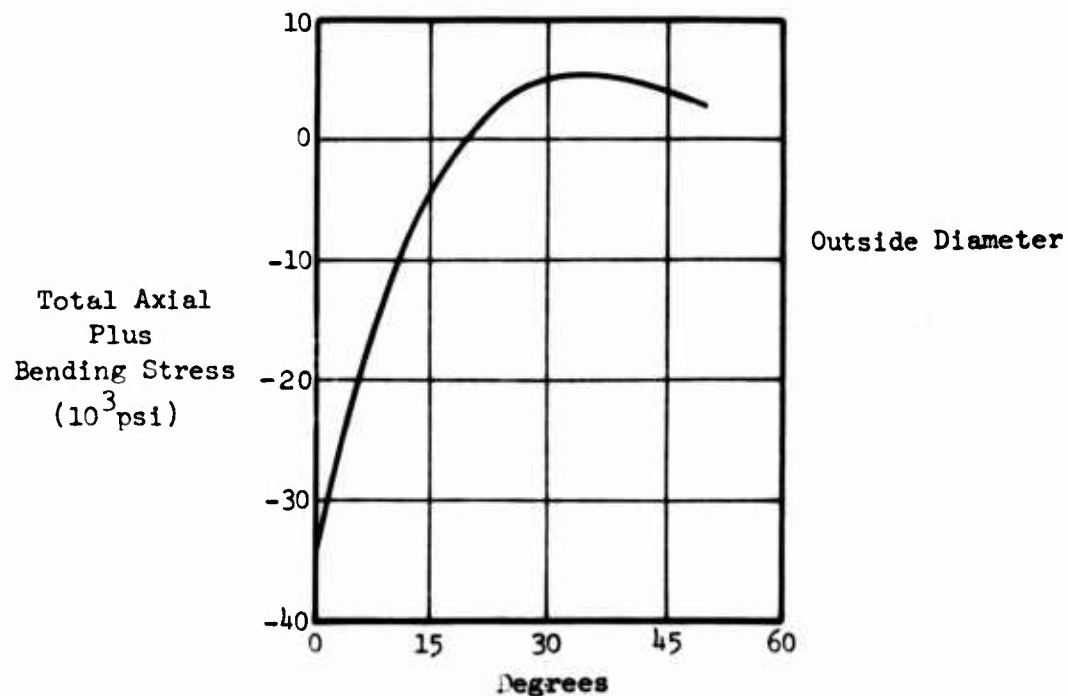
Figure D-13. Gear Rim Stresses - Sun Gear.

223
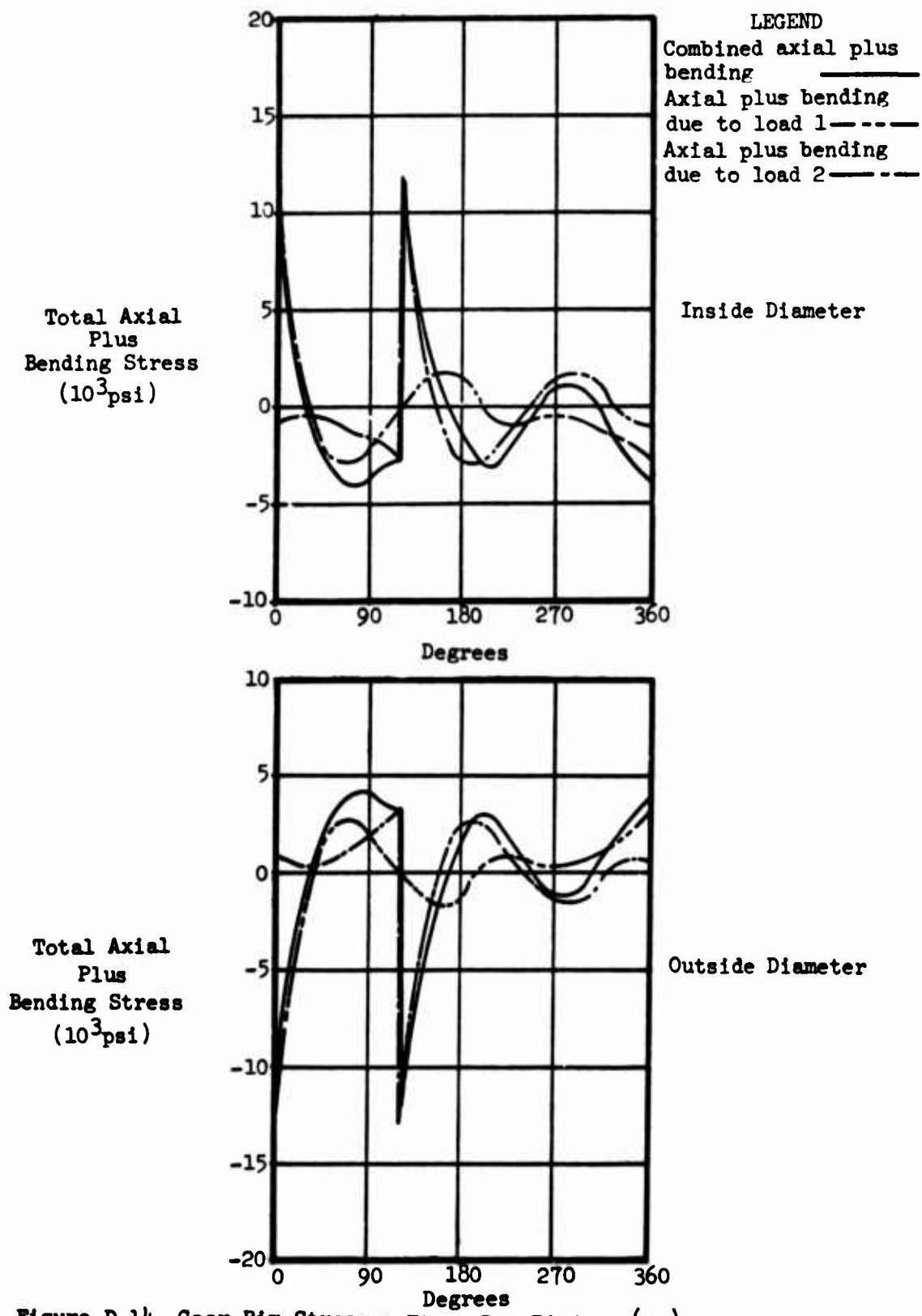
Figure D-14. Gear Rim Stresses-First-Row Pinion $(y_1)$.
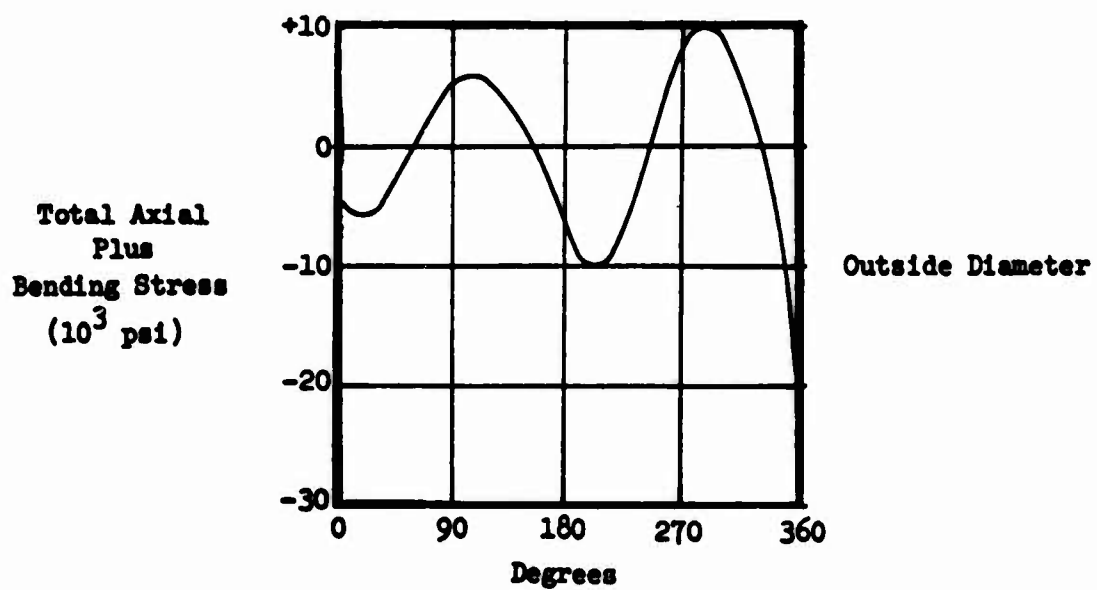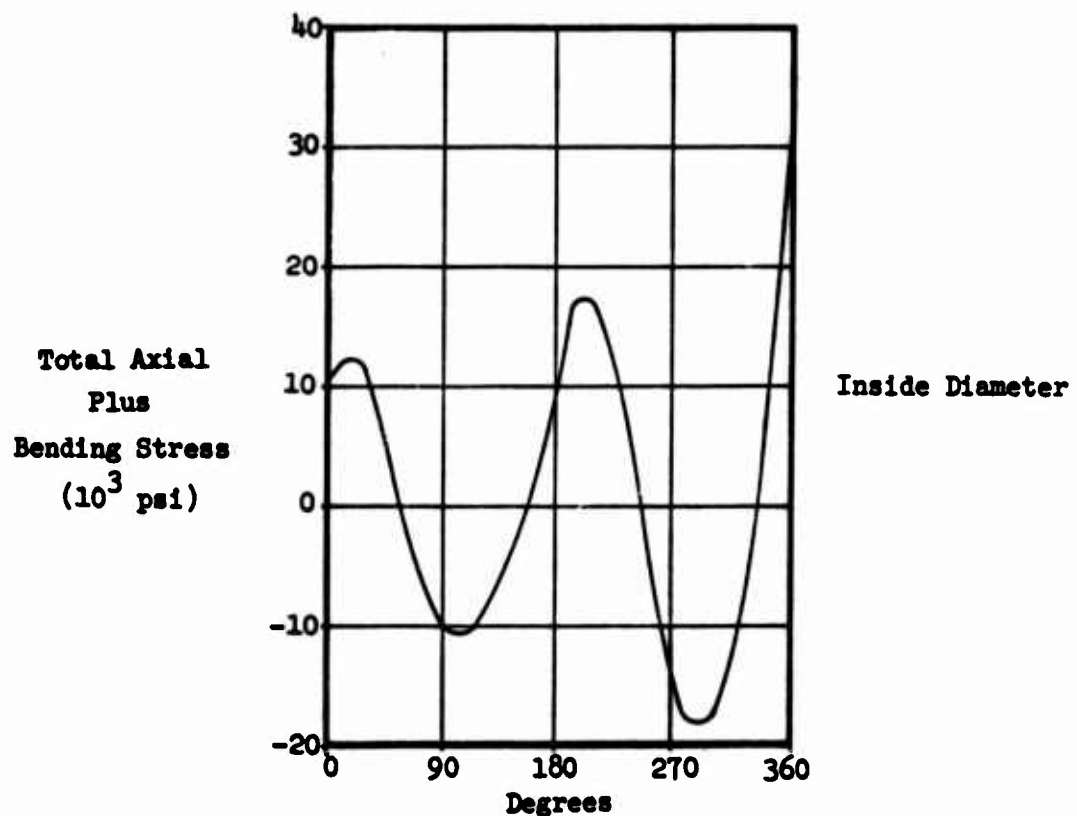
Figure D-15.   Gear Rim Stresses - First-Row Pinion ($x_1$).
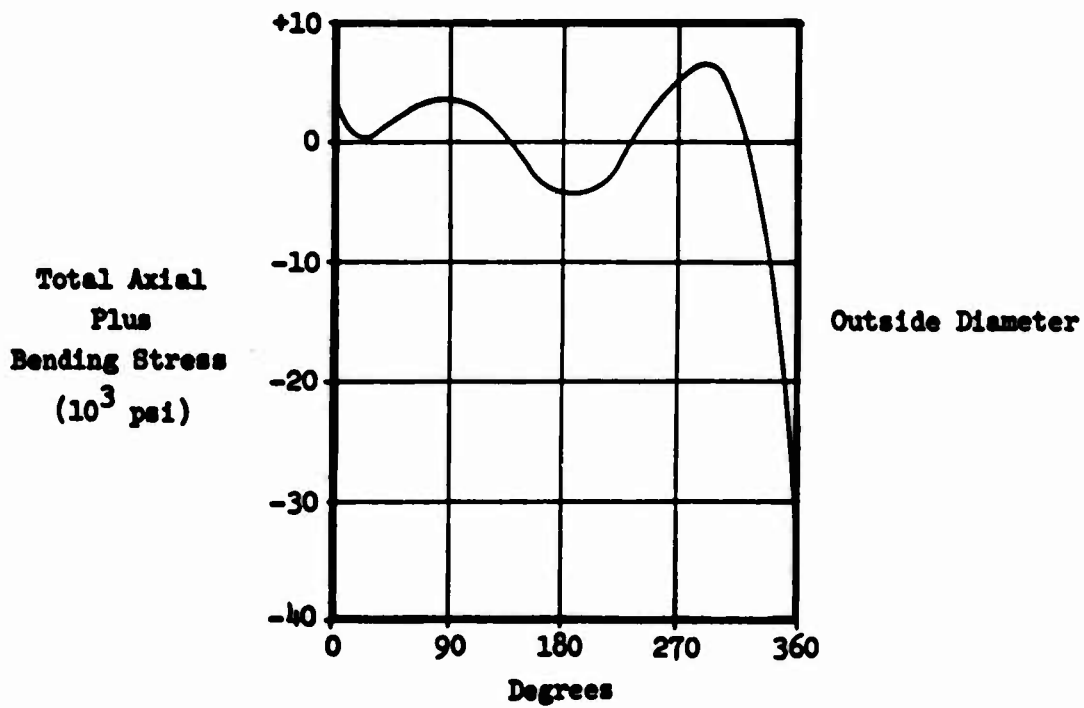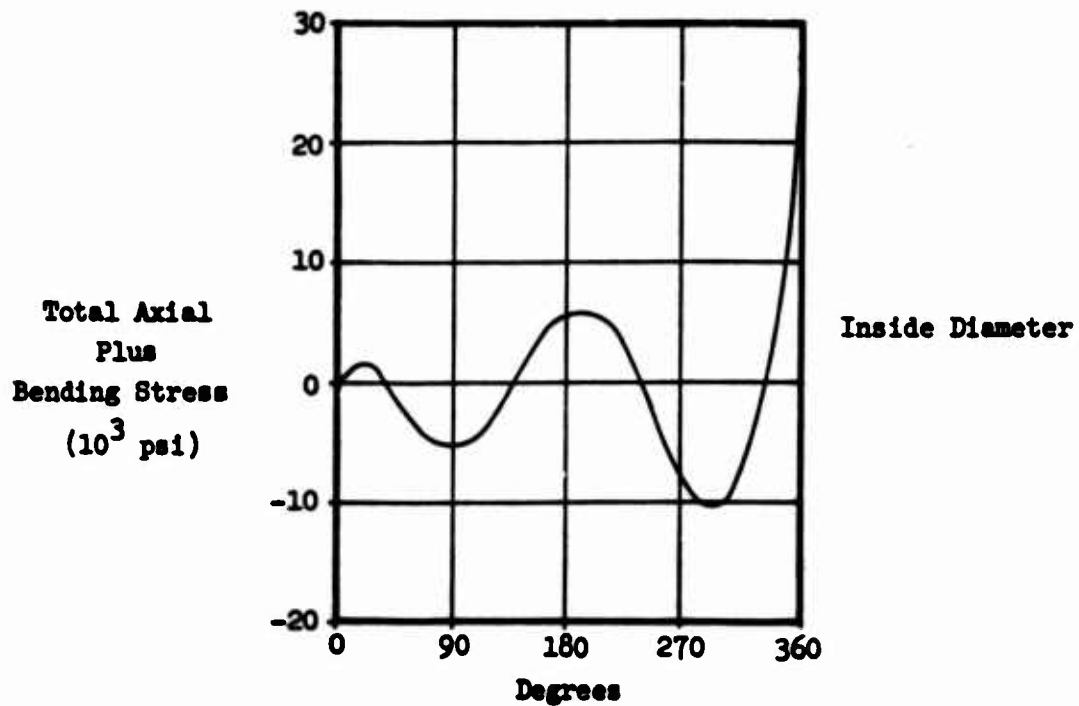
Figure D-16.   Gear Rim Stresses - Second-Row Pinion ($y_2$).

Figure D-17.  Gear Rim Stresses - Second-Row Pinion $(X_2)$.
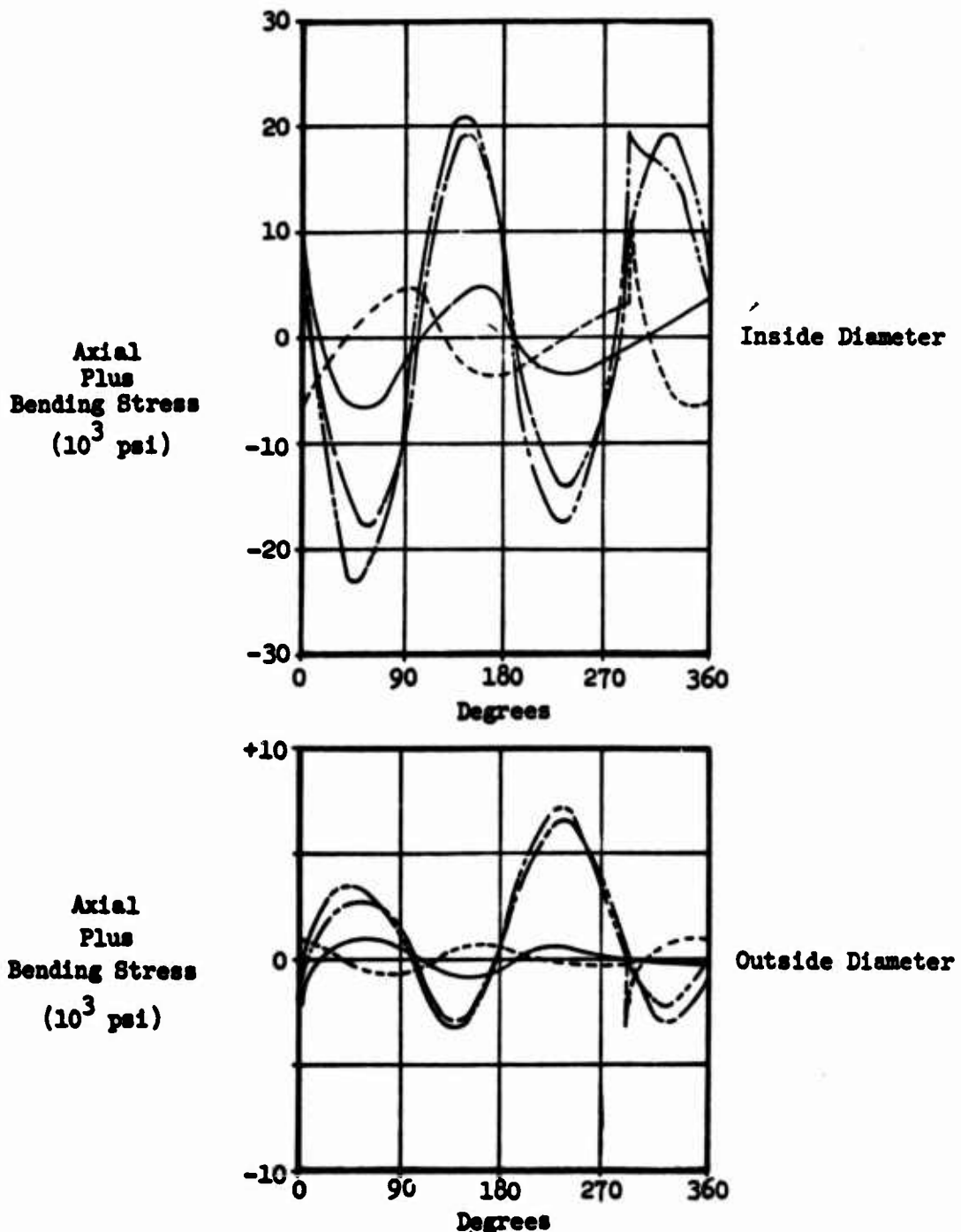
LEGEND:
——— Axial Plus Bending Stress due to Load 1
——— Axial Plus Bending Stress due to Load 2
—·— Axial Plus Bending Stress due to Load 3
—··— Total Axial Plus Bending Stress

227
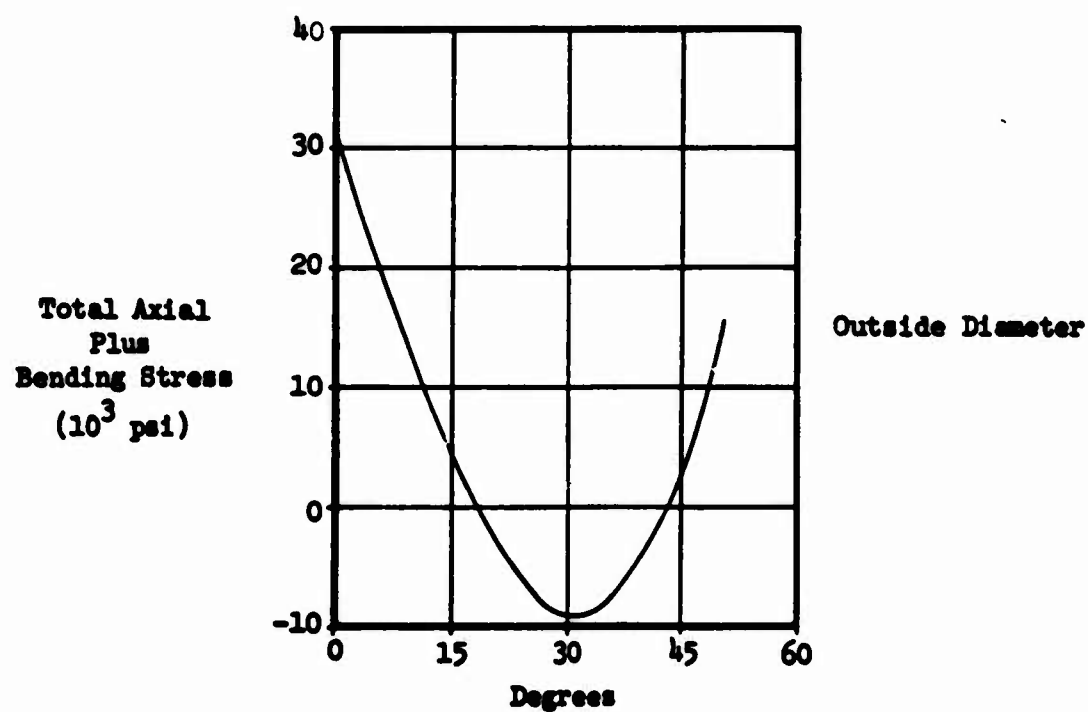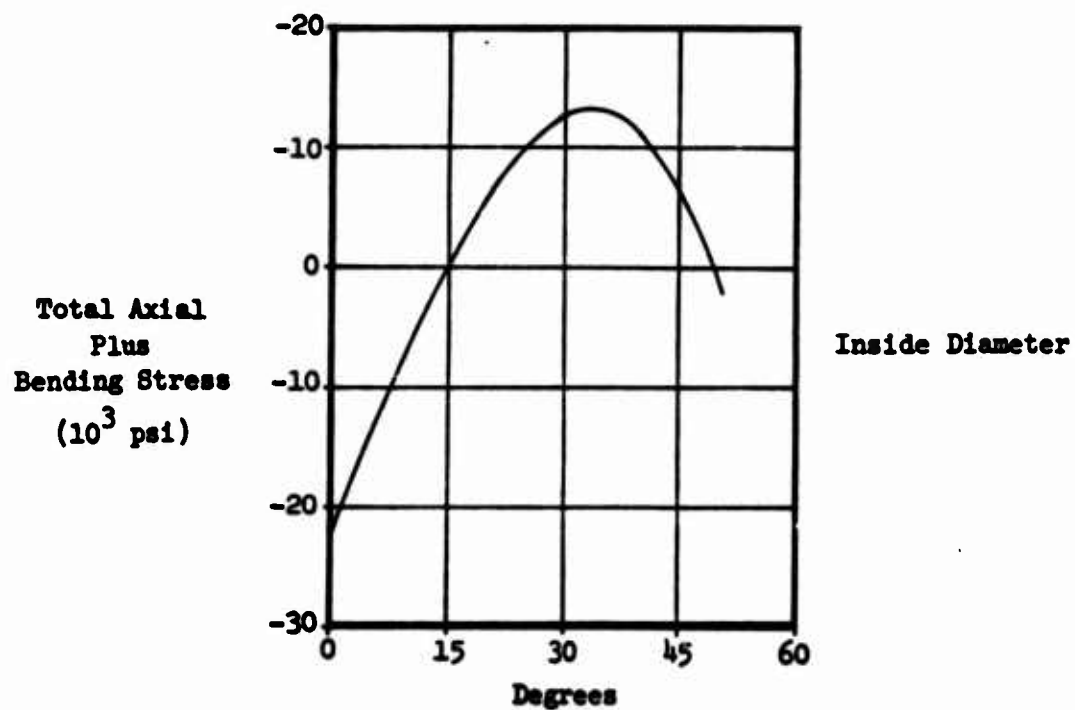
Figure D-18.    Gear Rim Stresses - Ring Gear (c).
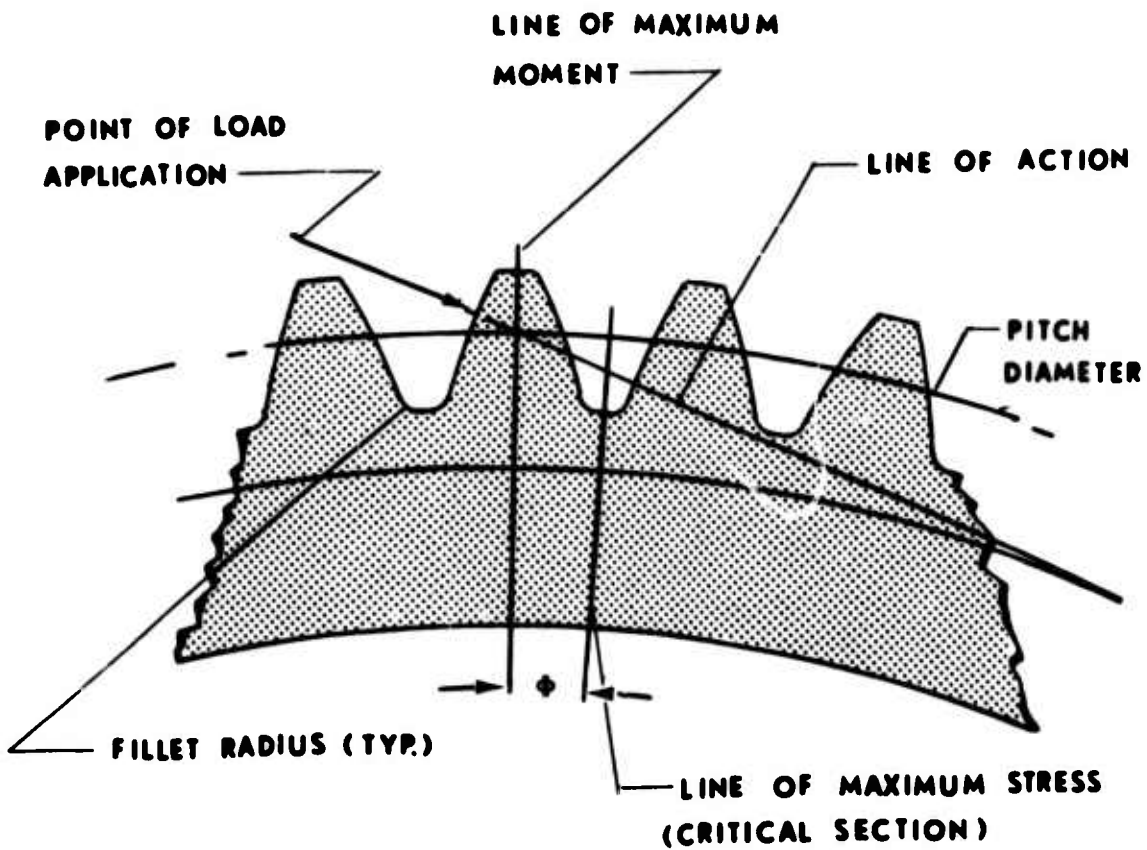
Figure D-19.   Typical Gear Tooth.

plus vibratory stress at the tooth roots are determined from

$$\text{Steady Stress} = \frac{1}{2} \left( f_{a_{max}} + f_{b_{max}} + f_{a_{min}} + f_{a_{max}} \right)$$

$$\text{Vibratory Stress} = \frac{1}{2} \left( f_{a_{max}} + f_{b_{max}} - f_{a_{min}} - f_{b_{min}} \right)$$

where:

$$f_a = \text{axial stress}$$

$$f_b = \text{bending stress}$$

The margin of safety is calculated from

$$MS = \frac{1}{\left[ \dfrac{f_{st}}{F_{ty}} + \dfrac{K_t \, f_v}{F_{en}} \right]} - 1$$

where

$$f_{st} = \text{steady stress}$$

$$f_v = \text{vibratory stress}$$

Figure D-20 shows the assumed cross sections used in the analysis.

The minimum margin of safety for each gear with the applied loads and section properties used is included in Table D-10.
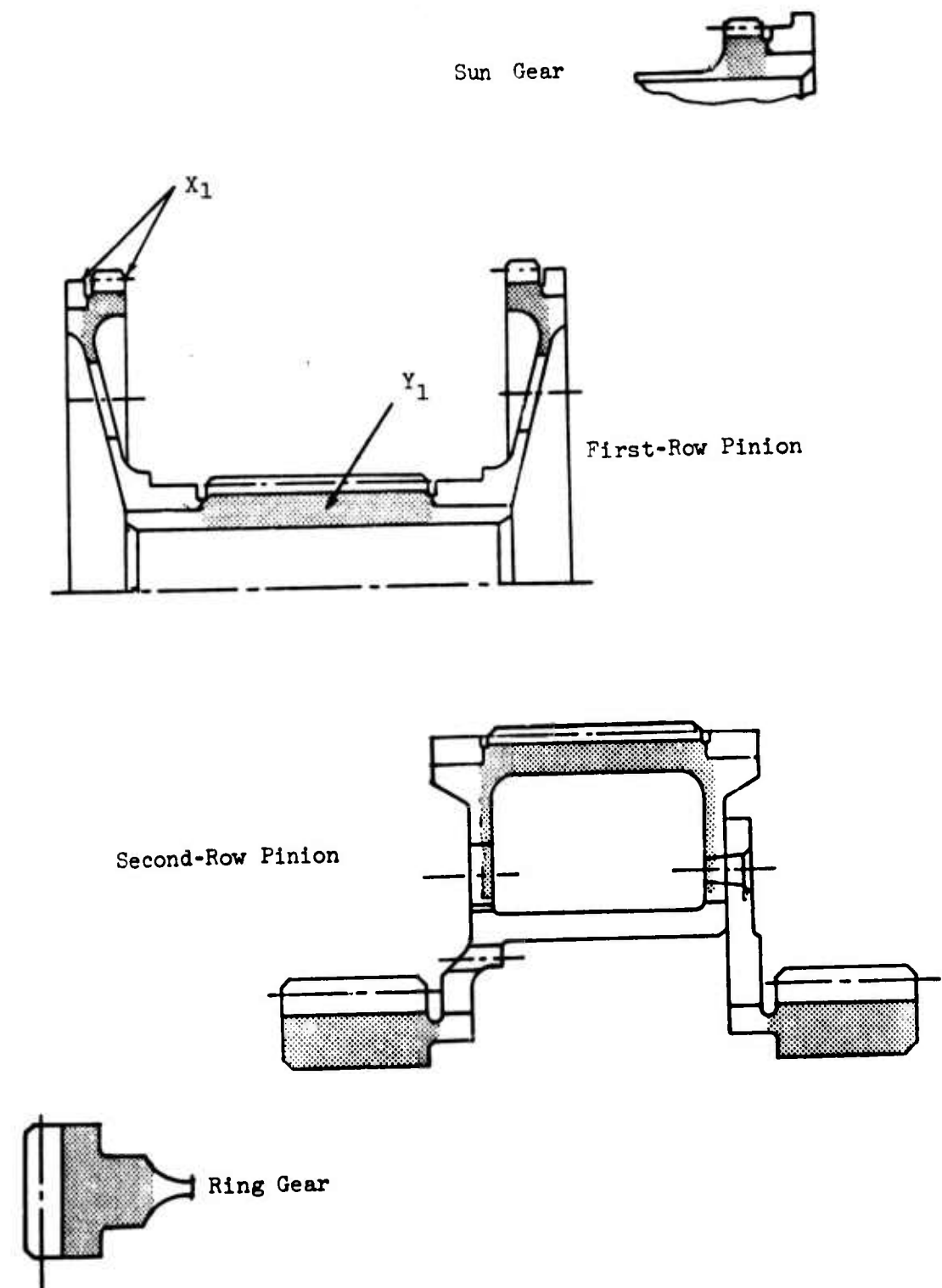
Figure D-20. Assumed Cross Section for Gear Rim Stress Analysis.

| | Radial (lbs) | Tangential (lbs) | Moment (lb-in) | Critical Zone | $Z$ (inches$^3$) | Minimum Margin of Safety |
|---|---|---|---|---|---|---|
| Sun Gear | 315 | 755 | 339 | Outside | 0.0086 | + .02 |
| 1st-Row Pinion $X_1$ | 315 | 755 | 227 | Inside | 0.00955 | + .04 |
| 1st-Row Pinion $Y_1$ | 1060 | 2270 | 566 | Outside | 0.0315 | |
| 2nd-Row Pinion $X_2$ | 1060 | 2270 | 689 | Inside | 0.1295 | + .09 |
| 2nd-Row Pinion $Y_2$ | 2790 | 4830 | 2403 | Outside | 0.07976 | +0.0 |
| Ring Gear | 2790 | 4830 | 3028 | Inside | 0.1864 | + .04 |

TABLE D-10.
ROLLER GEAR DRIVE RIM STRESSES - MARGIN OF SAFETY

As an example of the method of analysis, consider the 2nd-row pinion, $x_2$, with the applied loads as shown in Figure D21 . The gear is subjected to two load contact points and a sinusoidal bearing load. For each applied radial, tangential, moment and sinusoidal load, the ring is placed in equilibrium by uniform shear flow. The solutions for each case are then superimposed on each other, taking into account the proper phase relationship.

$$\overline{X} = 4.463 \quad \text{in.}$$
$$I = 0.1051 \quad \text{in.}^4$$
$$A = 1.110 \quad \text{in.}^2$$
$$Z_o = 0.5402 \quad \text{in.}^3$$
$$Z_i = 0.1295 \quad (\text{in.}^3)$$
$$W_r = 1060 \quad \text{lb}$$
$$W_t = 2270 \quad \text{lb}$$
$$M = 689 \quad \text{lb-in.}$$
$$Q = 10950 \quad \text{lb}$$
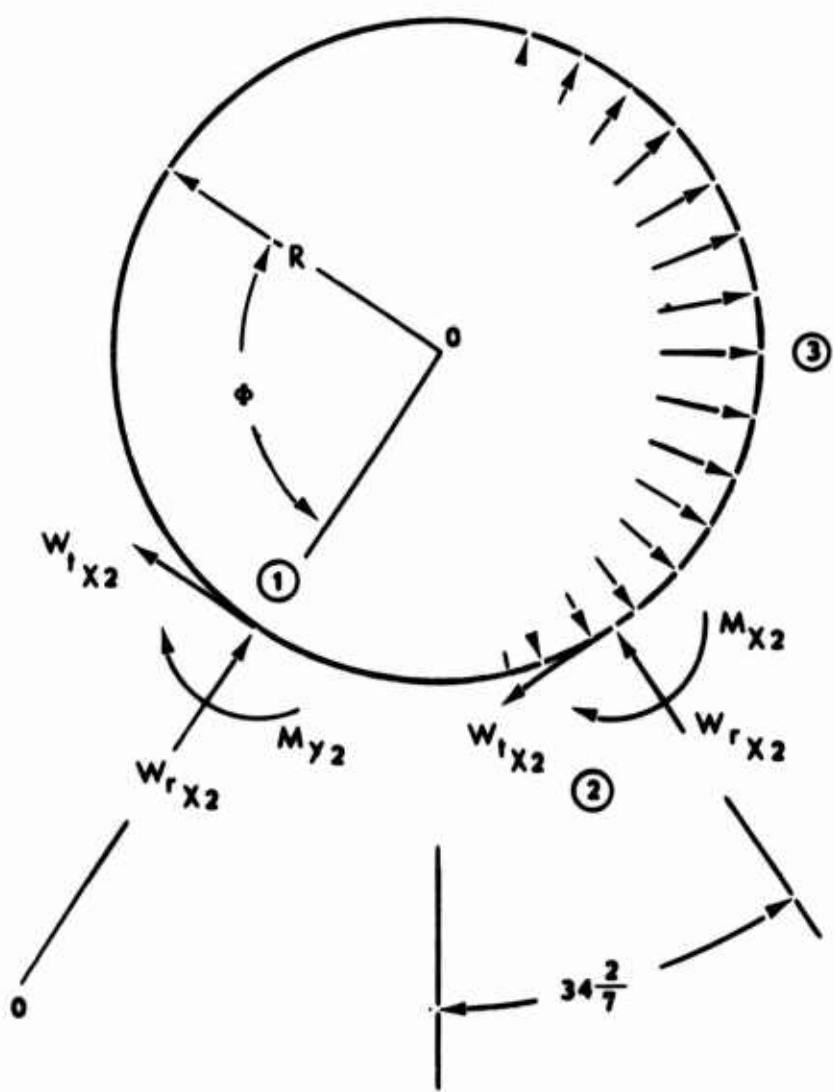
Figure D-21.   Second-Row Pinion, $X_2$ - Applied Loads.

233

The only case which has not as yet been discussed is the sinusoidal bearing load reacted by uniform shear flow.

$$Q_{max} = \frac{2 Q}{\pi R}$$

$$Q_{max} = \frac{(2)(10950)}{\pi (4.463)}$$

$$Q_{max} = 1560$$

The internal moment and internal circumferential force is force are given by

$$M_B = K_{12} Q_{max} R^2$$

$$N_B = K_{13} Q_{max} R$$

where

$$K_{12} = \left\{ \left[ -\frac{\theta \sin\theta}{4} - \frac{\cos\theta}{4} + \frac{1}{\pi} \right]\Big|_0^{\pi/2} \quad \left[ -\frac{(\pi-\theta)\sin\theta}{4} + \frac{\cos\theta}{4} + \frac{1}{\pi} \right]\Big|_{\pi/2}^{\pi} \right\}$$

$$K_{13} = \left\{ \left[ \frac{\theta \sin\theta}{4} + \frac{3}{4}\cos\theta \right]\Big|_0^{\pi/2} \quad \left[ \frac{(\pi-\theta)\sin\theta}{4} + \frac{\cos\theta}{4} \right]\Big|_{\pi/2}^{\pi} \right\}$$

The values of the internal stresses for the two gear loads and
bearing load are summarized in Table D-11.

On the outside of the gear rim:

$$K_t = 1.63$$

$$F_{en} = 22740 \text{ psi}$$

$$F_{ty} = 115000 \text{ psi}$$

$$f_s = 1920 \text{ psi}$$

$$f_v = \pm 5310 \text{ psi}$$

$$MS = \cfrac{1}{\left( \cfrac{f_s}{F_{ty}} + \cfrac{K_t \, f_v}{F_{en}} \right)} - 1$$

$$MS = \cfrac{1}{\left[ \cfrac{1920}{115000} + \cfrac{(1.63)(5310)}{22740} \right]} - 1$$

$$MS = +1.51$$

On the inside of the gear rim:

$$K_t = 1.0$$

$$F_{en} = 22740 \text{ psi}$$

$$F_{ty} = 115000 \text{ psi}$$

$$f_s = 290 \text{ psi}$$

$$f_v = 20,780 \text{ psi}$$

TABLE D-11. INTERNAL STRESSES, SECOND-ROW PINION ($x_2$).

| | Angle* | | Stress From Gear Loads | | Stress From Bearing Loads | |
|---|---|---|---|---|---|---|
| $\theta_1$ | $\theta_2$** | $\theta_3$*** | $\sigma_T$ Outside | $\sigma_T$ Inside | $\sigma_T$ Outside | $\sigma_T$ Inside |
| 0 | 291.42 | 235.28 | -3530 | 11140 | 6607 | -13806 |
| 22.5 | 313.92 | 257.78 | 524 | -1121 | 5458 | -9414 |
| 45.0 | 336.42 | 280.28 | 879 | -6121 | 2500 | -1694 |
| 67.5 | 358.92 | 302.78 | 1099 | -6018 | -924 | 13859 |
| 90.0 | 21.42 | 325.28 | 609 | -2889 | -2957 | 19267 |
| 112.5 | 43.92 | 347.78 | -102 | 940 | -2264 | 12518 |
| 135.0 | 66.42 | 10.28 | -653 | 3709 | 24 | -781 |
| 157.5 | 88.92 | 32.78 | -821 | 4435 | 2222 | -12650 |
| 180.0 | 111.42 | 55.28 | -576 | 3058 | 3104 | -17308 |
| 202.5 | 133.92 | 77.78 | 491 | -1970 | 2222 | -12650 |
| 225.0 | 156.42 | 100.28 | 755 | -3691 | 24 | -781 |
| 247.5 | 178.92 | 122.78 | 594 | -3441 | -2264 | 12518 |
| 270.0 | 201.42 | 145.28 | 301 | -2289 | -2957 | 19267 |
| 292.5 | 223.92 | 167.78 | 40 | -825 | -924 | 13859 |
| 315.0 | 246.42 | 190.28 | -184 | 907 | 2500 | -1694 |
| 337.5 | 268.92 | 212.78 | -130 | 1726 | 5458 | -9414 |
| 360.0 | 291.42 | 235.28 | -249 | 3326 | 6607 | -13806 |

*All angles are measured from point ① Figure D-21
**The angle $\theta_2$ is the angle for the stresses and internal loads due to gear loads ② measured with respect to point ①

***The angle $\theta_3$ is the angle for the stresses and internal loads due to bearing loads measured with respect to point ①

236

$$MS = \left( \frac{1}{\dfrac{f_s}{F_{ty}} + \dfrac{K_t \, f_v}{F_{en}}} \right)^{-1}$$

$$MS = \left[ \frac{1}{\dfrac{(290)}{115000} + \dfrac{(1.0)(20780)}{22740}} \right]^{-1}$$

$$MS = +0.09$$

## PLATE AND POST ASSEMBLY

The plate and post assembly reacts the torque of the roller gear drive unit. The distance between the plates of the plate and post assembly is small and the plates are assumed to react the load as a solid member. Figure D-22 is a sketch of the model used to determine the plate slope and stress where

Q = applied bearing load

$\phi$ = angle of rotation

g = height of post from center of plate
to $\mathcal{C}$ of bearing

d = mean diameter of post

l = length of plate betwen points of inflection

t = thickness of plate

Z = radius to $\mathcal{C}$ of bearing

$d_o$ = plate outside diameter

$d_i$ = plate inside diameter

h = distance between plates to inside edges

H = distance between plates to outside edges

$$L = \frac{1 - .8d}{2}$$

Equating the strain energy of the trunnion to the strain energy of the cantilever leads to

$$\phi = \frac{16 \, Q \, g \, L^3}{E \, 1^2 \, (d_o - d_i) \, (H^3 - h^3)}$$

$$f_b = \frac{12 \, Q \, g \, L \, H}{1 \, (d_o - d_i - 1.2d)(H^3 - h^3)}$$

238
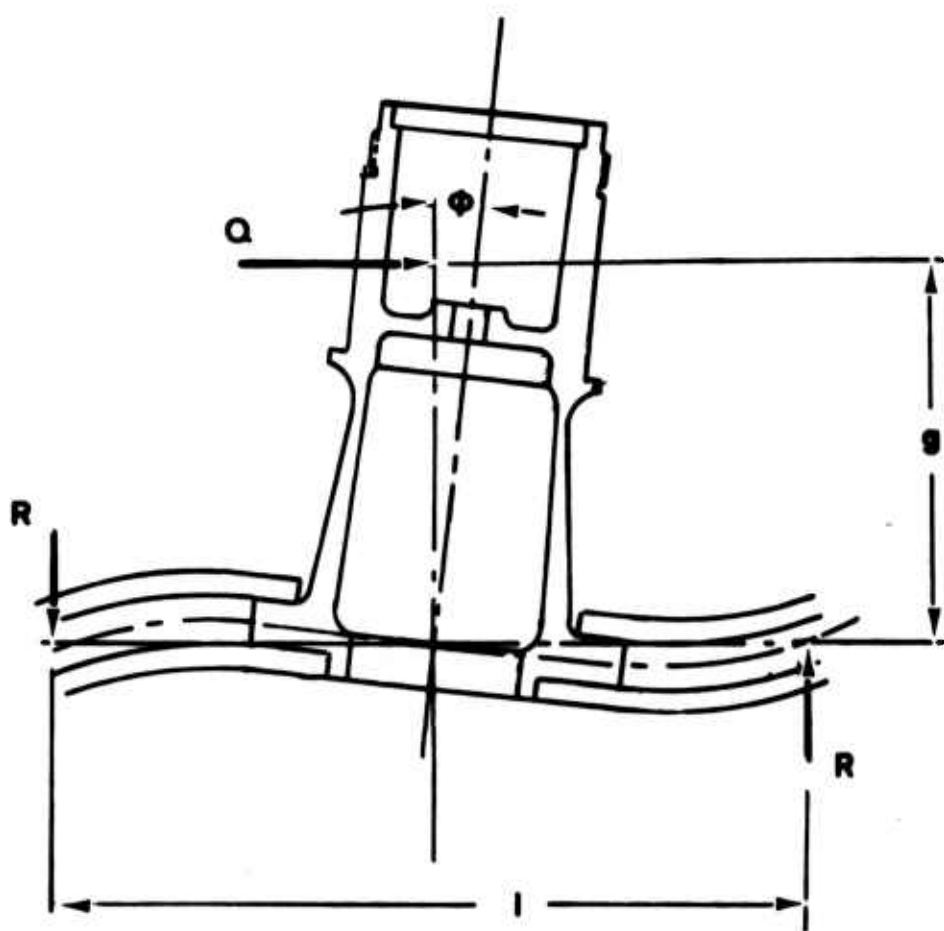
Figure D-22. Sketch of Plate and Post Assembly.

For the plate and post

$$d_o = 27.125 \text{ in}$$

$$d_i = 18.250 \text{ in}$$

$$H = 1.00 \text{ in}$$

$$h = .50 \text{ in}$$

$$Q = 10950 \text{ lb}$$

$$l = 10.025 \text{ in}$$

$$g = 3.95 \text{ in}$$

$$d = 2.83 \text{ in}$$

$$L = 3.880 \text{ in}$$

Substituting into the equation for slope:

$$\phi = \frac{(16)(10950)(3.95)(3.880^3)}{(29.0)(10^6)(10.025^2)(27.125 - 18.250)(1.00^3 - 0.50^3)}$$

$$\phi = 0.00178 \frac{\text{in}}{\text{in}} = \text{slope in plate}$$

Substituting into the equation for plate stress:

$$f_b = \frac{(12)(10950)(3.95)(3.880)(1.00)}{(10.025)(27.125 - 18.250 - (1.2)(2.83))(1.00^3 - 0.50^3)}$$

$$f_b = 41900 \text{ psi} = \text{stress in plate}$$

$$MS = \frac{F_{tu}}{(1.5) f_b} - 1$$

$$MS = \frac{150,000}{(1.5)(41900)} - 1$$

$$MS = +1.39$$

240

The critical section of the post occurs at the base of the post near the plate attachment. At this section:

$$d_o = 2.830 \text{ in}$$

$$d_i = 2.250 \text{ in}$$

$$Q = 10950 \text{ lb}$$

$$M = 38,820 \text{ in-lb}$$

$$Z = \frac{\pi}{32}\left(\frac{d_o^4 - d_i^4}{d_o}\right)$$

$$= \frac{\pi}{32}\left(\frac{2.830^4 - 2.250^4}{2.830}\right)$$

$$Z = 1.3360 \text{ in}^3$$

$$f_b = \frac{M}{Z} = \frac{38820}{1.3360}$$

$$f_b = 29050 \text{ psi}$$

$$F_{tu} = 136000 \text{ psi}$$

$$MS = \frac{F_{tu}}{1.5\, f_b} - 1$$

$$= \frac{136000}{(1.5)(29050)} - 1$$

$$= + 2.12$$

## FLANGE ASSEMBLY

The flange assembly and the hub transmit torque between the ring gear of the roller gear drive and the main rotor shaft. Figure D-23 shows the hub with the critical section A-A.

$$T_{limit} = \frac{63025 \; HP_{limit}}{rpm} = \frac{(63025)(3000)}{203} = 931,400 \; in\text{-}lb$$

The shear area is given by

$$A = \pi D t = (\pi)(9.70)(.240) = 7.31 \; in^2$$

The shear force is equal to

$$F = \frac{2T}{D} = \frac{(2)(931,400)}{9.70} = 192,000 \; lb$$

$$f_s = \frac{F}{A} = \frac{192,000}{7.31} = 26,300 \; psi$$

$$F_{ty} = 132,000 \; psi$$

$$MS = \frac{F_{ty}}{(2)(1.15)(f_s)} - 1 = \frac{132,000}{(2)(1.15)(26,300)} - 1 = 1.18$$

Figure D-23 shows the flange assembly consisting of the plate and flange with critical sections at B-B and C-C. At the critical section of the plate section B-B (12.77 inch diameter),

$$T_{limit} = 931,400 \; in\text{-}lb$$

The shear area is given by

$$A = \pi D t = \pi(12.77)(.115) = 4.613 \; in^2$$

The shear force is equal to:

$$F = \frac{2T}{D} = \frac{(2)(931,400)}{12.77} = 145,870 \; lb$$

$$f_s = \frac{F}{A} = \frac{145,870}{4.613} = 31,610 \; psi$$
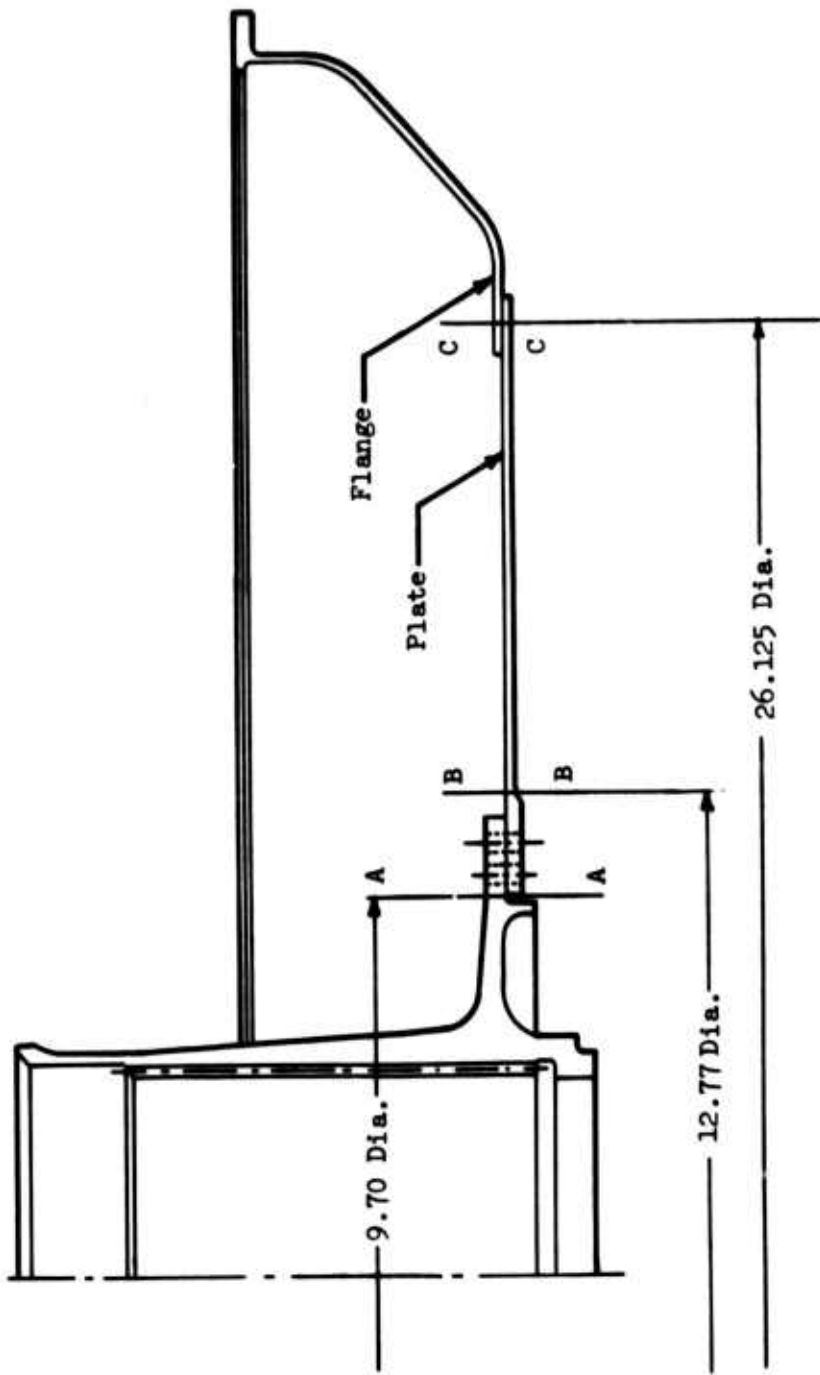
Figure D-23. Flange Assembly.

243

$F_{ty}$ = 103,000 psi

$$MS = \frac{F_{ty}}{(1.15)(2)(f_s)} - 1 = \frac{103,000}{(1.15)(2)(31610)} - 1 = +.41$$

The critical section of the flange occurs at section CC (bolt circle diameter of 26.125 inches) where

The shear area is given by

$$A = \pi D t - d n t$$

where

D = bolt circle diameter

t = thickness

d = diameter of fastener hole

n = number of fasteners

$$A = (\pi)(26.125)(.115) - (.249)(60)(.115) = 7.72 \text{ in}^2$$

The shear force is given by

$$F = \frac{2T}{D} = \frac{2(931,400)}{26.125} = 71300 \text{ lb}$$

$$f_s = \frac{F}{A} = \frac{71300}{7.72} = 9,230 \text{ psi}$$

$F_{ty}$ = 103,000 psi

$$MS = \frac{F_{ty}}{(1.15)(2)(f_s)} - 1 = \frac{103,000}{(1.15)(2)(9230)} - 1 = +3.85$$

## SECOND-ROW PINION, REDUCED $Y_2$ GEAR FACE WIDTH

The $Y_2$ gears of the second-row pinion were modified by decreasing the face width from 1.440 inches to 1.350 inches. This allowed a heavier blade-to-shield to be positioned in the wider undercut to protect the gears from the "blast-through" of the electron beam weld.

The structural difference between the modified and original gears is the gear tooth stresses which do not detract from the function of the gears. Figure D-24 shows the difference between the assemblies.

The gear tooth bending stress is a function of the face width of the gear, while the compressive stress is dependent upon the actual length of gear tooth contact.

The gear tooth bending stress is given by

$$f_b = \frac{W_t K_o}{K_v} \cdot \frac{P_d}{F} \cdot \frac{K_s K_m}{J}$$

and the compressive stress by:

$$f_c = \sqrt{\frac{21 \times 10^6 \ W_t}{\sin 2\phi \ F} \left( \frac{1}{d_p} \pm \frac{1}{d_g} \right)}$$

From Table B-2, the gear stresses for bending and compression, based on a gear face width of 1.440 and a contact width of 1.310, are

$$f_b = 33780 \text{ psi}$$

$$f_c = 129000 \text{ psi}$$

Therefore, when the face width is reduced to 1.350 and the contact path to 1.220,

$$f_b = 33780 \ \frac{1.440}{1.350} = 36030 \text{ psi}$$

$$f_c = 129000 \ \frac{1.310}{1.220} = 138500 \text{ psi}$$

The ring gear contact tooth stress will increase by a similar amount.

With the reduction in gear face width, the compressive stress is 6-1/2% above the allowable tabulated in Table B-1. Investigation into gear stress allowable shows the tabulated data to be conservative. Fatigue testing conducted under contracts DAAJ02-69-C-0060 and DAAJ02-70-C-0034 indicates an allowable compressive stress of up to 160,000 psi to be practical and also consistent with industry practice for aircraft gearing.

245
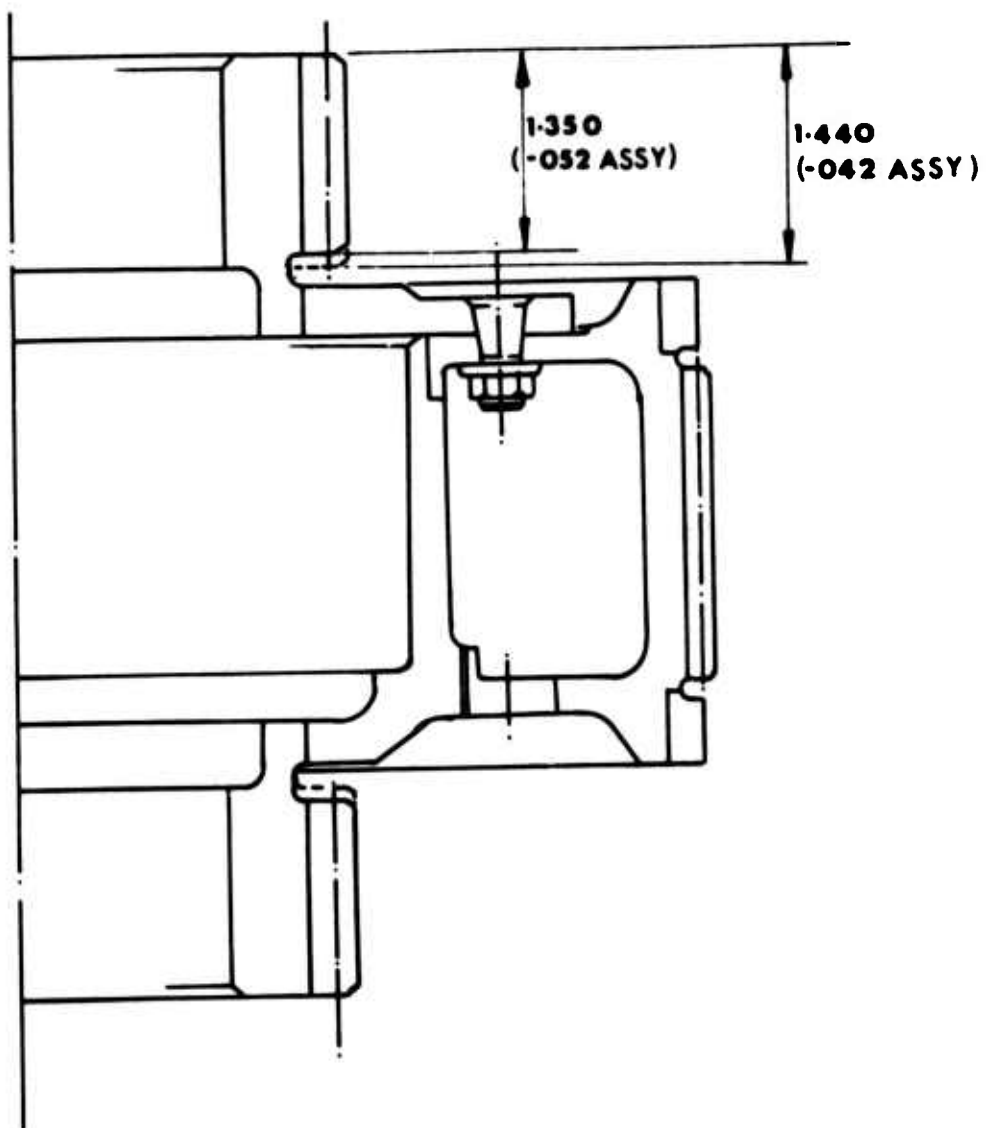
Figure D-24.   Reduced $Y_2$ Gear Face Width,
Second-Row Pinion.

## BUTT-WELD CONFIGURATION, FIRST-ROW PINION

The first-row pinion was redesigned to eliminate the deep electron beam weld. The redesigned gears are joined by a butt weld as shown in Figure D-25. The assembly has a heavier cross section than the original, resulting in high margins of safety for the $Y_1$ roller and gear rim loads listed in Tables D-5 and D-10. The purpose of this analysis is to determine the roller and gear rim stresses by ring analysis and the gear shaft bending stresses of the redesigned first-row pinion.
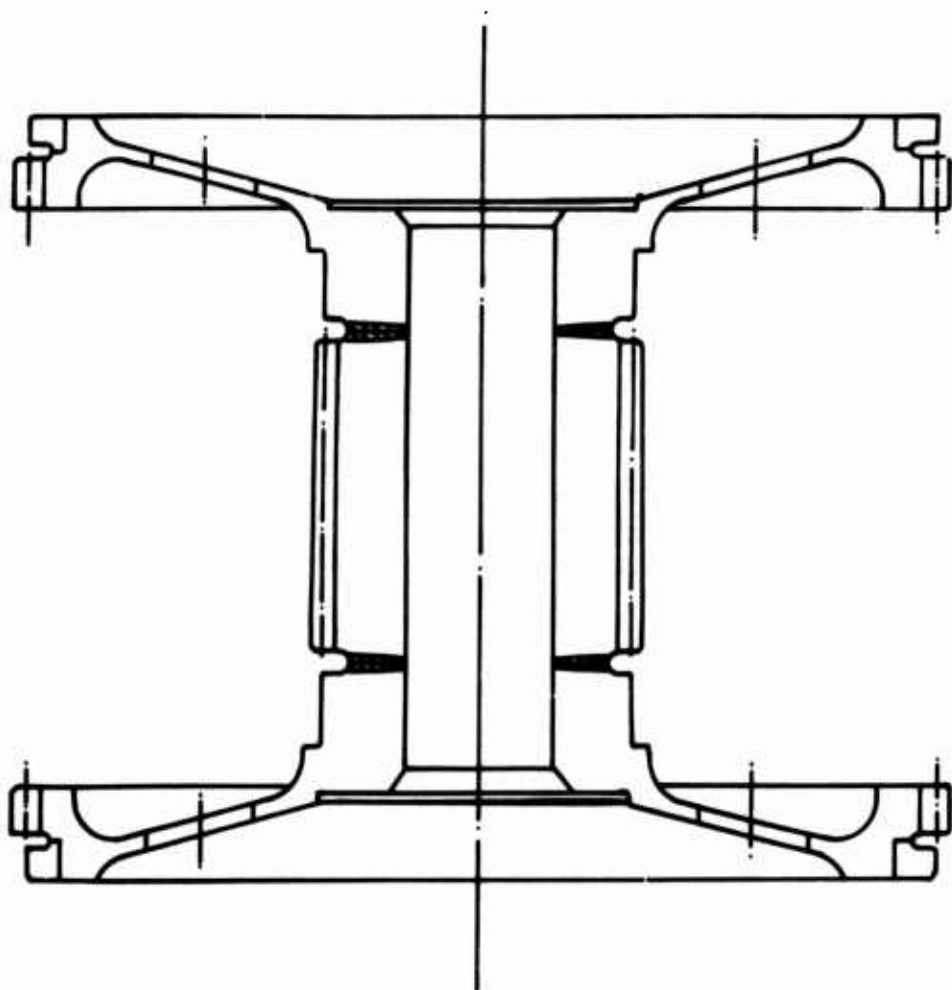


Figure D-25. Butt-Weld Design, First-Row Pinion.

<u>ROLLER RIM STRESS</u>

The roller rim stresses are calculated for the assembly using the section shown in Figure D-25.
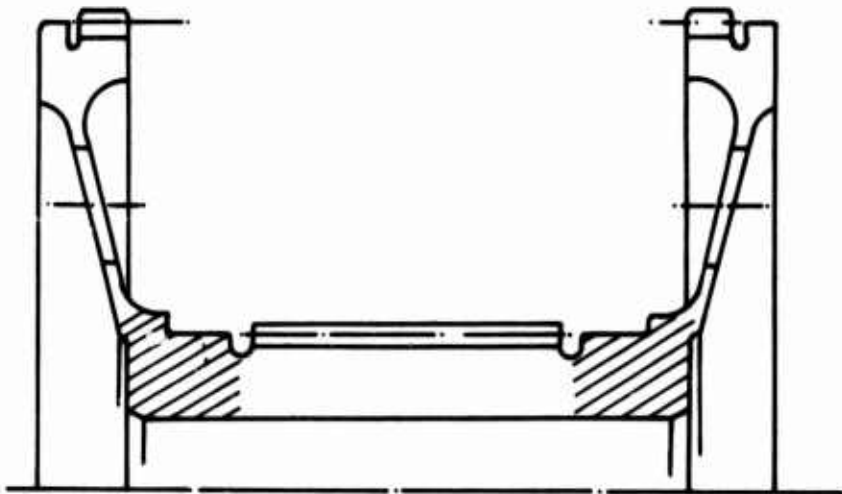


Figure D-26.   Assumed Cross Section for Roller Rim Stress Analysis, First-Row Pinion, $Y_1$.

Assumed cross section for roller rim stress analysis,

$$\bar{x} = 0.7943 \text{ in}$$
$$I = 0.01582 \text{ in}^4$$
$$Z_o = 0.0415 \text{ in}^3$$
$$Z_{in} = 0.0537 \text{ in}^3$$

Load per roller   $P = 2250 \text{ lb}$
$$R = 0.7943 \text{ in}$$

The internal moment M and internal circumferential force N are given by

$$M = K_m \frac{PR}{2}$$

$$N = K_n \frac{P}{2}$$

where

$$K_m = \frac{-(\pi - \phi)\ \sin\phi + .5\cos\phi + 1}{\pi}$$

$$K_n = \frac{(\pi - \phi)\ \sin\phi + 1.5\cos\phi}{\pi}$$

For the inside diameter, the maximum and minimum values of stress occur at 0 degrees and 72 degrees. Table D-12 summarizes the bending and tensile stresses in the first-row pinion.

TABLE D-12. MAXIMUM AND MINIMUM VALUES OF STRESS, INSIDE DIAMETER, FIRST-ROW PINION.

| Position (deg) | $K_m$ | $K_n$ | M | N | $f_b$(psi) | $f_a$(psi) |
|---|---|---|---|---|---|---|
| 0 | +0.47746 | +0.47746 | 427. | 537. | 7950. | 1000. |
| 72 | -0.20314 | +0.71818 | -182. | 808. | -3390. | 1510. |

Steady Stress $f_{st} = 1/2\ (f_{a_{max}} + f_{b_{max}} + f_{a_{min}} + f_{b_{min}})$.

Vibratory Stress $f_v = 1/2\ (f_{a_{max}} + f_{b_{max}} - f_{a_{min}} - f_{b_{min}})$.

Therefore, for the inside, the steady and vibratory stresses are

$$f_{st} = 3535\ \text{psi}$$
$$f_v = \pm 5415\ \text{psi}$$

The margin of safety is calculated from

$$MS = \left(\frac{1}{\dfrac{f_{st}}{F_{ty}} + \dfrac{K_t\ f_v}{F_{en}}}\right) - 1$$

for $K_t = 1.0$

$$F_{en} = 22430\ \text{psi}$$
$$F_{ty} = 115000\ \text{psi}$$

$$MS = \frac{1}{\left(\dfrac{3535}{115000} + \dfrac{1.0\ (5415)}{22430}\right)} - 1 = +2.67$$

For the outside diameter, the maximum and minimum values of stress occur at 0 degrees and 84 degrees and are given by Table D-13.

| Position (deg) | $K_m$ | $K_n$ | M | N | $f_b$(psi) | $f_a$(psi) |
|---|---|---|---|---|---|---|
| TABLE D-13. MAXIMUM AND MINIMUM VALUES OF STRESS, OUTSIDE DIAMETER - FIRST-ROW PINION. | | | | | | |
| 0 | +0.47746 | +0.47746 | 427. | 537. | +10300. | 1000. |
| 84 | -0.19546 | +0.58032 | 175. | 653. | - 4220. | 1215 |

$$f_{st} = 4150 \text{ psi}$$
$$f_v^{st} = \pm 7150 \text{ psi}$$

for

$$K_t = 1.0$$
$$F^t = 22430 \text{ psi}$$
$$F_{ty}^{en} = 115000 \text{ psi}$$

$$MS = \cfrac{1}{\left(\cfrac{4150}{115000} + \cfrac{1.0\,(7150)}{22430}\right)} -1 = 1.81$$

GEAR RIM STRESS

The gear rim is analyzed as a ring subjected to radial, tangential and moment loads which are reacted by uniform shear flow forces.

The gear rim stresses result in a margin of safety of +3.71 for the $Y_1$ gear. Figure D-27 shows the cross section used for the analysis.
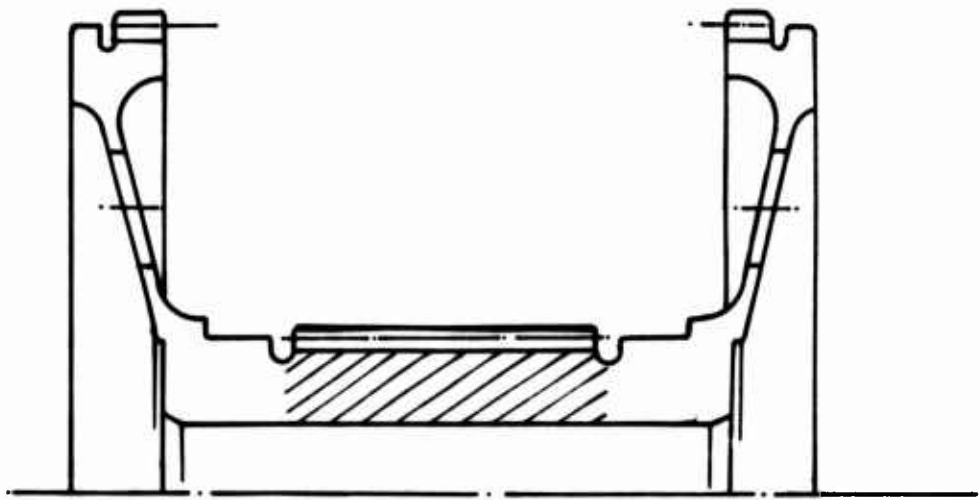
Figure D-27.  Assumed Cross Section for Gear Rim Stress Analysis,
First-Row Pinion, $Y_1$.

## BENDING STRESS ANALYSIS, ELECTRON-BEAM BUTT WELD

The first-row pinion assembly is analyzed as a simply supported shaft
with applied loads at the gear meshes and reaction points at the rollers.
Since the gear is rotating, the stresses at any point on the shaft are
subjected to totally reversed fatigue bending.

The butt weld  joining the gears to the shaft is the critical section.
Figure D-28 shows the loads imposed on the pinion due to the action of
the gear teeth and the roller forces.  (These loads are also shown in
Figure D-2, Free Body Diagram - First-Row Pinion.)  The $Y_1$ gear loads act
over the full gear width inducing shear forces in the weld.  The roller
loads and $X_1$ gear loads induce vibratory moment forces in the weld.

As the gear is symmetrical and the loads are in symmetry with the gear,
only one-half is analyzed.

Resolving all forces into planes 'A-A' and 'B-B' as shown in Figure D-28

As $N_2 = N_3$ and are products of $W_{rc}$

$$N_2 = \frac{W_{rc}}{4 \cos \alpha} = \frac{5580}{4(0.8262)} = 1685$$

251
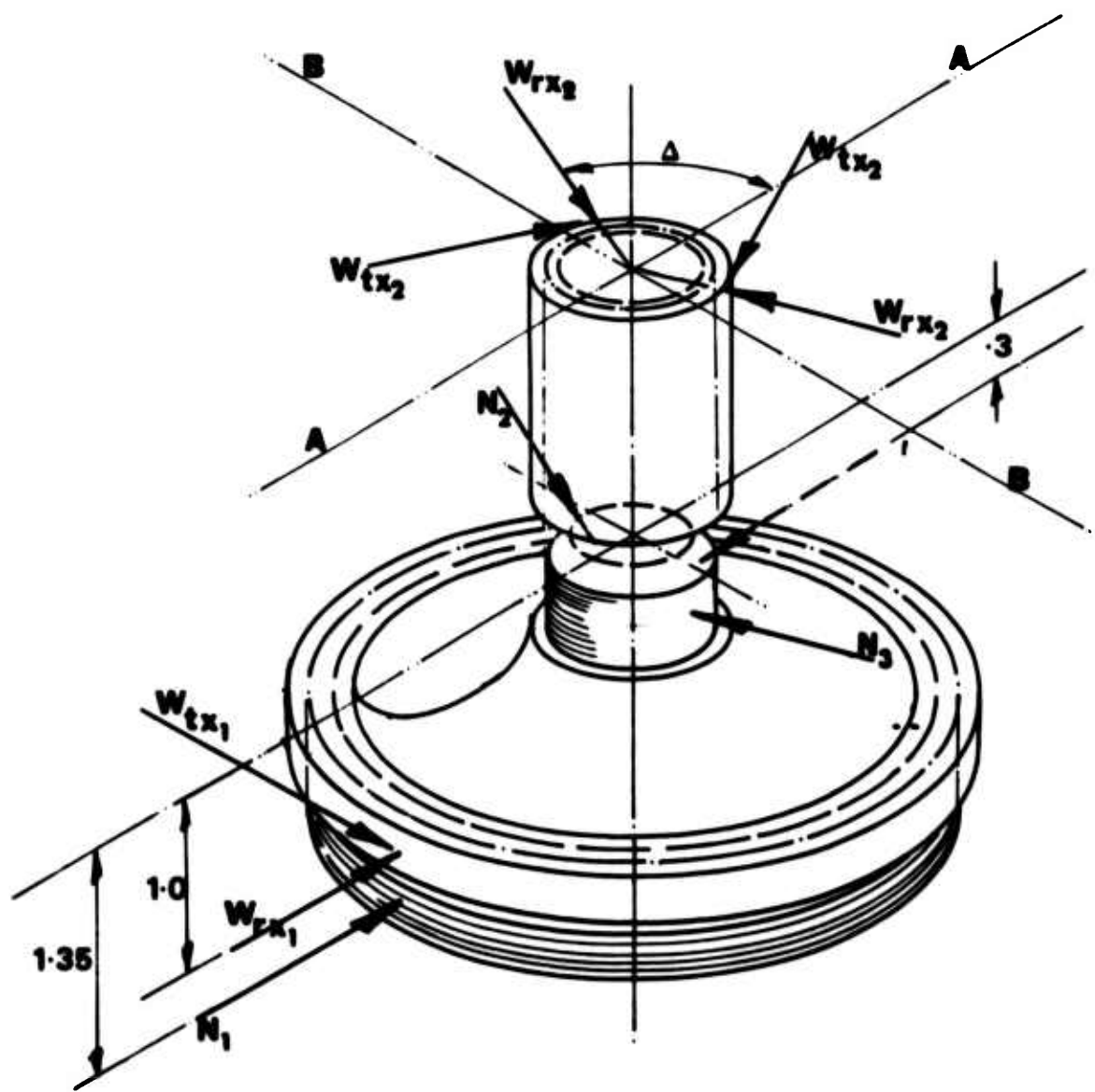
Figure D-28. Free Body Diagram - First-Row Pinion.

Plane AA

$$N_{2_{AA}} + N_{3_{AA}} = 2(N_2 \cos \Delta) = 2\left(1685(.5)\right) = 1685$$

$$N_1 = N_{2_{AA}} + N_{3_{AA}} = 1685$$

$$2(W_{r_{x2}})_{AA} = W_{e_{x2}} \cos \Delta = 1060(.5) = 530$$

$$2(W_{t_{x2}})_{AA} = 0$$

$$1/2(W_{r_{x1}}) = \frac{630}{2} = 315$$

Plane BB

$$N_{2_{BB}} + \left(-N_{3_{BB}}\right) = 0.$$

$$2(W_{t_{x2}})_{BB} + = 2 \, W_{t_{x2}}\left(\sin(90-\Delta)\right) = 2(2270)(.5) = 2270$$

$$1/2(W_{t_{x1}}) = \frac{1510}{2} = 755$$

At the weld

$$M_{AA} = 1685(1.35) + 315(1.0) - 1685(.3) = 2080 = \text{moment in} \\ \text{plane A-A}$$

$$M_{BB} = 755(1.0) = 755 = \text{moment in plane BB}$$

$$M = \sqrt{2080^2 + 755^2} = 2220 = \text{resultant moment}$$

$$F_s = \sqrt{2270^2 + 530^2} = 2330 = \text{resultant shear force}$$

The minimum section at the weld is

$d_o = 1.700$ in
$d_i = 1.002$ in
$A = 1.481$ in$^2$
$Z = 0.3835$ in$^3$

$$f_a = \frac{2330}{1.481} = 1570 = \text{shear stress}$$

$$f_v = \frac{2220}{0.3835} = 5780 = \text{vibratory stress}$$

The allowable stresses for the parent material, AMS 6265 Heat Treat $R_c$ 30-45, are given below.

$$F_{tu} = 136000 \text{ psi (min)}$$
$$F_{ty} = 115000 \text{ psi}$$
$$F_{en} = 44500 \text{ psi (machined surface)}$$

The allowable stresses for the weld are weld endurance strength 86% of the parent material, yield strength 97%, and ultimate strength 92% of the parent material.

$$F_{tu} = 0.92 (136000) = 125100 \text{ psi}$$
$$F_{ty} = 0.97 (115000) = 111550 \text{ psi}$$
$$F_{en} = 0.86 (44500) = 38270 \text{ psi}$$

The volume of stressed material for a hollow shaft with a fillet radius of 0.07 as shown in Figure D-29 is

$$\text{Volume} = .87 (0.07) 1.700^2 = .178$$

$$\text{Volume Ratio} = \frac{.178}{.009} = 19.5$$

$$\text{SEF} = .765 = \text{size effect factor.}$$

For 3 $\sigma$ reliability with $\nu = .13$ for weld material

$$\text{RF} = .61 = \text{reliability factor}$$
$$F_{en}' = F_{en} (\text{SEF}) (\text{RF})$$

$$F_{en}' = 38270 (.765) (.61) = 17860 = \text{working endurance limit}$$
$$\text{for } 3 \sigma$$

It is conservatively assumed that the stress concentration at the radius is effective at the weld. Figure D-29 shows the geometry used to calculate the stress concentration factor $K_t$.
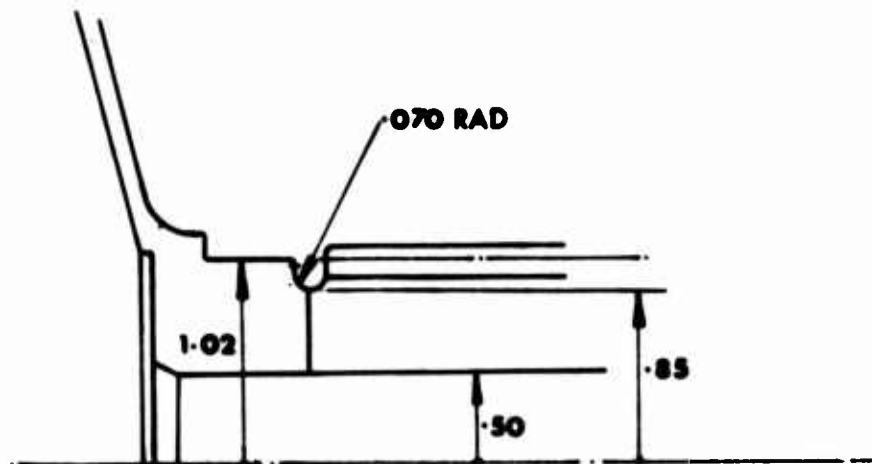
Figure D-29.  Groove Geometry.

$$K_t = 2.60$$

The margin of safety for the weld section is

$$MS = \left[ \cfrac{1}{\left( \cfrac{f_a}{F_{ty}} + \cfrac{K_t f_v}{F_{en}'} \right)} \right] -1$$

$$MS = \left[ \cfrac{1}{\left( \cfrac{1570}{111350} + \cfrac{2.60 \ (5780)}{17860} \right)} \right] -1 = .17$$

Therefore, the redesigned first-row pinion has a positive margin of safety in bending and in rim stresses, indicating infinite life under maximum operating load.

To safeguard against the possibility of the gears separating at the electron beam weld, a one-inch-diameter bolt placed through the center bore will clamp the gears to the pinion.  The bolt will react some of the bending moments, will put the weld in compression, and will increase the positive margin of safety at the critical section of the first-row pinion.

255

## SECOND-ROW PINION REDESIGN

As a result of fractures initiating from the "blind" electron beam welds of the initial design, the second-row pinion was redesigned.

The redesigned pinion shown in Figure D-30 incorporates a split housing for the spherical roller bearing. The design requires only two electron beam welds (identical to those of the preceding design).
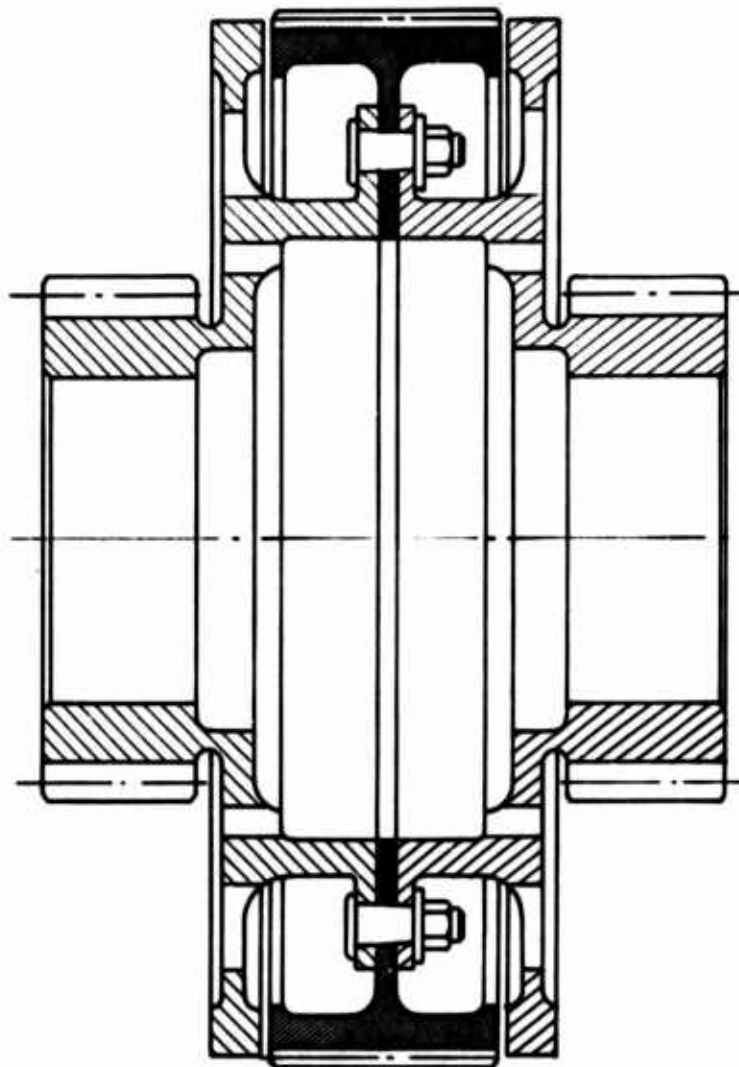


Figure D-30.   Redesigned Second-Row Pinion.

256

The stresses in the roller rim and gear rim of the redesigned second-row pinion are identical to those of the original design; i.e., the roller rim section and gear rim section are designed to have section properties identical to those of the preceding design. Figure D-31 shows the areas used to obtain the roller and gear rim section properties.
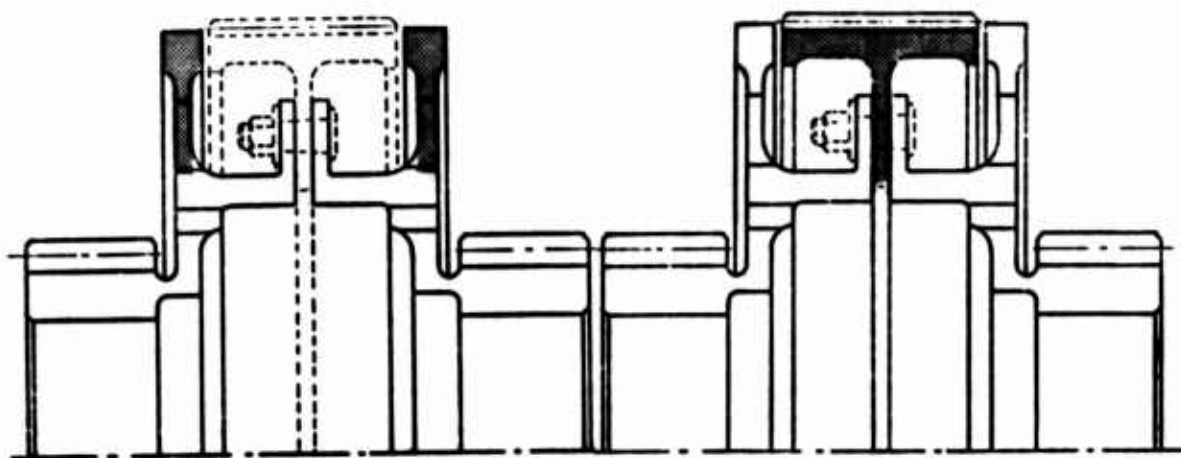


Figure D-31. Assumed Cross Sections for Roller and Gear
Rim Stress Analysis.

FATIGUE ANALYSIS

The pinion is analyzed for steady torsion and vibratory shear and bending
stress for the sites depicted in Figure D-32.
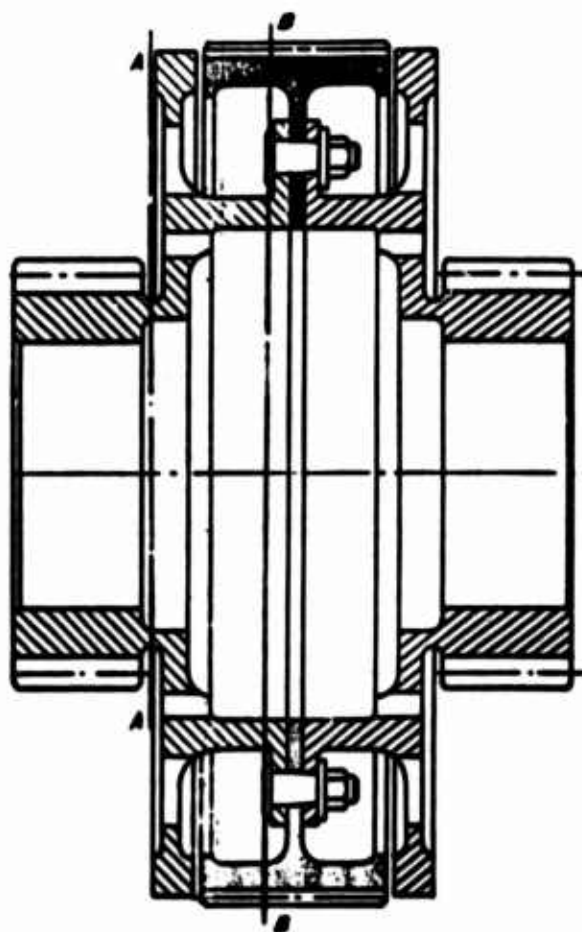


Figure D-32. Fatigue Analysis, Site Locations.

Each section is subjected to steady torsional and vibratory loads. The
margin of safety equations are conservatively based on the maximum shear
theory. Also included is the trunnion loading analysis of the vertical
web adjacent to section A-A and the bolt analysis.

Resolving the forces from Figure D-3 into 'X' and 'Y' planes gives the
values depicted in Figure D-33.
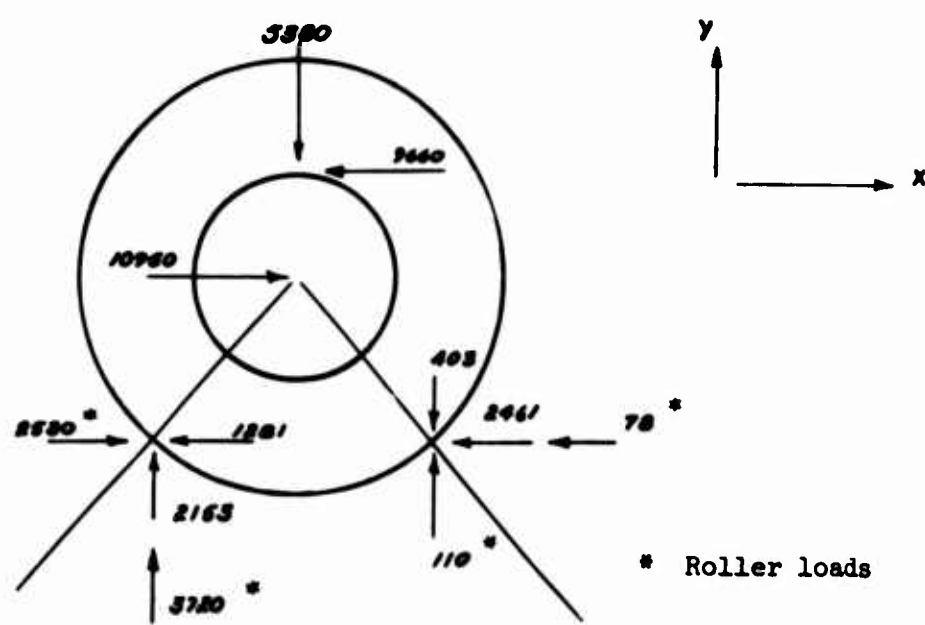
Figure D-33.  Free Body Diagram, X and Y Planes,
Second-Row Pinion.

'X' Plane Forces

$$\text{Net Roller Load} = 2530 - 78 = 2452$$

$$\text{Net } X_2 \text{ Gear Load} = -1281 - 2461 = -3742$$
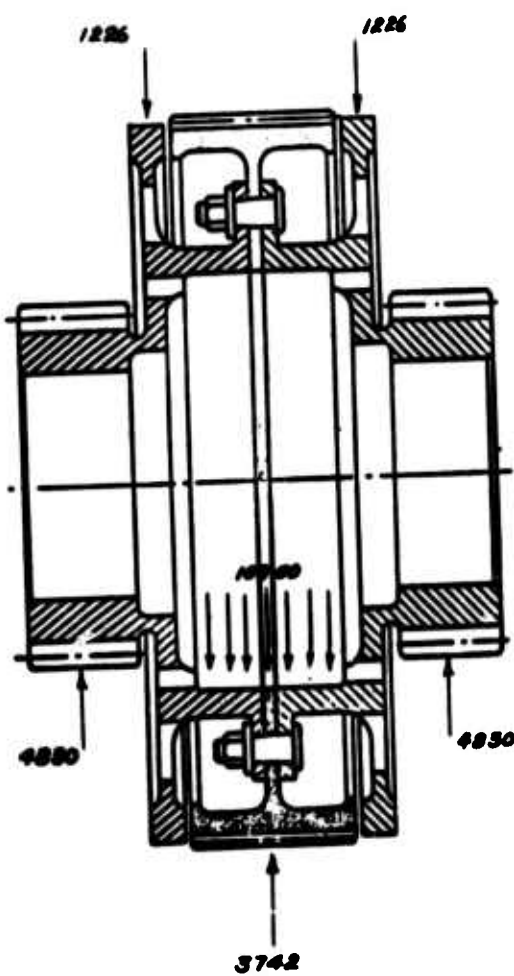


Figure D-34.  'X' Plane Forces.

'Y' Plane Forces

$$\text{Net Roller Load} = 3720 + 110 = 3830$$

$$\text{Net X}_2 \text{ Gear Load} = 2153 - 403 = 1750$$
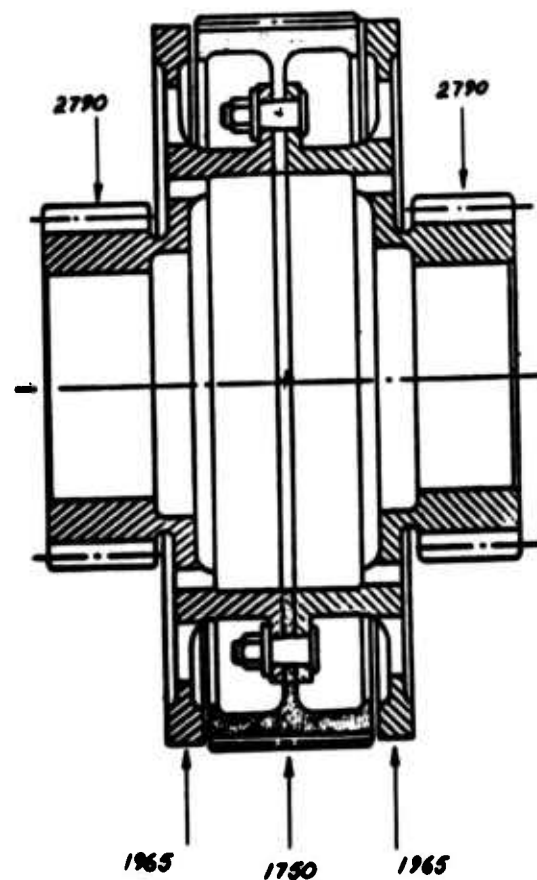
Figure D-35.  'Y' Plane Forces.

Section A-A (0.8 inch  from point of  load application)

$d_o = 3.875$ in

$d_i = 3.500$ in

$A = 2.172$ in$^2$

$Z = 1.865$ in$^3$

$T = W_{t_c} \dfrac{d}{2} = \dfrac{9660}{2}\left(\dfrac{4.477}{2}\right) = 10{,}820$ in $-$lb

$M = 0.8\,(2790^2 + 4830^2)^{\frac{1}{2}} = 4462$ in $-$lb

$f_a = \dfrac{T}{2Z} = \dfrac{10820}{2(1.864)} = 2900$ psi

$f_b = \dfrac{M}{Z} = \dfrac{4462}{1.864} = 2400$ psi

$f_s = \dfrac{2400}{2}$ psi

$F_{t_y} = 115000$ psi

$F_{en} = 26800$ psi

$K_t = 3.92$ (combined)

$K_{ts} = 1.20$

$$MS = \dfrac{1}{\sqrt{4\left(\dfrac{f_a}{F_{t_y}} + \dfrac{K_{t_s}\,f_s}{F_{en}}\right)^2 + \left(\dfrac{K_t\,f_b}{F_{en}}\right)^2}} - 1$$

$$MS = \dfrac{1}{\sqrt{4\left[\dfrac{2900}{115000} + \dfrac{1.2(1200)}{26800}\right]^2 + \left[\dfrac{392(2400)}{26800}\right]^2}} - 1 = +1.60$$

Also analyzed as a plate with edges supported at 2.9 inch radius and subjected to central couple (trunnion loading).

Max Radial Stress $= \dfrac{\beta\,M}{\alpha\,t^2}$

where $\alpha = 18.2$        when $\dfrac{1.99}{2.99} = .686$

$\beta = .71$

262

$$f_r = \frac{.71(4462)}{18.2(.187)^2} = 4980 \text{ psi}$$

$$f_a = 1450 \text{ psi}$$

$$K_t = 2.85 \text{ (external SCF)}$$

$$MS = \frac{1}{\sqrt{4\left(\frac{f_a}{F_{t_y}}\right)^2 + \left(\frac{K_t\, f_r}{F_{en}}\right)^2}} - 1$$

$$MS = \frac{1}{\sqrt{4\left[\frac{2900}{115000}\right]^2 + \left[\frac{2.85(4980)}{26800}\right]^2}} - 1 = + .88$$

Section B-B

'X' Plane

do = 6.210 in

di = 5.510 in
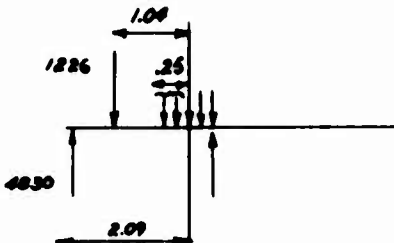
A = 6.443 in$^2$

Z = 8.941 in$^3$

M = 4830 (2.09) - 1226(1.04) - 2880(.25) - 12,000 in -lb

$$f_a = \frac{T}{2Z} = \frac{10820}{2(8.941)} = 608 \text{ psi}$$

$$f_{b_{xx}} = \frac{M}{Z} = \frac{12000}{8.941} = 1340 \text{ psi}$$

'Y' Plane
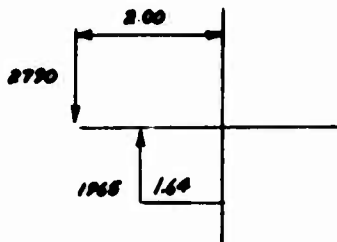
M = 2790(2.09) - 1965(1.04) = 3800 in -lb

$$f_{b_{yy}} = \frac{3800}{8.941} = 425 \text{ psi}$$

263

Pressure due to bearing interference fit of 0.0025/0.0035 inch = 820 psi

For thick wall cylinder

$$f_{xx} = 0$$

$$f_{yy} = 820 \left( \frac{3.105^2 + 2.755^2}{3.105^2 - 2.755^2} \right) = 6890 \text{ psi}$$

$$f_s = 820 \text{ psi}$$

$$f_{b_{(max)}} = \left[ 1340^2 + (6870 + 425)^2 \right]^{\frac{1}{2}} = 7440 \text{ psi}$$

$$f_{s_{(max)}} = \frac{7440}{2} = 3720 \text{ psi}$$

$$K_t = 3.2$$

$$K_{t_s} = 1.75$$

$$F_{t_y} = 115000 \text{ psi}$$

$$F_{en} = 26900 \text{ psi}$$

$$MS = \frac{1}{\sqrt{4 \left[ \frac{608}{115000} + \frac{1.65(3720)}{26900} \right]^2 + \left[ \frac{3.1(7440)}{26900} \right]^2}} - 1 = + .024$$

BOLT ANALYSIS

Briles Manufacturing, 5/16in- diameter, Taper-Lok

No. bolts = 16

Material = H-11 Steel Alloy 220/260 KSI

Properties per BPS 278 for TL 100 series

Ultimate double shear = 20200 lb  (min)

Ultimate tensile strength = 12500 lb  (min)

Fatigue load = 6000 lb  (high)

Transmitted Torque = $W_{t_c} \frac{d}{2}$ = 9660 $\left( \frac{4.4778}{2} \right)$ = 21640 lb

Nut torque = 165 in -lb

Bolt tension $P_1$ = $\frac{165}{.2(.3125)}$ = 2640 lb

Transmitted Torque $= \mu$PiRn $= .2(2640)(3.55)$ 16 $= 30,000$ in -lbs

Thus, sixteen 5/16in. bolts can transmit torque by friction.
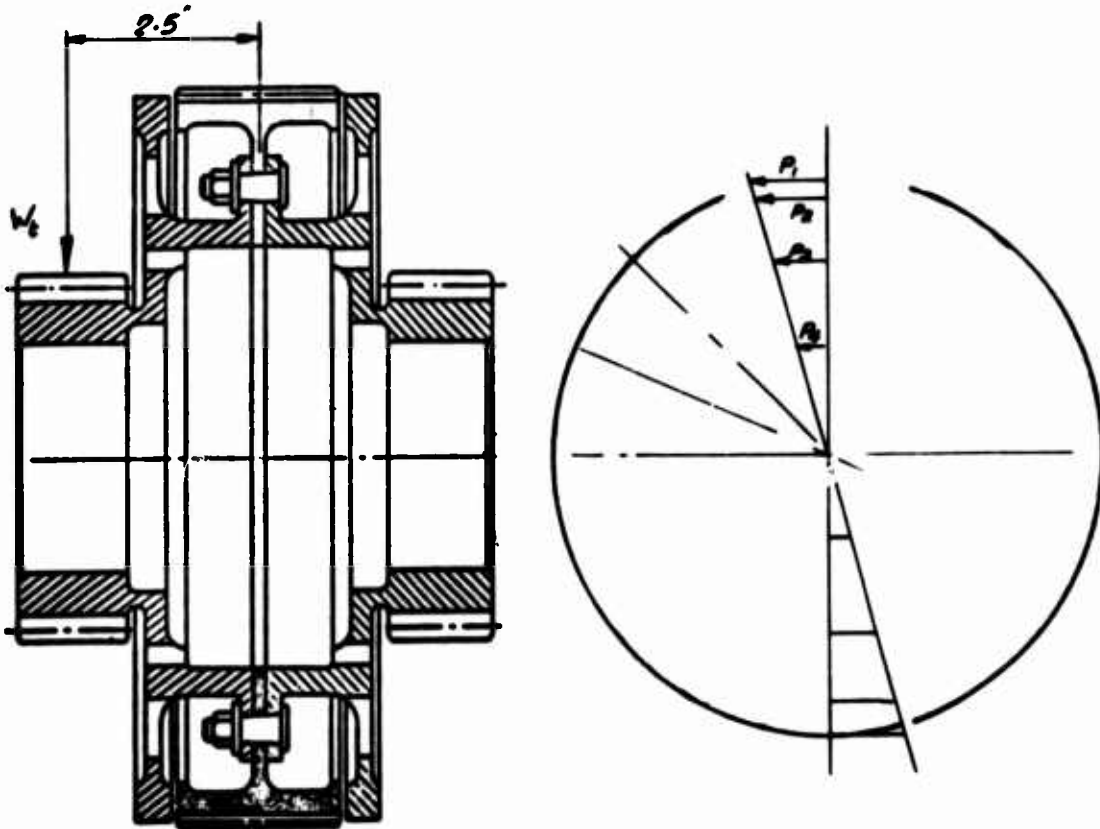


Figure D-36.  Bolt Forces,
Second-Row Pinion.

Moment on flange $M = \dfrac{W_t}{\cos}$ (2.5) $= \dfrac{4880}{\cos 30}$ (2.5) $= 14100$ in -lb

$$M = 7.2 \ P1 + 13.2 \ P2 + 10P3 + 5.6 \ P4$$

Also

$$\frac{P1}{3.6} = \frac{P2}{3.3} = \frac{P3}{2.5} = \frac{P4}{1.4}$$

Thus

P1 $=$ 500 lb

Max axial force on bolts $=$ 1000 lb

Bolt preload $=$ 2650 lb

Thus bolts will not separate under load.

Static margin of safety

Max tension in bolt = 2640 + 1000 = 3640 lb

Tension stress ratio = $\dfrac{1.5(3640)}{12500}$ = .437

Applied shear load = $(3742^2 + 1750^2)^{\frac{1}{2}}$ = 4130 lb

Assume 8 bolts react this shear load; then

Maximum shear load = 1025 lb

Shear stress ratio = $\dfrac{1.5(1025)}{20200}$ = .076

Then static MS = $\dfrac{.1}{.076}$ -1 = + .31

Fatigue Margin of Safety

Maximum fatigue load = $P_1 \pm P_a$ = 2640 ± 1000

= 3640 lb (max)/1640 lb (min)

Allowable fatigue load = 6000 lb

Thus, sixteen 5/16 in bolts torqued to 165 in -lb are adequate.

# STRUCTURAL ANALYSIS OF MAIN
## GEARBOX INPUT SECTION

## INPUT PINION

Power from each engine is transmitted through a shaft angle of 86°
via spiral bevel gears.

The gears have been primarily designed for surface durability, and
to obtain a requisite bearing life and required contact ratio.  The input
bevel pinion is a right-hand spiral gear driving counterclockwise and is
straddle mounted by a roller bearing and a stack bearing comprised of four
angular contact bearings.

Individual bearing loads have been calculated by a  computer program
which views the entire assembly of shaft, bearings and support
structure as a single, nonlinear elastic system.  Syroscopic and
centrifugal rolling element forces combine to give the individual bearing
loads depicted in Figure E-1 for the gear tangential, separating and axial
forces shown.

$$N = 21$$
$$HP = 1870 \text{ engine input}$$
$$rpm = 18966 \text{ engine rpm}$$

The basic gear data for the input pinion is

$$F = 2.100 \qquad = \text{face width}$$
$$d_p = 5.008 \qquad = \text{pitch diameter}$$
$$\phi = 20° \qquad = \text{pressure angle}$$
$$\psi = 30° \qquad = \text{spiral angle}$$
$$\gamma = 17° \; 45' \qquad = \text{pitch angle}$$

$$R_m = \frac{1}{2}\left( d_p - F \sin\gamma \right)$$

$$= \frac{1}{2}\left[ 5.008 - 2.1 \,(.3048) \right] = 2.184 = \text{mean radius}$$

The loads on the input bevel pinion are calculated as follows:

$$T = \frac{63025 \,(HP)}{rpm}$$

$$T = \frac{63025 \,(1870)}{18966} = 6220 \text{ in -lb}$$
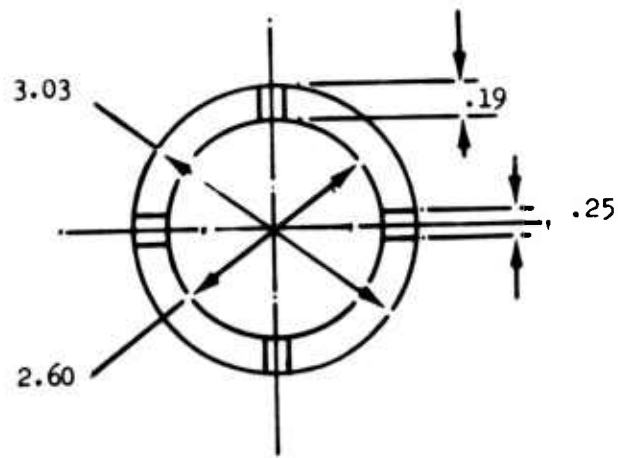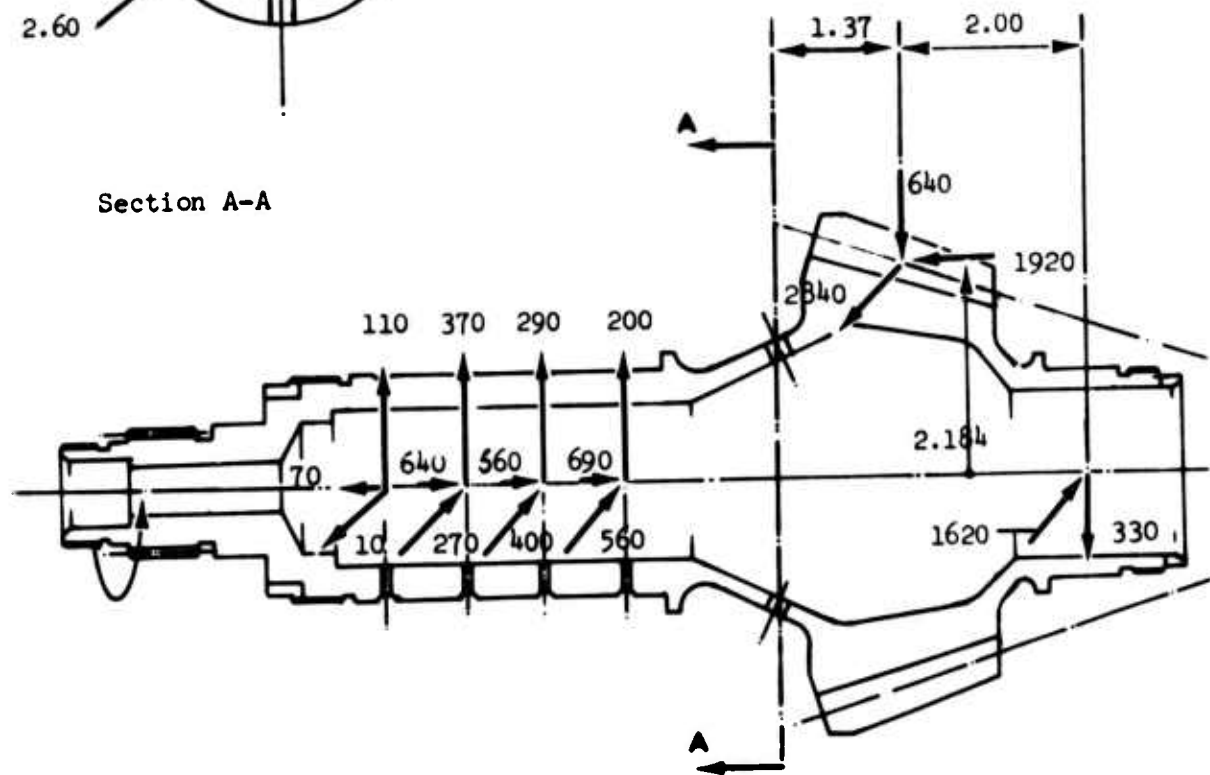
Figure E-1.   Input Bevel Pinion.

$$W_t = \frac{T}{R_m} = \frac{6220}{2.184} = 2840 \text{ lb}$$

$$W_a = \frac{W_t}{\cos\psi}\left(\tan\phi\,\sin\gamma + \sin\psi\,\cos\gamma\right)$$

$$= \frac{2840}{.866}\left[(.364)(.3048) + (.5)(.9524)\right] = 1930 \text{ lb}$$

$$W_r = \frac{W_t}{\cos\psi}\left(\tan\phi\,\cos\gamma - \sin\psi\,\sin\gamma\right)$$

$$= \frac{2840}{.866}\left[(.364)(.9524) - (.5)(.3048)\right] = 640 \text{ lb}$$

The critical section in fatigue is section A-A as shown in **Figure E-1.**
This section carries fatigue bending stresses as well as steady axial and
torsional stresses. For section A-A,

$$d_o = 3.03 \text{ in}$$

$$d_i = 2.60 \text{ in}$$

$$A = 1.711 \text{ (including holes)}$$

$$Z = 1.121 \text{ (including holes)}$$

$$K_t = 4.18$$

$$P_a = 1920 \text{ lb}$$

$$M = \sqrt{\left[(2840)(1.37) - (1620)(3.37)\right]^2 + \left[(640)(1.37) + (330)(3.37) - (1920)(2.184)\right]^2}$$

$$M = 2705$$

$$f_a = \frac{P_a}{A} = \frac{1930}{1.711} = 1130 \text{ psi}$$

$$f_b = \frac{M}{Z} = \frac{2705}{1.121} = 2410 \text{ psi}$$

$$f_s = \frac{T}{2(Z)} = \frac{6220}{2(1.121)} = 2770 \text{ psi}$$

For this shaft:

Material   = AMS 6265 Heat Treat $R_c$ 30 - 45

$$F_{tu} = 136,000 \text{ psi}$$

$$F_{ty} = 115,000 \text{ psi}$$

$$F_{en} = 22,400 \text{ psi}$$

$$MS = \cfrac{1}{\sqrt{\left(\cfrac{f_a}{F_{ty}} + \cfrac{K_t\, f_b}{F_{en}}\right)^2 + 4\left(\cfrac{f_s}{F_{ty}}\right)^2}} - 1$$

$$MS = \cfrac{1}{\sqrt{\left[\cfrac{1130}{115000} + \cfrac{(4.18)(2410)}{22400}\right]^2 + 4\left[\cfrac{2770}{115000}\right]^2}} - 1 = +1.16$$

## BEVEL GEAR ASSEMBLY

The bevel gear assembly as shown in Figure E-2  consists of the
following components:

- Splined Shaft
- Spur Pinion
- Outer Shaft
- Bevel Gear
- Quill Shaft
- Freewheel Unit Assembly

  - Housing
  - Cam
  - Roller
  - Pin/Spring

Power is transmitted from the input spiral bevel pinion to the
spiral bevel gear into the outer shaft.  The quill shaft connects the
freewheel unit to the outer shaft by means of floating splines.

The reaction loads from the lower ball bearing of the spur pinion
splined shaft are transmitted to the outer housing of the spiral bevel
gear.  The shafts are analyzed as simply supported straddle-mounted beams
subjected to fatigue bending stresses combined with steady torsional and
axial stresses.

Due to the angular location of the spur gear mesh as shown in
Figure E-3, and the method by which the loads combine, the right-hand
outer shaft is the more highly stressed assembly.

$$HP = 1870 \text{ (single engine maximum)}$$

$$rpm = 6223$$

$$T = \frac{63025 \text{ HP}}{rpm} = \frac{63025 \ (1870)}{6223} = 18940 \text{ in -lb}$$
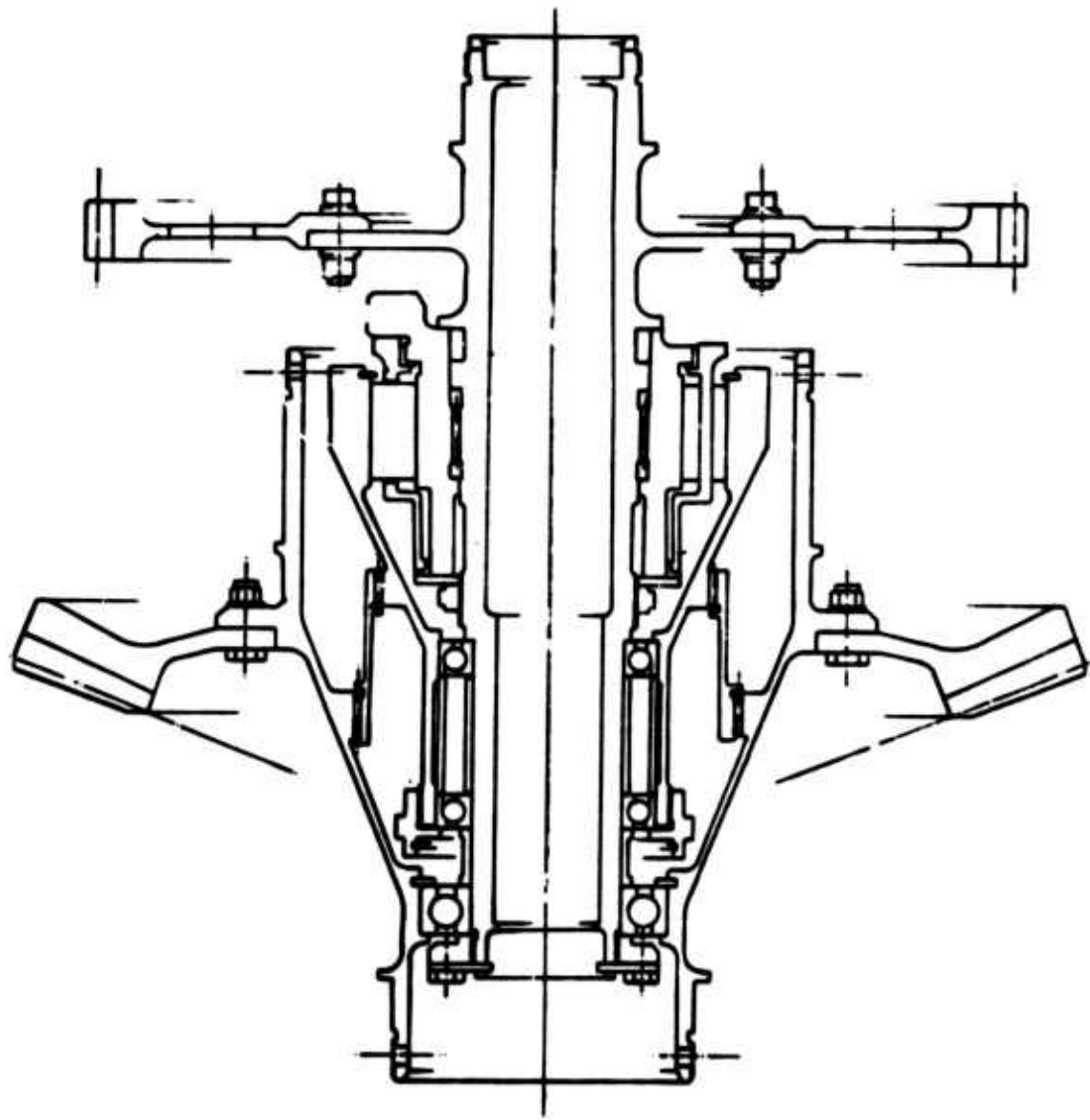
Figure E-2.   Bevel Gear Assembly.

## SPLINED SHAFT

The freewheel unit transmits torque from the cam through a locked spline into the shaft and hence to the spur pinion. A roller bearing mounted in the top cover and a ball bearing housed in the outer shaft are located at either end of the shaft to react the spur gear loads.
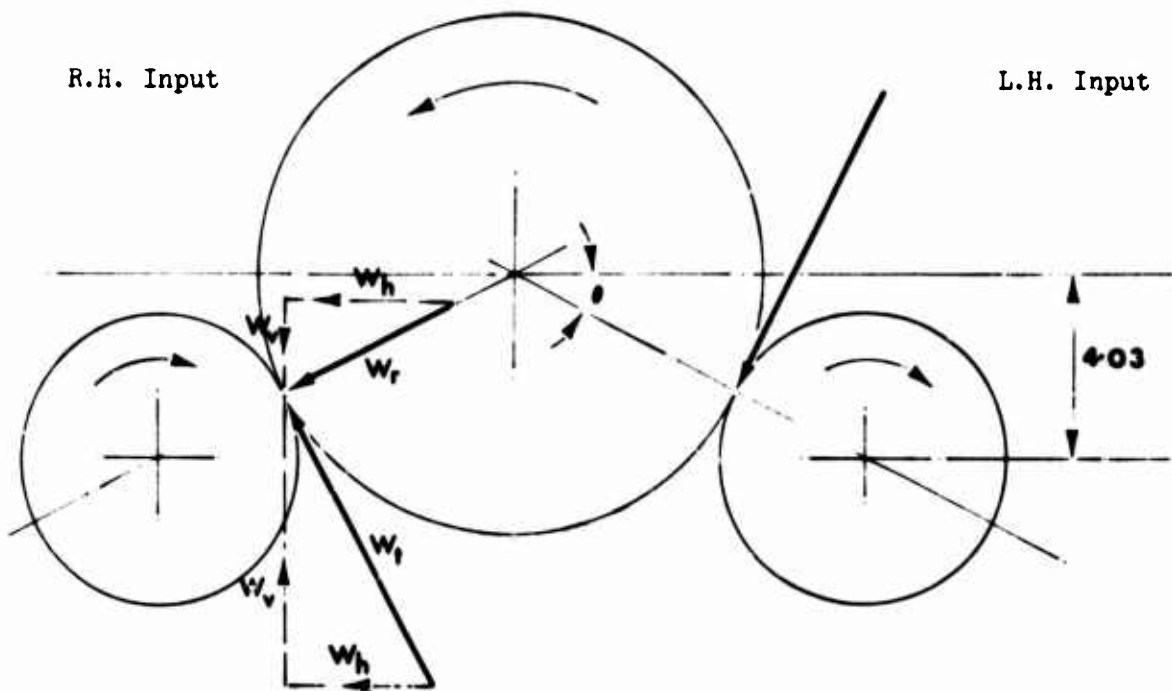


Figuré E-3.    Spur Gear Loads - Plan View.

| | | | |
|---|---|---|---|
| $N_p$ | = | 78 | = no. of teeth in pinion |
| $N_g$ | = | 120 | = no. of teeth in gear |
| $\phi$ | = | 22.5 | = pressure angle |
| Pitch | = | 6.0 | = diametral pitch |
| $\theta$ | = | 13° 43' | |
| $d_p$ | = | $\dfrac{78}{6}$ | = 13.00 = pinion pitch diameter |

Figure E-4  shows the splined shaft and spur pinion with the location of the critical section.
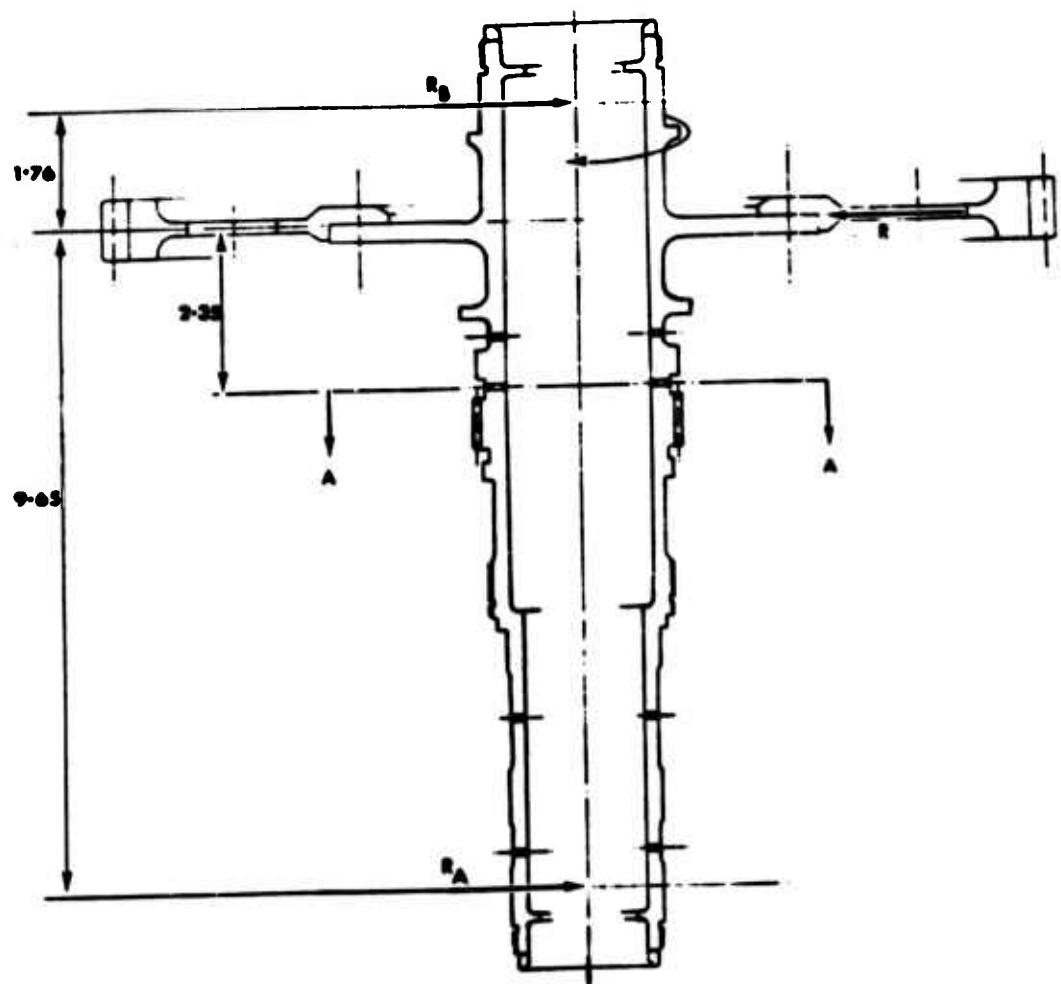
Figure E-4.  Splined Shaft.

274

The loads on the pinion from the gear mesh are given by

$$W_t = \frac{2\,T}{d_p} = 2\left(\frac{18940}{13.00}\right) = 2920 \textbf{ lb}$$

$$W_r = W_t \tan\phi = 2920\,(.4142) = 1210 \textbf{ lb}$$

Due to $W_t$:

$$W_h = W_t \sin\theta = 2920(.2370) = 690 \textbf{ lb}$$

$$W_v = W_t \cos\theta = 2920(.9715) = 2840 \textbf{ lb}$$

Due to $W_r$:

$$W_h = W_r \cos\theta = 1210(.9715) = 1170 \textbf{ lb}$$

$$W_v = W_r \sin\theta = 1210(.2370) = 290 \textbf{ lb}$$

The total loads are

$$W_h = 690 + 1170 = 1860 \textbf{ lb}$$

$$W_v = 2840 - 290 = 2550 \textbf{ lb}$$

$$R = \sqrt{1860^2 + 2550^2} = 3155 = \text{resultant load on centerline of shaft}$$

The loads on bearing A are

$$R_{Ah} = W_h\left(\frac{1.76}{11.41}\right) = 1860\left(\frac{1.76}{11.41}\right) = 290 \textbf{ lb}$$

$$R_{Av} = W_v\left(\frac{1.76}{11.41}\right) = 2550\left(\frac{1.76}{11.41}\right) = 390 \textbf{ lb}$$

$$R_A = \sqrt{290^2 + 390^2} = 485 \textbf{ lb}$$

The loads on bearing B are:

$$R_{Bh} = 1860 - 290 = 1570 \text{ lb}$$

$$R_{Bv} = 2550 - 390 = 2160 \text{ lb}$$

$$R_B = \sqrt{1570^2 + 2160^2} = 2670 \text{ lb}$$

Section A-A as shown in Figure E-4 is the critical section for this shaft. The gear mesh point remains stationary while the shaft is rotating; and hence, fully reversed fatigue bending stresses are induced along the shaft. Additionally at section A-A, steady torsional and steady axial (from nut preload) stresses are combined with the fatigue bending stress. The stress concentration factor is conservatively assumed to be the product of the hole and groove stress concentration factor. Figure E-5 is section A-A showing oil holes.
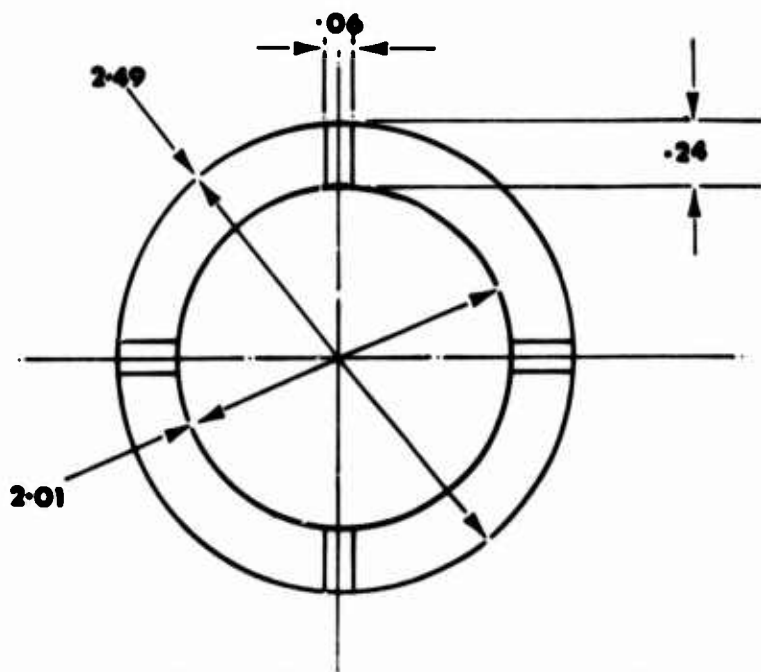


Figure E-5. Section A-A of Splined Shaft

276

At Section A-A,

$$d_o = 2.49 \text{ in}$$

$$d_i = 2.01 \text{ in}$$

$$A = 1.639 \text{ (including effect of holes)}$$

$$Z = .843 \text{ (including effect of holes)}$$

$$K_t = 4.74$$

The axial load produced by nut NAS 1493-14 for a torque of 1440 inch-pounds is given by

$$P = \frac{T_N}{K(d_p)} = \frac{1440}{.2(2.548)} = 2820 \text{ lb}$$

$$f_a = \frac{P}{A} = \frac{2820}{1.639} = 1720 \text{ psi}$$

$$f_b = \frac{M}{Z} = \frac{485(9.65 - 2.35)}{.843} = 4200 \text{ psi}$$

$$f_s = \frac{T}{2(Z)} = \frac{18940}{2(.843)} = 11230 \text{ psi}$$

$$MS = \frac{1}{\sqrt{\left(\dfrac{f_a}{F_{ty}} + \dfrac{K_t f_b}{F_{en}}\right)^2 + 4\left(\dfrac{f_s}{F_{ty}}\right)^2}} - 1$$

$$MS = \frac{1}{\sqrt{\left[\dfrac{1720}{115000} + \dfrac{4.74(4200)}{22600}\right]^2 + 4\left[\dfrac{11230}{115000}\right]^2}} - 1 = +.09$$

## OUTER SHAFT

The outer shaft transmits power from the input bevel gear to a splined quill shaft. Duplex bearings and a roller bearing, located at either end of the shaft straddle mount the gear. Radial loads from the splined shaft, as shown on page 274, are transferred into the outer shaft via the ball bearings. Figure E-6 shows the outer shaft with bearing reaction loads, bearing loads transferred from the splined shaft, and the bevel gear loads transferred to the shaft centerline.

$$N = 64$$

$$F = 2.100 = \text{face width}$$

$$d_p = 15.264 = \text{pitch diameter}$$

$$\phi = 20^\circ = \text{pressure angle}$$

$$\psi = 30^\circ = \text{spiral angle}$$

$$\gamma = 68^\circ 15' = \text{pitch angle}$$

$$R_m = \frac{1}{2}\left(d_p - F\sin\gamma\right)$$

$$= \frac{1}{2}\left[15.264 - 2.1\,(.9288)\right] = 6.66 = \text{mean radius}$$

The bevel gear loads are given by

$$W_t = \frac{T}{R_m} = \frac{18940}{6.66} = 2850\ \text{lb}$$

$$W_a = \frac{W_t}{\cos\psi}\left(\tan\phi\sin\gamma - \sin\psi\cos\gamma\right)$$

$$= \frac{2850}{.866}\left[(.364)(.9288) - (.5)(.3706)\right] = 500\ \text{lb}$$

$$W_r = \frac{W_t}{\cos\psi}\left(\tan\phi\cos\gamma + \sin\psi\sin\gamma\right)$$

$$= \frac{2850}{.866}\left[(.364)(.3706) + (.5)(.9288)\right] = 1970\ \text{lb}$$

The loads on bearing A are

$$R_{Av}(7.67) = 390(1.41) + 1970(4.6) + 500\,(6.66)\ (\Sigma M_{Bv} = 0)$$

$$R_{Av} = 1690\ \text{lb}$$

278
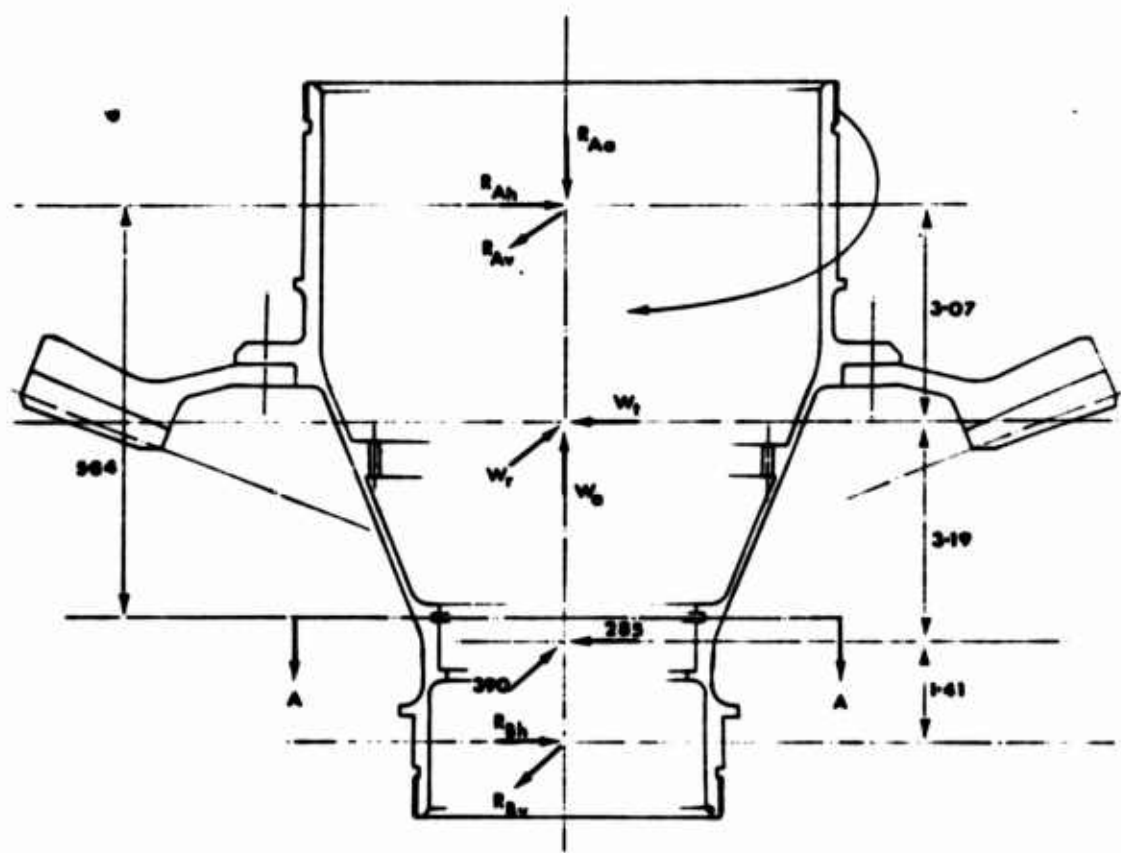
Figure E-6. Outer Shaft.

$$R_{Ah}(7.67) = 285(1.41) + 2850(4.6) \qquad (\Sigma M_{Bh} = 0)$$

$$R_{Ah} = 1760 \text{ lb}$$

$$R_A = \sqrt{1690^2 + 1760^2} = 2440 \text{ lb}$$

The loads on bearing B are

$$R_{Bv}(7.67) = 1970(3.07) + 390(6.26) - 500(6.66) \quad (\Sigma M_{Av} = 0)$$

$$R_{Bv} = 670 \text{ lb}$$

$$R_{Bh}(7.67) = 2850(3.07) + 285(6.26) \qquad (\Sigma M_{Ah} = 0)$$

$$R_{Bh} = 1370 \text{ lb}$$

$$R_B = \sqrt{670^2 + 1370^2} = 1530 \text{ lb}$$

Section A-A shown in **Figure E-6** is the critical section for the outer shaft. This section has induced fatigue bending stresses only. Cross sections along the conical portion of the shaft are not critical, as current manufacturing techniques limit the minimal wall thickness.

At section A-A

$$d_o = 4.014 \text{ in}$$

$$d_i = 3.782 \text{ in}$$

$$Z = \frac{\pi}{32}\left[\left(\frac{d_o^4 - d_i^4}{d_o}\right)\right] = \frac{\pi}{32}\left[\frac{(4.014^4 - 3.782^4)}{4.014}\right] = 1.345 \text{ in}^3$$

$$K_t = 2.75$$

$$M_h = 1930 + 1090(6.26 - 5.84) = 2387 \text{ lb-in}$$

$$M_v = 950 + 282(6.26 - 5.84) = 1068 \text{ lb-in}$$

$$M = \sqrt{2387^2 + 1068^2} = 2615 \text{ lb-in}$$

$$f_b = \frac{M}{Z} = \frac{2615}{1.345} = 1940 \text{ psi}$$

For this shaft

Material $\quad = \quad$ AMS 6260 $\quad$ Heat treat $R_c$ 30-45

$F_{tu} \quad = \quad 136,000 \text{ psi}$

$F_{ty} \quad = \quad 115,000 \text{ psi}$

$F_{en} \quad = \quad 23,600 \text{ psi}$

$$MS = \frac{F_{en}}{K_t (f_b)} - 1$$

$$MS = \frac{23,600}{2.75(1940)} - 1 = +3.4$$

## INPUT QUILL SHAFT

The input quill shaft transmits power from the input bevel gear
shaft to the freewheel unit housing. The mating splines are loose to
take up any misalignment; hence, the shaft acts as a simply supported
beam with torsional stresses only. The design parameters are

$$\text{HP limit} = 2805$$

$$\text{rpm} = 6223$$

Figure E-7 is a sketch of the input quill shaft.
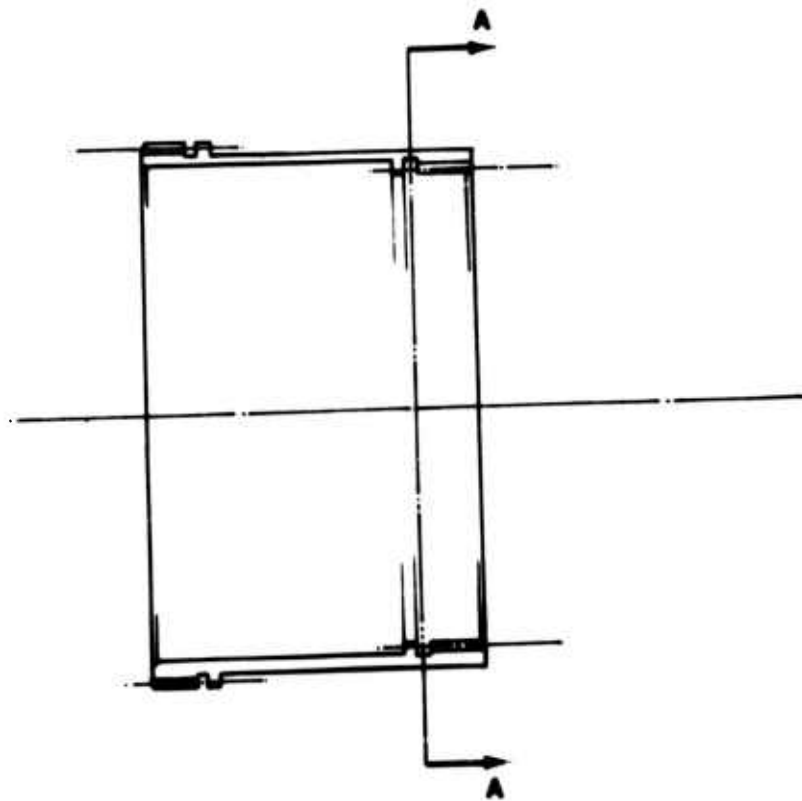


Figure E-7.    Input Quill Shaft.

The shaft is analyzed for torsional buckling using limit horsepower. The torsional modulus of rupture is a function of length, diameter, and wall thickness. At Section A-A in Figure E-7,

$$T = \frac{63025 \; HP}{rpm} = \frac{63025 \; (2805)}{6223} = 28410 \; \text{in-lb}$$

$$d_o = 5.375 \; \text{in.}$$

$$d_i = 5.151 \; \text{in.}$$

$$Z = \frac{\pi}{32} \left[ \frac{(d_o^4 - d_i^4)}{d_o} \right] = \frac{\pi}{32} \left[ \frac{(5.375^4 - 5.151^4)}{5.375} \right] = 2.387 \; \text{in}^3$$

$$f_s = \frac{T}{2 \; Z} = \frac{28410}{2(2.387)} = 5950 \; \text{psi}$$

$$F_{st} = 88000 \; \text{psi}$$

$$MS_{ult} = \frac{F_{st}}{1.5 \; f_s} - 1 = \frac{88000}{1.5(5950)} - 1 = +8.9$$

## INPUT FREEWHEEL UNIT ASSEMBLY

The freewheel unit allows power to be transmitted from the engines to the output member. When the torque direction is reversed, the unit over-runs. Fourteen rollers are located by a spring-loaded roller retention cage such that the rollers are always in contact with the inner and outer freewheel unit members. The freewheel unit assembly is depicted in Figure E-8. The following nomenclature is used for the freewheel unit analysis:

$$b = 3.10 = \text{housing outside radius}$$
$$R = 2.5264 = \text{housing bore radius}$$
$$K = 1.900 = \text{cam flat to cam center line}$$
$$d = 1.50 = \text{cam inside radius}$$
$$\rho = .3125 = \text{roller radius}$$
$$l = 1.255 = \text{roller effective length}$$
$$N = 14 = \text{number of rollers}$$
$$\nu = .32 = \text{Poisson's ratio}$$

Horsepower    HP    = 1870 maximum

Rotational speed rpm = 6223

$$T = \frac{63025 \; HP}{rpm} = \frac{63025 \; (1870)}{6223} = 18940 \text{ in -lb}$$

The following analysis determines the roller contact angle, commonly called the nip angle, for the fully loaded freewheel unit. The analysis includes the expansion of the housing and the contraction of the cam. Figure E-9 shows the loads on the roller.
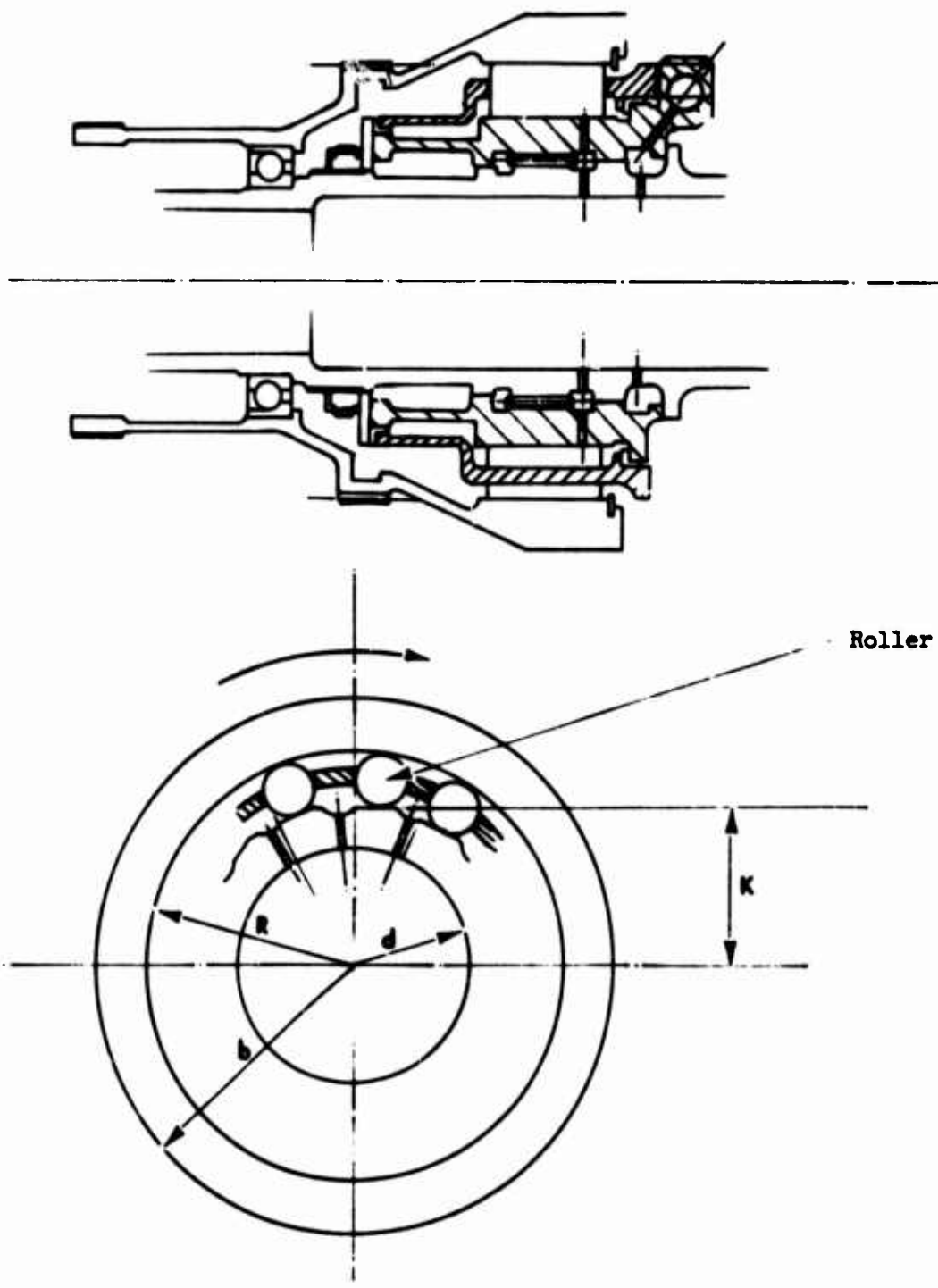
Figure E-8. Freewheel Unit Assembly.
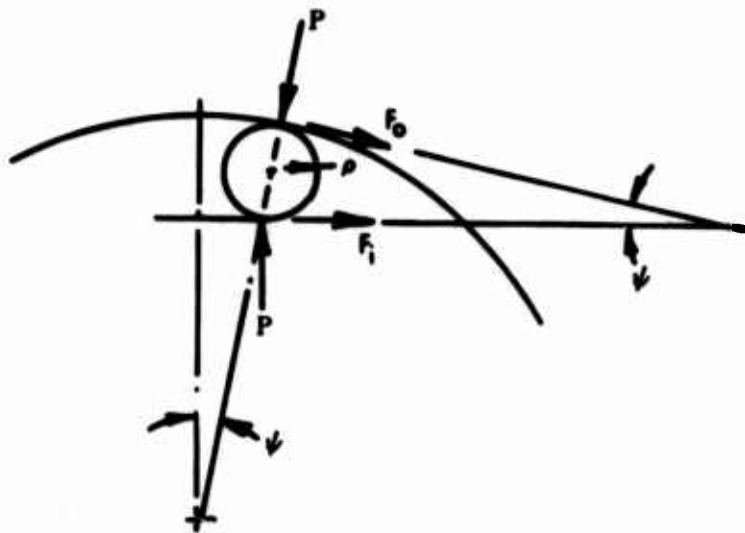
Figure E-9.   Loads Imposed on Roller.

For equilibrium of the roller:

$$F_o \, \rho \; = \; F_i \, \rho$$

$$F_o \; = \; F_i$$

Also from Figure E-9

$$F_i + F_o \cos \psi - \; P_o \sin \psi \; = \; 0$$

which reduces to:

$$P \; = \; F_o \cot \left( \frac{\psi}{2} \right)$$

To determine the cam and roller nip angle,

$$l_h \; = \; 1 + b - R \; = \; 1.255 + 3.10 - 2.5264$$

$$l_h \; = \; 1.8286 \qquad = \quad \text{effective housing length}$$

$$A_h \; = \; 2 \pi \quad R \, l_h \; = \; 2 \pi \; (2.5264)(1.8286)$$

$$A_h \quad = \quad 29.027 \quad = \quad \text{effective expansion area of housing}$$

$$l_c \quad = \quad 1 + K - d \quad = \quad 1.255 + 1.900 - 1.500 \quad = \quad 1.655$$

$$A_c \quad = \quad 2 \, \pi \, K \, l_c \quad = \quad 2 \, \pi \, (1.900)(1.655)$$

$$A_c \quad = \quad 19.757 \quad = \quad \text{effective contraction area of cam}$$

The radial contraction of the cam is given by

$$\mu_c \quad = \quad \frac{-K \, p_c}{E} \left[ \frac{K^2 + d^2}{K^2 - d^2} - \nu \right]$$

$$p_c \quad = \quad \frac{P \, N}{A_c} \quad = \quad \frac{F_o \, N}{A_c} \left( \cot \frac{\psi}{2} \right) \quad = \quad \frac{T}{R \, A_c} \left( \cot \frac{\psi}{2} \right)$$

$$\mu_c \quad = \quad \frac{-T}{E \, A_c} \left( \frac{K}{R} \right) \left[ \frac{K^2 + d^2}{K^2 - d^2} - \nu \right] \cot \frac{\psi}{2}$$

let:

$$W \quad = \quad \frac{-T}{E \, A_c} \left( \frac{K}{R} \right) \left[ \frac{K^2 + d^2}{K^2 - d^2} - \nu \right]$$

$$\mu_c \quad = \quad W \cdot \cot \frac{\psi}{2}$$

The radial expansion of the housing is given by

$$\mu_h \quad = \quad \frac{R \, p_h}{E} \left[ \frac{b^2 + R^2}{b^2 - R^2} + \nu \right]$$

$$p_h \quad = \quad \frac{T}{R \, A_h} \left( \cot \frac{\psi}{2} \right)$$

$$\mu_h \quad = \quad \frac{T}{E \, A_h} \left[ \frac{b^2 + R^2}{b^2 - R^2} + \nu \right] \cot \frac{\psi}{2}$$

Let

$$X = \frac{T}{E \, A_h} \left[ \frac{b^2 + R^2}{b^2 - R^2} + \nu \right]$$

$$\mu_h = X \cdot \cot \frac{\psi}{2}$$

Substituting for W and X,

$$W = \frac{-18940}{29 \times 10^6 \, (19.757)} \left( \frac{1.900}{2.5264} \right) \left[ \frac{1.900^2 + 1.500^2}{1.900^2 - 1.500^2} - .32 \right]$$

$$W = -99.16 \times 10^{-6}$$

$$X = \frac{18940}{29 \times 10^6 \, (29.027)} \left[ \frac{3.100^2 + 2.5264^2}{3.100^2 - 2.5264^2} + .32 \right]$$

$$X = 118.69 \times 10^{-6}$$

Now

$$\cos \frac{\psi}{2} = \frac{K + \mu_c + \rho}{R + \mu_h - \rho}$$

Substituting for $\mu_c$ and $\mu_h$,

$$\left[ \frac{R - \rho}{2} \right] \sin 2\psi + \left[ X \cos \psi - W \right] \left[ 1 + \cos \psi \right] = \sin \psi \left[ K + \rho \right]$$

$$\left[ \frac{2.5264 - .3125}{2} \right] \sin 2\psi + 10^{-6} \left[ 118.69 \cos \psi - 99.16 \right] \left[ 1 + \cos \psi \right] = \sin \psi \left[ 1.9 + .3125 \right]$$

By an iterative solution procedure, $\psi$ in the above equation is solved for the full load contact angle, giving

$$\psi = 4° \, 29'$$

A full load roller contact angle of less than $8^\circ$ at the maximum
design horsepower has been shown by experience to be sufficient to
retain the rollers in position and prevent roller "spit out".  A
full load angle greater than $2^\circ$ has been shown by experience to be
sufficient to prevent self-locking.  Hence, the input freewheel unit
cam assembly meets the design requirements for roller contact angle.

## FREEWHEEL UNIT HOUSING

The freewheel unit outer housing is analyzed as a ring subjected to 14 equally spaced loads induced by the rollers. The housing cross section with dimensions is shown in Figure E-10.
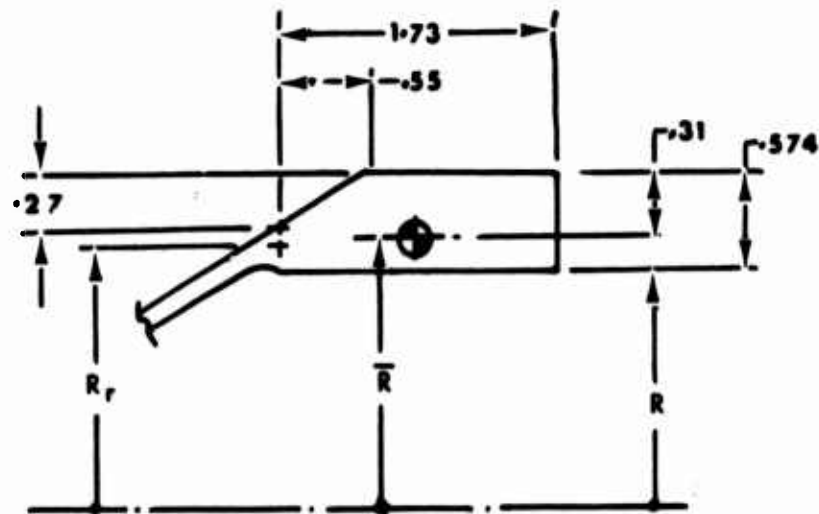


Figure E-10.  Freewheel Unit Outer Housing
Cross Section.

$A_H$ = .918 = cross sectional area of housing

$Y_o$ = .31 in

R = 2.5264 in

$\overline{R}$ = 2.79 in

$R_r$ = 2.70 in

$I_H$ = .0237 in$^4$

$$F_o = \frac{T}{R\,N} = \frac{18940}{2.5264\,(14)} = 535 \text{ lb}$$

$$P = F_o \cdot \cot \frac{\psi}{2} = 535\left(\cot \frac{4^\circ 29'}{2}\right) = 13680 \text{ lb}$$

The radial loads P and tangential loads F at each roller contact point are transferred to the centroid of the housing cross section at radius $\bar{R}$ as shown in Figure E-11.
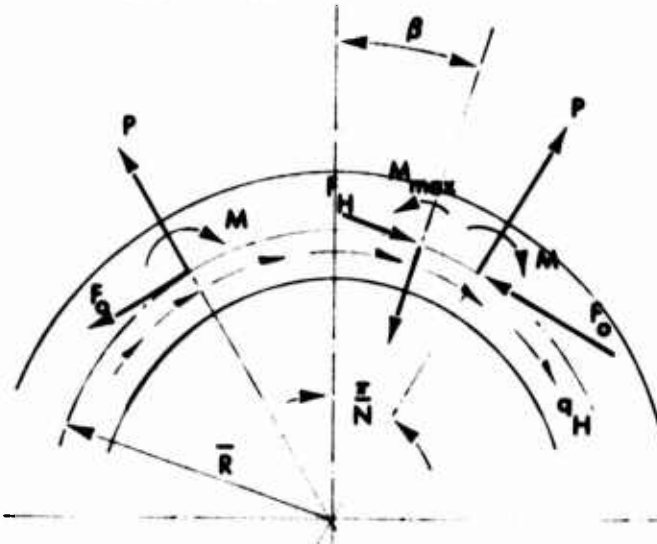


Figure E-11.  Roller Loads Transferred to
Centroid of Ring.

Shear flow $q_H = \dfrac{T}{2\pi R_r^2} = \dfrac{18940}{2\pi(2.7^2)} = 413$

The critical sections through the housing are at the roller contact points $(\theta = \beta)$

$$M_{max} = \frac{P\bar{R}}{2}\left(\frac{1}{\theta} - \frac{\cos\beta}{\sin\theta}\right) + \frac{Fo\,\bar{R}\sin\beta}{2\sin\theta} - q_H \cdot R_r^2\,\beta$$

$$\theta = \frac{\pi}{N} = \frac{\pi}{14} = .2244 = 12°51' = \beta$$

$$M_{max} = \frac{13680(2.79)}{2}\left(\frac{1}{.2244} - \frac{\cos 12°51}{\sin 12°51}\right)$$

$$+ \frac{535(2.79)}{2} - 413(2.7)^2\,.2244 = 1460 \text{ in-lb}.$$

291

The internal tensile load is given by

$$F_H = \frac{-P \cos \beta}{2 \sin \theta} + \frac{F_o \sin \beta}{2 \sin \theta}$$

$$= \frac{-13680. \cos 12°51}{2 \sin 12°51} + \frac{535}{2} = -29710 \text{ lbs}$$

The maximum stress occurs at the outside of the housing and is given by

$$f_b = \frac{M_{max} Y_o}{I_H} = \frac{1460(.31)}{.0237} = 19100 \text{ psi}$$

The axial stress is given by

$$f_a = \frac{-F_H}{A_H} = \frac{29710}{.918} = 32360 \text{ psi}$$

The material properties for the freewheel unit housing are

<u>Material</u>    AMS   6265 Heat Treat $R_c$ 30 - 45.

$$F_{tu} = 136000 \text{ psi}$$

$$F_{ty} = 115000 \text{ psi}$$

$$F_{bu} = 180000 \text{ psi}$$

$$MS_{ult} = \frac{1}{1.5\left(\dfrac{f_a}{F_{tu}} + \dfrac{f_b}{F_{bu}}\right)} -1$$

$$MS_{ult} = \frac{1}{1.5\left(\dfrac{32360}{136000} + \dfrac{19100}{180000}\right)} -1 = +.94$$

## FREEWHEEL UNIT CAM

The freewheel unit cam is analyzed as a ring subjected to 14 equally
spaced loads induced by the rollers. The cam cross-section with
dimensions is shown in Figure E-12.
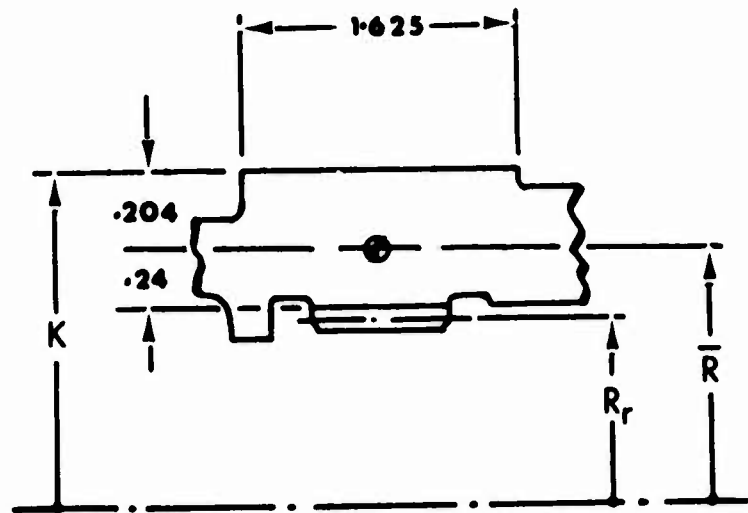


Figure E-12. Freewheel Unit Cam Cross section.

$A_c$ = .656 = cross-sectional area of cam

$Y_o$ = .204 in

$K$ = 1.90 in

$\bar{R}$ = 1.696 in

$R_r$ = 1.375 in

$I_c$ = .0095 in$^4$

The loads on the rollers, Figure E-9, are reacted by the cam loads shown
in Figure E-13

293
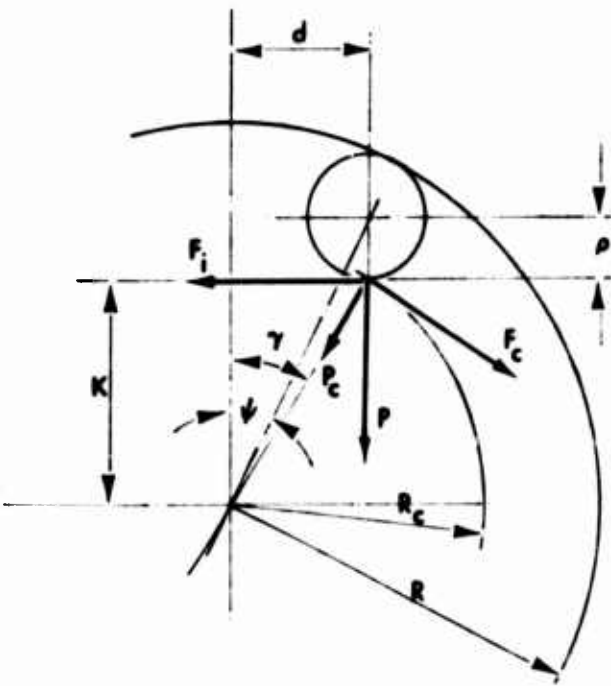
Figure E-13. Freewheel Unit Cam Loads.

where

$$d = (R - \rho) \sin \psi = (2.5264 - .3125) \sin 4°29' = .1729$$

$$\gamma = \tan^{-1}\left(\frac{d}{K}\right) = \tan^{-1}\left(\frac{.1729}{1.90}\right) = 5°12'$$

$$R_c = \frac{K}{\cos \gamma} = \frac{1.90}{\cos 5°12'} = 1.9078 \text{ in}$$

$$P = 13680 \text{ lb}$$

$$F_i = F_o = 535 \text{ lb}$$

$$P_c = P \cos\gamma + F_i \sin\gamma = 13680.\cos 5°12' + 535.\sin 5°12' = 13670 \text{ lb}$$

$$F_c = P \sin\gamma - F_i \cos\gamma = 13680.\sin 5°12' - 535.\cos 5°12' = 710 \text{ lb}$$

The radial loads P and tangential loads F at each roller contact point are transferred to the centroid of the cam cross section at radius R as shown in Figure E-14.
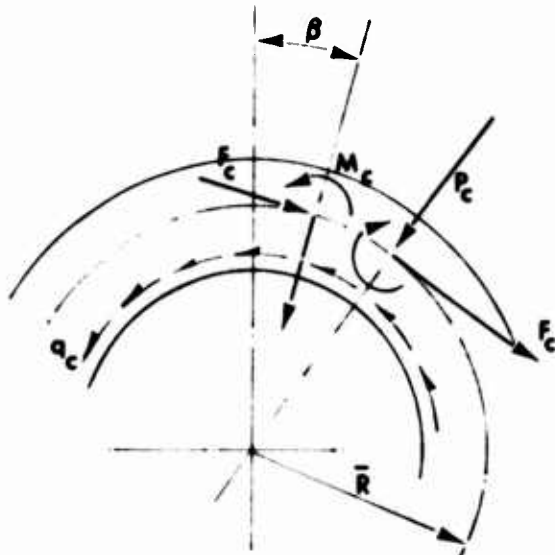
Figure E-14. Cam Loads Transferred to Centroid of Cam.

$$\text{Shear flow } q_c = \frac{T}{2 \pi R_r^2} = \frac{18940}{2 \pi (1.375)^2} = 1595 \text{ lb/in.}$$

The critical sections through the cam are at the roller contact points ($\theta = \beta$)

$$M_{max} = \frac{-P_c \bar{R}}{2} \left[ \frac{1}{\theta} - \frac{\cos \beta}{\sin \theta} \right] - \frac{F_c \bar{R} \sin \beta}{2 \sin \theta} + q_c \; R_r^2 \beta$$

$$\theta = \frac{\pi}{N} = \frac{\pi}{14} = .2244 = 12°51' = \beta$$

$$M_{max} = \frac{-13670(1.696)}{2} \left[ \frac{1}{.2244} - \frac{\cos 12°51'}{\sin 21°51} \right] - \frac{710(1.696)}{2} + 1595(1.375)^2 (.2244)$$

$$= -770 \text{ in-lbs}$$

The internal tensile load is shown by

$$F = \frac{P_c \cos \beta}{2 \sin \theta} - \frac{F_c \sin \beta}{2 \sin \theta}$$

$$= \frac{13670.\cos 12°51}{2.\sin 12°51} - \frac{710}{2} = 29600 \text{ lb}$$

**295**

## DYNAMIC ANALYSIS, ROLLER RETAINER PIN SPRING ASSEMBLY

The pin and spring assembly as shown in Figure E-8 exerts a force on the roller retention cage which causes the rollers to contact the outer housing and freewheel unit cam at all times. Improper design can cause the torque on the roller retention cage to reverse under dynamic conditions due to centrifugal forces. This phenomenon is critical when the cam and rollers are in the freewheel position, i.e., initial contact angle. $P_p$, as shown in Figure E-15, is the total force on the roller retention cage due to static and dynamic forces. In the ideal design $P_p$ should remain constant under all conditions.
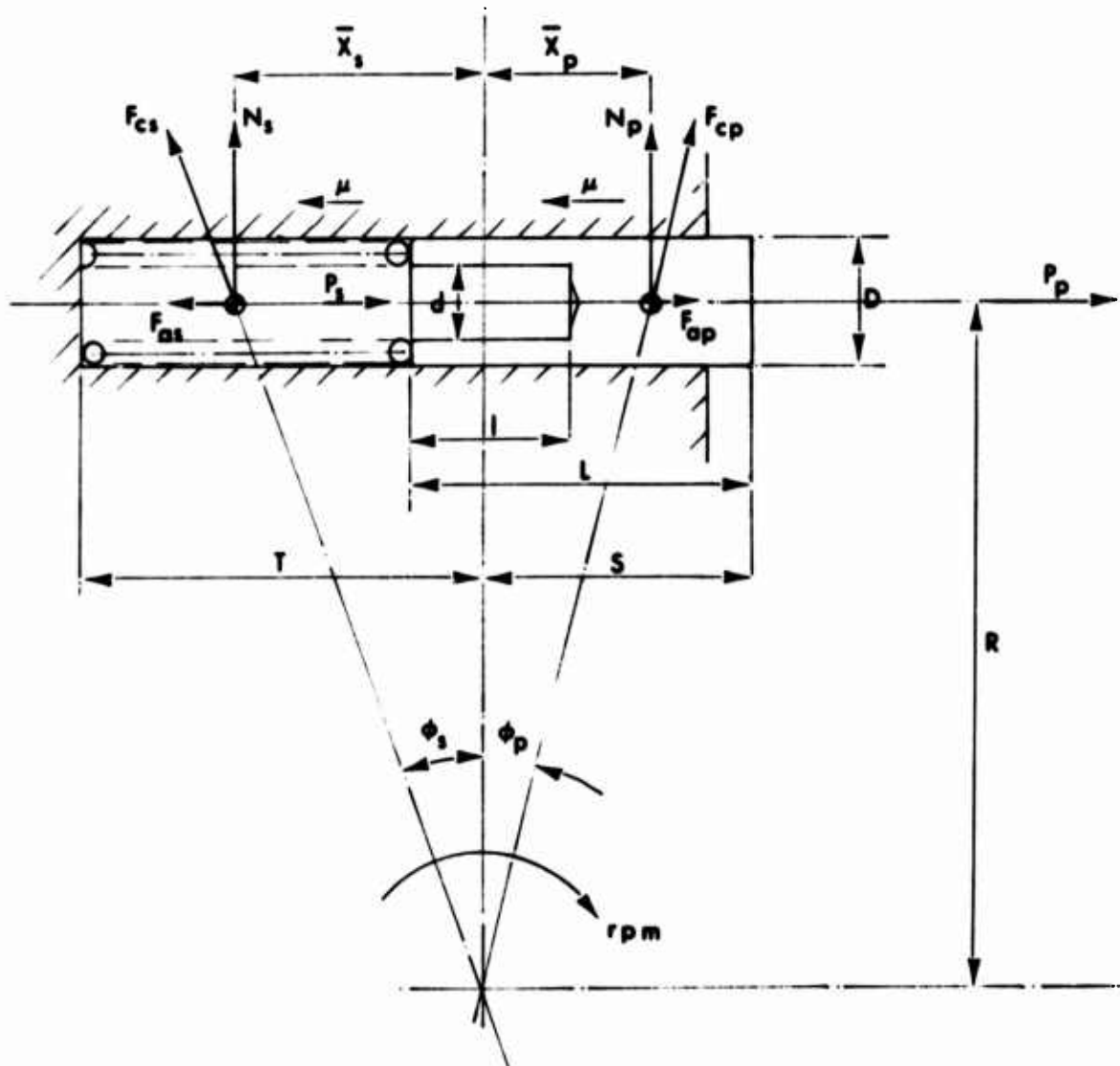


Figure E-15.    Pin and Spring Assembly.

The spring analysis is given below:

$$f_s = 1.125 \text{ in} = \text{free length of spring}$$

$$K_s = 10.8 \text{ lb/in} = \text{spring rate}$$

$$W_s = .00143 \text{ lb} = \text{weight of spring}$$

$$\overline{X}_s = \frac{T - S + L}{2} = \frac{1.06 - .715 + .85}{2} = .597 \text{ in}$$

$$F_{cs} = \frac{\pi^2 (.00143) \text{ rpm}^2}{900(386)} \cdot \sqrt{(2.187)^2 + (.597)^2} = 9.21(10^{-8}) \text{ rpm}^2$$

$$N_s = \frac{F_{cs} \cdot R}{\sqrt{R^2 + \overline{X}_s^2}}$$

$$= \frac{9.21(10^{-8})2.187}{\sqrt{(2.187)^2 + (.597)^2}} \left( \text{rpm}^2 \right) = 8.885 \ (10^{-8}) \ \text{rpm}^2$$

$$F_{as} = \frac{N_s \overline{X}_s}{R} = \frac{8.885(10^{-8})(.597)}{2.187} \left( \text{rpm}^2 \right) = 2.425(10^{-8}) \ \text{rpm}^2$$

$$F_s = K_s (f_s - T - S + L) = 10.8(1.125-1.06-.715 + .85) = 2.16$$

$$P_s = F_s - (F_{as} + \mu N_s)$$

$$= 2.16 - \text{rpm}^2 \left[ 2.425 + (8.885)\mu \right] 10^{-8} = \text{resultant force from spring on pin}$$

The pin analysis is as follows:

$$\left. \begin{matrix} D = .187 \text{ in} \\ L = .85 \text{ in} \\ d = .094 \text{ in} \\ 1 = .5 \text{ in} \end{matrix} \right\} \quad \text{See Figure E-15.}$$

$$W_p = .0057 = \text{pin weight, lb}$$

$$\overline{X}_p = \frac{DL^2 - dl^2}{2(DL - dl)} + S - L$$

$$= \frac{.187(.85)^2 - .094(.5)^2}{2\left[.187(.85) - .094(.5)\right]} + .715 - .85 = .363\,in$$

$$F_{cp} = \frac{\pi^2 W_p \cdot rpm^2}{900\,g}\sqrt{R^2 + \overline{X}_p^2}$$

$$= \frac{\pi^2(.0057)\,rpm^2}{900\,(386)}\sqrt{(2.187)^2 + (.363)^2} = 35.9(10^{-8})\,rpm^2$$

$$N_p = \frac{F_{cp} \cdot R}{\sqrt{R^2 + \overline{X}_p^2}}$$

$$= \frac{35.9(10^{-8})\,2.187}{\sqrt{(2.187)^2 + (.363)^2}}\left(rpm^2\right) = 35.41(10^{-8})\,rpm^2$$

$$F_{ap} = \frac{N_p \cdot \overline{X}_p}{R} = \frac{35.41(10^{-8})(.363)}{2.187}\left(rpm^2\right) = 5.88(10^{-8})\,rpm^2$$

$$P_p = P_s + F_{ap} - \mu N_p = \text{resultant pin force on cage}$$

$$= 2.16 + rpm^2(3.455 - 44.295\mu)\,10^{-8}$$

Hence, the resultant load $P_p$ is a function of coefficient of friction and rpm. Figure E-16 is a plot of resultant pin load vs rpm for various values of coefficient of friction. It shows that for a range of practical values of $\mu$, the resultant pin load is always positive and is essentially constant for $\mu = .075$ which is estimated to be the actual coefficient of friction.
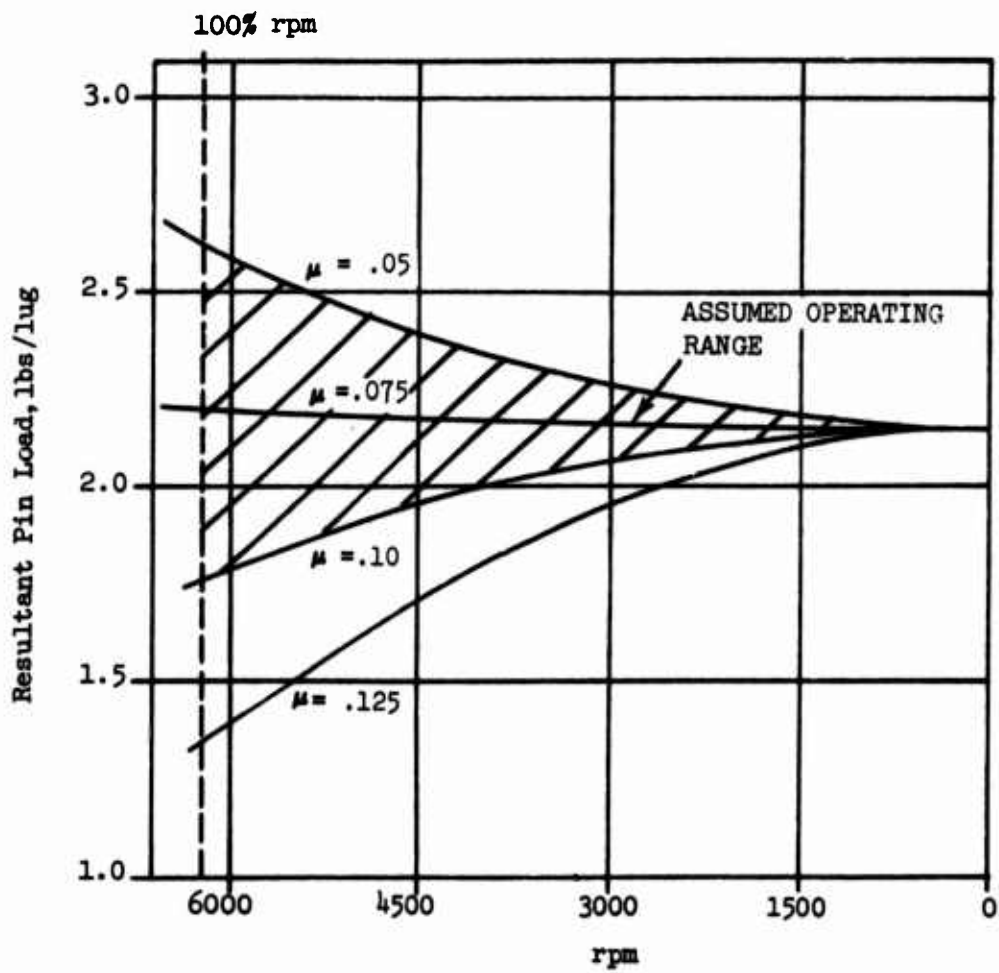
Figure E-16.  Load per Pin on Roller Retention Cage versus rpm for
Various Values of Coefficient of Friction.

# APPENDIX F
## STRUCTURAL ANALYSIS OF MAIN
## GEARBOX CENTER SECTION

### OUTER SHAFT

The spur bull gear receives power from the right and left inputs and transmits the combined power to the tail takeoff spiral bevel gear and to the roller gear drive reduction unit. This shaft is analyzed as a rotating beam with fully reversed bending stresses and steady torsional stress. The maximum stresses are induced in the shaft during single engine operation on the right input with maximum tail takeoff power. During normal dual operation, the loads on the spur bull gear tend to cancel, thereby inducing lower stresses in the shaft.

$$HP = 1870 \quad \text{single engine input}$$

$$HP = 700 \quad \text{tail takeoff}$$

$$rpm = 4045 \quad \text{outer shaft}$$

For single engine input

$$T = \frac{63025(1870)}{4045} = 29140 \text{ in-lb outer shaft}$$

$$T = \frac{63025(700)}{4045} = 10910 \text{ in-lb tail takeoff}$$

The bevel gear data for the tail takeoff pinion is

$$N = 73 = \text{number of teeth on pinion}$$

$$F = 1.40 = \text{face width}$$

$$d_p = 12.898 = \text{pitch diameter, in.}$$

$$\phi = 20^\circ = \text{pressure angle}$$

$$\psi = 35^\circ = \text{spiral angle}$$

$$\gamma = 52^\circ 56' = \text{pitch angle}$$

$$R_m = \frac{1}{2}\left(d_p - F \cdot \sin\gamma\right)$$

$$= \frac{1}{2}\left[12.898 - 1.4(.798)\right] = 5.89 = \text{mean radius}$$

300

Figure F-1 is a plan view of the bull gear mesh showing loads on bull gear and tail takeoff pinion.
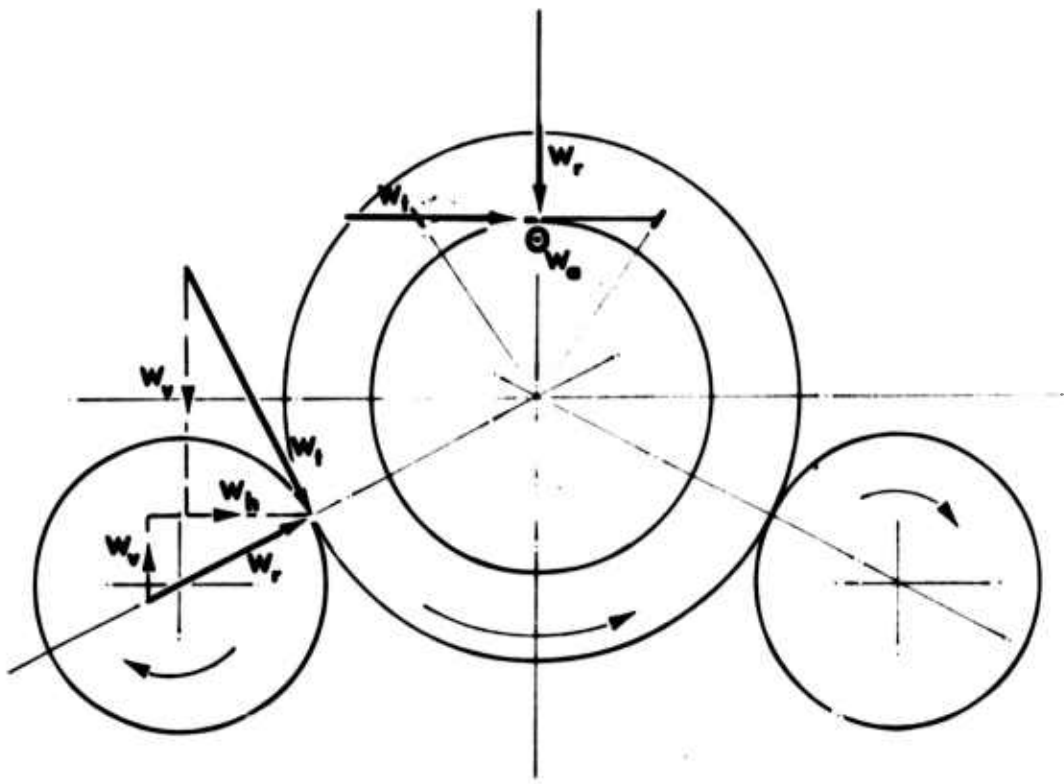


Figure F-1.    Gear Loads on Bull Gear
             and Tail Takeoff Pinion.

Figure F-2 shows the outer shaft with bull gear and tail takeoff pinion, critical section, and loads. $W_h$ and $W_v$ shown at the bull gear are obtained from page 275 of the splined shaft analysis.  For the right-hand spiral tail takeoff pinion driving clockwise,

$$W_t = \frac{T}{R_m} = \frac{10910}{5.89} = 1860 \text{ lb}$$

$$W_a = \frac{W_t}{\cos \psi} \left( \tan \phi \, \sin \gamma - \sin \psi \, \cos \gamma \right)$$

$$= \frac{1860}{.819} \left[ (.364)(.798) - (.574)(.603) \right] = -120 \text{ lb}$$

301
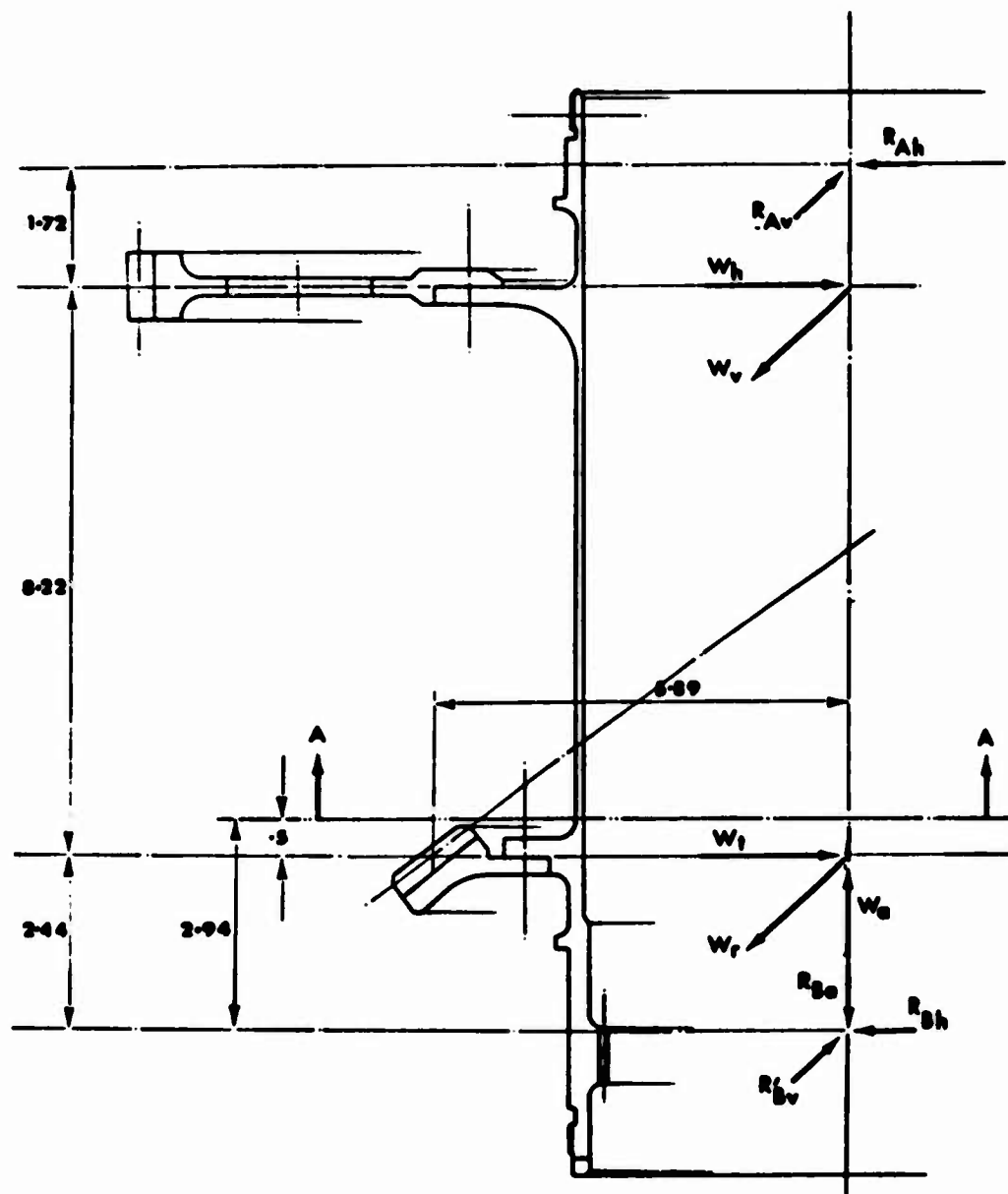
Figure F-2.   Outer Shaft.

302

$$W_r = \frac{W_t}{\cos\psi}\left(\tan\phi\,\cos\gamma + \sin\psi\,\sin\gamma\right)$$

$$= \frac{1860}{.819}\left[(.364)(.603)+(.574)(.798)\right] = 1530 \text{ lb}$$

From a static analysis of **Figure F-2** the bearing loads are found to be

$$R_{Av} = 2550 \text{ lb}$$

$$R_{Ah} = 1970 \text{ lb}$$

$$R_{Bv} = 1530 \text{ lb}$$

$$R_{Bh} = 1750 \text{ lb}$$

At critical section A-A,

$$d_o = 7.565 \text{ in}$$

$$d_i = 7.385 \text{ in}$$

$$Z = \frac{\pi}{32}\left[\frac{(d_o^4 - d_i^4)}{d_o}\right] = \frac{\pi}{32}\left[\frac{(7.565^4 - 7.385^4)}{7.565}\right] = 3.903 \text{ in}^3$$

$$K_t = 1.85$$

$$M = \sqrt{(2.94\cdot R_{Bh} - .5\,W_t)^2 + (2.94\cdot R_{Bv} - .5\,W_r)^2}$$

$$M = \sqrt{\left[2.94(1750) - .5(1860)\right]^2 + \left[2.94(1530) - .5(1530)\right]^2}$$

$$M = 5630 \text{ lb-in}$$

$$f_b = \frac{M}{Z} = \frac{5630}{3.903} = 1440 \text{ psi}$$

$$f_s = \frac{T}{2\,Z} = \frac{29140}{2(3.903)} = 3730 \text{ psi}$$

303

$$MS = \sqrt{\dfrac{1}{\left(\dfrac{K_t \; f_b}{F_{en}}\right)^2 + 4\left(\dfrac{f_s}{F_{ty}}\right)^2}} \quad -1$$

$$MS = \sqrt{\dfrac{1}{\left[\dfrac{1.85(1440)}{22700}\right]^2 + 4\left[\dfrac{3730}{115000}\right]^2}} \quad -1 \quad = \; +6.4$$

## INPUT QUILL SHAFT

The input quill shaft transmits power from the outer shaft to
the sun gear of the roller gear unit  The mating splines are loose
to take up any misalignment; hence, the shaft acts as a simply supported
beam with torsional stresses only.  The design parameters are

$$HP_{limit} = 1.5(3000) = 4500$$

$$rpm = 4045$$

Figure F-3 is a sketch of the input quill shaft.
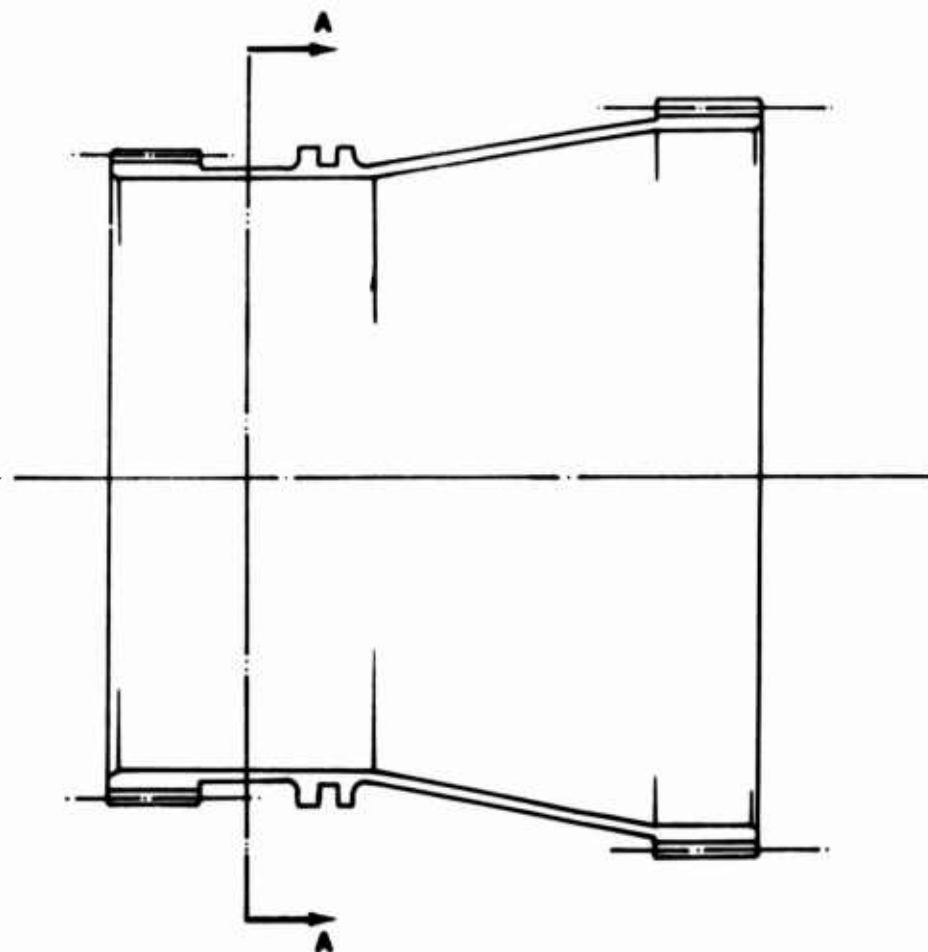
Figure F-3.  Input Quill Shaft.

The shaft is analyzed for torsional buckling using limit horsepower.
The torsional modulus of rupture is a function of length, diameter, and
wall thickness. At Section A-A in Figure F-3,

$$T = \frac{63025 \; HP}{rpm} = \frac{63025 \; (4500)}{4045} = 70110 \; in-lb$$

$$d_o = 6.615 \; in$$

$$d_i = 6.447 \; in$$

$$Z = \frac{\pi}{32}\left[\frac{d_o^4 - d_i^4}{d_o}\right] = \frac{\pi}{32}\left[\frac{(6.615^4 - 6.447^4)}{6.615}\right] = 2.779 \; in^3$$

$$f_s = \frac{T}{2 \; Z} = \frac{70110}{2(2.779)} = 12610 \; psi$$

$$F_{st} = 64000 \; psi$$

$$MS_{ult} = \frac{F_{st}}{1.5 \; f_s} - 1 = \frac{64000}{1.5(12610)} - 1 = + 2.37$$

## TAIL TAKEOFF BEVEL GEAR

The tail takeoff bevel is a left-hand spiral bevel gear driven counter-clockwise. Power is transmitted through a shaft angle of $80^\circ 15'$ to the tail takeoff quill shaft and hence to the accessory section of the main gearbox.

$$HP = 700 \text{ Tail tail takeoff}$$

$$rpm = 4045 \left(\frac{73}{42}\right) = 7031$$

The basic gear data for the bevel gear is

$$N = 42 = \text{ number of teeth on gear}$$

$$F = 1.40 \text{ in} = \text{ face width}$$

$$d_p = 7.420 \text{ in} = \text{ pitch diameter}$$

$$\phi = 20^\circ = \text{ pressure angle}$$

$$\psi = 35^\circ = \text{ spiral angle}$$

$$\gamma = 27^\circ 19' = \text{ pitch angle}$$

$$R_m = \frac{1}{2}\left(d_p - F\sin\gamma\right)$$

$$= \frac{1}{2}\left[7.42 - 1.4(.459)\right] = 3.39 = \text{ mean radius, in}$$

The loads on the bevel gear are calculated as follows:

$$T = \frac{63025(HP)}{rpm} = \frac{63025(700)}{7031} = 6275 \text{ in-lb}$$

$$W_t = \frac{T}{R_m} = \frac{6275}{3.39} = 1850 \text{ lb}$$

$$W_a = \frac{W_t}{\cos\psi}\left(\tan\phi\sin\gamma + \sin\psi\cos\gamma\right)$$

$$= \frac{1850}{.819}\left[(.364)(.459) + (.574)(.888)\right] = 1530 \text{ lb}$$

307

$$W_r = \frac{W_t}{\cos \psi} \left( \tan \phi \cos \gamma - \sin \psi \sin \gamma \right)$$

$$= \frac{1850}{.819} \left[ (.364)(.888) - (.574)(.459) \right] = 135 \text{ lb}$$

Figure F-4 shows the tail takeoff bevel gear with load and bearing reaction locations. From a static analysis of the figure, the bearing loads are found to be

$$R_{A_v} = 850 \text{ lb}$$

$$R_{B_v} = 985 \text{ lb}$$

$$R_{A_h} = 2320 \text{ lb}$$

$$R_{B_h} = 470 \text{ lb}$$

The critical section in fatigue is section A-A, as shown in Figure F-4. This section carries fatigue bending stresses as well as steady axial and torsional stresses. For section A-A

$$d_o = 2.57 \text{ in}$$

$$d_i = 2.37 \text{ in}$$

$$A = \frac{\pi}{4} \left( d_o^2 - d_i^2 \right) = \frac{\pi}{4} \left( 2.57^2 - 2.37^2 \right) = .776 \text{ in}^2$$

$$Z = \frac{\pi}{32} \left[ \frac{(d_o^4 - d_i^4)}{d_o} \right] = \frac{\pi}{32} \left[ \frac{(2.57^4 - 2.37^4)}{2.57} \right] = .461 \text{ in}^3$$

$$K_t = 1.5$$
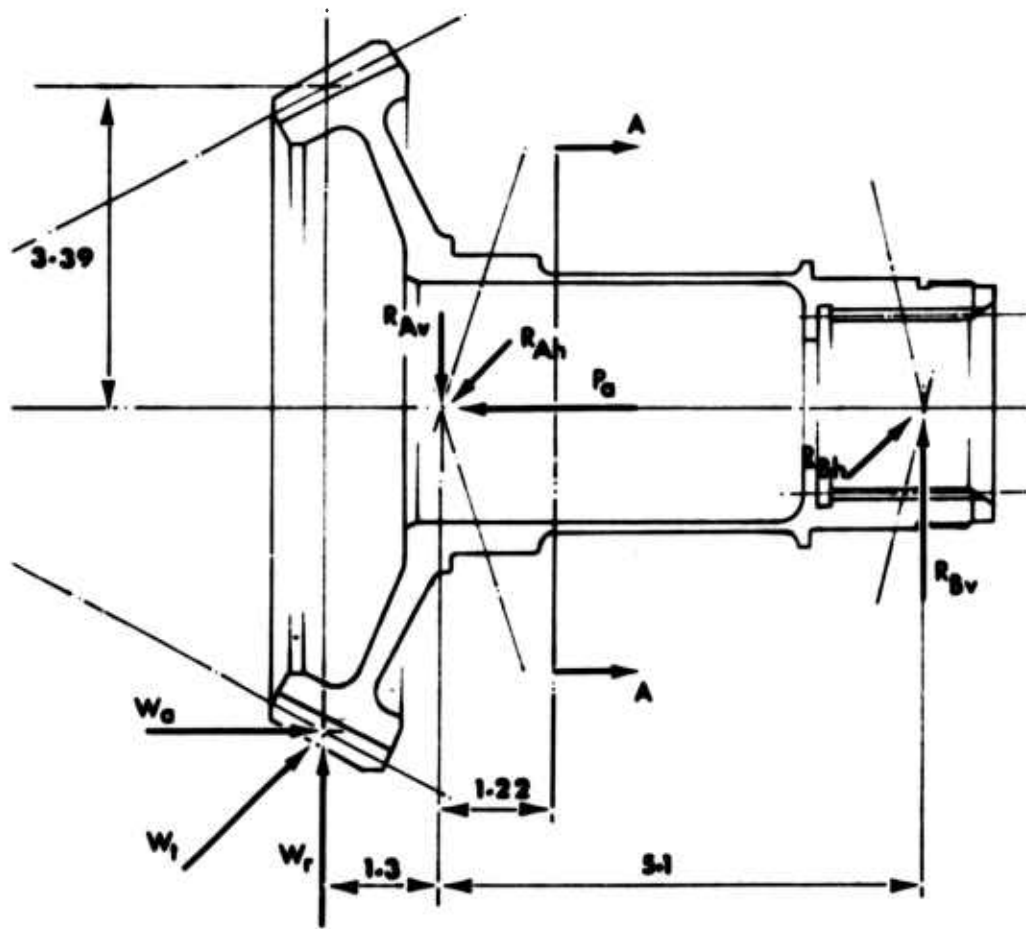
Figure F-4.  Tail Takeoff Bevel Gear.

$$P_a = 1530 = W_a$$

$$M = \sqrt{\left[985(5.1 - 1.22)\right]^2 + \left[470(5.1 - 1.22)\right]^2} = 4234 \text{ lb-in}$$

$$f_a = \frac{P_a}{A} = \frac{1530}{.776} = 1970 \text{ psi}$$

$$f_b = \frac{M}{Z} = \frac{4234}{.461} = 9185 \text{ psi}$$

$$f_s = \frac{T}{2\,Z} = \frac{6275}{2(.461)} = 6805 \text{ psi}$$

For this shaft:

Material = AMS 6265.  Heat Treat $R_c$ 30-45

$$F_{tu} = 136000 \text{ psi (min)}$$

$$F_{ty} = 11\text{?}00 \text{ psi}$$

$$F_{en} = 23200 \text{ psi}$$

$$MS = \sqrt{\frac{1}{\sqrt{\left(\dfrac{f_a}{F_{ty}} + \dfrac{K_t\, f_b}{F_{en}}\right)^2 + 4\left(\dfrac{f_s}{F_{ty}}\right)^2}}} - 1$$

$$MS = \frac{1}{\sqrt{\left[\dfrac{1970}{115000} + \dfrac{1.5(9185)}{23200}\right]^2 + 4\left[\dfrac{(6805)}{115000}\right]^2}} - 1 = +.60$$

## TAIL TAKEOFF QUILL SHAFT

The tail takeoff quill shaft transmits power from the tail takeoff bevel gear to the tail takeoff spur gear. The splines are not clamped axially; hence, the shaft acts as a simply supported beam with torsional stresses only. The design parameters are

$$HP_{limit} = 1050$$

$$rpm = 7031$$

Figure F-5 is a sketch of the tail takeoff quill shaft.
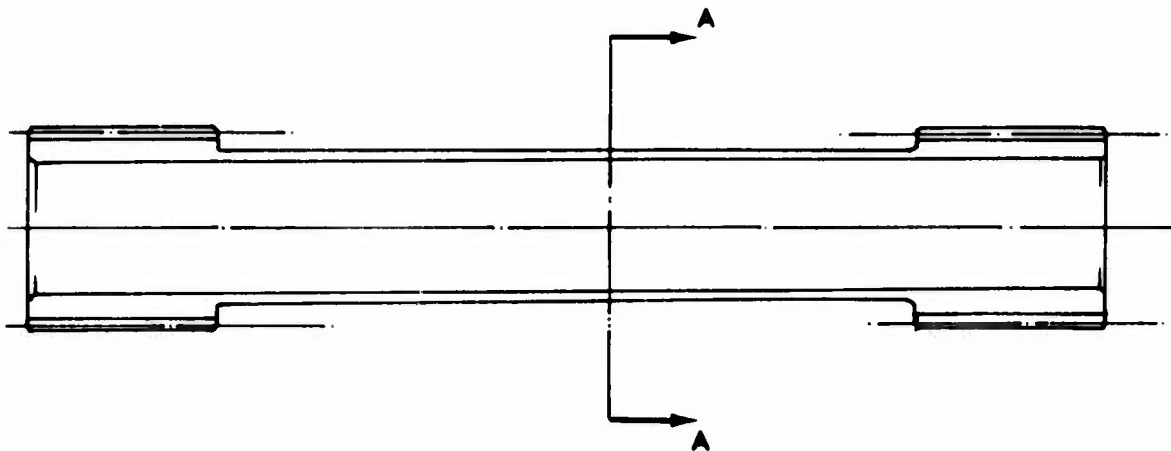
Figure F-5. Tail Takeoff Quill Shaft.

The shaft is analyzed for torsional buckling using limit horsepower.
The torsional modulus of rupture is a function of length, diameter, and
wall thickness.   At section A-A in Figure F-5,

$$T = \frac{63025 \text{ HP}}{\text{rpm}} = \frac{(63025)(1050)}{7031} = 9410 \text{ in -lb}$$

$$d_o = 1.584 \text{ in}$$

$$d_i = 1.385 \text{ in}$$

$$Z = \frac{\pi}{32} \left( \frac{d_o^4 - d_i^4}{d_o} \right) = \frac{\pi}{32} \left[ \frac{(1.584^4 - 1.385^4)}{1.584} \right] = .162 \text{ in}^3$$

$$f_s = \frac{T}{2 Z} = \frac{9410}{2(.162)} = 29030 \text{ psi}$$

$$F_{st} = 71000 \text{ psi}$$

$$M S_{ult} = \frac{F_{st}}{1.5 \, f_s} -1 = \frac{71000}{1.5 \, (29030)} -1 = + .63$$

# APPENDIX G

## STRUCTURAL ANALYSIS OF MAIN
## GEARBOX ACCESSORY GEARS

The accessory gear drive train provides power for the accessories listed in Table G-1. For the accessory drives, it is conservatively assumed that the fatigue design power is equal to the maximum power.

| TABLE G-1. ACCESSORY DRIVE TRAIN - MAIN GEARBOX. | | |
|---|---|---|
| Output Location | Fatigue Design HP | rpm |
| Generator Drive, Left Side | 53.6 | 8010 |
| Generator Drive, Right Side | 53.6 | 8112 |
| Auxiliary Hydraulic Pump Drive | 6.5 | 4005 |
| Utility Hydraulic Pump Drive | 13.0 | 4005 |
| Lubrication Pump Drive | 4.0 | 5149 |
| Tail Takeoff Drive | 565.0 | 4005 |
| Oil Cooler Drive | 15.0 | 7031 |
| Primary Hydraulic Pump Drive | 6.5 | 4197 |
| Tachometer Generator Drive | 1.0 | 3906 |
| Rotor Brake Drive | 825.0* | 4334 |
| *Corresponds to a limit torque brake capacity of 11990 inch-pounds at 450 psi and 4334 rpm. | | |

Figure G-1 is a sketch of the accessory drive train of the main gearbox with directions of rotation, numbers of teeth, and diametral pitch for each gear pair.

generator 45 t 10 p

auxiliary hydraulic
pump 90 t 10 p

primary hydraulic pump 67 t 10 p

generator 39 t 8 p

input $\left\{\begin{array}{l} 40 \text{ t } 10\text{p} \\ 45 \text{ f } 8\text{p} \end{array}\right.$

tachometer 72 t 10 p

rotor brake 73 t 8 p

output $\left\{\begin{array}{l} 79\text{t } 8\text{ P} \\ 90\text{ t } 10\text{ P} \end{array}\right.$

lubrication pump 70 t 10 p

utility hydraulic pump 90 t 10 P
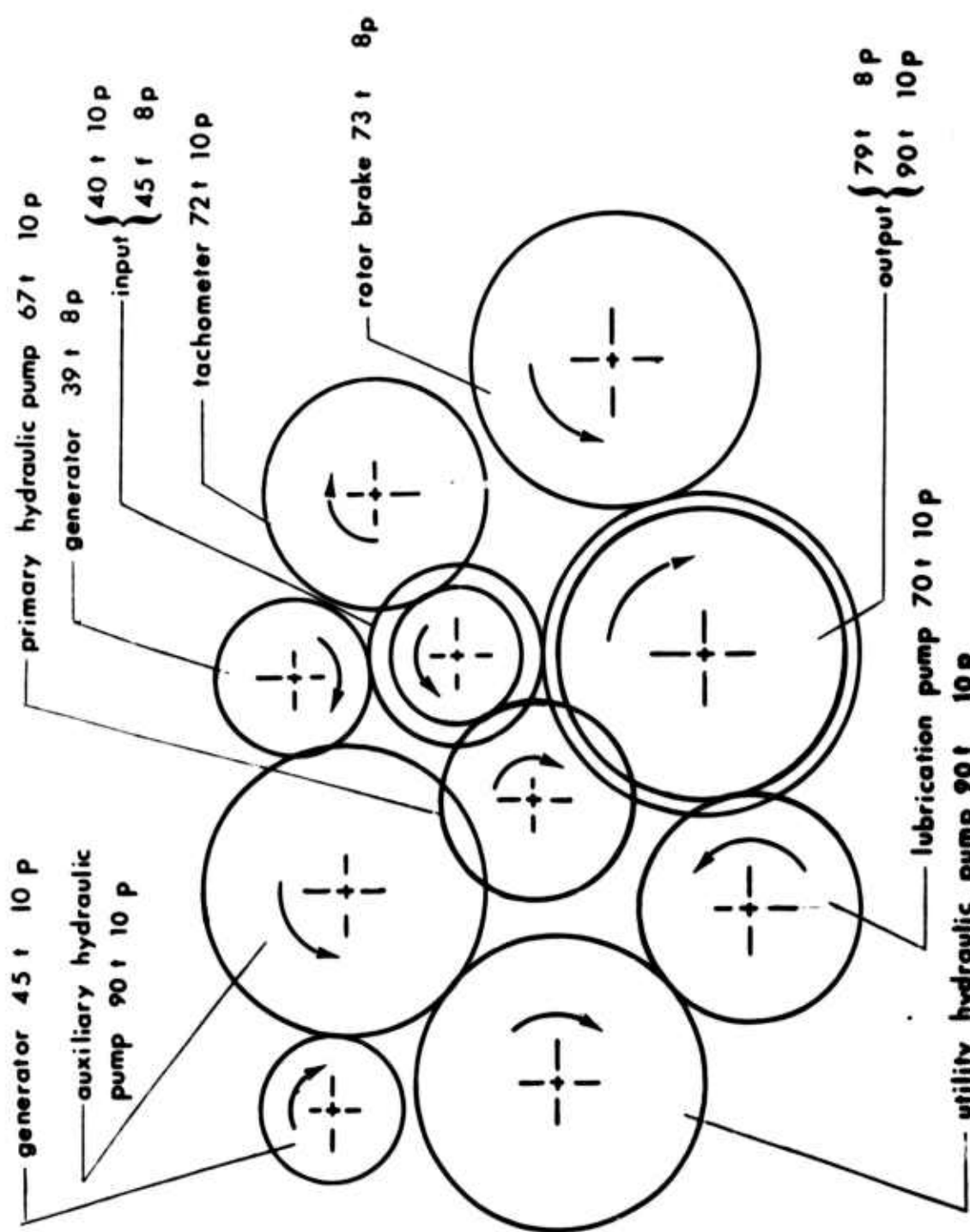
Figure G-1. Schematic, Accessory Drive Train.

314

## GEAR, SPUR, GENERATOR (LEFT SIDE)

The generator gear shaft is driven by the auxiliary hydraulic pump gear
and provides power to drive the left-side generator. Figure G-2
illustrates the actual shaft geometry and reactions for the left-side
generator.

$$T = \frac{63025 \text{ HP}}{\text{rpm}} = \frac{63025(53.6)}{8010} = 422 \text{ in -lb}$$

$$W_t = \frac{2 \text{ T}}{D} = \frac{(2)(422)}{4.5} = 188 \text{ lb}$$

$$W = \frac{W_t}{\cos 20^\circ} = \frac{188}{.93969} = 200 \text{ lb}$$

The reactions at A and B are

$$R_A = 304 \text{ lb}$$

$$R_B = 103 \text{ lb}$$

The critical section for fatigue design conditions occurs at
Section A-A (1.18 inches from point of load application).

$$M_{A-A} = (W)(1.18) - R_A(.312)$$

$$M_{A-A} = (200)(1.18) - (304)(.312) = 141 \text{ lb-in}$$

$$T_N = 684 \text{ in-lb} = \text{nut torque}$$

$$P = \frac{T_N}{.2 \text{ d}} = \frac{684}{(.20)(1.276)} = 2680 \text{ lb} = \text{nut preload}$$

$$d_o = 1.3781 \text{ in}$$

$$d_i = 1.110 \text{ in}$$
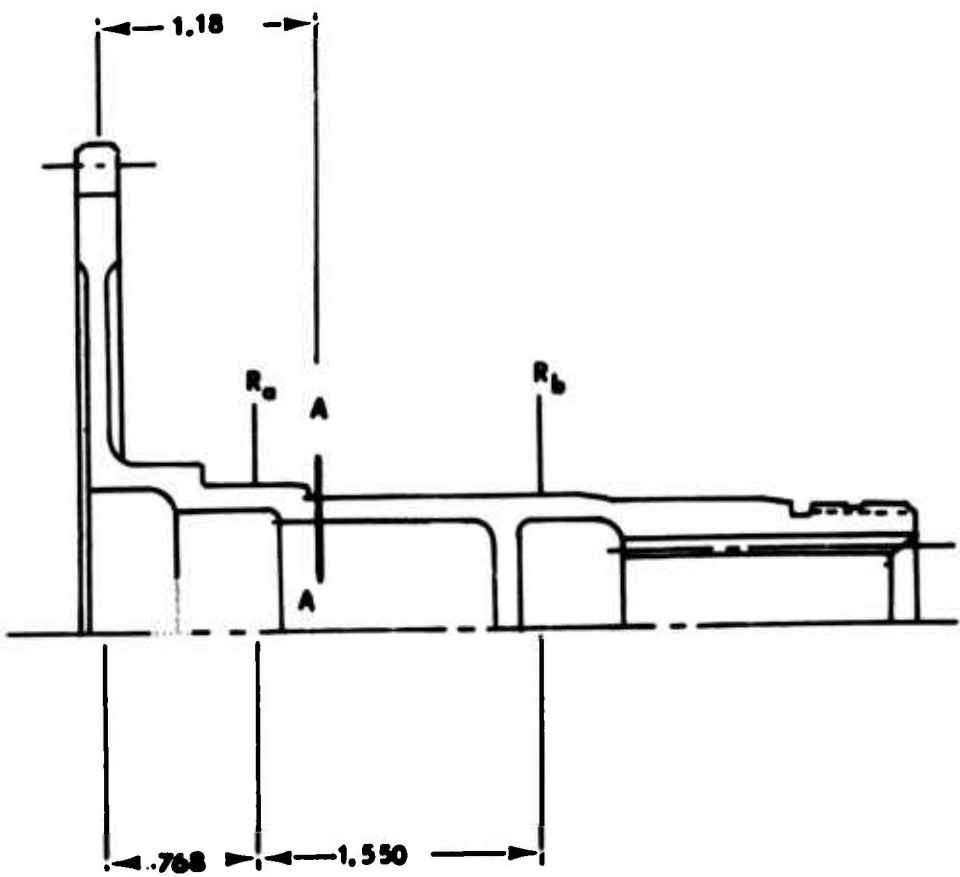
Figure G-2. Gear, Spur, Generator (Left Side).

$$Z = \frac{\pi}{32}\left(\frac{d_o^{\ 4} - d_i^{\ 4}}{d_o}\right) = \frac{\pi}{32}\left(\frac{1.3781^4 - 1.110^4}{1.3781}\right) = 0.1488 \text{ in}^3$$

$$A = \frac{\pi}{4}\left(d_o^{\ 2} - d_i^{\ 2}\right) = \frac{\pi}{4}\left(1.3781^2 - 1.110^2\right) = .525 \text{ in}^2$$

$$f_s = \frac{T}{2\ Z} = \frac{422}{(2)(.1488)} = 1400 \text{ psi}$$

$$f_b = \frac{M}{Z} = \frac{141}{0.1488} = 940 \text{ psi}$$

$$f_a = \frac{P}{A} = \frac{2680}{.525} = 5110 \text{ psi}$$

$$K_t = 2.30$$

$$F_{ty} = 115000 \text{ psi}$$

$$F_{en} = 23300 \text{ psi}$$

$$MS = \frac{1}{\sqrt{\left(\dfrac{f_a}{F_{ty}} + \dfrac{K_t\ f_b}{F_{en}}\right)^2 + 4\left(\dfrac{f_s}{F_{ty}}\right)^2}} - 1$$

$$MS = \frac{1}{\sqrt{\left(\dfrac{5110}{115000} + \dfrac{(2.30)(940)}{23300}\right)^2 + 4\left(\dfrac{1400}{115000}\right)^2}} - 1$$

$$MS = +6.18$$

## GEAR, SPUR, GENERATOR (RIGHT SIDE)

The generator gear shaft is driven by the accessory tail takeoff input gear and provides power to drive the right-hand generator. Figure G-3 illustrates the shaft geometry for the right-side generator shaft.

$$T = \frac{(63025)(HP)}{rpm} = \frac{(63025)(53.6)}{8112.0} = 416 \text{ in } -lb$$

$$W_t = \frac{2\,T}{dg} = \frac{(2)(416)}{4.875} = 171 \text{ lb}$$

$$W = \frac{W_t}{\cos 22\tfrac{1}{2}} = \frac{171}{0.92388} = 185 \text{ lb}$$

The reactions at points A and B are

$$R_A = 237 \text{ lb}$$

$$R_B = 52 \text{ lb}$$

The critical section for fatigue design conditions occurs at Section A-A (1.18 inches from point of load application).

$$M_{A-A} = W\,(1.18) - R_A\,(.312)$$

$$M_{A-A} = (185)(1.18) - (237)(.312) = 144 \text{ lb-in}$$

$$T_N = 685 \text{ in-lb} = \text{nut torque}$$

$$P = \frac{T_N}{(.20)(d)} = \frac{685}{(.20)(1.276)} = 2680 \text{ lb} = \text{nut preload}$$

$$d_o = 1.3781 \text{ in}$$

$$d_i = 1.110 \text{ in}$$
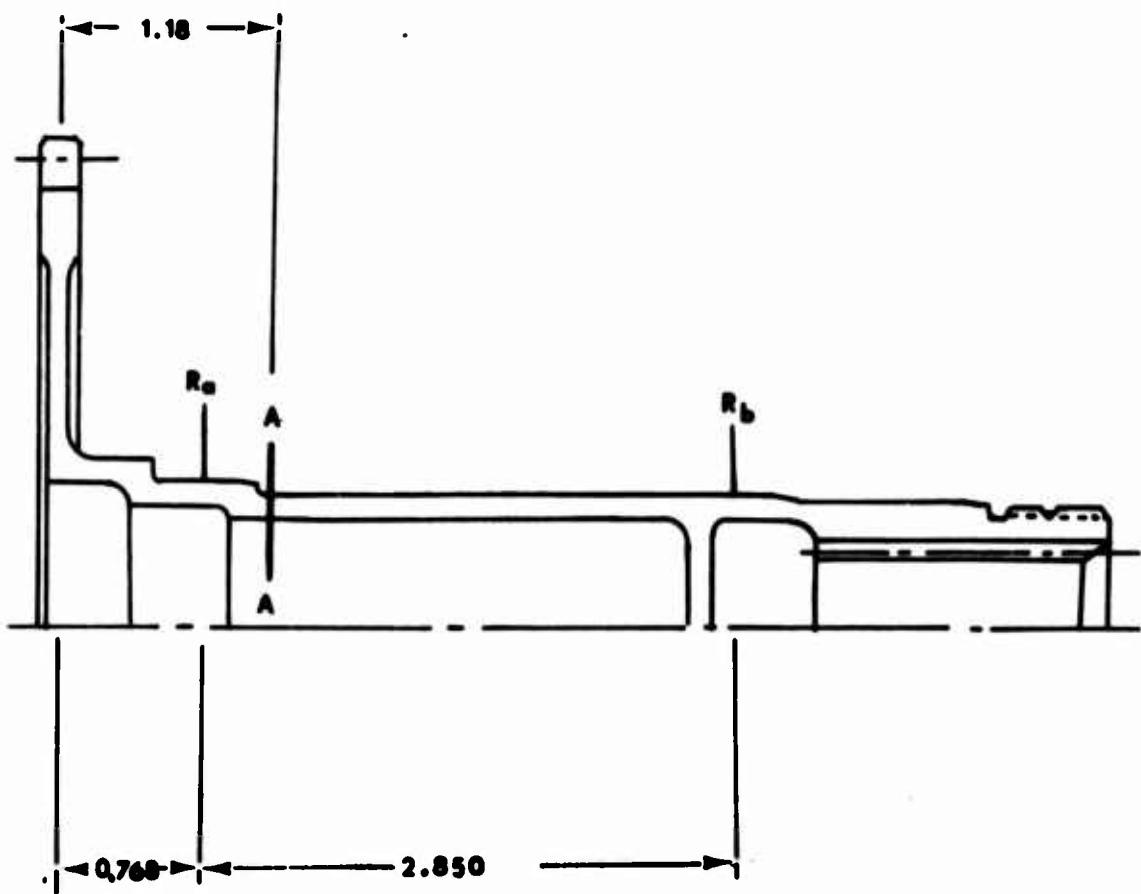
Figure G-3.  Gear, Spur, Generator (Right Side).

$$A = \frac{\pi}{4}(d_o^2 - d_i^2) = \frac{\pi}{4}(1.3781^2 - 1.110^2) = .525 \text{ in}^2$$

$$Z = \frac{\pi}{32}\left(\frac{d_o^4 - d_i^4}{d_o}\right) = \frac{\pi}{32}\left(\frac{1.3781^4 - 1.110^4}{1.3781}\right) = 0.1488 \text{ in}^3$$

$$f_s = \frac{T}{2Z} = \frac{416}{(2)(.1488)} = 1400 \text{ psi}$$

$$f_b = \frac{M}{Z} = \frac{144}{0.1488} = 970 \text{ psi}$$

$$f_a = \frac{P}{A} = \frac{2680}{.525} = 5110 \text{ psi}$$

$$K_t = 2.30$$

$$F_{ty} = 115000 \text{ psi}$$

$$F_{en} = 22900 \text{ psi}$$

$$MS = \frac{1}{\sqrt{\left(\dfrac{f_a}{F_{ty}} + \dfrac{K_t f_b}{F_{en}}\right)^2 + 4\left(\dfrac{f_s}{F_{ty}}\right)^2}} - 1$$

$$MS = \frac{1}{\sqrt{\left(\dfrac{5110}{115000} + \dfrac{(2.30)(970)}{22900}\right)^2 + 4\left(\dfrac{1400}{115000}\right)^2}} - 1$$

$$MS = +5.94$$

## GEAR, SPUR, AUXILIARY SERVO PUMP

The auxiliary servo pump gear is driven by the utility pump gear
and in turn, drives the left-side generator and auxiliary hydraulic pump.
The auxiliary servo pump spur gear is identical to the utility hydraulic
pump gear and is illustrated by Figure G-4. Figure G-5 is a sketch of
the applied gear loads and reactions for the auxiliary servo pump gear.
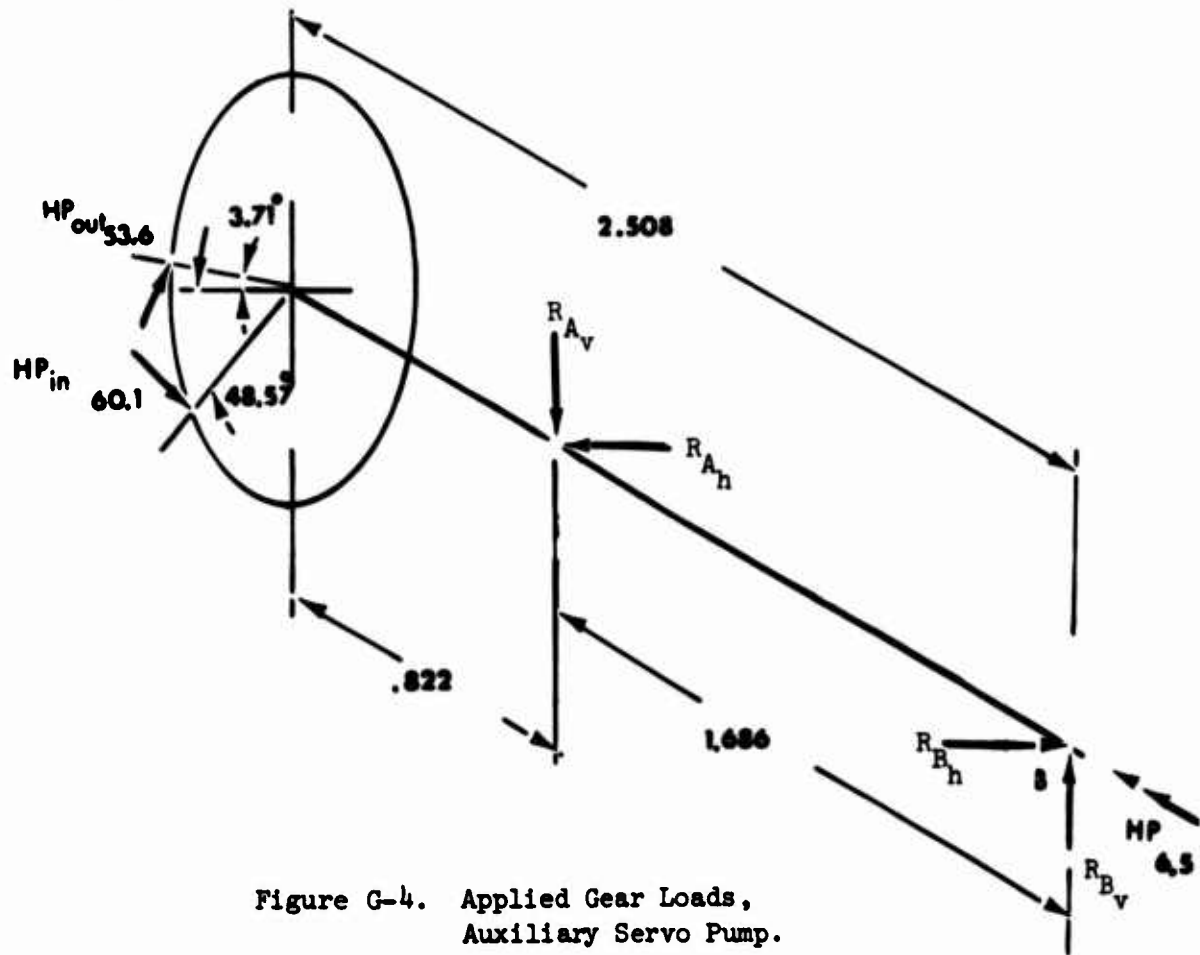


Figure G-4.  Applied Gear Loads,
Auxiliary Servo Pump.

$$T_{in} = \frac{63025 \; HP}{rpm} = \frac{(63025)(60.1)}{4005} = 945 \; in\text{-}lb$$

$$W_{tin} = \frac{T_{in}(2)}{dg} = \frac{(945)(2)}{9.0} = 210 \; lb$$

$$W_{rin} = W_{tin} \tan 20^{o} = (210)(0.36397) = 76 \; lb$$

321
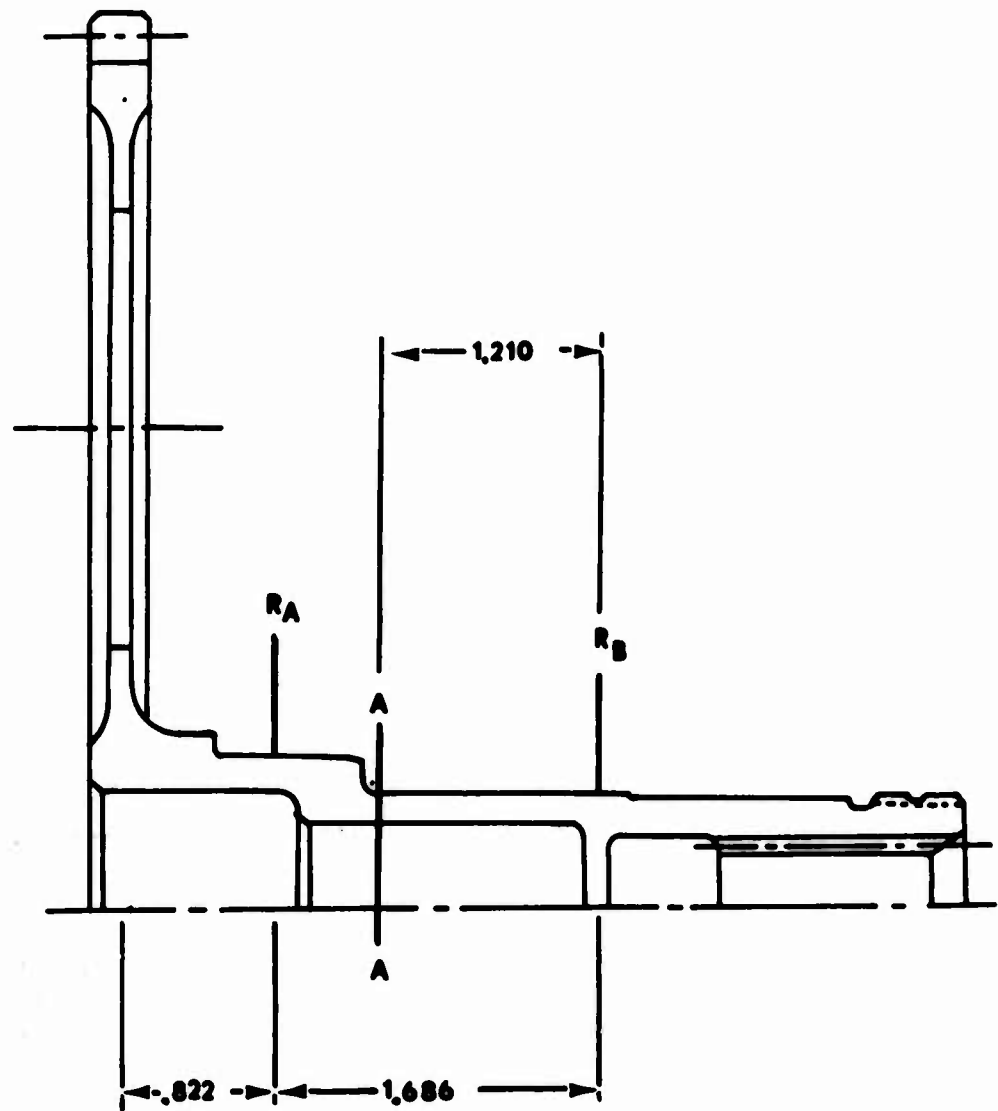
Figure G-5.  Gear, Spur, Auxiliary Servo Pump.

$$T_{out} = \frac{(63025)(HP)}{rpm} = \frac{(63025)(53.6)}{4005} = 843 \text{ in -lb}$$

$$W_{t_{out}} = \frac{T_{out}(2)}{dg} = \frac{(843)(2)}{9.0} = 187 \text{ lb}$$

$$W_{r_{out}} = W_{t_{out}} \tan 20^{\circ} = (187)(0.36397) = 68 \text{ lb}$$

From a static analysis of the shaft, the reactions at A and B are

$$R_{Av} = 150 \text{ lb}$$

$$R_{Ah} = 429 \text{ lb}$$

$$R_{Bv} = 49 \text{ lb}$$

$$R_{Bh} = 141 \text{ lb}$$

The critical section occurs at A-A (1.298 inches from point of load application) where

$$M_{A-A_v} = 59 \text{ lb-in}$$

$$M_{A-A_h} = 170 \text{ lb-in}$$

$$M_{A-A} = \sqrt{M_{A-A_v}^2 + M_{A-A_h}^2} = \sqrt{59.0^2 + 170^2} = 181 \text{ lb-in}$$

$$T_N = 102 \text{ lb-in}$$

$$P = \frac{T_N}{.2 \, d} = \frac{591}{(.20)(1.173)} = 2510 \text{ lb} = \text{nut preload}$$

323

$d_o$ = 1.1812 in

$d_i$ = 0.900 in

$Z$ = $\frac{\pi}{32}\left(\frac{d_o^4 - d_i^4}{d_o}\right)$ = $\frac{\pi}{32}\left(\frac{1.1812^4 - 0.90^4}{1.1812}\right)$ = 0.1073 in$^3$

$A$ = $\frac{\pi}{4}(d_o^2 - d_i^2)$ = $\frac{\pi}{4}(1.1812^2 - 0.90^2)$ = 0.458 in$^2$

$f_s$ = $\frac{T}{2Z}$ = $\frac{102}{(2)(.1073)}$ = 480 psi

$f_b$ = $\frac{M}{Z}$ = $\frac{181}{0.1073}$ = 1680 psi

$f_a$ = $\frac{P}{A}$ = $\frac{2510}{.458}$ = 5460 psi

$K_t$ = 2.3

$F_{en}$ = 23100 psi

$F_{ty}$ = 115000 psi

$MS$ = $\dfrac{1}{\sqrt{\left(\dfrac{f_a}{F_{ty}} + \dfrac{K_t\, f_b}{F_{en}}\right)^2 + 4\left(\dfrac{f_s}{F_{ty}}\right)^2}}$ $-1$

$MS$ = $\dfrac{1}{\sqrt{\left(\dfrac{5460}{115000} + \dfrac{(2.3)(1680)}{23100}\right)^2 + 4\left(\dfrac{480}{115000}\right)^2}}$ $-1$

$MS$ = + 3.65

## GEAR, SPUR, UTILITY HYDRAULIC PUMP

The utility hydraulic pump gear shaft is driven by the lubrication pump gear and in turn drives the auxiliary hydraulic pump gear as well as provides power to drive the utility hydraulic pump. Figure G-6 is a sketch of the applied gear loads and reactions, while Figure G-5 illustrates the geometry for the utility hydraulic pump shaft.
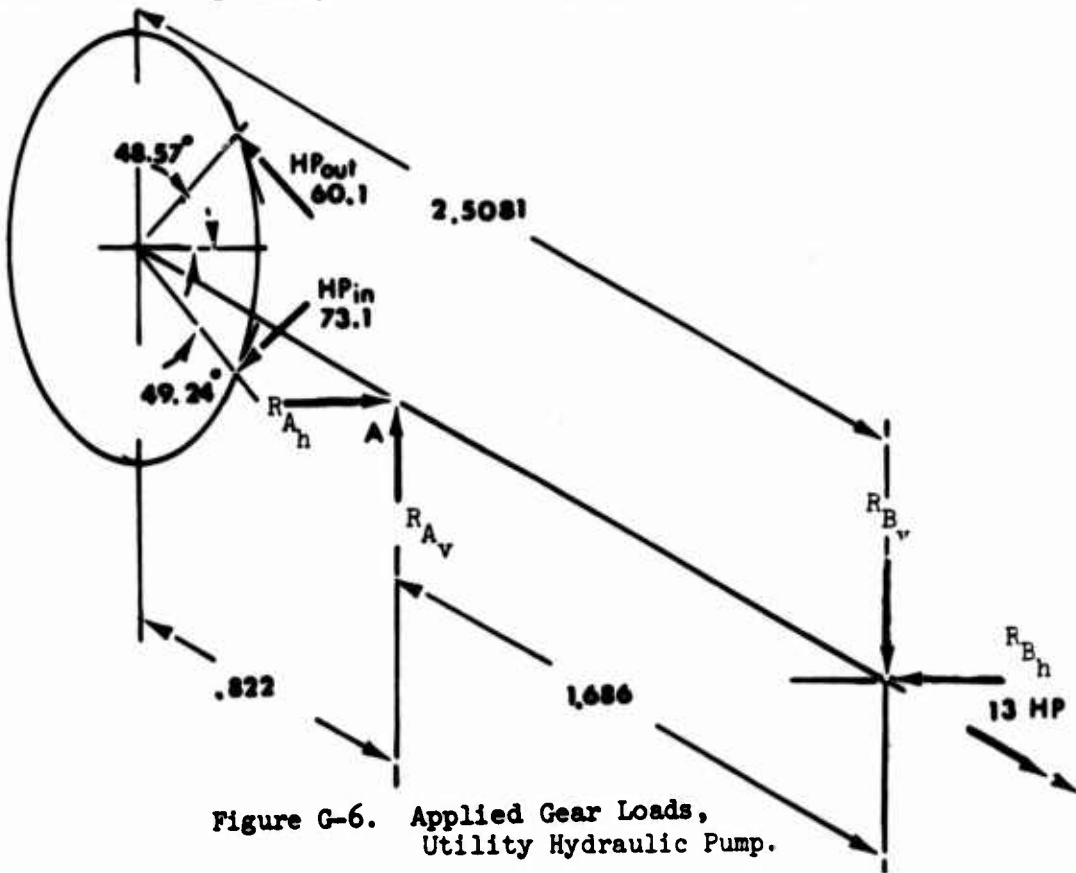


Figure G-6. Applied Gear Loads, Utility Hydraulic Pump.

$$T_{in} = \frac{(63025)(HP)}{rpm} = \frac{(63025)(73.1)}{4005} = 1150 \text{ in -lb}$$

$$W_{t_{in}} = \frac{2T_{in}}{dg} = \frac{2(1150)}{9.000} = 255 \text{ lb}$$

$$W_{r_{in}} = W_{t_{in}} \tan 20^\circ = (255)(.36397) = 93 \text{ lb}$$

325

$$T_{out} = \frac{(63025)(HP)}{rpm} = \frac{(63025)(60.1)}{4005} = 945 \text{ in -lb}$$

$$W_{t_{out}} = \frac{2\ T_{out}}{D} = \frac{2(945)}{9.0} = 210 \text{ lb}$$

$$W_{r_{out}} = W_{t_{out}} \tan 20^{o} = (210)(.36397) = 76 \text{ lb}$$

$$T_{spl} = \frac{(63025)(HP)}{rpm} = \frac{(63025)(13)}{4005} = \mathbf{205} \text{ in - lb}$$

From a static analysis of the load system as shown in Figure G-6, the reactions at A and B are

$$R_{Av} = 22.0 \text{ lb}$$

$$R_{Ah} = 688 \text{ lb}$$

$$R_{Bv} = 7.0 \text{ lb}$$

$$R_{Bh} = 225 \text{ lb}$$

The critical section for fatigue design conditions occurs at Section A-A (1.210 inches from the reaction at B) where

$$M_{A} = \sqrt{(1.210\ R_{Bh})^2 + (1.210\ R_{Bv})^2}$$

$$M_{A} = \sqrt{\left[1.210(225)\right]^2 + \left[1.210(7)\right]^2}$$

$$M_{A} = 272 \text{ lb-in}$$

$$T_N \quad = \quad 591 \text{ in -lb} = \text{nut torque}$$

$$P \quad = \quad \frac{T_N}{.2 \ d} \quad = \quad \frac{591}{(.2)(1.173)} \quad = \quad 2510 \text{ lb - nut preload}$$

$$d_o \quad = \quad 1.1812 \text{ in}$$

$$d_i \quad = \quad 0.900 \text{ in}$$

$$A \quad = \quad \frac{\pi}{4} \ (d_o^2 - d_i^2) \quad = \quad \frac{\pi}{4} \ (1.1812^2 - 0.90^2) \quad = \quad .458 \text{ in}^2$$

$$Z \quad = \quad \frac{\pi}{32} \left( \frac{d_o^4 - d_i^4}{d_o} \right) = \quad \frac{\pi}{32} \left( \frac{1.1812^4 - 0.900^4}{1.1812} \right) = \quad 0.1073 \text{ in}^3$$

$$f_a \quad = \quad \frac{P}{A} \quad = \quad \frac{2510}{.458} \quad = \quad 5460 \text{ psi}$$

$$f_s \quad = \quad \frac{T}{2 \ Z} \quad = \quad \frac{205}{(2)(0.1073)} \quad = \quad 960 \text{ psi}$$

$$f_b \quad = \quad \frac{M}{Z} \quad = \quad \frac{272}{0.1073} \quad = \quad 2550 \text{ psi}$$

$$K_t \quad = \quad 2.3$$

$$F_{en} \quad = \quad 23100 \text{ psi}$$

$$F_{ty} \quad = \quad 115000 \text{ psi}$$

$$MS \quad = \quad \frac{1}{\sqrt{\left( \dfrac{f_a}{F_{ty}} + \dfrac{K_t \ f_b}{F_{en}} \right)^2 + 4 \left( \dfrac{f_s}{F_{ty}} \right)^2}} \quad -1$$

$$MS \quad = \quad \frac{1}{\sqrt{\left( \dfrac{5460}{115000} + \dfrac{(2.3)(2550)}{23100} \right)^2 + 4 \left( \dfrac{960}{115000} \right)^2}} \quad -1$$

$$MS \quad = \quad +2.31$$

## GEAR, SPUR, LUBRICATION PUMP

The lubrication pump gear is driven by accessory tail takeoff gear and in turn drives the utility pump gear and the lubrication pump. Figure G-7 is a sketch of the applied gear loads and reactions, while Figure G-8 illustrates the geometry of the lubrication pump shaft.
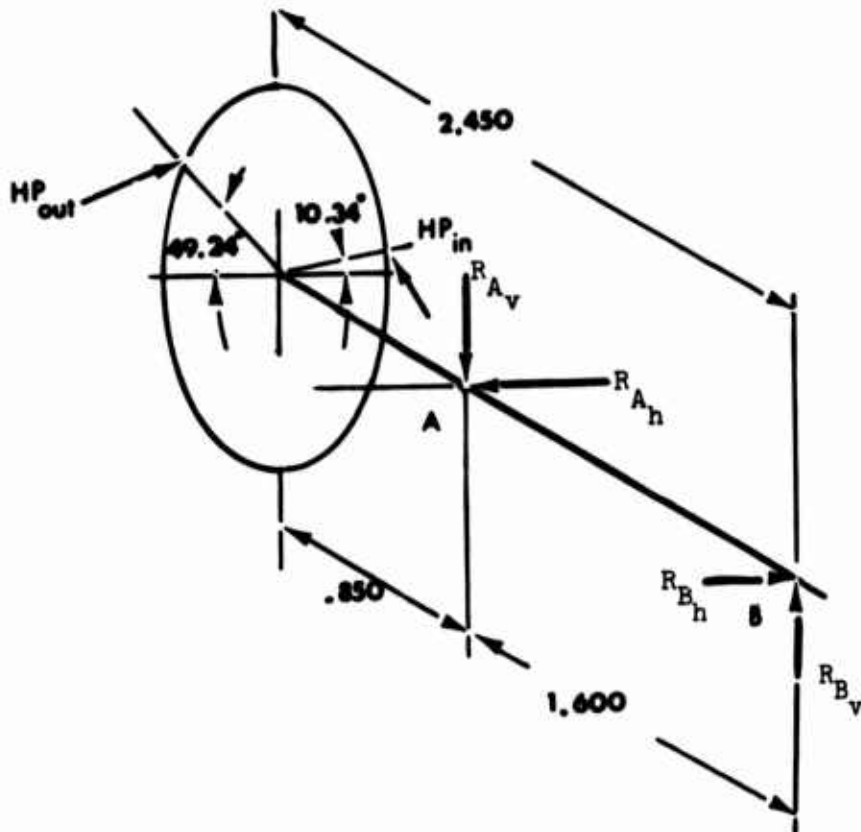


Figure G-7. Applied Gear Loads, Lubrication Pump.

$$T_{in} = \frac{63025 \; HP_{in}}{rpm} = \frac{63025 \; (77)}{5149} = 943 \; in\text{-}lb$$

$$W_{t_{in}} = \frac{T_{in}(2)}{dg} = \frac{(943)(2)}{7.0} = 270 \; lb$$

$$W_{r_{in}} = W_{t_{in}} \; \tan 20^{\circ} = (270)(.36397) = 98 \; lb$$
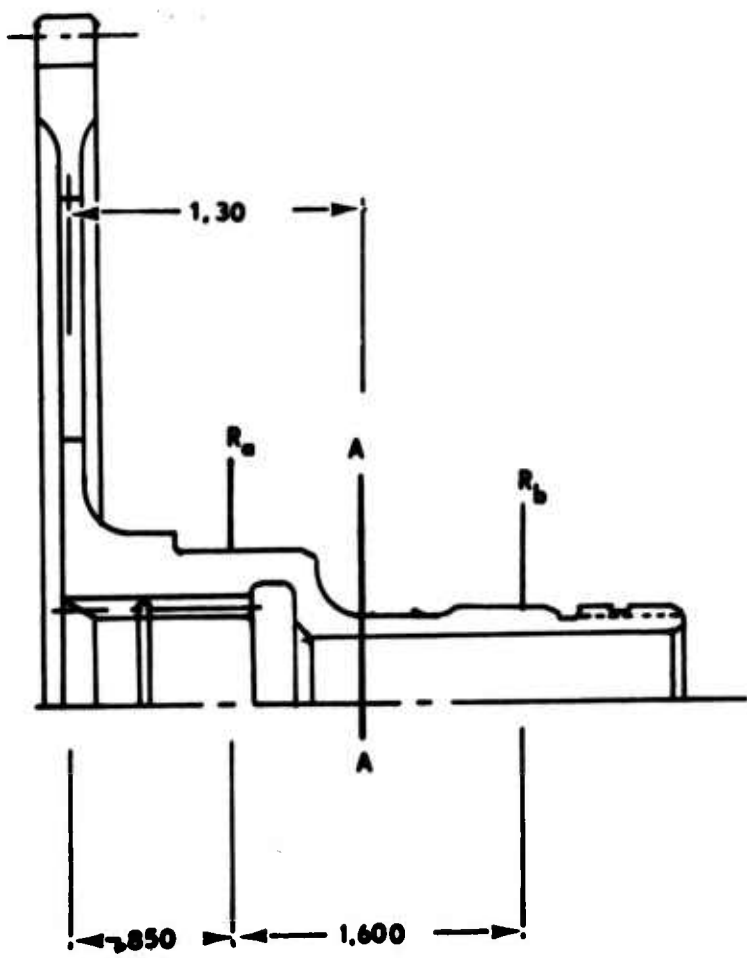
Figure G-8.  Gear, Spur, Lubrication Pump.

$$T_{out} = \frac{63025 \ HP_{out}}{rpm} = \frac{(63025)(73)}{5149} = 894 \ in{-}lb$$

$$W_{t_{out}} = \frac{T_{out} \ (2)}{Dia} = \frac{(894)(2)}{7.0} = 256 \ lb$$

$$W_{r_{out}} = W_{t_{out}} \ tan \ 20^o = (256)(.36397) = 93.0 \ lb$$

$$T_{spline} = \frac{63025 \ HP_{pump}}{rpm} = \frac{(63025)(4.0)}{5149} = 50 \ in{-}lb$$

From a static analysis of the shaft the reactions at A and B are

$$R_{Ah} = 168 \ lb \qquad\qquad R_{Bh} = 58 \ lb$$

$$R_{Av} = 527 \ lb \qquad\qquad R_{Bv} = 183 \ lb$$

The critical section for fatigue design conditions occurs at Section A-A (1.300 inches from point of load application) where

$$M_{A{-}A_h} = 67 \ lb{-}in$$

$$M_{A{-}A_v} = 211 \ lb{-}in$$

$$M = \sqrt{M_{A{-}A_h}^{\ 2} + M_{A{-}A_v}^{\ 2}} = \sqrt{67^2 + 211^2} = 221 \ lb{-}in$$

$$T = 49 \ in{-}lb$$

$$P = \frac{T_p}{.2d} = \frac{400}{(.20)(.969)} = 2070 \ lb = nut \ preload$$

330

$$d_o = .914 \text{ in}$$

$$d_i = .698 \text{ in}$$

$$Z = \frac{\pi}{32}\left(\frac{d_o^4 - d_i^4}{d_o}\right) = \frac{\pi}{32}\left(\frac{.914^4 - .698^4}{.914}\right) = 0.04945 \text{ in}^3$$

$$A = \frac{\pi}{4}(d_o^2 - d_i^2) = \frac{\pi}{4}(.914^2 - .698^2) = .277 \text{ in}^2$$

$$f_s = \frac{T}{2Z} = \frac{49}{(2)(.04945)} = 494 \text{ psi}$$

$$f_b = \frac{M}{Z} = \frac{221}{0.04945} = 4466 \text{ psi}$$

$$f_a = \frac{P}{A} = \frac{2070}{.277} = 7500 \text{ psi}$$

$$K_t = 1.42$$

$$F_{en} = 22700 \text{ psi}$$

$$F_{ty} = 115000 \text{ psi}$$

$$MS = \frac{1}{\sqrt{\left(\dfrac{f_a}{F_{ty}} + \dfrac{K_t\, f_b}{F_{en}}\right)^2 + 4\left(\dfrac{f_s}{F_{ty}}\right)^2}} - 1$$

$$MS = \frac{1}{\sqrt{\left(\dfrac{7500}{115000} + \dfrac{(1.42)(4466)}{22700}\right)^2 + 4\left(\dfrac{494}{115000}\right)^2}} - 1$$

$$MS = +1.90$$

## SHAFT, QUILL, LUBRICATION PUMP DRIVE

The lubrication pump quill shaft transmits power between the lubrication pump gear and the lubrication pump. Figure G-9 is an illustration of the lubrication pump quill shaft with the critical section at A-A.
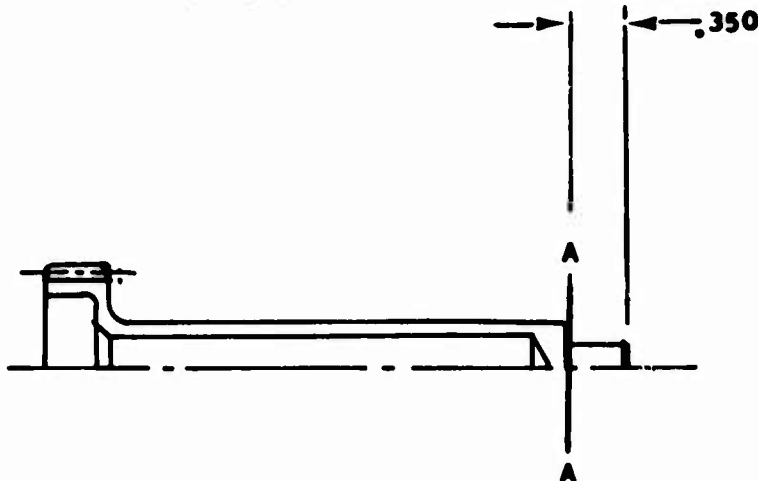


Figure G-9. Shaft, Quill, Lubrication Pump Drive.

$$T = \frac{63025 \; HP}{rpm} = \frac{(63025)(4)}{5149} = 50 \; in -lb$$

For a square section subjected to torsion

$$f_s = \frac{T}{a \, b \, h}$$

where $a = 0.208$

$$f_s = \frac{50}{(0.208)(0.273)(0.273^2)} = 11800 \; psi$$

$$F_{ty} = 115000 \; psi$$

$$MS = \frac{F_{ty}}{(1.15)(2 \, f_s)} - 1 = \frac{115000}{(1.15)(2)(11800)} - 1$$

$$= +3.23$$

332

## GEAR, SPUR, TAIL TAKEOFF

The tail takeoff input spur gear is driven by the quill shaft of the tail
takeoff bevel gear and in turn drives the right-side generator gear, the
tachometer generator gear, the primary hydraulic pump gear, the accessory
tail takeoff output, and the oil cooler driveshaft. Figure G-10 is a
sketch of the applied gear loads and reactions, while Figure G-11
illustrates the geometry for the tail takeoff input shaft.
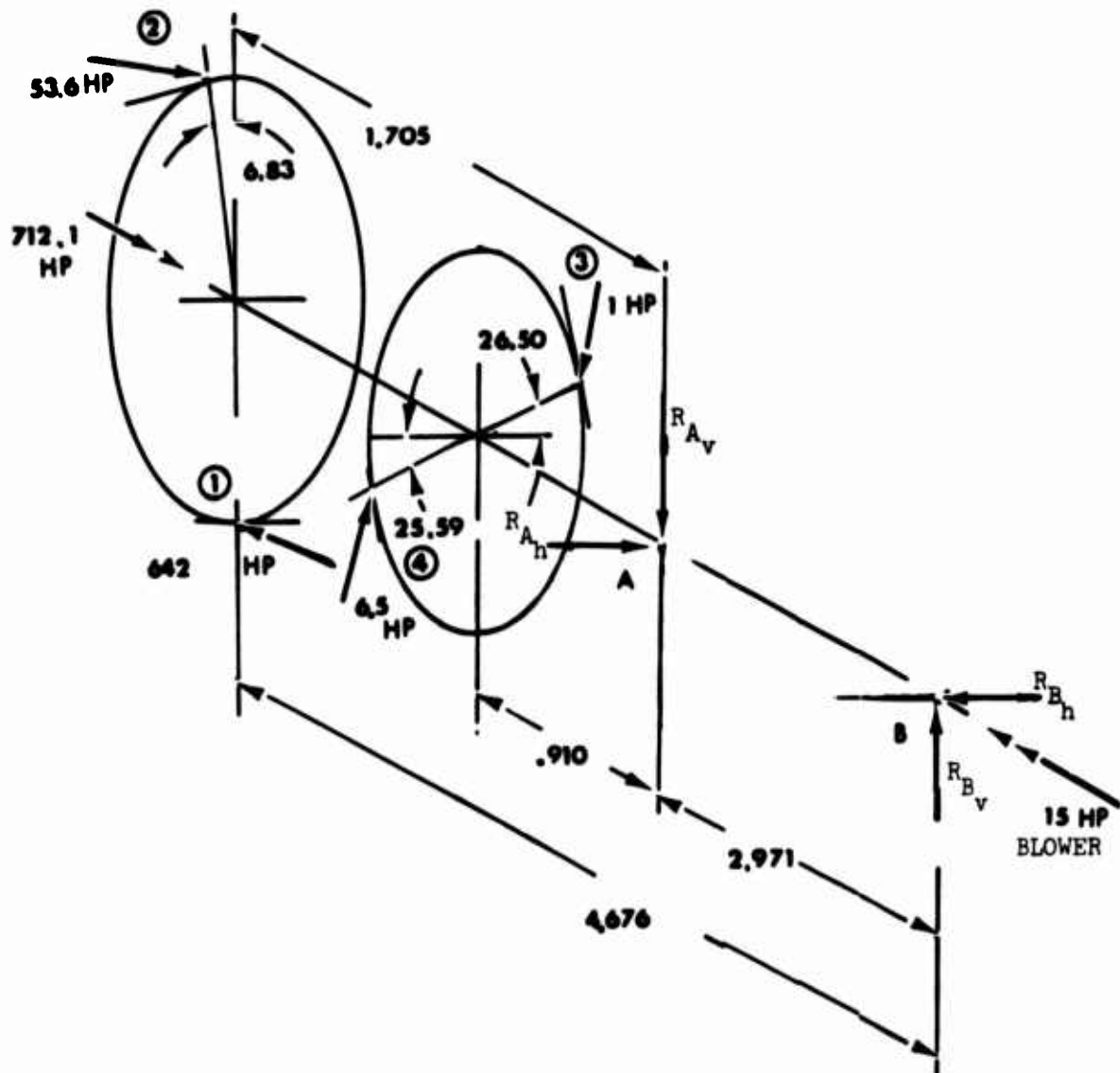


Figure G-10. Applied Gear Loads, Tail Takeoff Input.
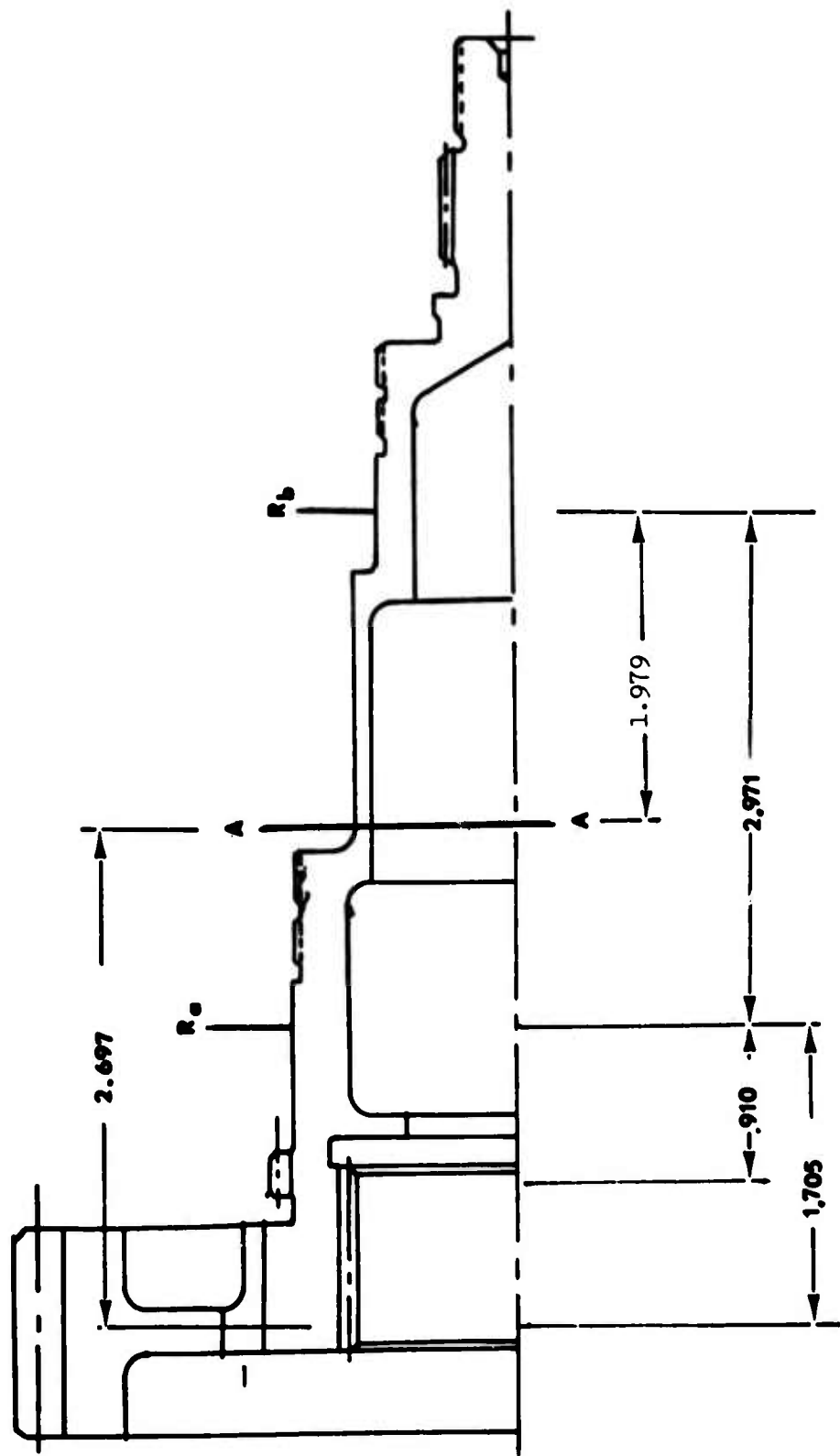
Figure G-11. Shaft, Spur, Tail Takeoff Input.

From a static analysis of Figure G-11, the reaction at A and B are

$$R_{A_v} = 1290 \text{ lb}$$

$$R_{B_v} = 466 \text{ lb}$$

$$R_{A_h} = 3210 \text{ lb}$$

$$R_{B_h} = 1170 \text{ lb}$$

The critical section for fatigue design conditions occurs at
Section A-A (1.979 inches from the reaction at B)

where

$$M_h = 1.979 \, R_{B_h} = 1.979 \, (1170) = 2320 \text{ lb-in}$$

$$M_v = 1.979 \, R_{B_v} = 1.979 \, (466) = 920 \text{ lb-in}$$

$$M = \sqrt{M_h^2 + M_v^2} \qquad \sqrt{2320^2 + 920^2} = 2490 \text{ lb-in}$$

$$d_o = 1.815 \text{ in}$$

$$d_i = 1.615 \text{ in}$$

$$Z = \frac{\pi}{32} \left( \frac{d_o^4 - d_i^4}{d_o} \right) = \frac{\pi}{32} \left( \frac{1.815^4 - 1.615^4}{1.815} \right) = 0.2191 \text{ in}^3$$

$$f_s = \frac{T}{2 \, Z} = \frac{134}{(2)(0.2191)} = 307 \text{ psi}$$

$$f_t = \frac{M}{Z} = \frac{2490}{0.2191} = 11375 \text{ psi}$$

$$T_1 \quad = \quad \frac{63025 \text{ HP}}{\text{rpm}} \quad = \quad \frac{63025 \, (642)}{7031} \quad = \quad 5740 \text{ in -lb}$$

$$W_{t_1} \quad = \quad \frac{T_1 \, (2)}{d} \quad = \quad \frac{5740 \, (2)}{5.625} \quad = \quad 2050 \text{ lb}$$

$$W_{r_1} \quad = \quad W_{t_1} \tan 22.5^{\circ} \quad = \quad 2050 \, (.41421) \quad = \quad 847 \text{ lb}$$

$$T_2 \quad = \quad \frac{63025 \text{ HP}_2}{\text{rpm}} \quad = \quad \frac{63025 \, (53.6)}{7031} \quad = \quad 480 \text{ in -lb}$$

$$W_{t_2} \quad = \quad \frac{T_2 \, (2)}{d} \quad = \quad \frac{480 \, (2)}{5.625} \quad = \quad 171 \text{ lb}$$

$$W_{r_2} \quad = \quad W_{t_2} \tan 22.5^{\circ} \quad = \quad 171 \, (0.41421) \quad = \quad 71 \text{ lb}$$

$$T_3 \quad = \quad \frac{63025 \text{ HP}_3}{\text{rpm}} \quad = \quad \frac{63025 \, (1.0)}{7031} \quad = \quad 9.0 \text{ in-lb}$$

$$W_{t_3} \quad = \quad \frac{T_3 \, (2)}{d} \quad = \quad \frac{9.0 \, (2)}{4.0} \quad = \quad 4.5 \text{ lb}$$

$$W_{r_3} \quad = \quad W_{t_3} \tan 22.5^{\circ} \quad = \quad 4.5 \, (0.41421) \quad = \quad 1.9 \text{ lb}$$

$$T_4 \quad = \quad \frac{63025 \text{ HP}}{\text{rpm}} \quad = \quad \frac{63025 (6.5)}{7031} \quad = \quad 58. \text{in -lb}$$

$$W_{t_4} \quad = \quad \frac{T_4 \, (2)}{d} \quad = \quad \frac{58 \, (2)}{4.0} \quad = \quad 29 \text{ lb}$$

$$W_{r_4} \quad = \quad W_{t_4} \tan 22.5^{\circ} \quad = \quad 29 \, (0.41421) \quad = \quad 12 \text{ lb}$$

$$T_{cooler} = \quad \frac{63025 \; \text{HP}_{blower}}{\text{rpm}} \quad = \quad \frac{63025 \, (15)}{7031} \quad = \quad 134 \text{ in -lb}$$

336

$$K_t \quad = \quad 1.35$$

$$F_{en} \quad = \quad 21800 \text{ psi}$$

$$F_{ty} \quad = \quad 115000 \text{ psi}$$

$$MS \quad = \quad \frac{1}{\sqrt{\left(\dfrac{K_t \ f_b}{F_{en}}\right)^2 + 4\left(\dfrac{f_s}{F_{ty}}\right)^2}} \quad -1$$

$$MS \quad = \quad \frac{1}{\sqrt{\left(\dfrac{1.35 \ (11375)}{218000}\right)^2 + 4\left(\dfrac{307}{115000}\right)^2}} \quad -1$$

$$MS \quad = \quad +.41$$

## SHAFT, GEAR, TAIL TAKEOFF

The tail takeoff gear shaft receives power from the tail takeoff input
and transmits power to the lubrication pump, auxiliary pump, utility pump,
generator, and adapter gearbox input as well as provides a torque path
for the rotor brake.

Figure G-12 is a sketch of the applied gear loads and reactions, while
Figure G-13 illustrates the shaft geometry for the tail takeoff spur gear.
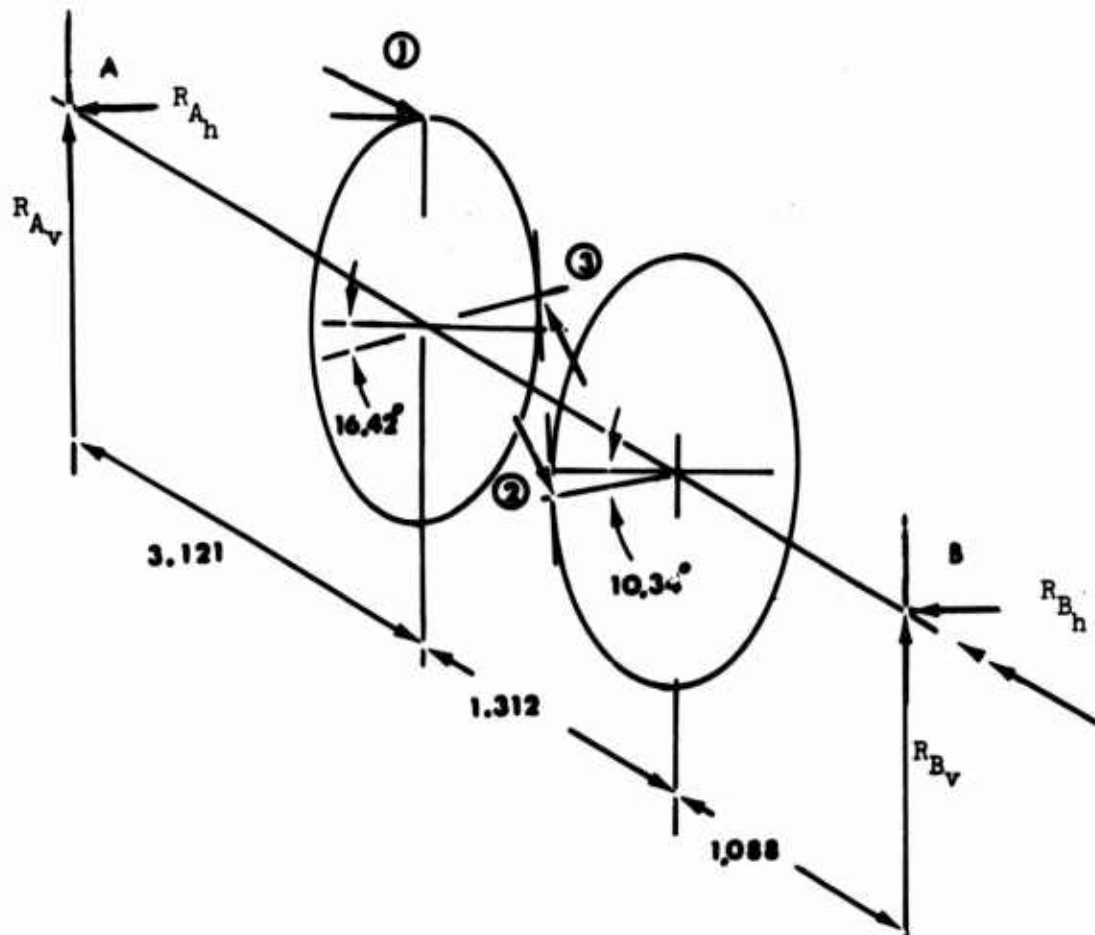


Figure G-12.   Applied Tail Takeoff Shaft Loads.
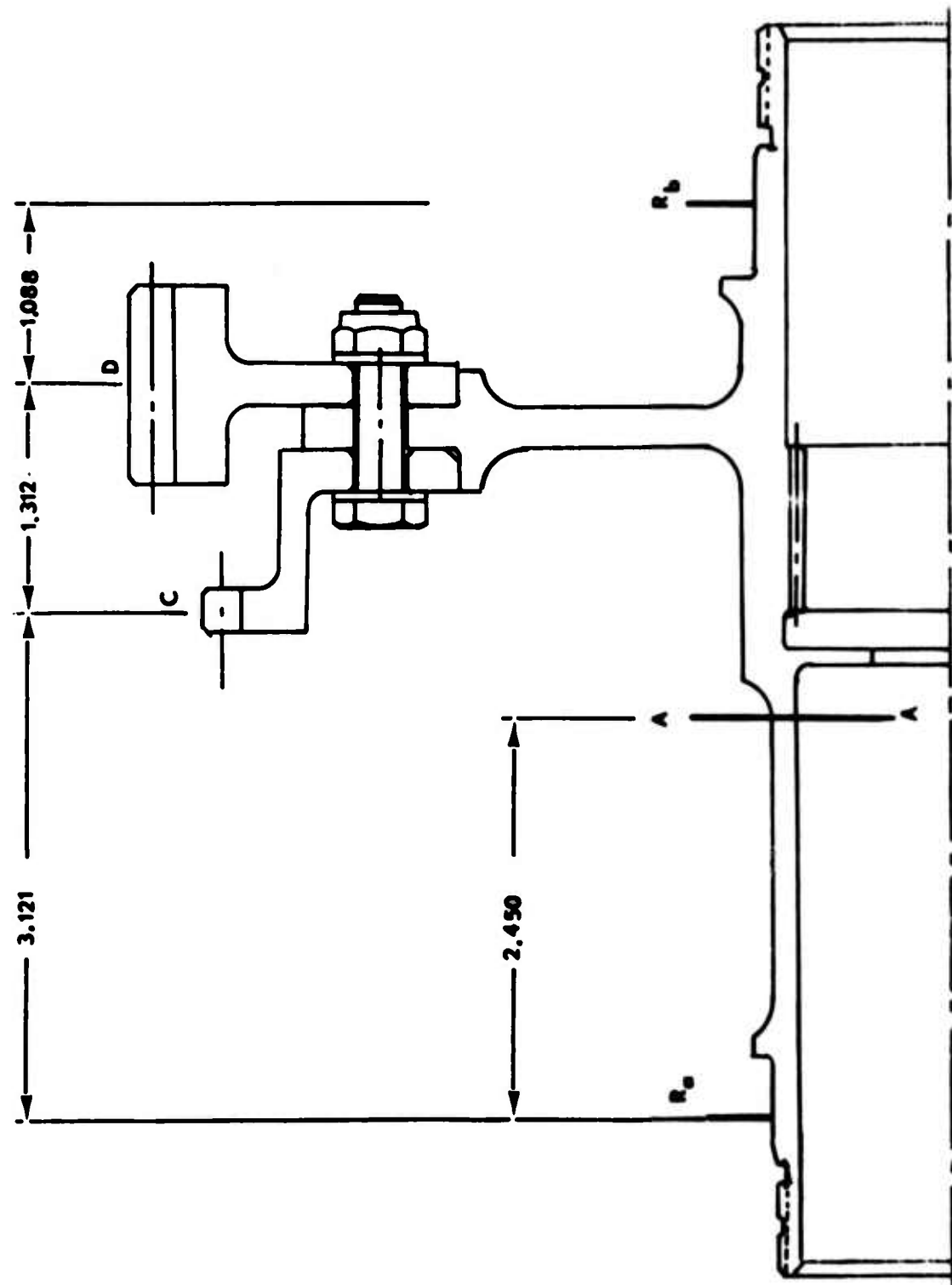
Figure G-13.  Shaft, Gear, Tail Takeoff.

339

Two design conditions exist: normal operation (power to tail rotor, no rotor brake application) and rotor brake application (rotor brake applied, no power to tail rotor). The highest stresses are induced in this shaft during normal operation.

### Normal Operation

| | | | | | |
|---|---|---|---|---|---|
| $T_1$ | = 10100 in-lb | $W_{t_1}$ | = 2050 lb | $W_{r_1}$ | = 847 lb |
| $T_2$ | = 1213 in-lb | | | | |
| $T_3$ | = 0.0 in-lb | $W_{t_2}$ | = 270 lb | $W_{r_2}$ | = 98 lb |
| $T_{TTO}$ | = 8890 in-lb | $W_{t_3}$ | = 0 | $W_{r_3}$ | = 0 |

### Rotor Brake Application

| | | | | | |
|---|---|---|---|---|---|
| $T_1$ | = 14190 in-lb | $W_{t_1}$ | = 2874 lb | $W_{r_1}$ | = 1190 lb |
| $T_2$ | = 1213 in-lb | $W_{t_2}$ | = 270 lb | $W_{r_2}$ | = 98 lb |
| $T_3$ | = 11990 in-lb | | | | |
| $T_{TTO}$ | = 0 | $W_{t_3}$ | = 2427 lb | $W_{r_3}$ | = 1014 lb |

From a static analysis of Figure G-13, the reactions at points A and B are

$$R_{Av} = 60 \text{ lb}$$

$$R_{Ah} = 467 \text{ lb}$$

$$R_{Bv} = 541 \text{ lb}$$

$$R_{Bh} = 1725 \text{ lb}$$

The critical section for fatigue design conditions occurs at
Section A-A (2.45 inches from reaction A) under normal operation.
Operation.

$$M_{A-A} = \sqrt{\left(R_{Ah}\, 2.45\right)^2 + \left(R_{Av}\, 2.45\right)^2}$$

$$M_{A-A} = \sqrt{\left[60(2.45)\right]^2 + \left[467\,(2.45)\right]^2} = 1152 \text{ lb-in}$$

$$d_o = 2.115 \text{ in}$$

$$d_i = 1.853 \text{ in}$$

$$Z = \frac{\pi}{32}\left(\frac{d_o^4 - d_i^4}{d_o}\right) = \frac{\pi}{32}\left(\frac{2.115^4 - 1.853^4}{2.115}\right) = 0.3816 \text{ in}^3$$

$$f_b = \frac{M}{Z} = \frac{1152}{0.3816} = 3020 \text{ psi}$$

$$K_t = 1.72$$

$$F_{ty} = 115000 \text{ psi}$$

$$F_{en} = 21900 \text{ psi}$$

$$MS = \frac{F_{en}}{K_t\, f_b} - 1 = \frac{21900}{(1.72)(3020)} - 1 = +3.21$$

## GEAR, SPUR, PRIMARY SERVO PUMP

The primary servo pump spur gear is driven by the tail takeoff input gear and in turn drives the primary servo pump. Figure G-14 illustrates the primary servo pump gear and shaft geometry and reactions.

$$T = \frac{63025 \text{ HP}}{\text{rpm}} = \frac{(63025)(6.5)}{4197} = 97 \text{ in -lb}$$

$$W_t = \frac{2T}{dg} = \frac{(2.0)(97)}{6.7} = 29 \text{ lb}$$

$$W = \frac{W_t}{\cos \emptyset} = \frac{29}{.92388} = 32 \text{ lb}$$

Determining the reactions at A and B,

$$R_A = 47 \text{ lb}$$

$$R_B = 15 \text{ lb}$$

The critical section for fatigue design conditions occurs at Section A-A (1.30 inches from the applied load). This section is subjected to fatigue bending, steady torsion and steady axial stress (from nut preload). At this section

$$M_{A-A} = W(1.30) - R_A (.478)$$

$$M_{A-A} = (32)(1.30) - (47)(.478) = 18 \text{ lb-in}$$

The nut preload is found from

$$P = \frac{T_N}{(.2)(d)} = \frac{591}{(.2)(1.173)} = 2510 \text{ lb} = \text{nut preload}$$

$$d_o = 1.1812 \text{ in}$$

$$d_i = .900 \text{ in}$$
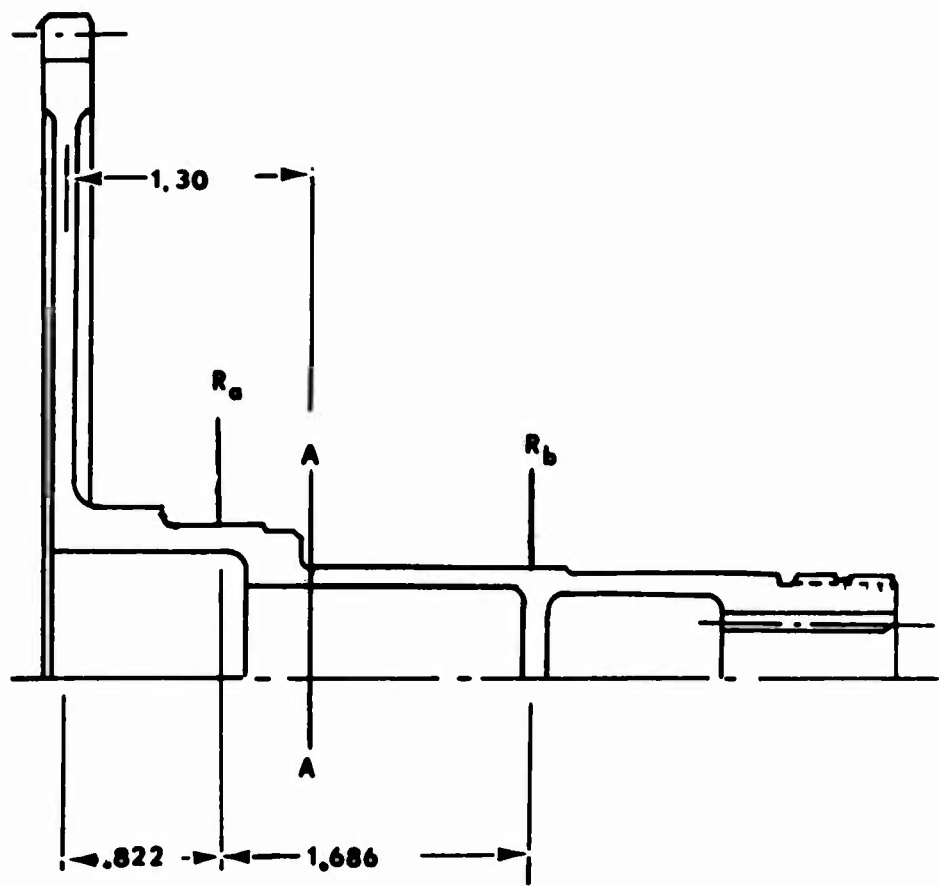
Figure G-14.  Gear, Spur, Primary Hydraulic Pump.

$$A = \frac{\pi}{4}(d_o^2 - d_i^2) = \frac{\pi}{4}(1.1812^2 - .900^2) = 0.458 \text{ in}^2$$

$$Z = \frac{\pi}{32}\left(\frac{d_o^4 - d_i^4}{d_o}\right) = \frac{\pi}{32}\left(\frac{1.1812^4 - .900^4}{1.1812}\right) = 0.1073 \text{ in}^3$$

$$f_a = \frac{P}{A} = \frac{2510}{.448} = 5480 \text{ psi}$$

$$f_b = \frac{M}{Z} = \frac{18.}{0.1073} = 165 \text{ psi}$$

$$f_s = \frac{T}{2Z} = \frac{97}{(2)(0.1073)} = 455 \text{ psi}$$

$$K_t = 2.45$$

$$F_{ty} = 115000 \text{ psi}$$

$$F_{en} = 23100 \text{ psi}$$

$$MS = \frac{1}{\sqrt{\left(\dfrac{f_a}{F_{ty}} + \dfrac{K_t \, f_b}{F_{en}}\right)^2 + 4\left(\dfrac{f_s}{F_{ty}}\right)^2}} - 1$$

$$MS = \frac{1}{\sqrt{\left(\dfrac{5480}{115000} + \dfrac{(2.45)(165)}{23100}\right)^2 + 4\left(\dfrac{455}{115000}\right)^2}} - 1$$

$$MS = + \text{ high}$$

## SHAFT, TACHOMETER DRIVE

The tachometer drive gear is driven by the accessory tail takeoff input
and provides power to drive the tachometer generator.  Figure G-15
illustrates the geometry for the tachometer driveshaft.
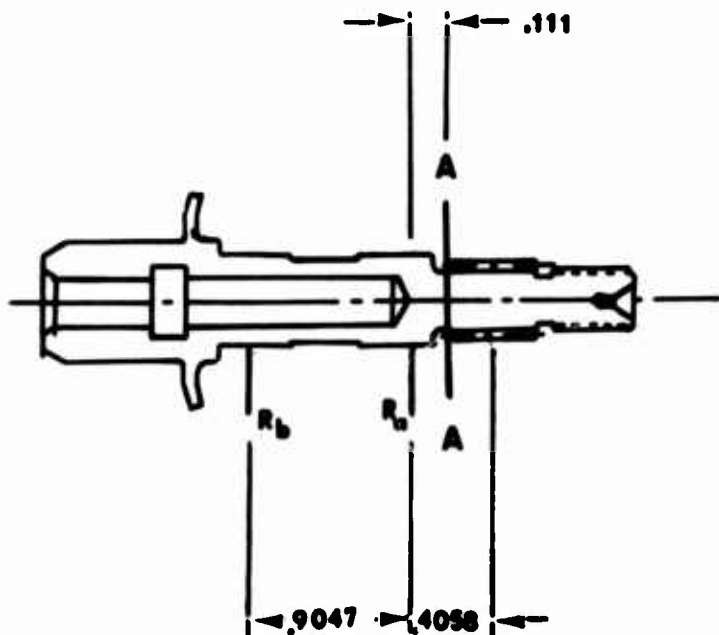


Figure G-15.  Shaft, Tachometer Drive.
S6135-20075-0

$$T = \frac{(63025)(HP)}{rpm} = \frac{(63025)(1.0)}{3906} = 16 \text{ in -lb}$$

$$W_t = \frac{T(2)}{dg} = \frac{(16)(2)}{7.2} = 4.5 \text{ lb}$$

$$W_r = W_t \tan 22.5^\circ = (4.48)(.414213) = 1.9 \text{ lb}$$

345

The critical section for fatigue design conditions occurs at
Section A-A ( .111 inch from the reaction point A) where

$$M_{A-A} = \sqrt{(4.5)(0.2947)^2 + (1.9)(.2947)^2} = 1.4 \text{ lb-in}$$

$$T = 16 \text{ in -lb}$$

$$P = \frac{T_p}{.2d} = \frac{185}{(.2)(0.285)} = 3250 \text{ lb} = \text{nut preload}$$

$$d_o = 0.270$$

$$Z = \frac{\pi}{32} d_o^3 = \frac{\pi}{32} (0.270^3) = 0.001932 \text{ in}^3$$

$$A = \frac{\pi}{4} d_o^2 = \frac{\pi}{4} (.270^2) = .0572 \text{ in}^2$$

$$f_s = \frac{T}{2Z} = \frac{16}{(2)(0.001932)} = 4140 \text{ psi}$$

$$f_b = \frac{M}{Z} = \frac{1.4}{0.001932} = 720 \text{ psi}$$

$$f_a = \frac{P}{A} = \frac{3250}{.0572} = 56,800 \text{ psi}$$

$$K_t = 2.0$$

$$F_{en} = 24,900 \text{ psi}$$

$$F_{ty} = 115,000$$

$$MS = \frac{1}{\sqrt{\left(\dfrac{f_a}{F_{ty}} + \dfrac{K_t \, f_b}{F_{en}}\right)^2 + 4\left(\dfrac{f_s}{F_{ty}}\right)^2}} - 1$$

$$MS = \sqrt{\cfrac{1}{\left(\cfrac{56800}{115000} + \cfrac{(2.0)(720)}{24900}\right)^2 + 4\left(\cfrac{4140}{115000}\right)^2}} - 1$$

$$MS = +.78$$

## GEAR, SPUR, ROTOR BRAKE

The rotor brake gear shaft carries the rotor brake disc and is driven by accessory tail takeoff output gear. Figure G-16 illustrates the rotor brake shaft geometry, while Figure G-17 is a sketch of the applied loads and reactions.
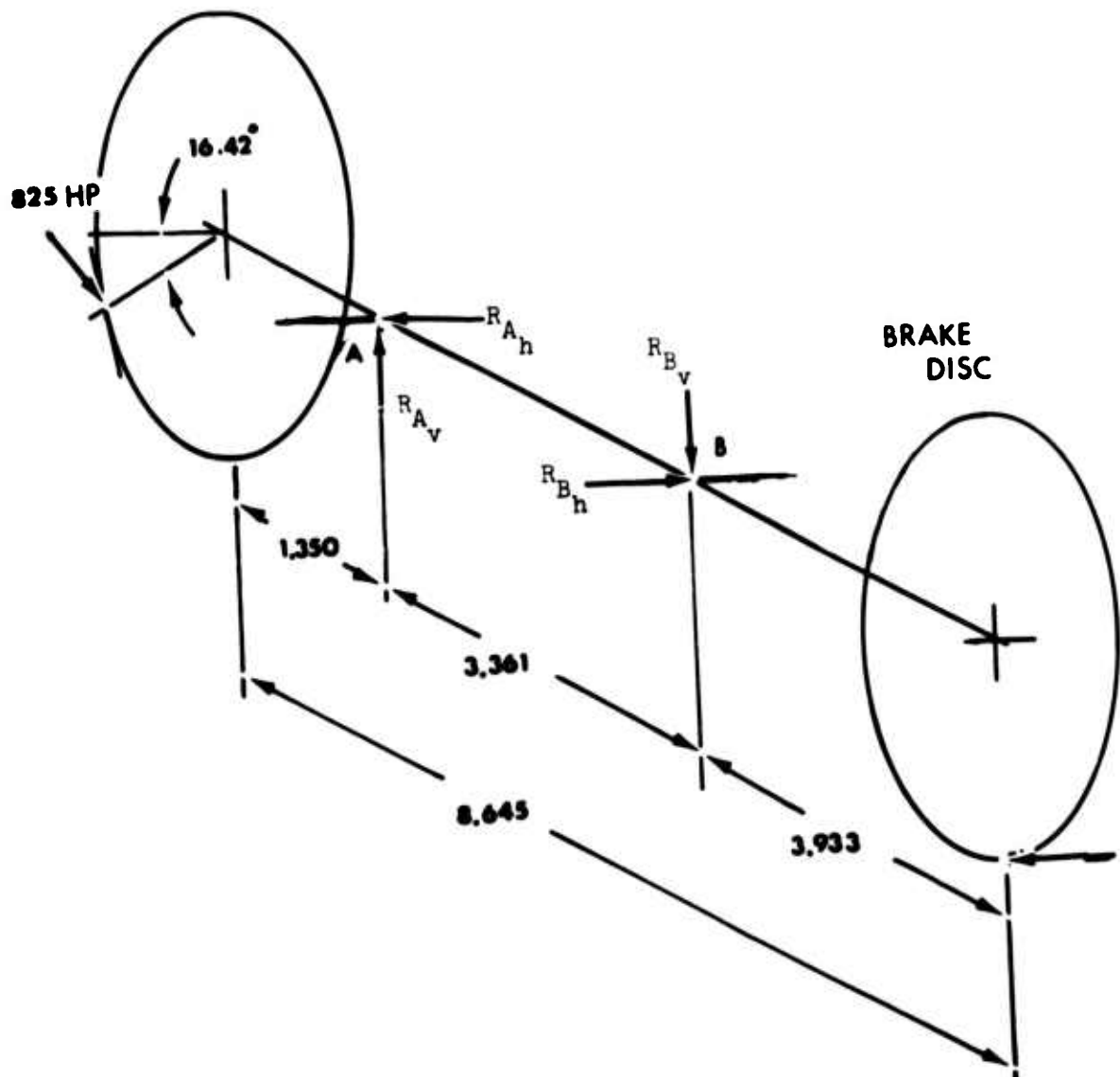
Figure G-16. Applied Gear and Brake Loads, Rotor Brake Shaft.
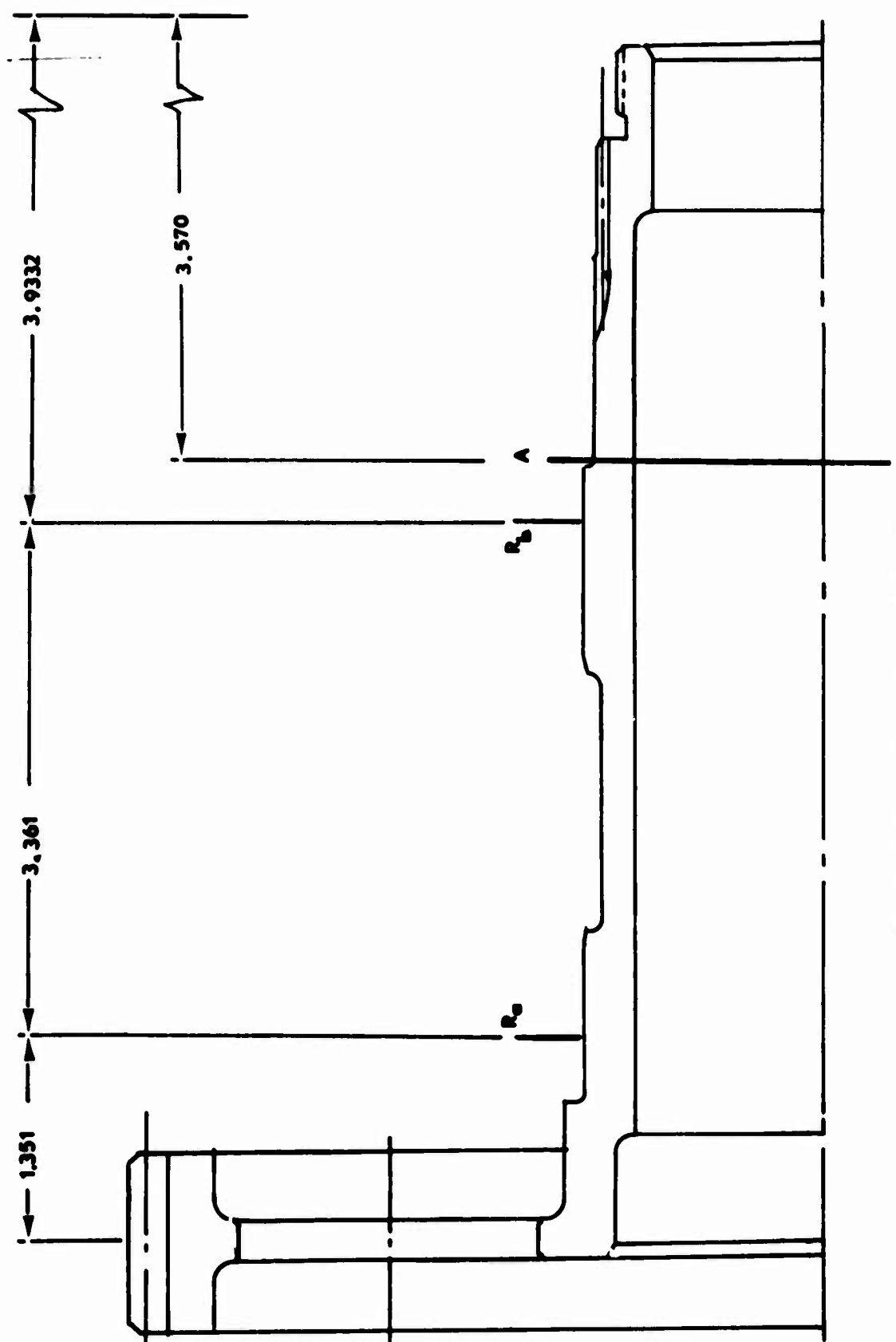
Figure G-17. Gear, Spur, Rotor Brake.

$$A = \frac{\pi}{4}(2.5^2) = 4.90 \text{ in}^2 = \text{area per pad}$$

$$N = PA = 450(4.90) = 2200 \text{ lb} = \text{normal force per pad}$$

$$W_{t_{brake}} = \mu N = .275(2200) = 605 \text{ lb}$$

Brake Friction Radius = 4.950 in

$$T_{brake} = 4(605)(4.95) = 11990 \text{ in-lb} = \text{total torque for 4 pads}$$

The critical section for fatigue design conditions occurs at Section A-A where

$$M = W_{t_{brake}}(3.570)$$

$$M = (2420)(3.570) = 8650 \text{ lb-in}$$

$$T = 11990 \text{ in-lb}$$

$$P = \frac{T_p}{.2 \, d} = \frac{1960}{(.2)(2.75)} = 3570 \text{ lb} = \text{nut preload}$$

$$d_o = 3.072 \text{ in}$$

$$d_i = 2.510 \text{ in}$$

$$Z = \frac{\pi}{32}\left(\frac{d_o^4 - d_i^4}{d_o}\right) = \frac{\pi}{32}\left(\frac{3.072^4 - 2.510^4}{3.072}\right) = 1.577 \text{ in}^3$$

$$A = \frac{\pi}{4}(d_o^2 - d_i^2) = \frac{\pi}{4}(3.072^2 - 2.510^2) = 2.45 \text{ in}^2$$

$$f_s = \frac{T}{2Z} = \frac{11990}{(2)(1.577)} = 3800 \text{ psi}$$

$$f_b \quad = \frac{M}{Z} \quad = \frac{8650}{1.577} \quad = 5480 \text{ psi}$$

$$f_a \quad = \frac{P}{A} \quad = \frac{3570}{2.45} \quad = 1460 \text{ psi}$$

$$K_t \quad = 3.30$$

$$F_{en} \quad = 21800 \text{ psi}$$

$$F_{ty} \quad = 115000 \text{ psi}$$

$$MS \quad = \frac{1}{\sqrt{\left(\dfrac{f_a}{F_{ty}} + \dfrac{K_t\, f_b}{F_{en}}\right)^2 + 4\left(\dfrac{f_s}{F_{ty}}\right)^2}} \quad -1$$

$$MS \quad = \frac{1}{\sqrt{\left(\dfrac{1460}{115000} + \dfrac{3.30(5480)}{21800}\right)^2 + 4\left(\dfrac{3800}{115000}\right)^2}} \quad -1$$

$$MS \quad = + .18$$

## LUBRICATION ANALYSIS

The primary aim of the lubrication system is to provide lubricant to all rotating/contacting surfaces. This analysis determines the optimum jet size for the lubrication requirements of the gears, bearings and rollers of the roller gear drive transmission.

### GEAR EFFICIENCY

In order that the oil requirements for gear meshes may be determined, it is first necessary to calculate the efficiency of each individual gear mesh.

The theoretical efficiency formula for the two-row, ring output, carrier fixed, sun gear input, roller gear drive can be calculated from the efficiencies of the individual meshes. Since all gears are on fixed centers, the overall efficiency is the product of the three individual mesh efficiencies and is given by

$$\eta \text{overall} = \eta ax_1 \, \eta y_1 \, x_2 \, \eta y_2 c$$

where

$\eta$overall = overall efficiency of roller gear drive unit

$\eta_{ax_1}$ = efficiency of sun gear with first row gear

$\eta y_1 x_2$ = efficiency of first row pinion with second-row gear

$\eta y_2 c$ = efficiency of second-row pinion with ring gear

The efficiency formula for individual gear meshes assumes that the coefficients of friction remain constant throughout the areas of approach and recess of tooth engagement.

The efficiency of spiral bevel gears is

$$\eta = 1 - \left(\frac{\cos \phi}{\cos \phi_n \cos \psi}\right) \left[\frac{1 + (1/m)}{(\beta_a + \beta_r) \cos \psi}\right] \frac{f}{2} \left(\beta_a^2 + \beta_r^2\right)$$

where

$\psi$ = spiral angle at middle of tooth space

$\phi_n$ = normal pressure angle

$\phi$ = pressure angle in plane of rotation of equivalent helical gear

$$\tan \phi = \frac{\tan \phi_n}{\cos \psi}$$

$$B_a = \frac{\sqrt{R_{og}^2 - R_{bg}^2} - R_{vg} \sin \phi}{R_{bp}}$$

$$B_r = \frac{\sqrt{R_{op}^2 - R_{bp}^2} - R_{vp} \sin \phi}{R_{bp}}$$

where

$R_{vp}$, $R_{vg}$ = pitch radial of equivalent spur pinion and gear respectively

$R_{op}$, $R_{og}$ = outside radius of equivalent spur pinion and gear respectively

$R_{bp}$, $R_{bg}$ = base radius of equivalent spur pinion and gear respectively

$\phi$ = pressure angle

$m$ = equivalent spur gear ratio = $\dfrac{R_{vg}}{R_{vp}}$

$$R_{op} = R_{vp} + a_p$$

$$R_{og} = R_{vg} + a_g$$

$$R_{bp} = R_{vp} \cos \emptyset$$

$$R_{bg} = R_{vg} \cos \emptyset$$

where

$a_p$, $d_g$ = addendum of pinion and gear respectively

$R_{vg}$, $R_{vp}$ = pitch radius of equivalent spur pinion and gear

$$R_{vp} = \frac{R_p}{\cos \gamma_p}$$

$$R_{vg} = \frac{R_g}{\cos \gamma_g}$$

where

$R_p$, $R_g$ = pitch radius of bevel pinion and gear at large end

$\gamma_p$, $\gamma_g$ = pitch angle of bevel pinion and gear

For hardened steel gears,

$$f = \frac{2}{3} \left( .002 \sqrt{V_s} \right)$$

where

$V_s$ = sliding velocity (average)

$$V_s = \frac{2 \pi R_p (rpm)}{12} \left[ 1 + \frac{N_p}{N_g} \right] \left[ \frac{\beta_a + \beta_r}{4} \right] \cos \emptyset$$

354

The efficiency of external spur gears is

$$\eta = 1 - \left[ 1 + \frac{N_p}{N_G} \right] \frac{f}{2} \left( \frac{\beta_a^2 + \beta_r^2}{\beta_a + \beta_r} \right)$$

where

a  =  arc of approach of driver

r  =  arc of recess of driver

f  =  coefficient of friction  (is derived for hardened
            spur gears as for hardened spiral bevel gears)

$$\beta_a = \frac{\sqrt{R_{og}^2 - R_{bg}^2} - R_g \sin \phi}{R_{bp}}$$

$$\beta_r = \frac{\sqrt{R_{op}^2 - R_{bp}^2} - R_p \sin \phi}{R_{bp}}$$

where

$R_p, R_g$  =  pitch radius of pinion and gear respectively

$R_{op}, R_{og}$  =  outside radius of pinion and gear respectively

$R_{bp}$  =  base circle radius of pinion

$\phi$  =  pressure angle

The efficiency of internal spur gears is

$$\eta = 1 - \left[ 1 - \frac{N_p}{N_g} \right] \frac{f}{2} \left( \frac{\beta_a^2 + \beta_r^2}{\beta_a + \beta_r} \right)$$

355

where

$$\beta_a = \frac{R_g \sin \phi - \sqrt{R_{ig}^2 - R_{bg}^2}}{2}$$

where

$R_{ig}$ = inside radius of gear

Values of $\beta_r$ and f are derived as for external spur gears.

Table H-1 , summarizes the efficiencies of the individual gear meshes for the roller gear drive transmission.

| TABLE H-1.   INDIVIDUAL GEAR MESH EFFICIENCIES. | | |
|---|---|---|
| Location | Coefficient of Friction | Efficiency $\eta$ |
| Input Bevel Gear Mesh | .061 | .9907 |
| Input Spur Gear Mesh | .044 | .9975 |
| TTO Bevel Gear Mesh | .036 | .9966 |
| TTO Spur Gear Mesh | .039 | .9964 |
| Roller Gear Drive Unit | | |
| Sun-1st Row Gear Mesh | .034 | .9974 |
| 1st Row Pinion – 2nd-Row Gear Mesh | .023 | .9975 |
| 2nd Row Pinion – Ring Gear Mesh | .013 | .9991 |

Thus, the gear mesh efficiency of the roller gear drive unit is

$\eta_{RGD}$ = (.9974)(.9975)(.9991) = .9940

ROLLER EFFICIENCY

## Efficiency due to Rolling

The rollers straddling the gears of the roller gear drive unit are subjected to pure rolling only. Rolling losses are due to the material deformation at the zone of contact caused by the roller preloads.

Consider the pressure distribution due to a cylinder on a flat surface carrying a load with unit length. Let the total Hertzian zone width be 2 b.
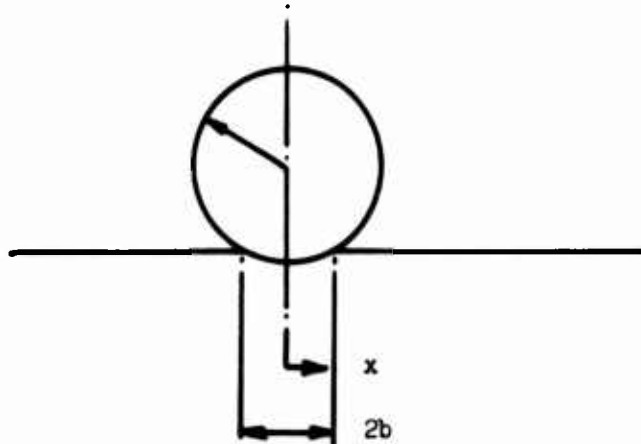


Figure H-1. Cylinder on a Flat Surface.

The pressure p at any point is given by

$$p = p_o \left(1 - \frac{x^2}{b^2}\right)^{\frac{1}{2}}$$

where

$$p_o = \text{pressure at the center} = \frac{2w}{\pi b}$$

357

Work done, $\emptyset$, by the cylinder in rolling forward unit distance is $G/r$

$$\emptyset = \frac{2\,wb}{3\pi r}$$

Energy loss $= \alpha\,\emptyset$

Energy lost by hysteresis during rolling of a cylinder over unit distance is

$$F = 3.5\,\alpha\left(\frac{2\,wb}{3\pi r}\right) = 3.5\,\alpha\,\emptyset$$

where

$\alpha =$ fractional hysteresis loss in static loading – unloading cycles

$\alpha = .01$ (Bowden and Tabor)
$\phantom{\alpha =} .005$ (K.L. Johnson)

$$b = 4\sqrt{\frac{R\,w}{2\pi E'}}$$

where

$E' =$ effective elastic modulus $= 33 \times 10^6$ lb/in$^2$

$R =$ effective radius of two surfaces

Dividing the equation for F through by the load, then the resistance to rolling is

$$\mu_r = 3.5\,\alpha\left(\frac{b}{3\pi r}\right)$$

$$= \frac{28\,\alpha}{3\pi r}\sqrt{\frac{w\,R}{2\pi E'}}$$

Then rolling efficiency, $\eta = 1 - \mu_r$

Table H-2 lists the efficiency per roller contact due to the preload forces given on page 102 of the main report. As there are two identical rolling contacts at each mesh, the value N is equal to half the preload force

| | Preload/Roller | Load/Inch | Efficiency |
|---|---|---|---|
| Location | N | w | $\eta$ |
| Sun - 1st-Row Roller | 1375 | 8590 | .9997 |
| 1st-Row/2nd-Row Rollers | 70 | 155 | .9999 |
| 1st-Row/2nd-Row Roller | 2250 | 5000 | .9997 |

TABLE H-2. ROLLER ROLLING EFFICIENCY.

## Shoulder Efficiency

In previous programs it was found that the sun gear has a tendency to move axially. This axial movement is a result of the various minute imperfections in the manufacture of the parts. To limit the movement, shoulders are machined on the rollers of the sun and first-row pinion. Friction forces at these shoulder contacts add to the efficiency losses of the rollers. The axial force is assumed to be 2% of the total preload on the sun gear.

At each sun - 1st - Row Roller Contact

$$N_1 = 2750$$

Axial force $F_a = 7\left[2750\left(\frac{2}{100}\right)\right] = 385$ lb

friction force $F = \mu F_a$

where $\mu = .02$

Sun roller shoulder - 1st - row rollers

$$F = .02(385) = 7.7$$

Friction Torque $= 7.7(9.035) = 70$

359

$$F_{HP}/_{contact} = \frac{2 \pi (70)(4045)}{7(12)(33,000)} = .64$$

$$\eta = 1 - \frac{.64}{3000}(7) = .9985$$

1st-Row Roller Shoulder - 2nd-Row Roller

$$F = 7.7$$

$$\text{Friction torque} = 7.7 (2.196) = 17.0$$

$$F_{HP}/_{contact} = \frac{2 \pi (17)(5858)}{7(12)(33,000)} = .22$$

$$\eta = 1 - \frac{.22}{3000}(7) = .9995$$

Table H-3 tabulates the overall roller efficiency per contact as the product of the shoulder efficiency and the rolling efficiency.

| TABLE H-3. OVERALL ROLLER EFFICIENCY PER CONTACT. | | | |
|---|---|---|---|
| Location | Efficiency Rolling | Shoulder | Efficiency Per Contact |
| Sun - 1st-Row Roller | .9997 | .9985 | .9982 |
| 1st-Row/2nd-Row Roller | .9999 | .9995 | .9994 |
| 1st-Row/2nd-Row Roller | .9997 | .9995 | .9992 |

BEARINGS

The friction torque for a rolling bearing is the sum of the load torque and viscous friction torque.

$$\text{i.e.,} \quad M \quad = \quad M_1 + M_v$$

The load torque is given by

$$M_1 \quad = \quad f_1 \; F_\beta \; d_m$$

in which $f_1$ is a factor depending on bearing design and relative bearing load. For ball bearings,

$$f_1 \quad = \quad Z \left(\frac{F_s}{C}\right)^y$$

where

$$F_s \; = \quad \text{static equivalent lead}$$

$$C \; = \quad \text{basic static capacity}$$

$$d_m \; = \quad \text{pitch diameter}$$

TABLE H-4 gives values of $Z$ and $y$.

| TABLE H-4. BALL BEARING FRICTION PARAMETERS. | | | |
|---|---|---|---|
| Ball Bearing Type | Contact Angle | Z | y |
| Deep Groove | $\alpha = 0^\circ$ | .0009 | .55 |
| Angular Contact | $\alpha = 30^\circ$ | .001 | .33 |
| Angular Contact | $\alpha = 40^\circ$ | .0013 | .33 |
| Thrust | $\alpha = 90^\circ$ | .0012 | .33 |
| Self-Aligning | $\alpha = 10^\circ$ | .0003 | .4 |

Table H-5 gives empirical values of $f_1$ for roller bearings.

| TABLE H-5. ROLLER BEARING FRICTION PARAMETERS. | |
|---|---|
| Roller Bearing Type | $f_1$ |
| Cylindrical | .0003 |
| Spherical (self-aligning) | .0005 |
| Tapered | .0005 |

For radial ball bearings

$$F_\beta = 0.9 \, F_a \cot \alpha - 0.1 \, F_r$$

or                                                          Larger value
                                                               used

$$F_\beta = F_r$$

where

$$F_a = \text{thrust load}$$

$$F_r = \text{radial load}$$

For roller bearings

$$F_\beta = F_r$$

The viscous torque is given by

$$M_v = 1.42 \times 10^{-5} \, f_o \, (v_o \cdot \text{rpm})^{2/3} \, d_m^3$$

where

$v_o$ = oil viscosity (centistokes) and $f_o$ is a factor depending upon type of bearing and method of lubrication. Table H-6 gives values of $f_o$ used for the bearings in the roller gear drive transmission.

362

| TABLE H-6. BEARING FRICTION FACTORS. | |
| --- | --- |
| Bearing Type | $f_o$ |
| Deep-groove ball bearing (single row) <br> Self-aligning ball bearing (double row) <br> Angular contact ball bearing (single row) | 4 |
| Angular contact ball bearing (double row) <br> Single-row tapered roller bearing | 8 |
| Cylindrical roller bearing (single row) | 6 |
| Spherical roller bearing (double row) | 12 |

For the bearings in roller gear drive transmission, Table H-7 gives the values for the friction torque for lubrication oil MIL-L-23699 which has a viscosity of 5.0 centistokes at $210^\circ$ F.

| Location | Friction Torque $M_1$ | Viscosity Torque $M_v$ | Total M |
|---|---|---|---|
| **TABLE H-7. BEARING FRICTION TORQUE** | | | |
| Input Bevel Pinion Ball Stack | 7.28 | 18.36 | 27.6 |
| Input Bevel Pinion Roller | 1.6 | 5.14 | 6.74 |
| Input Bevel Gear Ball Duplex | 8.5 | 70.0 | 78.5 |
| Input Bevel Gear Roller | 2.93 | 4.17 | 7.1 |
| Input Spur Pinion Ball | .46 | 1.34 | 1.8 |
| Input Spur Pinion Roller | 2.93 | 4.17 | 7.1 |
| Outer Shaft Roller | 3.73 | 44.27 | 48.0 |
| Outer Shaft Taper | 4.01 | 55.5 | 59.5 |
| Roller Gear 2nd-Row Spherical* | 22.0 | 4.0 | 26.0 |
| Main Rotor Shaft Ball Duplex | 149.0 | 8.0 | 157.0 |
| Main Rotor Shaft Roller | 23.5 | 13.5 | 37.0 |
| TTO Bevel Pinion Inboard Taper | 7.7 | 7.65 | 15.35 |
| TTO Bevel Pinion Outboard Taper | 1.87 | 5.53 | 7.4 |
| Spur Pinion TTO Roller | 2.2 | 2.3 | 4.5 |
| Spur Pinion TTO Ball | .6 | .85 | 1.45 |
| Spur Gear TTO Roller | .6 | 1.5 | 2.1 |
| Spur Gear TTO Ball | 3.4 | 1.6 | 5.0 |

*Torque values are per bearing.

LUBRICATION REQUIREMENTS AND HEAT GENERATED

The lubricating oil for the roller gear drive transmission is MIL-L-23699, a synthetic turbine engine lubricant widely used in helicopter transmissions.

Lubrication requirements for the gear meshes, roller contacts, and bearings are based on the prorated powers specified in Table C-2. The total heat generated is required at maximum continuous power in order that the oil cooler size may be determined.

The required oil flow rate is that amount of oil, in gallons per minute, necessary to dissipate a temperature rise at the gears, rollers, and bearings of $50^{\circ}$F. It is anticipated that the average oil temperature will be $210^{\circ}$F, at which temperature MIL-L-23699 has a specific heat of .51 Btu/lb $^{\circ}$F.

The oil required, in gallons per minute, is

$$Q = \frac{.13 \, H_1}{c_p \, \Delta_T}$$

where

$c_p$ = oil specific heat = .51 Btu/lb $^{\circ}$F

$\Delta_T$ = change in oil temperature = $50^{\circ}$F

$H_1$ = heat generated (Btu/min)

$Q$ = .005 $H_1$

where

$H_1$ = $F_{HP}$ x 42.42

For gears and rollers, the frictional horsepower is given by

$F_{HP}$ = $(1 - \eta)$ HP

where

HP = power being transmitted

$\eta$ = efficiency, specified in Table H-1 for gears and Table H-2 for rollers

365

For Bearings,

$$F_{HP} = M \frac{rpm}{63025}$$

where

M = total retarding torque specified in Table H-7

For the individual gear meshes and roller contacts, Table H-8 tabulates the friction power and heat generated at the maximum and prorated powers quoted in Table C-2. The required oil flow, Q, is specified for the prorated power.

| Location | At Maximum Power | | At Prorated Power | |
|---|---|---|---|---|
| | $F_{HP}$ | $H_1$ | $F_{HP}$ | Q |
| **TABLE H-8. GEARS AND ROLLERS, HEAT GENERATED AND OIL FLOW REQUIREMENTS.** | | | | |
| Input Bevel Gear Mesh | 17.4 | 740 | 10.0 | 2.0 |
| Input Spur Gear Mesh | 4.7 | 200 | 2.8 | .6 |
| TTO Bevel Gear Mesh | 2.4 | 100 | 1.1 | .25 |
| TTO Spur Gear Mesh | 2.5 | 107 | 1.2 | .25 |
| _Roller Gear Drive Unit_ | | | | |
| Sun-1st·Row Gear Mesh | 1.11 | 48 | .7 | .15 |
| 1st-Row Pinion - 2nd-Row Gear Mesh | 1.07 | 45 | .7 | .15 |
| 2nd-Row Pinion - Ring Gear Mesh | .38 | 16 | .24 | .05 |
| Sun-1st-Row Roller Contact | .8 | 32 | .5 | .1 |
| 1st-Row/2nd-Row Roller Contact | .26 | 10 | .16 | .03 |
| 1st-Row/2nd-Row Roller Contact | .34 | 14 | .2 | .04 |

366

Table H-9 tabulates the friction power, heat generated and oil flow required for each individual bearing set. These values are for the speed and retarding torques specified in Tables C-2 and H-7, respectively.

Part of the bearing torque is due to viscous losses which are independent of load; thus, oil requirements differ slightly for prorated powers.

| Location | $F_{HP}$ | $H_1$ | Q |
|---|---|---|---|
| **TABLE H-9. BEARING FRICTION TORQUE AND OIL REQUIREMENT.** | | | |
| Input Bevel Pinion Ball Stack | 8.3 | 350 | 1.75 |
| Input Bevel Pinion Roller | 2.0 | 86 | .43 |
| Input Bevel Gear Ball Duplex | 7.76 | 330 | 1.62 |
| Input Bevel Gear Roller | 1.38 | 58 | .30 |
| Input Spur Pinion Ball | .177 | 7.5 | .04 |
| Input Spur Pinion Roller | .70 | 30 | .15 |
| Outer Shaft Roller | 3.1 | 130 | .65 |
| Outer Shaft Taper | 3.8 | 160 | .80 |
| Roller Gear 2nd-Row Spherical | .51 | 22 | .11* |
| Main Rotor Shaft Ball Duplex | .5 | 21 | .10 |
| Main Rotor Shaft Roller | .12 | 5 | .03 |
| TTO Bevel Pinion Inboard Taper | 1.72 | 73 | .36 |
| TTO Bevel Pinion Outboard Taper | .82 | 35 | .17 |
| Spur Pinion TTO Roller | .62 | 26 | .13 |
| Spur Pinion TTO Ball | .16 | 7 | .04 |
| Spur Gear TTO Roller | .14 | 6 | .03 |
| Spur Gear TTO Ball | .32 | 14 | .07 |
| *Oil flow is per bearing. | | | |

The total oil flow required for the roller gear drive transmission at prorated power is

Oil flow for gears     = 9.3 includes 3.6 for RGD gears and rollers

Oil flow for bearings = 11.5 **includes .77 for RGD bearings**

Total oil flow        = 20.8 gallons per minute

The requirement for the adaptor box has not been tabulated but requires

                    .25 for the gears

                    .8  for the bearings

Total oil flow        = 21.8 gallons per minute.

The total heat generated for the roller gear drive transmission at maximum power is

Heat generated from gears    = 2900 Btu's/min includes 815 Btu's/min from RGD gears and rollers

Heat generated from bearings = 2355 Btu's/min includes 154 Btu's/min from RGD bearings

Total heat generated       = 5255 Btu's/minute

The analysis of the adaptor box has not been included but that generates

                  140 Btu's/min from the gear meshes

                  100 Btu's/min from the bearings

Total heat generated        = 5500 Btu's/minute

Sikorsky has previously sized their oil coolers on maximum continuous power and without consideration to viscous effects in bearings. Therefore, for the roller gear drive transmission, the oil cooler requirement at 1770 HP/input maximum continuous power is given in Table H-10.

| TABLE H-10. HEAT GENERATED AT MAXIMUM CONTINUOUS POWER | | |
|---|---|---|
| Heat Source | Maximum Power (Btu/min) | Maximum Continuous Power (Btu/min) |
| Main Drive Gears | 2900 | 2740 |
| Adaptor Box Gears | 140 | 130 |
| Bearing Friction Torque (Main Drive) | | 553 |
| Bearing Friction Torque (Adaptor Box) | | 78 |
| Heat Generated at Max Continuous Power, 3500 Btu/min | | |

## LUBRICATION SYSTEM

The required oil flow for the roller gear drive transmission is 22 gallons per minute. Two fixed displacement vane pumps, one mounted in the sump and driven off the main rotor shaft through speed increasing gears, and the other mounted on the rear cover and driven by the primary hydraulic gear, are each capable of delivering 22 gallons per minute.

Oil from the sump is fed to each pump which delivers oil at 75 psi. This high pressure oil combines into one line at the inlet to the oil filter. Upon exit, the oil passes through the oil cooler and onto the jets. It is anticipated that the pressure at the jets will be 50 psi. The relief valve at the pump can be adjusted to ensure the desired pressure. In order to limit the amount of oil to the roller gear drive unit, an in-line restrictor decreases the oil pressure to 30 psi. Also affected by this restrictor are the lubrication jets to the tapered roller bearings on the outer shaft and tail takeoff bevel gear shaft.

Figure H-2 is a schematic of the oil lubrication system. Both the input bevel gear meshes and the tail takeoff bevel gear mesh are lubricated in and out of mesh.

Lubrication is also directed to the bearings, rollers, and plungers of the freewheel units and the splines of the quill shafts.

## LUBRICATION JET DIAMETERS

Flow through an orifice (jet) is related to the upstream and downstream pressure by the square law equation

$$Q = C_d A_o \sqrt{\frac{2 \Delta P}{\rho}}$$

where

$Q$ = volume rate of flow, $in^3/sec$

$C_d$ = discharge coefficient

$A_o$ = area of orifice opening, $in^2$

$\Delta P$ = change in pressure, $lb/in^2$

$\rho$ = mass density of fluid, $lb\text{-}sec^2/in^4$

Converting Q to gallons per minute leads to

$$Q = 29.84 \, C_d \, d_o^2 \sqrt{\frac{\Delta P}{S}}$$

where

$d_o$ = orifice diameter, in

$S$ = specific gravity of oil

Knowing Q from Tables H-8 and H-9, the jet diameter for MIL-L-23699 at S = .935 ($175°F$) is

$$d_o = \left( \frac{Q}{30.9 \, C_d \sqrt{\Delta P}} \right)^{\frac{1}{2}}$$
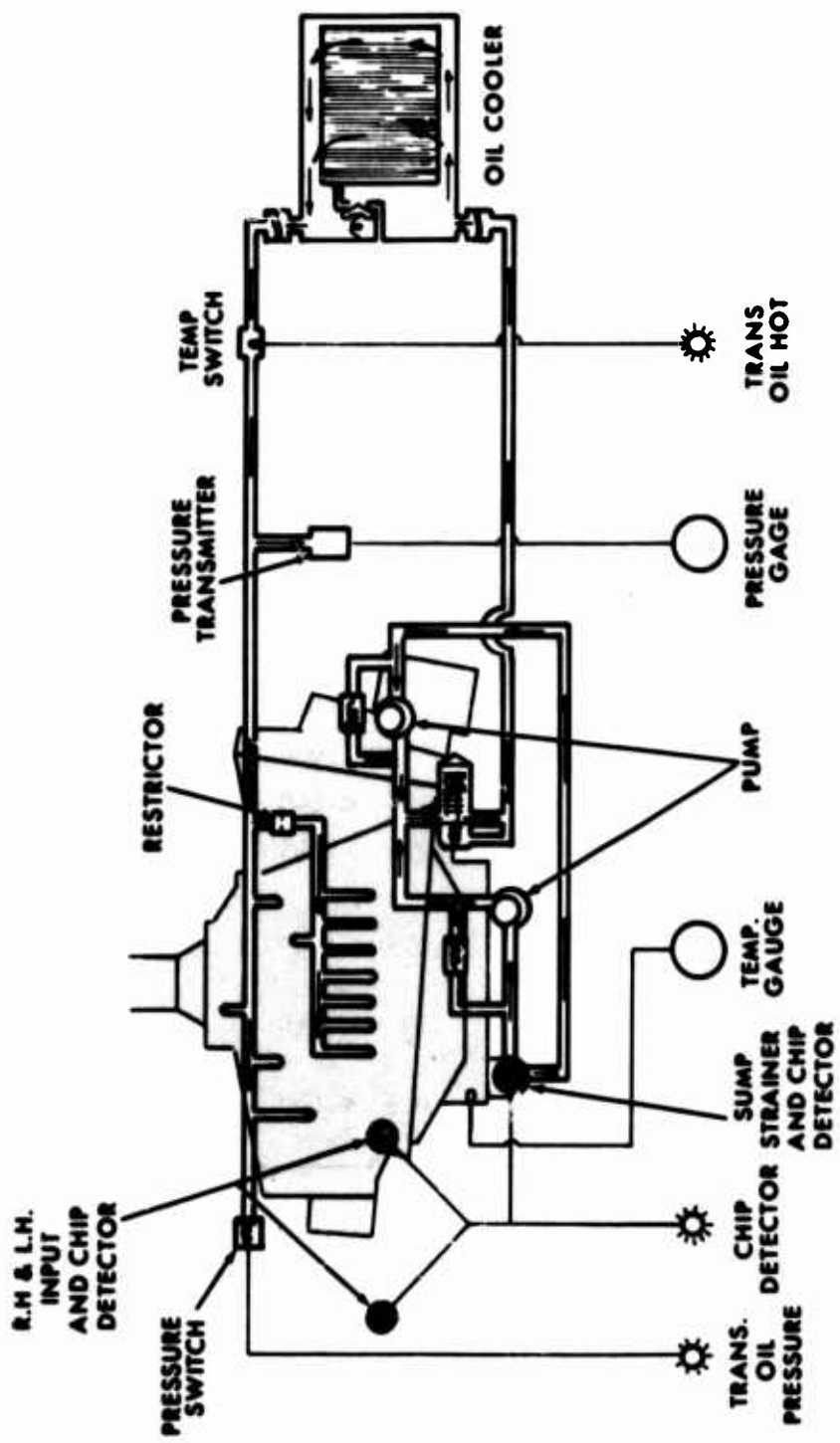
370

Figure H-2. Lubrication Schematic.

The theoretical flow per jet diameter is shown in Tables H-11 and H-12 for the gears and bearings respectively. The flow obtained through the jet diameter used is shown for comparison. These calculations are based on a coefficient of discharge which has been determined experimentally. A back pressure at the jet of 50 psi has been used except for the roller gear drive unit and the tapered roller bearings where 30 psi is used.

To reduce the possibility of jet blockage, a minimum jet diameter of .040 inch is specified.

| | | Theoretical | | Actual | |
|---|---|---|---|---|---|
| Location | No. Jets Per Mesh | Q/Jet | $d_o$ | Q/Jet | $d_o$ |
| Input Bevel Gear Mesh | 2 | 1.0 | .082 | .9 | .078 |
| Input Spur Gear Mesh | 1 | .6 | .066 | .18 | .040 |
| TTO Bevel Gear Mesh | 2 | .125 | <.040 | .18 | .040 |
| TTO Spur Gear Mesh | 1 | .25 | .045 | .44 | .055 |
| Roller Gear Drive Unit | | | | | |
| Sun-1st-Row Gear Mesh | 2 | .075 | <.040 | .14 | .040* |
| 1st-Row Pinion - 2nd-Row Gear Mesh | 1 | .15 | <.040 | .37 | .059* |
| 2nd-Row Pinion - Ring Gear Mesh | 2 | .025 | <.040 | .14 | .040 |

TABLE H-11. GEARS AND ROLLERS - JET DIAMETERS.

*At 30 psi

| Locations | No. Jets Per Brg. | Theoretical Q/Jet | $d_o$ | Actual Q/Jet | $d_o$ |
|---|---|---|---|---|---|
| TABLE H-12. BEARINGS - JET DIAMETERS. | | | | | |
| Input Bevel Pinion Ball | 1 | 1.75 | .11 | 2.55 | .125 |
| Stack Roller | 1 | .43 | .055 | .5 | .059 |
| Input Bevel Gear Ball | 4 | .405 | .052 | .18 | .040 |
| Duplex Roller | 1 | .3 | .047 | .44 | .055 |
| Input Spur Pinion Ball | | .04 | | | |
| Roller | 1 | .15 | <.04 | .51 | .060 |
| Outer Shaft Roller | 1 | .65 | .067 | .18 | .040 |
| Taper | 4 | .2 | .041 | .18 | .040 |
| Roller Gear 2nd-Row Spherical | 1 | .11 | <.04 | .14 | .040* |
| Main Rotor Shaft Ball Duplex | 1 | .10 | <.04 | .18 | .040 |
| Roller | 1 | .03 | <.04 | .18 | .040 |
| TTO Bevel Pinion Inboard Taper | 1 | .36 | .059 | .4 | .063* |
| Outboard Taper | 1 | .17 | .043 | .4 | .063* |
| Spur Pinion TTO Roller | 1 | .13 | <.04 | .18 | .040 |
| Ball | 1 | .04 | <.04 | .18 | .040 |
| Spur Gear TTO Roller | 1 | .03 | <.04 | .18 | .040 |
| Ball | - | .07 | <.04 | .51 | .060 |

*At 30 psi

373

TRANSMISSION EFFICIENCY

The efficiency of a transmission is a function of the heat that is generated in the gearbox. This heat, when converted to friction horsepower at the source of heat (the gear meshes and bearings) and compared to the input power, is the efficiency.

Heat is generated from friction, oil churning, windage and viscous shearing of the oil film at the contacts. In order to compare the calculated efficiency of the roller gear drive transmission, the effects of oil churning and windage have been ignored; viscous shearing has been incorporated in bearing friction horsepower but has been neglected in gear mesh calculations.

Tables H-13 and H-14 respectively tabulate the power path from the input to the main rotor shaft and from the tail takeoff bevel gear through the accessories to the tail takeoff shaft.

The overall efficiency is a function of the power out and the power in; thus,

$$\eta_{overall} = \frac{P_{out} \text{ main rotor} + P_{out} \text{ TTO} + P_{out} \text{ accessories}}{P_{in}}$$

and the efficiency of the roller gear drive unit is.

$$\eta_{RGD} = \frac{P_{out}}{P_{in}}$$

374

## TABLE H-13. INPUT - MAIN ROTOR SHAFT POWER PATH LOSSES.

| | Power In | Bearing Loss | Power Out | Mesh Loss |
|---|---|---|---|---|
| Input Bevel Pinion | 3740 | 20.6 | 3719.4 | 34.8 |
| Input Bevel Gear | 3684.6 | 18.28 | 3666.32 | - |
| Input Spur Pinion | 3666.32 | 1.75 | 3664.57 | 9.4 |
| Input Spur Gear | 3655.17 | 6.9 | 2948.27 | - |
| Roller Gear Drive | | | | |
| Input Sun | 2948.27 | 5.6 | 2942.67 | 7.77 |
| 1st Row | 2934.9 | 4.2 | 2930.7 | 7.49 |
| 2nd Row | 2923.1 | 3.57 | 2919.53 | 2.66 |
| Ring Gear - Main Rotor | 2916.87 | .62 | 2916.25 | - |

375

## TABLE H-14. ACCESSORY POWER PATH LOSSES.

| | Power In | Accessory Power Out | Losses | Power Out |
|---|---|---|---|---|
| TTO Bevel Gear | 700 | | 4.94 | 695.06 |
| TTO Spur Pinion | 695.06 | 150.0 Oil Cooler + $\left\{\begin{array}{l}\text{1.0 Tachometer}\\ \text{35.7 Generator}\\ \text{6.5 Primary Hyd.}\end{array}\right.$ | .216+.78+2.5 | 633.364 |
| TTO Spur Gear | 633.364 | $\left\{\begin{array}{l}\text{4.0 Lube Pump}\\ \text{13.0 Utility Pump}\\ \text{6.5 Auxiliary Pump}\\ \text{53.6 Generator}\end{array}\right.$ | .385 + .46 | 555.419 |

Overall efficiency is given by

$$\eta_{overall} = \frac{P_{out} \text{ Main Rotor} + P_{out} \text{ TTO} + P_{out} \text{ Accessory}}{P_{in}}$$

$$= \frac{2916.25 + 555.419 + 138.401}{3704}$$

$$\eta = .965$$

The roller gear drive unit efficiency is

$$\eta_{RGD} = \frac{P_{out}}{P_{in}} = \frac{2916.87}{2948.27}$$

$$\eta = .989$$

13980-75

377